



UNIVERSIDADE DE BRASÍLIA - UNB
INSTITUTO DE GEOCIÊNCIAS - IG
PROGRAMA DE PÓS-GRADUAÇÃO EM GEOLOGIA

**Geologia, geoquímica e geocronologia das rochas da Suíte
Rio Branco, Cinturão Nova Brasilândia e implicações na
evolução do orógeno Sunsás no sudoeste do Cráton
Amazônico**

Tese de Doutorado N.º 159

Marcos Luiz do Espírito Santo Quadros

Brasília-DF
2020



UNIVERSIDADE DE BRASÍLIA - UNB
INSTITUTO DE GEOCIÊNCIAS - IG
PROGRAMA DE PÓS-GRADUAÇÃO EM GEOLOGIA

**Geologia, geoquímica e geocronologia das rochas da Suíte Rio Branco,
Cinturão Nova Brasilândia e implicações na evolução do orógeno Sunsás no
sudoeste do Cráton Amazônico**

Discente:

Marcos Luiz do Espírito Santo Quadros

Banca Examinadora:

Profa. Maria Emília Schutesky Della Giustina (Orientadora)

Prof. Wilson Teixeira (USP)

Prof. Moacir José Buenano Macambira (UFPA)

Prof. Elton Luiz Dantas (IGD/UnB)

Prof. Reinhardt Adolfo Fuck (IGD/UnB/suplente)

Prof. Mauro Cesar Geraldês (UERJ/suplente)

Brasília, 22 de janeiro de 2020



UNIVERSIDADE DE BRASÍLIA - UNB
INSTITUTO DE GEOCIÊNCIAS - IG
PROGRAMA DE PÓS-GRADUAÇÃO EM GEOLOGIA

Tese de doutorado apresentada ao Programa de Pós-Graduação em Geologia do Instituto de Geociências da Universidade de Brasília em cumprimento ao requisito parcial para a obtenção do Título de Doutor em Geologia, área de concentração geologia regional.

Autor:

Marcos Luiz do Espírito Santo Quadros

Banca Examinadora:

Profa. Maria Emília Schutesky Della Giustina (IG/UnB) _____
(Orientadora)

Prof. Wilson Teixeira (USP) _____
Examinador Externo

Prof. Moacir José Buenano Macambira (UFPA) _____
Examinador Externo

Prof. Elton Luiz Dantas (IGD/UnB) _____
Examinador Interno

Brasília, 22 de janeiro de 2020

Qg

Quadros, Marcos Luiz do Espírito Santo
Geologia, geoquímica e geocronologia das rochas
da Suíte Rio Branco, Cinturão Nova Brasilândia e
implicações na evolução do orógeno Sunsás no sudoeste do
Cráton Amazônico / Marcos Luiz do Espírito Santo Quadros;
orientador Maria Emília Schutesky Della Giustina. --
Brasília, 2020.
120 p.

Tese (Doutorado - Doutorado em Geologia) -- Universidade
de Brasília, 2020.

1. Geologia Regional. 2. Geoquímica. 3. Geocronologia. 4.
Geotectônica. 5. Evolução Crustal. I. Giustina, Maria Emília
Schutesky Della , orient. II. Título.

DEDICATÓRIA

*A Alan Marcos Rocha Quadros,
Amanda Rocha Quadros,
Auricélia Almeida Rocha,
Laura Cristina Silveira Quadros,
Marcos Alonso de Quadros (in memoriam),
Raíza Karolina Almeida Rocha,
Terezinha de Jesus Espírito Santo Quadros*

Agradeço a **DEUS** pelo dom da vida.

Agradeço a **minha família** (pais, irmãos, esposa, sobrinhas e filhos) pelo apoio ao longo desta jornada, que começou na pequena cidade de Bragança-PA, trilhando caminhos posteriores em Belém-PA, Porto Velho-RO e chegando até Brasília-DF. Agradecimentos em especial aos meus pais Marcos Alonso de Quadros (*in memoriam*) e Terezinha de Jesus do Espírito Santo Quadros pela dedicação e incentivo aos meus estudos ao longo de toda a vida, a minha esposa Auricélia Almeida Rocha que sempre me apoiou e tomou as rédeas da família durante as minhas ausências e aos meus filhos (Alan Quadros, Amanda Quadros e Raíza Rocha) pelo incentivo e pela curiosidade em conhecer a importância de um curso de doutorado na vida pessoal e profissional.

Agradeço à Profa. Maria Emília Della Giustina (IG-UnB) pela orientação durante a execução da tese e pela confiança no meu trabalho. Ao amigo Prof. Valmir da Silva Souza (IG-UnB) pelo incentivo e apoio técnico durante as atividades do doutorado na UnB, em Brasília. Aos professores Reinhardt Adolfo Fuck (IG-UnB) e Catarina Labouré Benfica Toledo (IG-UnB) e aos geólogos (a) Joseneusa Brilhante Rodrigues (CPRM) e Jaime Estevão Scandolaro (CPRM) pelas revisões dos artigos e sugestões.

Aos amigos geólogos da CPRM Anderson Alves de Souza, Luciano Castro da Silva e Lívio Wagner Chaves Correa agradeço pelo apoio técnico necessário para elevar o nível das discussões geológicas, seja no campo ou nos trabalhos de escritório.

Às amigas da CPRM Maria Rosalva Campos Coelho (Técnica em Mineração) e a geóloga Joseneusa Brilhante Rodrigues agradeço pelo imenso apoio durante as atividades de preparação de amostras para análises isotópicas e interpretação dos resultados.

Aos colegas e amigos da CPRM Lúcia Travassos da Rosa-Costa, César Lisboa Chaves, Ardiles Gimax Henrique, Teresinha de Jesus Fôro, Homero Reis de Melo Junior, Cintia Maria Gaia da Silva, Marcelo Lacerda Vasquez, Raphael Neto Araújo e Nelma Fabricia da P. R. Botelho, pelo apoio técnico em momentos específicos ocorridos durante o andamento do curso de doutorado.

À Coordenação de Aperfeiçoamento de Pessoal de Nível Superior (CAPES) pelo apoio financeiro parcial a pesquisa realizada.

À instituição CPRM-Serviço Geológico do Brasil, unidades regionais em Porto Velho (REPO), Belém (SUREG-BE) e Brasília (SEDE), agradeço pelo apoio logístico e financeiro as etapas de campo, laboratório e escritório e ao Programa de Pós-graduação em Geologia do Instituto de Geociências, Universidade de Brasília.

E por fim, a todos que contribuíram de alguma forma direta ou indireta com a elaboração desta tese de doutorado.

A evolução geológica do Cinturão Nova Brasilândia no sudoeste do Cráton Amazônico, em Rondônia, ocorreu de forma progressiva durante o Mesoproterozoico e início do Neoproterozoico, entre aproximadamente 1241 Ma e 910 Ma, período que abrange estágios pré-orogênico, orogênico e pós-orogênico. Novos dados geológicos de campo, geoquímicos, geocronológicos U-Pb em zircão (LA-ICP-MS) e de isótopos de Sr-Nd obtidos na parte sul do cinturão, associados a reinterpretação de informações anteriormente publicadas, permitem estabelecer cronologia mais precisa entre os episódios de sedimentação, deformação, metamorfismo e magmatismo, bem como a caracterização da afinidade química do magmatismo máfico, fonte, ambiente tectônico da Suíte Rio Branco e os estágios ou fases de evolução do cinturão durante a orogenia Nova Brasilândia.

O ambiente tectônico de *emplacement* do magma máfico-félsico da Suíte Rio Branco é importante na caracterização dos eventos orogenéticos do Mesoproterozoico (Esteniano), no sudoeste do Cráton Amazônico, que antecederam à formação do supercontinente Rodínia. A Suíte Rio Branco, alvo de estudo, é composta por rochas máficas-félsicas que incluem metagabros, metagabro-noritos, metatroctolitos, metabasaltos maciços, metadiabásios, anfibolitos, metagranitos, rochas metavulcânicas félsicas e metatrandhjemitos (equivalentes de plagiogranitos), expostos na forma de *stocks* alongados, arredondados ou ovais, *sills* e enxames de diques, além de derrames. A encaixante regional (Formação Rio Branco) é representada por rochas de alto grau metamórfico, incluindo gnaisses calciossilicáticos, biotita paragneisses, gnaisses trondhjemiticos, anfibolitos e granulitos (paraderivados, máficos ou félsicos).

Idades U-Pb (LA-ICP-MS) obtidas em cristais de zircão em rochas do Domínio Rio Branco (constituído por rochas metavulcanossedimentares, metamáficas e metafélsicas), parte sul do Cinturão Nova Brasilândia, sugerem episódios de metamorfismo de alto grau entre 1137 ± 9 Ma e 1127.6 ± 2.3 Ma. Portanto, anterior ao *emplacement* das rochas máficas e félsicas da Suíte Rio Branco, datado entre 1119.7 ± 2.7 Ma e 1106.2 ± 2.8 Ma, portanto de geração muito próxima ao metamorfismo. Cristais de zircão recristalizados provenientes de paragneisse de alto grau e granito anatético da Formação Rio Branco e de metagabro da Suíte Rio Branco mostram, respectivamente, idades U-Pb (LA-ICP-MS) de 1019 ± 5 Ma, 1011.3 ± 9.6 Ma e 1016.7 ± 3.9 Ma que representam, possivelmente, registros isotópicos de episódio mais jovem de deformação, metamorfismo e migmatização ocorrido no Cinturão Nova Brasilândia.

Dados geoquímicos (rocha total) demonstram que as rochas metamáficas da Suíte Rio Branco são composicionalmente sub-alcalinas toleíticas de baixo a médio Ti, com assinaturas de sobreposição de MORB-like, IAT e BABB. Nos diagramas de multi-elementos normalizados ao Manto Primitivo, as rochas metamáficas da Suíte Rio Branco apresentam enriquecimento em

elementos litófilos de íons grandes (LILE) em relação elementos de elevado potencial iônico (HFSE), anomalias negativas de Nb e Ta, positivas de Pb, e enriquecimento gradativo em Th em relação a Nb e Ta. Por outro lado, apresentam razões $Ti/V = 10-50$, $La/Yb = 1,74-12,33$ e $Th/Yb = 0,10-3,56$, razões $Ce/Y (4,12-24,67)$ variando de baixa a alta e razões baixa para $Ce/Pb (3,3-20,5)$, $Nb/U (3,2-16,25)$ e $Th/La (0,01-0,30)$. A composição isotópica de Sr-Nd mostrou ϵNd com valores levemente negativos a positivos entre $-2,89$ e $+1,66$ (para $t=1120$ Ma), próximos ao CHUR, e variadas relações $^{87}Sr/^{86}Sr (0,702-0,714)$ e baixas relações $^{143}Nd/^{144}Nd (\sim 0,512)$ sugerindo contaminação crustal ou metassomatismo da cunha mantélica. Os dados geológicos e as assinaturas geoquímicas e isotópicas da Suíte Rio Branco, juntamente com os *trends* petrogenéticos definidos nos diagramas de variação, multi-elementos normalizados, ETR's normalizados e discriminantes tectônicos, foram considerados eficazes no diagnóstico de subducção.

A proposta de evolução tectônica para o Cinturão Nova Brasilândia, apresentada nessa tese de doutorado, sugere que a parte sul do Cinturão Nova Brasilândia representa um fragmento incompleto de um sistema arco-bacia, contendo registros de dois estágios evolutivos desenvolvidos durante a orogenia Nova Brasilândia. O primeiro acrecionário, entre aproximadamente 1137 Ma e 1106 Ma, envolve subducção intraoceânica, metamorfismo de alto grau (granulítico), magmatismo máfico-félsico e formação de sistema *arc – back-arc*. O segundo colisional, entre aproximadamente 1096 Ma e 1010 Ma, envolve espessamento crustal, deformação (tectônica transpressiva e transcorrência sinistral tardia), metamorfismo de alto grau (anfíbolito superior) e migmatização. Os estágios acrecionário e colisional da orogenia Nova Brasilândia no Mesoproterozoico (Esteniano), associados à evolução do orógeno Sunsás e a montagem de Rodínia, ocorreu mediante interações entre o bloco Paraguá, proto-Cráton Amazônico e fragmentos menores de terrenos, envolvendo articulações tectônicas oblíquas e/ou frontais entre grandes massas crustais representadas por Laurentia e Amazônia. Esse novo cenário tectônico é diferente do modelo de *rift* intracontinental proposto anteriormente, principalmente na fase de inversão da bacia e início do fechamento de um oceano porque envolve subducção intraoceânica e formação de um sistema *arc – back-arc*.

Nesse novo cenário tectônico considera-se a orogenia Nova Brasilândia no sudoeste do Cráton Amazônico como do tipo acrecionária-colisional, com evolução entre 1137 e 1010 Ma, posterior a formação de um oceano (fase de oceanização) entre o Bloco Paraguá (acrescido de terrenos alóctones e faixas móveis) e o proto-Cráton Amazônico entre 1241 e 1137 Ma.

Palavras-chave: Magmatismo Mesoproterozoico, Geoquímica, Geocronologia U-Pb, Isótopos de Sr-Nd, Cinturão Nova Brasilândia, Subducção

Geological evolution of the Nova Brasilândia belt in the southwestern Amazonian Craton in Rondônia occurred progressively during the Mesoproterozoic and early Neoproterozoic, between ca. 1241 Ma and 910 Ma, a period that encompasses pre-orogenic, orogenic and post-orogenic stages. New field geological, geochemical, geochronological U-Pb (LA-ICP-MS) and Sr-Nd isotopes data obtained from southern belt rocks, together with the reinterpretation of previously published information, allow for more accurate chronology of sedimentation, deformation, metamorphism and magmatism episodes, and to define the chemical affinity of mafic magmatism, sources, tectonic environment of the Rio Branco Suite. As well as the evolution stages of the belt during the Nova Brasilândia orogeny.

The tectonic emplacement environment of the Rio Branco Suite mafic-felsic magma is important in characterizing of the Mesoproterozoic (Stenian) orogenic events in the southwestern of the Amazonian Craton, prior to the Rodinia supercontinent assembly. The Rio Branco Suite, target of the studies, is composed by mafic-felsic rocks classified as metagabbros, metagabbronorites, metatroctolites, massive metabasalts, metadiabases, amphibolites, metagranites, metavolcanic rocks and metatrandhjemites (plagiogranite equivalents) exposed to rounded or elliptical stocks, sills, dike swarms and spills. The host rock of the Rio Branco Suite include high-grade rocks consisting of calc-silicate gneisses, biotite paragneisses, amphibolites and granulites (paraderived, mafic or felsic).

U-Pb ages (LA-ICP-MS) obtained from rock zircon crystals from the Rio Branco domain (composed of metavolcanosedimentary, metafelsic and metamafic rocks) in the southern part of the Nova Brasilândia belt suggest an episode of high-grade metamorphism that occurred between 1137 ± 9 Ma and 1127.6 ± 2.3 Ma. Therefore, prior to the emplacement of the Rio Branco Suite mafic-felsic magma dated between 1119.7 ± 2.7 Ma and 1106.2 ± 2.8 Ma, more of very close generation. Recrystallized zircon crystals from high-grade paragneiss and anatectic granite of the Rio Branco Formation, and Rio Branco Suite metagabbro presented, respectively, U-Pb ages (LA-ICP-MS) of 1019 ± 5 Ma, 1011.3 ± 9.6 Ma and 1016.7 ± 3.9 Ma possibly representing isotopic records of a youngest episode of deformation, metamorphism and migmatization that occurred during the evolution of the Nova Brasilândia belt.

Geochemical data (whole rock) demonstrates that the Rio Branco Suite metamafic rocks are compositionally low- to medium Ti tholeitic sub-alkaline, with overlap signatures of MORB-like, IAT and BABB. In the Mantle-normalized multi-element diagrams of the Rio Branco Suite, metamafic rocks show enrichment in large ion lithophile elements (LILE) relative to high-field-strength elements (HFSE), negative Nb and Ta anomalies, Pb positive anomalies, gradual Th

enrichment in relation to Nb and Ta, and enrichment in K and Sr. On the other hand, $Ti/V = 10-50$, $La/Yb = 1.74-12.33$ and $Th/Yb = 0.10-3.56$ ratios, $Ce/Y (4.12-24.67)$ ratios ranging from low to high and low ratios to $Ce/Pb (3.3-20.5)$, $Nb/U (3.2-16.25)$ and $Th/La (0.01-0.30)$. Sr-Nd isotopic composition showed ϵNd with slightly negative to positive values between -2.89 and $+1.66$ (for $T = 1120$ Ma), close to CHUR, and varied $^{87}Sr/^{86}Sr (0.702-0.714)$ and low ratios $^{143}Nd/^{144}Nd$ ratios (~ 0.512) suggesting enrichment/contamination or mantelic wedge metasomatism. The geological data, geochemical and isotopic signatures of the Rio Branco Suite metamafic component, together with the petrogenetic trends defined in the variation diagrams, normalized multi-elements patterns (spidergrams), normalized REEs patterns and tectonic discriminants were effective in the diagnostic of subduction.

The tectonic evolution proposal for the Nova Brasilândia belt presented in this doctoral thesis suggests that the southern part of the Nova Brasilândia belt is an incomplete fragment of arc-basin system containing records of two evolutionary stages developed during the Nova Brasilândia orogeny. The first accretionary, between ca. 1137 Ma and 1106 Ma, involves intra-oceanic subduction, high-grade metamorphism (granulitic) and arc - back-arc system formation. The second collision, between ca. 1096 Ma and 1010 Ma, involves crustal thickening, deformation (transpressive tectonics and late sinistral transurrence), high-grade metamorphism, and migmatization, as proposed in previous work. The accretionary and collisional stages of the Nova Brasilândia orogeny in the Mesoproterozoic (Stenian), associated with the evolution of the Sunsás orogen and Rodinia assembly, occurred through interactions between the Paraguá block, Amazonian proto-Craton and smaller terrane fragments, involving oblique and/or frontal tectonic joints between large crustal masses represented by Laurentia and Amazônia. This new tectonic scenario is partly different from the intracontinental rift model previously proposed, mainly in the basin inversion phase and the beginning of an ocean closure because it involves intra-oceanic subduction and formation of an arc - back-arc system.

In this new tectonic scenario it is considered that the nature of the Nova Brasilândia orogeny in southwestern Amazonian Craton, in Rondônia, is of the accretionary-collisional type between ca. 1137 and 1010 Ma. Therefore, after the formation of an ocean (oceanization phase) between a Paraguá block (increased of allochthonous terranes and mobile belts) and the Amazonian proto-Craton between ca. 1241 and 1137 Ma.

Keywords: Mesoproterozoic magmatism, Geochemistry, U-Pb Geochronology, Sr-Nd Isotopes, Nova Brasilândia belt, Subduction

	<i>pág.</i>
Figura 1. Cenário tectônico esquemático Mesoproterozoico do sudoeste do Cráton Amazônico com a localização da área estudada (adaptado de Ruiz, 2005; Bettencourt <i>et al.</i> , 2010; Teixeira <i>et al.</i> , 2010; D'Agrella-Filho <i>et al.</i> , 2012; Rizzotto <i>et al.</i> , 2014).....	3
Figura 2. Mapa de localização da área de estudo (imagem de fundo corresponde ao modelo digital SRTM).....	6
Figura 3. Províncias geocronológicas do Cráton Amazônico, segundo Tassinari e Macambira (1999) em (A) e Santos <i>et al.</i> (2003) em (B).....	14
Figura 4. Quadro comparativo entre a cronologia dos eventos orogenéticos mesoproterozoicos (Esteniano-Toniano) registrados nas províncias Sunsás e Grenville.....	20
Figura 5. Recobrimento aerogeofísico do Cinturão Nova Brasilândia e adjacências. Em (A) mapa de aeromagnetometria de Amplitude do Sinal Analítico (ASA), (B) mapa de aeromagnetometria primeira derivada horizontal (DZ) e (C) mapa de aerogamaespectrometria mostrando a composição ternária RGB (K, eTh, eU) (fonte: CPRM, 2014 - Projeto Aerogeofísico Sudoeste de Rondônia).....	22
Figura 6. Mapa geológico do Cinturão Nova Brasilândia, sudoeste do Cráton Amazônico, Rondônia. Compilado e modificado de Scandolara e Rizzotto (1998), Bahia e Silva (1998) e Bergami <i>et al.</i> (2018).....	23
Tabela 1. Principais características geológicas e tectônicas do cinturão Nova Brasilândia no sudoeste do Cráton Amazônico em Rondônia (Principais características geológicas e tectônicas do Cinturão Nova Brasilândia no sudoeste do Cráton Amazônico em Rondônia (após Scandolara e Rizzotto, 1998; Bahia e Silva, 1998; Rizzotto, 1999; Tohver <i>et al.</i> , 2004, 2005a; Santos <i>et al.</i> , 2008; Rizzotto <i>et al.</i> , 2014).....	106
Figura 7. Quadro comparativo com os cenários de evolução tectônica propostos para o Cinturão Nova Brasilândia, sudoeste do Cráton Amazônico, Rondônia, no Mesoproterozoico (Esteniano).....	107

CAPÍTULO 1 – INTRODUÇÃO	<i>pág.</i>
1. Introdução.....	1
1.1 Apresentação do tema.....	1
1.2 Justificativas técnico-científicas.....	2
1.3 Objetivos.....	4
1.4 Localização e acesso.....	5
1.5 Metodologia e materiais.....	5
1.5.1 Análise bibliográfica e aquisição de dados.....	6
1.5.2 Atividades de campo e elaboração do mapa geológico.....	6
1.5.3 Geoquímica em rocha total (elementos maiores e traços).....	7
1.5.4 Geocronologia U-Pb em zircão (LA-ICP-MS).....	8
1.5.5 Estudos isotópicos Sm-Nd e Sr-Sr em rocha total.....	10
1.6 Estrutura organizacional da Tese.....	12
CAPÍTULO 2 – CONTEXTO GEOLÓGICO REGIONAL	
2. Contexto geológico regional.....	13
2.1 Sudoeste do Cráton Amazônico em Rondônia.....	13
2.1.1 Província Rio Negro-Juruena.....	15
2.1.2 Província Rondoniana-San Ignácio.....	18
2.1.3 Província Sunsás.....	20
CAPÍTULO 3 - Artigo Científico 1.....	26
CAPÍTULO 4 - Artigo Científico 2	66
CAPÍTULO 5 – Discussões e conclusões	
5. Discussões e conclusões.....	105
5.1 Fase pré-orogênica (< 1241 Ma).....	105
5.2 Fase orogênica acrecionária (1137-1106 Ma).....	108
5.3 Fase orogênica colisional (1096-1010 Ma).....	110
Referências bibliográficas da Tese.....	112

1. Introdução

1.1 Apresentação do tema

Essa pesquisa abrange informações geológicas de campo, petrológicas e geocronológicas da região sudeste do Estado de Rondônia, enfocando rochas mesoproterozoicas da Suíte Rio Branco e encaixante regional. Tais informações constituem a base da proposta de um novo cenário tectônico de subducção para a porção sul do Cinturão metavulcanossedimentar Nova Brasilândia, apresentado nesta tese de doutorado intitulada “**Geologia, geoquímica e geocronologia das rochas da Suíte Rio Branco, Cinturão Nova Brasilândia e implicações na evolução do orógeno Sunsás no sudoeste do Cráton Amazônico**”, aplicado como requisito à obtenção do título/grau de Doutorado em Geologia pela Universidade de Brasília (UnB).

O estudo da gênese das suítes magmáticas máficas é importante porque estas representam registros geológicos que podem ser associados a diversos ambientes extensionais ou convergentes, continentais ou intraoceânicos, com índice de preservação relativamente baixo em função de serem, em geral, consumidas durante os processos orogenéticos acrecionários ou colisionais. Portanto, são registros de episódios magmáticos de natureza máfica ou máfica-ultramáfica de significância global e relevante importância geodinâmica e metalogenética, marcadoras de grandes eventos tectônicos globais. São também indicadores da natureza e composição das fontes mantélicas e dos processos de contaminação e metassomatismo do manto, durante subducção ou residência crustal. Neste contexto, o magmatismo máfico-félsico da Suíte Rio Branco no sudoeste do Cráton Amazônico em Rondônia se destaca pela sua importância no cenário de evolução do Cinturão Nova Brasilândia no Mesoproterozoico, possivelmente registro na Amazônia de uma fase de oceanização, seguida de subducção intraoceânica e formação de arco de ilhas e bacias *back-arc*.

O Cinturão metavulcanossedimentar Nova Brasilândia, conhecido também como Cinturão Nova Brasilândia, é entidade geotectônica de *trend* E-W, com inflexões para NW e SW, desenvolvido no Mesoproterozoico (Esteniano) entre o Bloco Paraguá (acrescido de terrenos alóctones) e o proto-Cráton Amazônico a partir da reativação da zona de sutura Guaporé que havia sido formada anteriormente, durante a orogenia Rondoniana-San Ignácio entre 1,47-1,35 Ga (Rizzotto *et al.*, 2014). Segundo Rizzotto (1999), pioneiro no estudo dessa região, as rochas metavulcanossedimentar que compõem o Cinturão Nova Brasilândia originaram-se a partir de um ciclo de Wilson, com abertura e fechamento de bacia do tipo *rift* intracontinental, que evoluiu para margem passiva e formação de proto-oceano. Na fase de inversão da bacia, as rochas do *rift* foram metamorfizadas em médio a alto grau (atingindo fácies granulito) durante a orogenia Nova Brasilândia, inicialmente atribuída ao intervalo de tempo entre 1180 e 1100 Ma.

1.2. Justificativas técnico-científicas

Diversos cenários tectônicos têm sido apresentados para explicar a formação do supercontinente Rodínia no final do Mesoproterozoico (Esteniano), envolvendo a colisão do proto-Cráton Amazônico com a parte leste da América do Norte representada pela Laurentia, envolvendo articulações locais com o Bloco Paraguá e o embasamento Arequipa-Antofala. Sadowski e Bettencourt (1996) apresentaram uma das primeiras tentativas de correlação global que sugerem a justaposição entre Amazônia e Laurentia, durante a amalgamação do Supercontinente Rodínia. Dados paleomagnéticos do sudoeste do Cráton Amazônico publicados anteriormente sugerem correspondências entre a deformação Grenvilliana e as do sudoeste do Cráton Amazônico, durante o Mesoproterozoico, conectando a Amazônia e a Laurentia (Rogers e Santosh, 2003; Tohver *et al.*, 2002, 2004, 2005a). Três importantes cinturões metassedimentares na borda sudoeste do Cráton Amazônico, denominados de Nova Brasilândia e Aguapeí expostos ao longo da fronteira entre Bolívia e Brasil, e Sunsás na Bolívia, são considerados áreas-chave para a compreensão dos eventos orogenéticos do Mesoproterozoico (Esteniano) porque preservam registros das atividades de aglutinação de massas cratônicas para formar o supercontinente Rodínia (Fig. 1). Portanto, são áreas geologicamente importantes para estabelecer correlações entre a Província Sunsás (ou Sunsás-Aguapeí), no Cráton Amazônico, e a Província Grenville, no sul da Laurentia (Fig. 1) (Rizzotto *et al.*, 1999; Litherland e Bloomfield, 1981; Litherland *et al.*, 1986; Boger *et al.*, 2005; Ruiz, 2005; Santos *et al.*, 2008, Teixeira *et al.*, 2010, Rizzotto *et al.*, 2014). Os cinturões Nova Brasilândia, Aguapeí e Sunsás foram, recentemente, considerados como pertencentes a uma única unidade geotectônica, denominada de Cinturão Móvel da Amazônia Ocidental, desenvolvida no final do Mesoproterozoico em ambiente de *rift* intracontinental (Rizzotto *et al.*, 2014).

No Cinturão Nova Brasilândia, área de interesse dessa pesquisa, estudos pioneiros realizados por Rizzotto (1999) e Rizzotto *et al.* (1999, 2001) na região de Nova Brasilândia, em Rondônia, permitiram a caracterização da Orogênese Nova Brasilândia, que corresponde a um Ciclo de Wilson desenvolvido aproximadamente entre 1,23 e 1,10 Ga, envolvendo abertura e fechamento de uma bacia denominada de *rift* Nova Brasilândia. Nesse *rift*, a sedimentação mesoproterozoica ocorreu no Esteniano e está representada na parte norte do cinturão pelas rochas da Formação Migrantinópolis (idades máximas de sedimentação em 1215 Ma, Rizzotto, 1999; 1211 Ma, Santos *et al.*, 2000; ou 1122 Ma, Rizzotto *et al.*, 2014), constituída por turbiditos de composição siliciclástica-carbonática. Na parte sul do Cinturão Nova Brasilândia, rochas metassedimentares em alto grau associam-se espacialmente com rochas plutônicas metamáficas, sendo este conjunto englobados na Formação Rio Branco, conforme a concepção original de Rizzotto (1999). Nesse contexto as unidades metassedimentares representam a sedimentação relacionada à fase *rift*

intracontinental, que evoluiu para margem passiva, e as rochas metamáficas associadas ao magmatismo gerado nas fases *rift-drift* a *drift*, com formação de proto-oceano (Rizzotto, 1999).

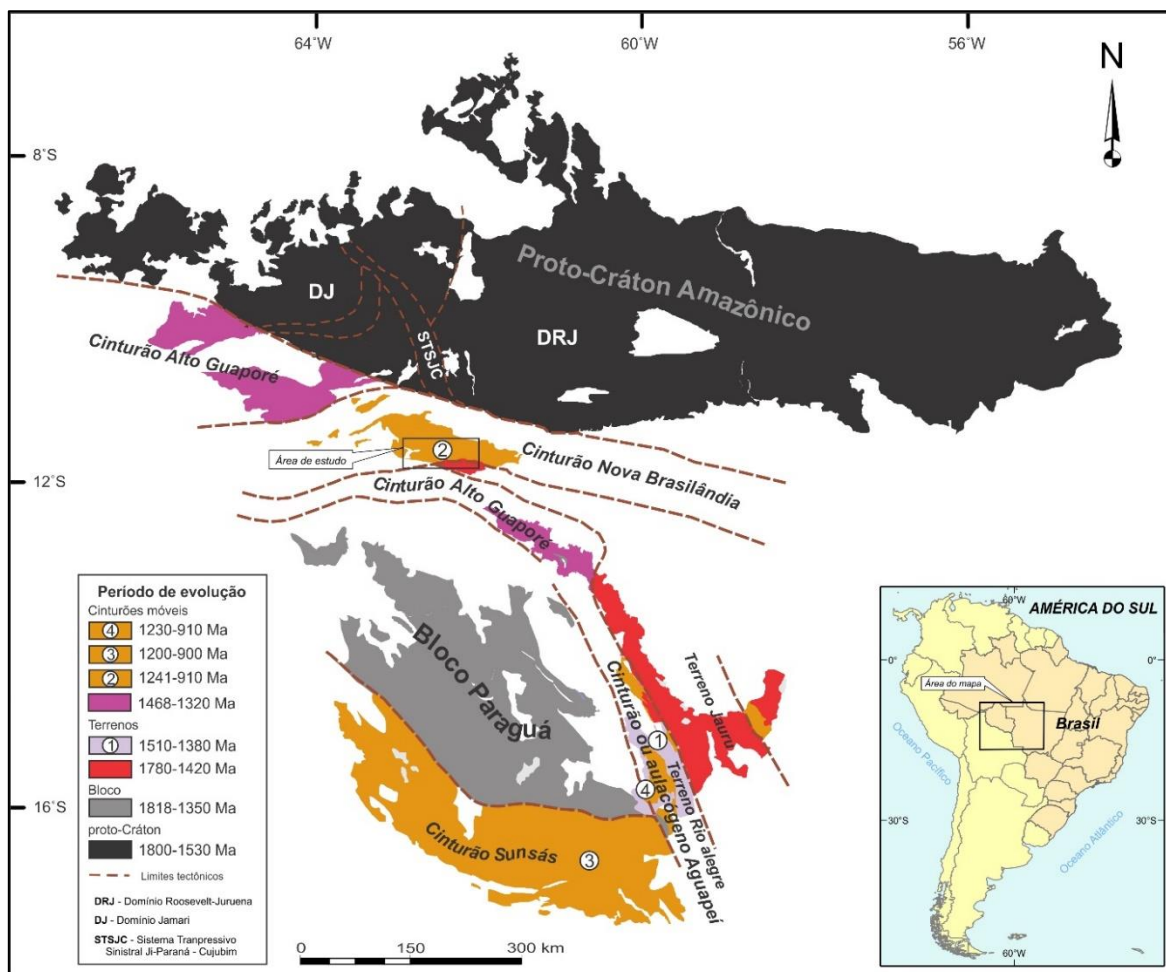


Fig. 1. Cenário tectônico esquemático Mesoproterozoico do sudoeste do Cráton Amazônico com a localização da área estudada (adaptado de Ruiz, 2005; Bettencourt et al., 2010; Teixeira et al., 2010; D'Agrella-Filho et al., 2012; Rizzotto et al., 2014).

Considerando cenário inicial de evolução em ambiente de *rift* intracontinental, duas relações geológicas observadas no campo chamaram a atenção em relação a sequência evolutiva neste tipo de ambiente. A primeira se refere à existência de rochas máficas intrusivas (*stocks*, *sills* e enxames de diques) em rochas metavulcanossedimentares em alto grau metamórfico, sugerindo a existência de episódio de metamorfismo de alto grau (granulítico) anterior ao *emplacement* do magma máfico. A segunda envolve existência de estruturas deformacionais (dobras, cavalgamentos oblíquos, zonas de cisalhamento/milonitização e lineações de estiramento) mais jovens e que afetam todo o conjunto rochoso, associadas à transpressão e transcorrência tardia, descritas anteriormente por Rizzotto (1999) e Tohver et al. (2004, 2005a, 2005b). Essas relações apontam para uma história geológica bem mais complexa do que simplesmente abertura e fechamento de um *rift* intracontinental, onde a

associação de rochas metavulcanossedimentares em alto grau teve seus protólitos depositados e metamorfizados anterior ao *emplacement* do magmatismo máfico da Suíte Rio Branco. Essas relações espaciais entre as rochas sinalizavam para a possibilidade de geração em ambiente orogênico compressional, como forma de explicar a deformação (dobras, cavalgamentos, transpressão e transcorrência), metamorfismo de alto grau (granulítico) e o magmatismo (máfico-félsico), espacialmente associados.

Neste contexto, o desenvolvimento da pesquisa de doutorado foi pautado na obtenção de dados geológicos, geoquímicos, geocronológicos U-Pb e isotópicos Sr-Nd das rochas da parte sul do Cinturão Nova Brasilândia, com ênfase principal na definição das idades das rochas, afinidade química, fonte e ambiente tectônico do magmatismo máfico da Suíte Rio Branco, bem como no estabelecimento dos intervalos de tempo dos eventos geológico reconhecidos na área de estudo. As informações obtidas serviram de base científica para elucidar dúvidas e questionamentos relacionados ao ambiente tectônico do magmatismo máfico e sua formação em cenários continentais ou oceânicos, divergentes ou convergentes. Dessa forma, o objetivo de nossa pesquisa foi estabelecido em busca do aperfeiçoamento do modelo de *rift* intracontinental, anteriormente proposto, bem como apresentar um novo cenário tectônico alternativo, diferente do que já havia sido proposto para o Cinturão Nova Brasilândia. Por fim, contribuir de forma pontual, através de nossos estudos, para o aperfeiçoamento dos modelos globais de reconstituição dos eventos tectônicos que levaram a formação do supercontinente Rodínia.

1.3 Objetivos

O objetivo principal da pesquisa consistiu no estudo das rochas metamáficas da Suíte Rio Branco, aflorantes no Domínio Rio Branco, parte sul do Cinturão Nova Brasilândia, mediante a caracterização geológica, petrográfica, geoquímica (rocha total), geocronológica U-Pb em zircão (LA-ICP-MS) e estudos dos isótopos de Sm, Nd e Sr. O estudo foi direcionado para a definição da idade, afinidade química, fonte e ambiente tectônico gerador do magmatismo máfico da Suíte Rio Branco, bem como na cronologia dos eventos geológicos. Pretendeu-se, também, definir se essas rochas metamáficas faziam parte de intrusões acamadadas, arco de ilhas ou se pertenciam a uma sequência ofiolítica, possivelmente marcadora de importante zona de sutura na região. Esta pesquisa de doutorado buscou, com base na caracterização da afinidade química e nos *trends* petrogenéticos apresentados pelas rochas metamáficas da Suíte Rio branco nos diagramas de classificação da série (AFM), diagramas de correlação tipo Harker, diagramas ETR (normalizados), diagramas multi-elementos ou *spidergrams* (normalizados) e nos diagramas discriminantes tectônicos específicos (que utilizam elementos menores), complementados pelos estudos de Sr-Nd, identificar se o magmatismo máfico da Suíte Rio Branco estava relacionado à evolução de *rift* intracontinental com

possível geração de proto-oceano (tipo MORB), conforme proposto inicialmente por Rizzotto (1999), ou se parte do magmatismo máfico da Suíte Rio Branco poderia ser correlacionado a ambiente orogenético compressivo, envolvendo subducção intraoceânica e formação de arco e bacias. Este estudo objetivou, também, a caracterização da natureza isotópica e geoquímica das fontes mantélicas com base na determinação das razões isotópicas de Sr e Nd e na análise de dados geoquímicos de elementos traços considerados imóveis. Finalizando, teve o objetivo de fornecer novos subsídios à evolução geodinâmica do Mesoproterozoico do sudoeste do Cráton Amazônico, em Rondônia, com base na definição do ambiente tectônico de geração do magmatismo máfico Suíte Rio Branco e seu contexto geotectônico regional na evolução do Cinturão Nova Brasilândia e do orógeno Sunsás.

1.4 Localização e acesso

Este estudo foi desenvolvido na porção sudoeste do Cráton Amazônico, Rondônia, mais especificamente na parte sul do Cinturão Nova Brasilândia, denominada de Domínio Rio Branco. A área estudada localiza-se mais especificamente no sudeste de Rondônia, distante aproximadamente 525 km por via rodoviária da capital Porto Velho. Corresponde a polígono retangular com vértices de coordenadas geográficas S11°48'55"/W61°41'25", S12°02'51"/W61°41'25", S12°02'51"/W62°26'55" e S11°48'55"/W62°26'55", medindo 26 km de largura e 82 km de comprimento, abrangendo área de aproximadamente 2132 km². A área estudada abrange partes dos municípios de Alta Floresta d'Oeste e Santa Luzia d'Oeste (Fig. 2). O acesso à área pode ser realizado a partir da cidade de Porto Velho, pela rodovia federal BR-364, até o entroncamento com a rodovia estadual RO-479, seguindo nessa rodovia estadual até Santa Luzia d'Oeste e em seguida em direção a Alta Floresta d'Oeste. Além desse principal acesso, outras rotas podem ser estabelecidas para acessar a área de pesquisa. O deslocamento no interior da área pode ser realizado por meio de estradas vicinais, denominadas de linhas de colonização, trafegáveis de forma satisfatória durante a época do verão amazônico. Alta Floresta d'Oeste é cidade que pode ser utilizada como base de apoio para as atividades de campo.

1.5 Metodologia e materiais

Para alcançar os objetivos proposto nesta pesquisa foram utilizadas técnicas e métodos de investigação, descritos a seguir:

1.5.1 Análise bibliográfica e aquisição de dados

Consistiu na análise e síntese de materiais bibliográfico de cunho científico, publicados anteriormente, que constituem acervo de informações geológicas das regiões de Rondônia, Mato Grosso e Bolívia. Foram consultadas diversas publicações científicas específicas e voltadas para a temática da pesquisa, métodos analíticos aplicados e problemas geológicos semelhantes. As informações analisadas que serviram de suporte científico a esta pesquisa estão contidas principalmente em livros, revistas, periódicos nacionais e internacionais, dissertações de mestrado e teses de doutorado.

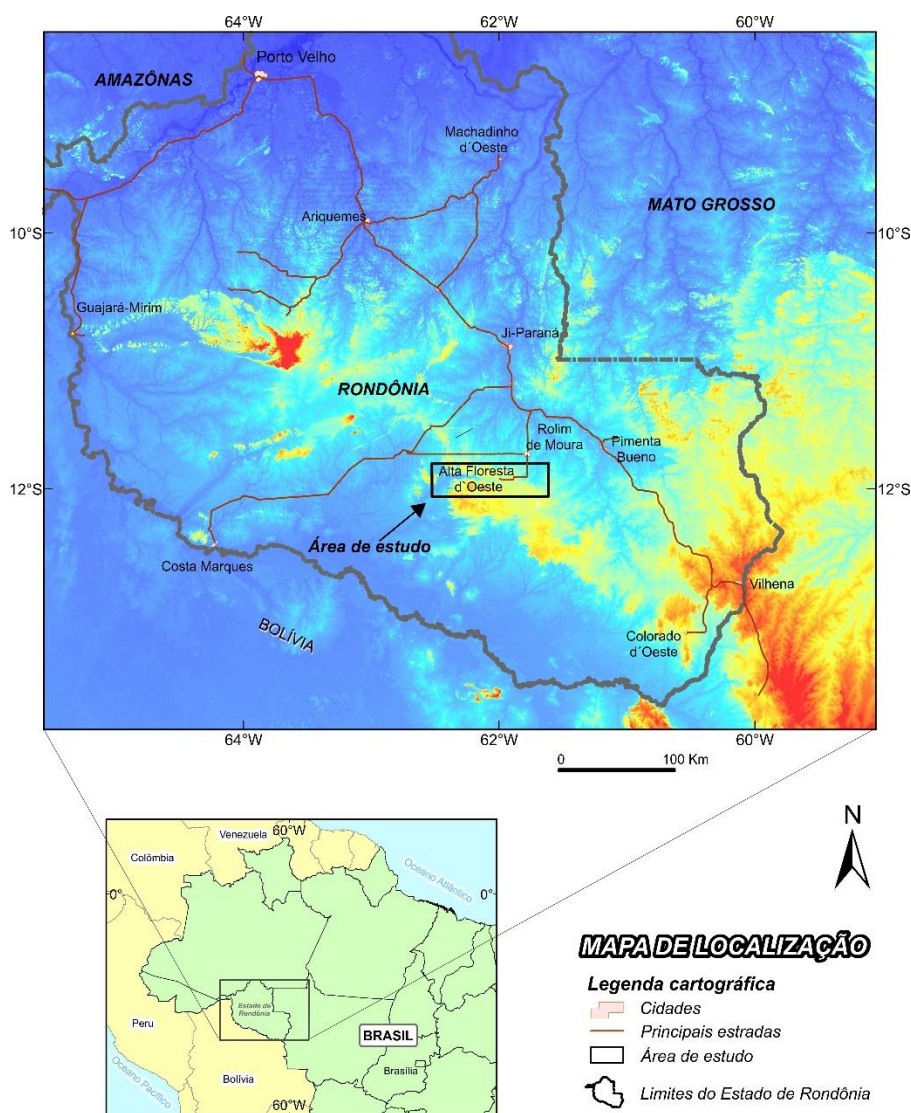


Fig. 2. Mapa de localização da área de estudo (imagem de fundo corresponde ao modelo digital SRTM).

1.5.2 Atividades de campo e elaboração do mapa geológico

Para caracterizar as rochas e compreender as relações geológicas entre as unidades litoestratigráficas da área de pesquisa, foram realizados trabalhos de campo mediante descrição de afloramentos, coleta de amostras de rocha para análises petrográficas, geoquímicas e isotópicas. O

mapa geológico foi elaborado a partir da compilação de informações geológicas existentes e disponibilizadas pela CPRM-Serviço Geológico do Brasil, obtenção de novas informações de campo, integração geológico-geofísico (aeromagnetometria e aerogamaespectrometria), acrescida de informações petrológicas e geocronológicas. O mapa geológico em formato digital (escala 1:100.000), inserido como figuras nos artigos e no texto da tese, foi elaborado mediante o emprego do *software* de geoprocessamento ArcGIS, ajustado as bases cartográfica do IBGE (escala 1:100.000), as imagens do SRTM-*Shuttle Radar Topographic Mission* e apresentado em valores UTM, *datum* SIRGAS 2000.

1.5.3 Geoquímica em rocha total (elementos maiores e traços)

Os estudos geoquímicos em rocha total envolveram coleta, descrição petrográfica, seleção e análise de 34 amostras de rochas metamáficas provenientes do Domínio Rio Branco, parte sul do Cinturão Nova Brasilândia. A geoquímica de rocha total foi realizada na ALS Laboratório, conforme certificado BH17273983. Os métodos analíticos incluem ICP-AES e ICP-MS para os principais óxidos e elementos traços. O trabalho analítico solicitou um pacote de preparação das amostras (PREP-31), com códigos da ALS de preparação CRU-31 (*fine crushing – 70% < 2 mm*), LOG-22 (*sample login – red w/o BarCode*), PUL-31 (*pulverize split to 85% < 75 µm*), SPL-21 (*split sample-riffle splitter*) and WEI-21 (*received sample weight*). O pacote analítico solicitado foram ME-4ACD81 (*base metals by 4-acid dig., instrument ICP-AES*) para análises dos elementos Ag, As, Cd, Co, Cu, Li, Mo, Ni, Pb, Sc, Tl e Zn, ME-ICP06 (*whole rock package-ICP-AES*) para a análise dos óxidos Al₂O₃, BaO, CaO, Cr₂O₃, Fe₂O₃, K₂O, MgO, MnO, Na₂O, P₂O₅, SiO₂, SrO e TiO₂, o pacote ME-MS81 (*lithium borate fusion ICP-MS*) para a análise dos elementos Ba, Ce, Cr, Cs, Dy, Er, Eu, Ga, Gd, Hf, Ho, La, Lu, Nb, Nd, Pr, Rb, Sm, Sn, Sr, Ta, Tb, Th, Tm, U, V, W, Y, Yb e Zr, o pacote OA-GRA05 (*loss on ignition at 1000°C, instrument ICP-MS*) para cálculo do LOI e o pacote TOT-ICP06/ME-MS81D (*total calculation for ICP06, instrument ICP-AES*) para o cálculo total de fechamento da amostra. Descrições detalhadas dos métodos e dos pacotes ALS de análises utilizados podem ser consultados ou obtidos na *home page* da ALS (www.alsglobal.com).

Para análise dos elementos maiores procedeu-se com os recálculos dos valores obtidos para base anidra, em seguida a utilização dos diagramas de classificação usando-se os gráficos AFM (Irvine e Baragar, 1971) e TAS (Cox *et al.*, 1979). O índice de diferenciação escolhido, isto é, os óxidos e elementos considerados imóveis que mais variam na série ou suíte, foi o MgO e Zr. Para elaboração dos diagramas discriminantes das séries, foram utilizados os diagramas de ETR's normalizados ao Condrito (Boynton, 1984) e diagramas de multi-elementos (*spidergrams*) normalizados ao Manto Primitivo (McDonough e Sun, 1995). Para a identificação do ambiente tectônico da Suíte Rio Branco, foram utilizados diagramas discriminantes tectônicos aplicados

especificamente a rochas máficas. Os *trends* petrogenéticos obtidos foram comparados com os padrões pré-estabelecidos em cada diagrama utilizado, conforme a concepção original do autor. Foram também comparados com outros *trends* petrogenéticos obtidos em outras regiões, bem mais estudadas, e com assinaturas geoquímicas semelhantes, tanto aquelas relacionadas a ambientes tectônicos antigos, como também modernos do Fanerozoico (Pearce, 1982, 2008; Pearce *et al.*, 1984; Shervais, 1982; Wood, 1980; Cabanis e Lecolle, 1989; Dilek e Furnes, 2011; Saccani *et al.*, 2013, 2014; Dey *et al.*; 2018; Chen *et al.*, 2014; Xia e Li, 2019).

A finalidade do uso desses diagramas de elementos maiores e traços foi estabelecer os *trends* petrogenéticos das rochas metamáficas da Suíte Rio Branco e, dessa forma, estabelecer afinidades geoquímicas que possam ser correlacionadas com basaltos alcalinos ou subalcalinos/toleíticos, bem como, estabelecer *trends* petrogenéticos que possam indicar o ambiente tectônico em que as rochas foram geradas, tais como basaltos de dorsais meso-oceânicas (MORBs), basaltos de ilhas oceânicas (IOBs), basaltos de grandes províncias ígneas (LIPs, p. ex. basaltos de platôs oceânicos-OFBs, basaltos de platôs continentais-CFBs, basaltos de *rift* intracontinental IRBs) ou basaltos associados à subducção (toleitos de arco de ilhas-IAT, basaltos de bacias de *back-arc*, basaltos de margens continentais ativas). Os resultados das análises químicas, diagramas elaborados, discussões e interpretações dos dados encontram-se em detalhe no artigo constante no Capítulo 4.

1.5.4 Geocronologia U-Pb em zircão (LA-ICP-MS)

O método U-Pb através da técnica analítica de “ablação” a laser associada com um espectrômetro de massas com plasma indutivamente acoplado, conhecida pela sigla LA-ICP-MS, é indicado para todos os tipos de rochas (magmáticas félsicas ou máficas, metamórficas e sedimentares), inclusive as polideformadas. Consiste na análise pontual (*in situ*), tamanho do *spot* mínimo de cerca de 25 µm, direcionada para áreas específicas dos grãos ou cristais minerais de interesse, tais como zircão, monazita, rutilo, titanita, perovskita, badeleíta, xenotima, e outros minerais ricos em U e pobres em Pb. Neste método, a informação obtida se refere as idades de cristalização magmática, metamorfismo e migmatização, além de informações isotópicas da derivação mantélica e fontes.

Nesse estudo isotópico o procedimento adotado envolve, inicialmente, descrição detalhada de afloramentos e amostragem de materiais geológicos direcionadas para análise geocronológica U-Pb, levando-se em consideração a identificação do problema geológico a ser solucionado. Considera-se, também, as relações geológicas de campo e o mapa geológico existente, como orientativo para a escolha do material e local mais adequado para coleta das amostras, bem como para espacialização dos pontos coletados em relação a área de estudo. Portanto, coletou-se sete amostras de rocha do Domínio Rio Branco, obtendo-se em torno 8 kg de rocha metassedimentar ou

metafésica e 20 a 30 kg de rocha metamáfica, por amostra. As amostras foram preparadas nos laboratórios da CPRM-Serviço Geológico do Brasil em Porto Velho e Belém, conforme os procedimentos laboratoriais de preparação de amostras descritos por Castro *et al.* (2012). Para identificar estruturas internas do mineral de interesse (no caso, zircão), os *mounts* foram imageados por elétrons retroespalhados (BSE) no microscópio eletrônico de varredura (MEV) do laboratório do Centro de Geocronologia do Instituto de Geociências da Universidade de Brasília (Geocron-IG/UnB). Os dados isotópicos de zircão U-Pb (LA-ICP-MS) foram obtidos no mesmo laboratório e seguiram o procedimento analítico descrito por Böhn *et al.* (2009). Antes das análises no LA-ICP-MS, os *mounts* foram limpos por lavagem com HNO₃ diluído (2%). Uma vez totalmente secas, as amostras foram montadas junto com o zircão padrão GJ1 (Jackson *et al.*, 2004) em uma célula especialmente adaptada para ser utilizada dentro do New Wave UP213 Nd: YAG (213 nm) laser, que se encontra conectado ao Thermo Finnigan Neptune Multicoletor ICP-MS. O Hélio (He) foi utilizado como gás de arraste, que foi misturado com Argônio (Ar) antes de entrar no ICP-MS (Plasma por Acoplamento Indutivo com Espectrômetro de Massa). O laser foi operado a uma frequência de 10 Hz. Os isótopos de Pb 204 e 207 foram coletados com contadores de íons e ²³⁸U e ²⁰⁶Pb foram analisados em um copo de Faraday. O conteúdo de ²⁰²Hg foi monitorado em um contador de íons para correção da interferência isobárica entre ²⁰⁴Hg e ²⁰⁴Pb. Os sinais durante a “ablação” a laser foram obtidos em 40 ciclos de 1 segundo cada e para avaliação dos dados, apenas intervalos coerentes de resposta do sinal foram considerados. A redução dos dados foi realizada em planilha do Excel desenvolvida pelos técnicos da Geocron-IG/UnB, que considera valores em branco, composição dos padrões de zircão e propagação de erros. A intensidade do sinal de ²⁰⁴Pb foi calculada usando uma razão natural de ²⁰²Hg/²⁰⁴Hg de 4,346. A correção de Pb comum foi aplicada para grãos de zircão com ²⁰⁶Pb/²⁰⁴Pb menor que 1000, aplicando uma composição de chumbo comum seguindo o modelo de Stacey e Kramers (1975). A plotagem dos dados de U-Pb foi realizada por ISOPLOT v. 4.15 (Ludwig, 2003). Erros para razões isotópicas são apresentados no nível 1σ. Para o cálculo dos diagramas integrados por idade, foram considerados apenas grãos de zircão de concordância > 90% paraderivadas e cristais de zircão > 95% de concordância para rochas ortoderivadas, principalmente para os cálculos das idades mais precisas (idades concórdia).

O sistema U-Th-Pb em zircão (LA-ICP-MS) foi utilizado no estudo das rochas da parte sul do Cinturão Nova Brasilândia na obtenção das idades de cristalização magmática e de metamorfismo das rochas metaígneas máficas e félsicas da Suíte Rio Branco e idades máximas de sedimentação das rochas metassedimentares em alto-grau da Formação Rio Branco. A partir da obtenção das idades pico, concórdia e de intercepto superior, foi definida idades das rochas e, conseqüentemente, a definição dos intervalos dos episódios magmáticos, deformação, metamorfismo e de sedimentação durante as fases pré, sin e pós-orogênica da orogenia Nova

Brasilândia. Os resultados das novas análises geocronológicas U-Pb (LA-ICP-MS) em zircão, bem como discussões e interpretações, constam em detalhes nos artigos da tese apresentados nos capítulos 3 e 4.

1.5.5 Estudos isotópicos Sm-Nd e Sr-Sr em rocha total

O Samário (Sm) e o Neodímio (Nd) são elementos terras raras (ETR) que ocorrem em pequenas quantidades em diversas minerais constituintes de rocha, tais como silicatos, fosfatos e carbonatos, enquanto que o Estrôncio (Sr) é um metal alcalino-terroso (do grupo 2 ou IIA) da Classificação Periódica dos Elementos, abundante na natureza na forma de sulfatos e carbonatos, sendo encontrado em vários tipos de rocha. Esses elementos, em função de suas propriedades químicas e isotópicas, apresentam informações sobre a evolução da Terra e do sistema solar, podendo ser utilizados como ferramenta para solucionar problemas geológicos (Sato e Tassinari, 1997; Gioia e Pimentel, 2000; Gerald, 2010). O Sm e o Nd são elementos litófilos fortemente enriquecidos na crosta continental e na crosta oceânica da ordem de 10 a 100 vezes mais do que em relação aos reservatórios mantélicos (Hermann, 1970). Sm e Nd são elementos terras raras (ETR) com valência +3 e raios iônicos similares, portanto, apresentam comportamento geoquímico equivalentes (Wassenburg *et al.*, 1981). São elementos químicos considerados incompatíveis durante a cristalização magmática, sendo apenas aceitos nos sítios cristalográficos das fases residuais, por isso, são muito utilizados em estudos de processos ígneos responsáveis pelas variações composicionais dos diversos reservatórios terrestres.

Para o estudo isotópico Sm-Nd e determinação da razão Sr-Sr ($^{87}\text{Sr}/^{86}\text{Sr}$) utilizamos o método descrito por Gioia e Pimentel (2000). As análises foram realizadas no Laboratório de Geocronologia da Universidade de Brasília. Os procedimentos químicos de preparação das amostras para as análises isotópicas foram realizados em salas limpas equipadas com capelas de fluxo laminar, destiladores em quartzo e em PTFE (tipo 2 garrafas), colunas de troca iônica em PTFE e quartzo, *clean boxes*, chapas quentes, purificadores de água do tipo Nanopure e Milli-Q e micro-balanças analíticas. Os brancos de procedimento para Sr e Nd foram menores que 100 pg. No laboratório, pós de rocha total (aprox. 50 mg) foram misturados com uma solução de ^{149}Sm - ^{150}Nd e dissolvidos em cápsulas de Savillex. A extração de Sm, Nd e Sr de amostras de rocha total seguiu as técnicas convencionais de troca catiônica, utilizando colunas de Teflon contendo resina LN-Spec (HDEHP - ácido dietil-hexil fosfórico suportado em pó de PTFE). As amostras de Sm e Nd foram carregadas em filamentos de re-evaporação e em conjuntos de filamentos duplos. As medições isotópicas de Sr-Nd foram realizadas em espectrômetro de massas de multi-coletor Finnigan MAT-262, equipamento termo-iônico dotado de sete coletores tipo copo Faraday móveis e uma multiplicadora de elétrons central.

As incertezas para as proporções Sm/Nd e $^{143}\text{Nd}/^{144}\text{Nd}$ são melhores que + 0,5% (2σ) e + 0,005% (2σ), respectivamente, com base em análises repetidas dos padrões internacionais de rocha BHVO-1 e BCR-1. As razões $^{143}\text{Nd}/^{144}\text{Nd}$ foram normalizadas para $^{146}\text{Nd}/^{144}\text{Nd}$ de 0,7219 e a constante de decaimento utilizada foi $6,54 \times 10^{-12} \text{ a}^{-1}$. Os valores de TDM foram calculados usando o modelo de De Paolo (1981). O cálculo das idades modelo TDM foram realizadas mediante o uso do *software* ISOPLOT 4.15 (Ludwig, 2008). Os resultados das análises constam em tabelas inseridas no artigo constante no capítulo 4 dessa tese, com suas respectivas interpretações geológicas.

Na metodologia Sm-Nd, o estudo se baseia no decaimento radioativo do ^{147}Sm para ^{143}Nd em taxa muito baixa, com meia-vida do ^{147}Sm próximo de 106 Ga, sendo equivalente a 23 vezes a idade da Terra (Anders e Ebihara, 1982). O método Sm-Nd foi aplicado no estudo de idades modelo de manto empobrecido (TDM) e de fonte (parâmetros petrogenéticos), a partir da análise das razões iniciais $^{143}\text{Nd}/^{144}\text{Nd}$ como indicadores da origem crustal ou mantélica das rochas metamáficas da Suíte Rio Branco, mediante o uso do parâmetro ϵNd (epsilon Nd) comparando as diferentes razões das rochas analisadas. Neste caso, utilizamos a notação matemática $\epsilon\text{Nd} = \{ [(^{143}\text{Nd}/^{144}\text{Nd})^0 / (^{143}\text{Nd}/^{144}\text{Nd})_{\text{CHUR}}] - 1 \} \times 10^4$, sendo $(^{143}\text{Nd}/^{144}\text{Nd})_{\text{CHUR}}$ correspondente ao valor da razão $^{143}\text{Nd}/^{144}\text{Nd}$ em meteoritos condríticos para a idade considerada e CHUR (reservatório condrítico uniforme). Neste caso, assumindo que a Terra foi formada por materiais semelhantes aos dos meteoritos condríticos, valores de ϵNd próximos de 0 (zero) teriam sido derivados de manto primitivo, entretanto, como a crosta continental se desenvolveu a partir do manto, por processos de cristalização, fusão, retrabalhamento e diferenciação, e o Nd é mais incompatível que o Sm, por ter raio iônico um pouco maior, com o decorrer do tempo o manto adquire razões Sm/Nd maiores que o CHUR, sendo este chamado de manto empobrecido, devido à perda de elementos litófilos, implicando em valores de ϵNd positivos (+), comuns em rochas derivadas de manto empobrecido (fonte mantélica). Por outro lado, rochas com ϵNd com valores negativos (-), razões Sm/Nd menores que o CHUR, são ditas crustais (fontes crustais), oriundas de magmas formados por fusão parcial na crosta continental.

As idades modelos T_{DM} (DM=Manto Empobrecido) das rochas metamáficas da Formação Rio Branco foram utilizadas associadas às idades “t” oriundas das idades de cristalização U-Pb obitadas, com o objetivo de definir rochas ou protólitos derivados do manto (idades TDM próximas das idades U-Pb cristalização), definindo se são rochas juvenis, e associá-las a eventos de formação crustal. Alternativamente, se são rochas de fontes crustais ou de fontes mistas, em que as idades modelo são um pouco mais antigas do que as idades de cristalização U-Pb (t), podendo em alguns casos não ter a componente juvenil ou em outros sugerir superposição de eventos magmáticos envolvendo fusão parcial.

Estrôncio (Sr) é um metal alcalino terroso pertencente ao Grupo 2 da Tabela Periódica. Possui número atômico 38, portanto, forma cátions com valência $+2$ e menos móveis do que os metais alcalinos (Faure e Powell, 1972; Faure, 1986). O que regula a ocorrência de Sr na natureza é a intensidade com a qual acontece a substituição de Ca por Sr. Portanto, Sr^{+2} (raio iônico de 1.13 Å) pode substituir Ca^{+2} (raio iônico de 0.99 Å) em diversos minerais, tais como apatita, calcita, clinopiroxênio, plagioclásio e titanita, sendo que a quantidade de Sr nos minerais vai ocorrer em função da coordenação de sítios (8 ou 6). Eventualmente, Sr^{+2} pode ser capturado pela estrutura de feldspatos potássicos no lugar do K^+ , devido à razão carga/raio, ou também, pode formar seus próprios minerais, tais como celestita (SrSO_4) e estroncianita (SrCO_3). O Sr tem quatro isótopos naturais, ^{84}Sr , ^{86}Sr , ^{87}Sr e ^{88}Sr , todos estáveis. Contudo, a composição isotópica do Sr é bastante variável e dependente da razão Rb/Sr, visto que ^{87}Sr é produzido a partir do decaimento radioativo de ^{87}Rb (constante de decaimento de $^{87}\text{Rb} = 1,42 \times 10^{-11} \text{ y}^{-1}$). O valor de $^{87}\text{Sr}/^{86}\text{Sr}$ do magma a partir do qual uma rocha ou mineral se cristalizaram depende não apenas do decaimento de ^{87}Rb para ^{87}Sr , mas também da razão Rb/Sr do sistema, que irá variar de acordo com o comportamento geoquímico destes elementos (Faure e Powell, 1972; Faure, 1986; Oliveira, 2015). Atualmente, considera-se que os isótopos de Sr, bem como de outros elementos pesados (p.ex., Nd), não são fracionados durante os processos de fusão parcial em equilíbrio ou cristalização fracionada. Desta maneira, considera-se que a composição isotópica do magma e das rochas cristalizadas a partir dele é igual à composição isotópica da área fonte. Logo, é possível utilizar a razão inicial das rochas ou minerais para identificar a origem dos diversos tipos de magma (Faure e Powell, 1972; Faure, 1986; Allègre e Othman, 2008).

1.6 Estrutura organizacional da Tese

Esta tese de doutorado está estruturada em cinco capítulos (introdução, contexto geológico regional, artigo científico 1, artigo científico 2 e discussões e conclusões) e direcionada para apresentação na forma de artigos destinados à publicação em periódicos científicos internacionais e especializados na linha de pesquisa que foi desenvolvida. Os dois artigos abordam principalmente aspectos relacionados a geologia, geocronologia U-Pb em zircão (LA-ICP-MS), geoquímica (rocha total) e estudos de isótopos de Sr-Nd (rocha total), conforme os objetivos estabelecidos visando responder questões relacionadas à geologia e evolução tectônica da região. O detalhamento de cada tópico proposto com as respectivas metodologias utilizadas, resultados obtidos e interpretações, encontram-se presentes de forma detalhada nos artigos e de forma sucinta no volume da tese.

2. Contexto geológico regional

2.1 Sudoeste do Cráton Amazônico em Rondônia

O Cráton Amazônico, uma das principais entidades geotectônicas pré-cambrianas da América do Sul, encontra-se exposto predominantemente em território brasileiro, mas estende-se para Guiana, Suriname, Venezuela, Colômbia e Bolívia. Corresponde a uma das maiores áreas cratônicas do mundo e com extensão de aproximadamente 5.600.000 km², sendo que em território brasileiro sua área é de aproximadamente 4.400.000 km². O Cráton Amazônico é limitado tectonicamente a leste pelo Cinturão Araguaia e a sul e sudeste pelo Cinturão Paraguai. Grande parte do Cráton Amazônico é coberto por sedimentos fanerozoicos, sendo a leste os da Bacia do Parnaíba, a sul das bacias do Xingu e Alto Tapajós, a sudoeste da Bacia dos Parecis, a oeste da Bacia do Solimões, a norte da Bacia do Tacutu e na porção central do cráton por sedimentos da Bacia do Amazonas. O Cráton Amazônico se estende sob os depósitos cenozoicos até a Pré-Cordilheira Andina, devido à presença de rochas com idades mesoproterozoicas na porção mais oriental do Cinturão Andino (Cordani *et al.*, 2000; Kroonenberg, 1982; Priem *et al.*, 1989).

O Cráton Amazônico foi inicialmente subdividido em dois escudos denominados de Escudo Brasil Central, a sul, e Escudo das Guianas, a norte, separados pelas extensas áreas sedimentares depositadas sobre a sinéclise do Amazonas. Amaral (1974) subdividiu o cráton em três províncias geocronológicas: Amazônia Oriental, Amazônia Central e Amazônia Ocidental. A partir do modelo proposto por Amaral (1974), diversos modelos evolutivos foram propostos com o intuito de aperfeiçoar e adaptar os modelos anteriormente propostos, todos fundamentados em dados geocronológicos (p. ex. Cordani *et al.*, 1979; Teixeira *et al.*, 1989). Hasui *et al.* (1984) e Costa e Hasui (1997) propuseram modelos alternativos com base em dados geofísicos e estruturas geológicas, definindo doze blocos ou placas de idades arqueanas a proterozoicas, separados por cinturões móveis, nos quais o processo tectônico gerador predominante envolveu a colisão de massas crustais, com posteriores reativações dos cinturões móveis durante eventos tectônicos mais jovens.

Cordani *et al.* (1979) propuseram modificações na nomenclatura das províncias geocronológicas mediante a introdução da Província Rondoniana. A Província Amazônia Central passou a ser denominada Província Maroni-Itacaiúnas (2,1 Ga a 1,8 Ga); a Província Amazônia Ocidental (>2,1 Ga) teve sua nomenclatura mantida; a Província Amazônia Ocidental foi subdividida nas províncias Rio Negro-Juruena (1,7 Ga a 1,45 Ga) e Rondoniana (1,4 Ga a 1,1 Ga). Teixeira *et al.* (1989) introduziram modificações no modelo de Cordani *et al.* (1979), com base em um vasto acervo de idades Rb-Sr e K-Ar, propondo apenas a caracterização da Província Amazônia

Central como uma província, propriamente dita, e as demais como faixas móveis. Teixeira *et al.* (1989) propuseram o desmembramento de parte da Província Maroni-Itacaiúnas e o agregaram à Província Amazônia Central.

Tassinari e Macambira (1999) com base em novos dados geocronológicos, em especial Sm-Nd, propuseram para a região sudoeste do Cráton Amazônico a subdivisão das províncias Rio Negro-Juruena (1,80-1,55 Ga), Rondoniana-San Ignácio (1,45-1,30 Ga) e Sunsás (1,25-1,00 Ga) (Fig. 3). Santos *et al.* (1999, 2000) e Santos (2004) reinterpretaram a configuração das províncias geocronológicas, com base em dados U-Pb e Sm-Nd, e individualizaram as províncias Rio Negro e Rondônia-Juruena, anteriormente definidas como uma única província denominada de Rio Negro-Juruena e também estenderam os limites da Província Sunsás mais para leste, avançando sobre o território brasileiro, englobando a Província Rondoniana-San Ignácio na Província Sunsás (1,25-1,00 Ga) (Fig. 3).

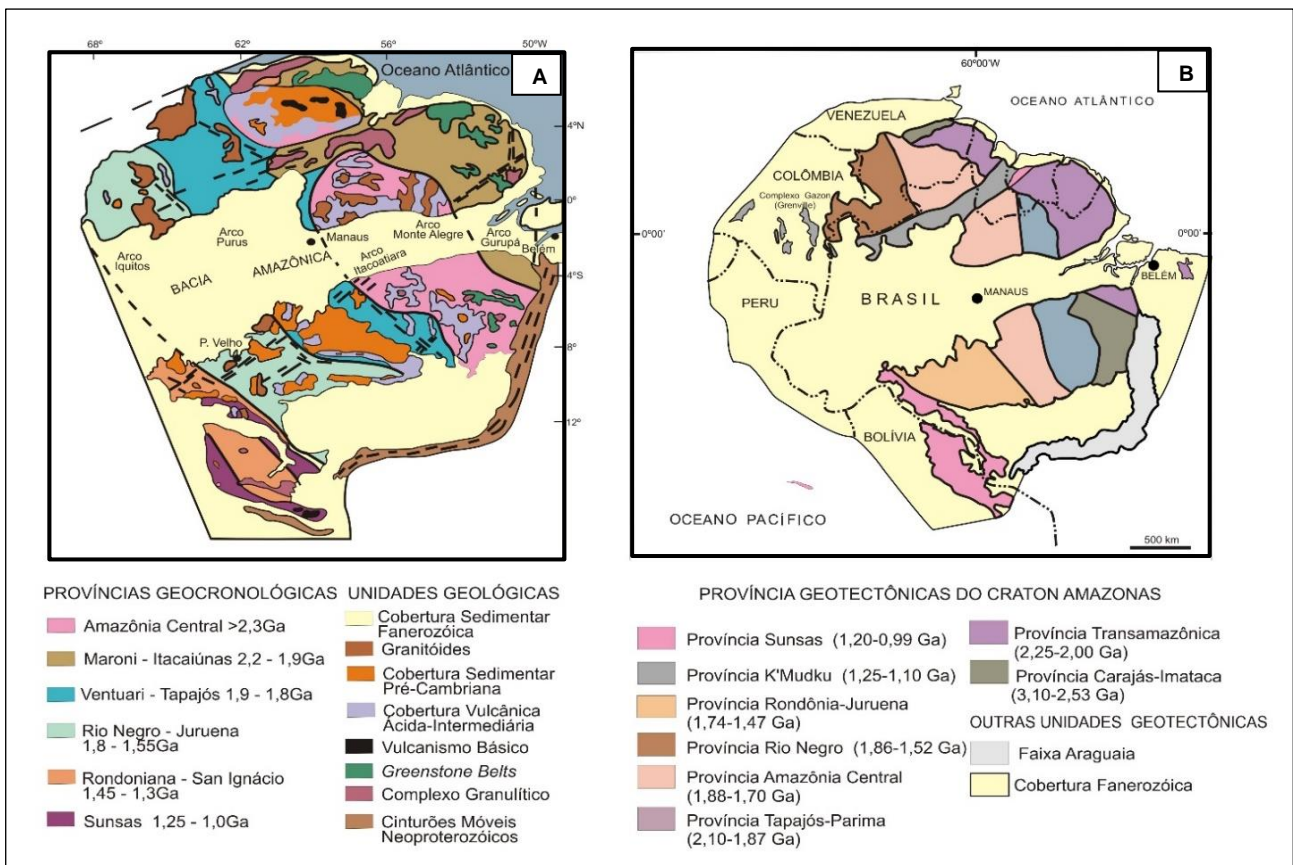


Fig. 3. Províncias geocronológicas do Cráton Amazônico, segundo Tassinari e Macambira (1999) em (A) e Santos *et al.* (2003) em (B).

A estruturação do setor sudoeste do Cráton Amazônico e adjacências também foi considerada em diversos trabalhos de síntese e de revisão regional (Pinto Filho *et al.*, 1977; Litherland e Bloomfield, 1981; Litherland *et al.*, 1986; Casquet *et al.*, 2006, 2008; Scandolara *et al.*, 1999; Loewy *et al.*, 2003, 2004) e em trabalhos específicos (Rizzotto, 1999; Rizzotto *et al.*, 1999; Rizzotto *et al.*, 2001; Rizzotto *et al.*, 2002; Ruiz, 2005; Ruiz *et al.*, 2007; Scandolara, 2006; Teixeira *et al.*, 2010), todos com ênfase na litoestratigráfica e evolução crustal. Outros trabalhos regionais discutiram a importância das rochas mesoproterozoicas da América do Sul na formação do supercontinente Rodinia e relacionaram parte delas à evolução tectônica do orógeno Sunsás, como produto da colisão entre o Cráton Amazônico e a borda leste e sudeste da Laurentia (Sadowski e Bettencourt, 1996; Geraldés *et al.*, 2001; Kroner e Cordani, 2003, Tohver *et al.*, 2002; Santos *et al.*, 2002; Tohver *et al.*, 2005a; Tohver *et al.*, 2005b; Li *et al.*, 2008; Bettencourt *et al.*, 2010; Rizzotto *et al.*, 2013; Rizzotto *et al.*, 2014; Cawood e Pisarevsky, 2017). Destes trabalhos citados, o arcabouço estrutural proposto por Tohver *et al.* (2005b) sugere a existência de uma zona de sutura oculta (*cryptic suture zone*) ao longo da qual se desenvolveu o Cinturão Nova Brasilândia, estando este relacionado a colisão do Cráton Amazônico com a Laurentia em aproximadamente 1,2-1,0 Ga. Alternativamente, Scandolara (2006) apresentou proposta de compartimentação tectonoestratigráfica para o sudoeste do Cráton Amazônico, em Rondônia, baseada na subdivisão terrenos, definidos descritivamente como entidades geológicas de extensão regional com características petrológicas, estruturais, geoquímicas, geofísicas e geocronológicas próprias, limitados por sistemas de falhas ou zonas de cisalhamento de grande expressão regional. Neste contexto individualizaram o Terreno Jamari, Terreno Roosevelt e o Terreno Nova Brasilândia.

Adotando-se as subdivisões de Províncias Geocronológicas de Tassinari e Macambira (1999), a região sudoeste do Cráton Amazônico em Rondônia abrange parte das províncias Rio Negro-Juruena, Rondoniana-San Ignácio e Sunsás, descritas nas seções 2.1.1, 2.1.2 e 2.1.3. A área de pesquisa deste doutorado ocupa parte da Província Sunsás (Fig. 3).

2.1.1 Província Rio Negro-Juruena

Na proposta de Tassinari e Macambira (1999), a Província Rio Negro-Juruena (1,80-1,55 Ga) estende-se desde o extremo oeste de Rondônia até a bacia hidrográfica do alto curso do rio Teles Pires, no Mato Grosso, a leste. A parte abrangida pelos estados de Rondônia e noroeste de Mato Grosso foi subdividida em dois terrenos, denominados de Roosevelt e Jamari (Scandolara, 2006).

O Terreno Roosevelt, também conhecido como Terreno Roosevelt-Juruena (Scandolara, 2006; Quadros *et al.*, 2011), abrange o extremo-nordeste do estado de Rondônia e o noroeste do estado de Mato Grosso e é constituído nestas regiões pelas unidades Suíte Intrusiva São Romão e Grupo Roosevelt. A Suíte Intrusiva São Romão (aproximadamente 1770 Ma) reúne vários corpos

de granitos metaluminosos a peraluminosos, cálcio-alcálicos de alto potássio, tardi- a pós-colisionais, representados por monzogranitos finos, subordinadamente magnetita microgranitos e granodioritos, com variáveis intensidades de deformação e metamorfismo. O Grupo Roosevelt (aproximadamente 1740 Ma) que é composto por rochas metavulcanossedimentares compreendendo dacitos e riolitos com intercalações de basaltos e tufos, ignimbritos e conglomerados vulcanoclásticos subordinados, sotopostos por meta-argilitos e metassiltitos interdigitados com *metacherts*, formações ferríferas e metatufos (Santos *et al.*, 2000; Lacerda Filho *et al.*, 2004; Quadros e Rizzotto, 2007).

O Terreno Jamari ocupa a porção centro-ocidental do Estado de Rondônia, sendo constituído, predominantemente, por rochas ortoderivadas e, subordinadamente, paraderivadas em alto grau metamórfico, rochas metavulcanossedimentares e metassedimentares em médio a baixo grau metamórfico, localmente na fácies xisto-verde, além de diversos metagranitos foliados a gnaissificados. No contexto do embasamento ortoderivado do Terreno Jamari, ocorre o Complexo Jamari (aproximadamente 1750 a 1730 Ma), denominação dada por Isotta *et al.*, (1978), composto por ortognaisses tonalíticos, enderbíticos e quartzo dioríticos, com intercalações subordinadas de lentes de gnaisses calciossilicáticos e anfibolitos, exibindo intensidades variáveis de migmatização e milonitização, em geral metamorfizados em condições P e T condizentes com a fácies anfibolito superior a granulito. As idades U-Pb do Complexo Jamari foram obtidas em ortognaisses tonalíticos, quartzo dioríticos e enderbíticos em 1750 ± 24 Ma, 1761 ± 3 Ma (MSWD = 0.43) e 1730 ± 22 Ma, respectivamente (Payolla *et al.*, 2002; Santos *et al.*, 2002; Scandolara, 2006). A deformação e o metamorfismo superimpostos em todas as rochas desse complexo são destacados por sobrecrescimentos de cristais de zircão, os quais forneceram idades de recristalização em torno de 1,33 Ga (Santos *et al.*, 2003; Scandolara, 2006). As paraderivadas em alto grau aflorantes no Terreno Jamari, nas porções central e norte-nordeste de Rondônia, foram englobadas posteriormente no Complexo Quatro Cachoeiras, designação dada por Rizzotto *et al.* (2004), constituído por alternâncias de gnaisses paraderivados de alto grau, extensão e espessura variáveis, aflorantes na região a norte de Jaru e Ouro Preto do Oeste, ao longo do igarapé Quatro Cachoeiras, e entre os municípios de Vale do Anari e Machadinho d'Oeste. Essa unidade litoestratigráfica é constituída por biotita-cordierita-granada gnaisses, gnaisses calciossilicáticos, sillimanita-granada gnaisses, biotita-quartzo gnaisses e gnaisses quartzo-feldspáticos finos, todos com intensidade variável de deformação e migmatização. As paragêneses dessa unidade são compatíveis com metamorfismo de alto grau, na transição da fácies anfibolito superior para a fácies granulito. Payolla *et al.* (2002) atribuiu a idade 1660 Ma como a máxima sedimentação dos protólitos sedimentares do Complexo Quatro Cachoeiras obtida em amostra de paragnaisse em alto grau da região de Machadinho d'Oeste.

Rochas metavulcanossedimentares de baixo grau ocorrem na parte noroeste do Terreno Jamari, sendo representada principalmente pela Formação Mutum-Paraná (Lobato *et al.*, 1966), constituída por uma unidade inferior de filitos, ardósias, meta-argilitos, meta-arenitos arcoseanos, quartzitos, metacherts e metatufos cinza e uma unidade superior de quartzo meta-arenitos e metassiltitos, depositados em ambiente marinho raso, epicontinental, com restritos episódios de sedimentação continental e vulcanismo. Uma amostra de metatufo félsico da base da sequência foi datada pelo método U-Pb (SHRIMP) e apresentou várias populações de grãos de zircão herdado e de idades arqueana até paleoproterozoica. A população principal apresentou idade concordante de 1731 ± 17 Ma, interpretada como a de cristalização do tufo (Santos *et al.*, 2001).

Na região da serra da Providência, parte leste do Terreno Jamari, ocorre a Formação Igarapé Lourdes composta por associação de rochas metavulcanossedimentares de baixo grau e idade atribuída inicialmente ao Paleoproterozoico, apenas com base em suas relações estratigráficas com as unidades espacialmente associadas (Quadros e Rizzotto, 2007). Nessa região, as rochas da Formação Igarapé Lourdes estão representadas por meta-arenitos e metaconglomerados, na base, e por metassiltitos, metapelitos manganésífero e metassiltitos avermelhados, no topo. Na região de Presidente Médici, ocorrem intercalações de meta-arenitos, metassiltitos, clorita xistos, quartzitos, metatufos, metavulcânicas ácida e formações ferrífera de origem hidrotermal. Essas rochas estão, em geral, metamorfizadas na fácies xisto-verde. Dados geocronológicos U-Pb, em amostra de xisto, apresentados por Quadros *et al.* (2011) revelaram idade de 1367 Ma, considerada como a máxima sedimentação dos protólitos sedimentares da Formação Igarapé Quinze, posicionando-a no Mesoproterozoico.

Nas regiões centro-leste, nordeste, noroeste e central do Terreno Jamari ocorre a Suíte Intrusiva Serra da Providência, constituída por monzogranitos porfiríticos (piterlitos e viborgitos), sienogranitos, charnockitos, mangeritos e gabros, intrusivos no embasamento do Terreno Jamari (Tassinari, 1984; Scandola, 2006; Quadros e Rizzotto, 2007). Trata-se de uma suíte subalcalina, metaluminosa a fracamente peraluminosa e intraplaca do tipo A, que se estende desde o noroeste de Mato Grosso, sul do Amazonas, porção centro-norte de Rondônia, chegando até próximo ao limite estadual com o Acre. Suas rochas variam de isotrópicas a deformadas, sendo que os tipos deformados mostram ampla variação estrutural e textural, desde fracamente foliados até protomilonitos e milonitos, até tipos bandados. Os protomilonitos são mais frequentes na borda oeste do batólito Serra da Providência e em largas zonas da associação charnockito-granito entre as cidades de Ouro Preto do Oeste e Ji-Paraná. As partes mais deformadas e gnaissificadas são observadas no maciço Rio Crespo, região de Ariquemes e adjacências. A Suíte Serra da Providência engloba diversos episódios magmáticos que ocorreram por um período de tempo superior a 80 Ma e seu pulso mais antigo está representado por biotita sienogranito porfirítico de idade U-Pb de 1606

± 24 Ma, seguida por hornblenda-biotita monzogranito de idade U-Pb de 1573 ± 15 Ma (Bettencourt *et al.*, 1999). Uma amostra de piterlito e outra de viborgito forneceram idades idênticas de 1566 ± 5 Ma e 1566 ± 3 Ma, respectivamente. Uma fácies de biotita-sienogranito pórfiro forneceu idade de 1554 ± 47 Ma. A fase final do magmatismo, representada pelo quartzo sienito do Maciço União, forneceu idade de 1532 ± 5 Ma (Bettencourt *et al.*, 1999). A deformação e o metamorfismo das rochas da Suíte Serra da Providência ocorreram em condições de médio a alto-grau com ápice, principalmente, em aproximadamente 1,33 Ga, associada à Orogenia Rondoniana-San Ignácio (Quadros e Rizzotto, 2007; Santos *et al.*, 2002, 2008; Scandolara, 2006; Scandolara *et al.*, 1999; Silva *et al.*, 2002; Bettencourt *et al.*, 2010; Quadros *et al.*, 2011).

2.1.2 Província Rondoniana-San Ignácio

A Província Rondoniana-San Ignácio (1,47-1,33 Ga) abrange a porção sudoeste do Cráton Amazônico e encontra-se representada em Rondônia, principalmente pelo Cinturão Alto Guaporé (1,47-1,31 Ga) que aflora na região de Colorado d'Oeste e Corumbiara, estendendo-se em direção à região de Nova Mamoré, no noroeste de Rondônia. No Terreno Jamari o reflexo dessa tectônica promoveu o retrabalhamento da crosta mais antiga na região de Ariquemes, Jaru e Ouro Preto do Oeste, em Rondônia (Scandolara, 2006; Quadros e Rizzotto, 2007; Bettencourt *et al.*, 2010; Rizzotto *et al.*, 2013).

O Cinturão Alto Guaporé consiste em segmento crustal NW-SE com rochas de ortoderivação e paraderivação, representado por sequências metavulcanossedimentares em alto grau metamórfico, rochas metamáficas e metaultramáficas, além de diversas gerações de granitos sin-, tardi- e pós-orogênicos, formado a partir da colisão do Bloco Paraguá com o proto-Cráton Amazônico durante a Orogenia Rondoniana-San Ignácio (Rizzotto *et al.*, 2013). Inclui-se no Cinturão Alto Guaporé o Complexo Nova Mamoré (definido por Rizzotto *et al.*, 2005a, 2005b), constituído por gnaisses polideformados e migmatizados expostos na região oeste-noroeste de Rondônia, entre as cidades de Guajará-Mirim, Nova Mamoré e Nova Califórnia, compreendendo rochas paraderivadas representadas por gnaisses quartzo-feldspáticos, granada-biotita-quartzo gnaisses, granofels quartzo-feldspáticos, gnaisses calciossilicáticos bandados e silimanita-granada-biotita-quartzo xistos. Essas rochas se encontram em grau metamórfico de fácies anfíbolito superior (zona da silimanita). Zonas de fusão parcial são comuns e não raro com geração de migmatitos com neossoma em forma lentes e bolsões pegmatóides, compostos por k-feldspato, quartzo e biotita e alongados segundo a estruturação regional. No limite norte-noroeste do Cinturão Alto Guaporé em Rondônia aflora o Complexo São Felipe, com área de ocorrência distribuída ao longo de uma faixa que se estende desde as imediações da cidade de São Felipe, a oeste, até o rio Pimenta Bueno, a leste (Quadros *et al.*, 2007). Em geral, as rochas desse complexo ocorrem como corpos alongados e

imbricados segundo a direção da foliação regional WNW-ESSE. As principais rochas são augen-gnaisses de composição granodiorítica a monzogranítica, paragneisses e ortogneisses monzograníticos com graus variados de migmatização.

Na região sudeste de Rondônia, o Cinturão Alto Guaporé é composto pelo Complexo Colorado (Rizzotto *et al.*, 2013) que foi inicialmente subdividido nas unidades metapelítica, metapsamítica e ferromanganesífera. O referido complexo tem ampla distribuição na região de Colorado do Oeste e Corumbiara, onde ocorre como faixa descontínua e alongada segundo a direção NNW-SSE, com cerca de 130 km de comprimento e 30 km de largura. É constituído por rochas supracrustais clastoquímicas compostas por plagioclásio-biotita-quartzo paragneisses bandados e parcialmente migmatizados, granada-silimanita paragneisses migmatíticos, xistos heterogêneos, biotita-gnaisses, formações ferríferas bandadas, gnaisses calciossilicáticos, metamargas, talco xistos, além de xistos grafitosos e anfíbolitos subordinados (Quadros e Rizzotto, 2007; Rizzotto e Hartmann, 2012; Rizzotto *et al.*, 2013). Nesta mesma região encontra-se o Complexo Trincheira (~1.47 Ga), designação dada inicialmente por Romanini (2000), que representa parte de uma sequência ofiolítica marcadora de uma zona de sutura na região (Sutura Guaporé), constituído predominantemente por anfíbolitos e gnaisses anfíbolíticos, com frequentes intercalações de gnaisses paraderivados, paranfíbolitos, formações ferríferas bandadas, metabasaltos e xistos. Metagabros, metagabronoritos e leucometagabros com texturas e estruturas ígneas reliquias também são comuns. Tremolitos, actinolita xistos e intercalações de gnaisses calciossilicáticos são litologias subordinadas (Rizzotto e Hartmann, 2012; Rizzotto *et al.*, 2013).

O magmatismo granítico Mesoproterozoico (Ectasiano) na Província Rondoniana-San Ignácio corresponde a uma série de corpos e maciços graníticos isotrópicos a foliados, de natureza sin-, tardi- a pós-colisional com idades de cristalização no intervalo entre 1387 Ma e 1309 Ma. Esses corpos são englobados nas suítes intrusivas Santo Antônio (monzogranitos, quartzo monzonitos, diques pegmatíticos e aplíticos, rochas híbridas e diques de diabásio), Teotônio (microclínio granitos, microclínio-quartzo sienitos e sienogranitos), Igarapé Enganado (sienogranitos, monzogranitos, granodioritos e raros tonalitos), Cerejeiras (granada-biotita monzogranitos, biotita sienogranitos e raros granodioritos), Alto Escondido (biotita sienogranitos e biotita monzogranitos), Alto Candeias (hornblenda-biotita monzogranitos, biotita monzogranitos, charnockitos e quartzo monzonitos) e São Lourenço-Caripunas (monzogranitos, sienogranitos, granitos pórfiros subvulcânicos, aplitos e quartzo sienitos, com mineralização de cassiterita e wolframita em *greisen* e em veios de quartzo), além da Suíte Laje (granitos tipo S leucocráticos com biotita e granada) (Rizzotto *et al.*, 2005a, 2005b; Scandola, 2006; Quadros e Rizzotto, 2007; Bettencourt *et al.*, 2010).

2.1.3 Província Sunsás

A Província Sunsás (1,25-0,95 Ga), também conhecida como Província Sunsás-Aguapeí, ocorre no extremo-sudoeste do Cráton Amazônico em Rondônia, Mato Grosso e Bolívia e tem sido cronologicamente correlacionada à Província Grenville na Laurentia, principalmente em relação as idades dos eventos orogênicos reconhecidos (Fig. 4). O termo Sunsás foi originalmente utilizado para denominar um cinturão orogênico de *trend* NW, na Bolívia, de idade em torno de 1000 Ma (Litherland *et al.*, 1989), conhecido como Cinturão Sunsás. Posteriormente, esse cinturão foi correlacionado com o Cinturão Aguapeí, no Brasil, passando a constituir uma única unidade geotectônica (Tassinari *et al.*, 1996). Estudos isotópicos, geoquímicos e de geologia estrutural em áreas-chaves da Província Sunsás (cinturões Nova Brasilândia, Sunsás e Aguapeí, além de áreas de cráton retrabalhado), no Brasil e na Bolívia, tem proporcionado avanços significativos na reconstituição do arcabouço dessa província e nas discussões sobre a evolução do orógeno Sunsás (Geraldés *et al.*, 2001; Rizzotto *et al.*, 2013; Santos *et al.*, 2003, 2008; Tassinari e Macambira, 1999, 2004; Tohver *et al.*, 2006; Boger *et al.*, 2005; Ruiz, 2005; Teixeira *et al.*, 1996, 2006, 2010; Vargas-Mattos, 2006; Cordani e Teixeira, 2007; Elming *et al.*, 2009).

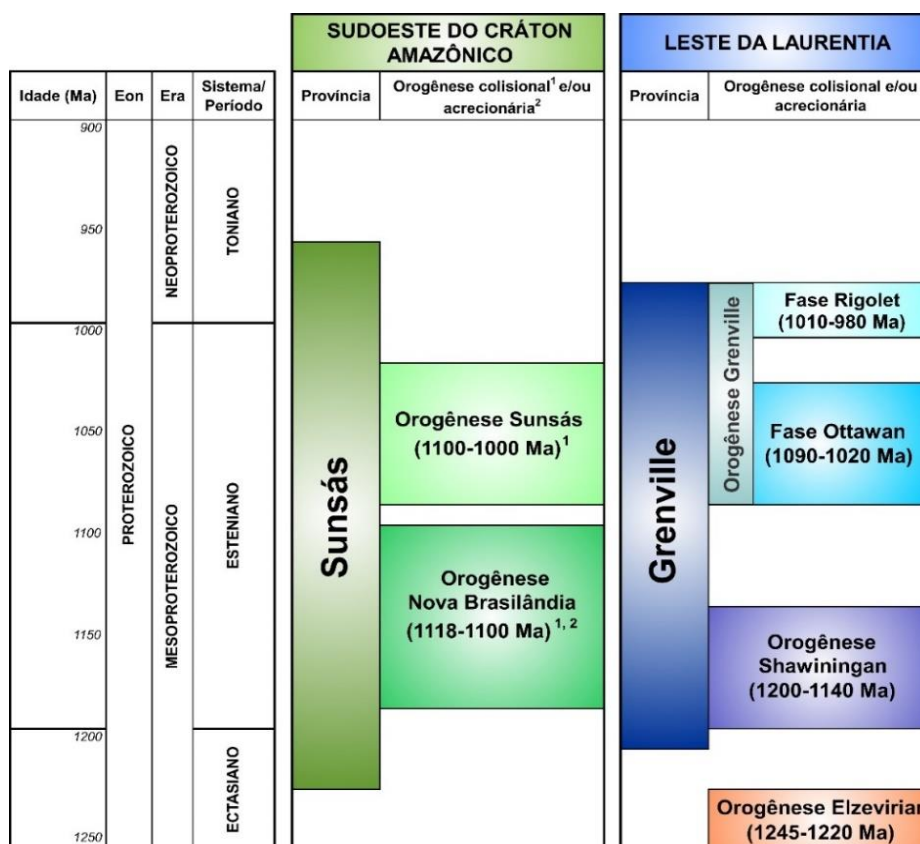


Fig. 4. Quadro comparativo entre a cronologia dos eventos orogênicos mesoproterozoicos (Esteniano-Toniano) registrados nas províncias Sunsás e Grenville (adaptado de Rizzotto, 1999; Rivers, 2008; Teixeira *et al.*, 2010; McLelland *et al.*, 2010).

No sudoeste do Cráton Amazônico, em Rondônia, consideramos que a Província Sunsás se encontra representada pelo Cinturão Nova Brasilândia e pelo Sistema Transpressivo Sinistral Ji-Paraná – Cujubim (STSJC) (Figs. 1, 5, 6). O Cinturão Nova Brasilândia constitui unidade geotectônica alongada na direção E-W a NW-SE, medindo 170 km de comprimento por 40 km de largura, aflorante em meio a sedimentos neoproterozoicos e fanerozoicos. Encontra-se limitado a norte pelo *Graben* Pimenta Bueno, a sul pelo complexo São Felipe, a leste pela Bacia dos Parecis e a oeste por coberturas sedimentares cenozoicas. Fortes anomalias magnéticas indicam que o Cinturão Nova Brasilândia se estende para leste e para sudoeste, além dos seus limites aflorantes (Figs. 5A, 5B). Sugere ainda a existência de estrutura tectônica E-W de escala regional, possivelmente marcadora de limites de blocos crustais. Essas anomalias magnéticas encontram-se bem evidenciadas na parte sul do cinturão, apresentando *trend* magnético regional E-W impresso nas rochas metassedimentares em alto-grau da Formação Rio Branco (gnaisses cálcio-silicáticos, biotita paragneisses e granulitos) (Figs. 5A, 6). Parte das anomalias magnéticas são geradas por corpos ígneos máficos e por diques máficos, enquanto que baixos magnéticos são evidenciados por materiais geológicos diversos, de origem sedimentar (rochas metassedimentares da Formação Migrantinópolis e sedimentos do Fanerozoico) e magmática félsica (granitos) (Fig. 5A). A interpretação qualitativa dos dados magnéticos revelou feições lineares magnéticas que podem representar estruturas geológicas que contornam corpos ígneos máficos, permitindo a identificação de domínios magnéticos distintos (Fig. 5B). A aerogamaespectrometria, principalmente o mapa de composição ternária RGB (K, eTh, eU), foi utilizada como ferramenta auxiliar na individualização das unidades geológicas e na delimitação mais precisa dos traçados dos contatos geológicos. Foi possível ainda estabelecer correlação entre as informações geológicas de campo e a resposta radiométrica apresentada no mapa de composição ternária, permitindo detalhar a cartografia geológica na área estudada (Fig. 5C).

O Cinturão Nova Brasilândia é constituído por rochas metavulcanossedimentares em médio a alto grau que fazem parte do Grupo Nova Brasilândia, composto de uma unidade dominante de metaturbiditos terrígeno-carbonáticos (Formação Migrantinópolis) e uma unidade máfico-félsica bimodal com intercalações de paragneisses (Formação Rio Branco), conforme definição inicial dada por Rizzotto (1999) (Fig. 6). Além destas, ocorre no extremo noroeste do cinturão a Formação Terra Boa composta por intercalações de meta-arenitos e metassiltitos metamorfizados em baixo-grau (Quadros e Rizzotto, 2007). A fase magmática tardi- a pós-orogênica encontra-se representada pelos granitos das suítes Rio Branco e Rio Pardo e anorogênica pelas rochas das suítes Novo Mundo (máfica) e Costa Marques (félsica). O modelo de evolução do Cinturão Nova Brasilândia proposto inicialmente envolve a abertura e fechamento de *rift* intracontinental, margem passiva e formação

de proto-oceano, desenvolvido em dois ciclos entre 1250 e 1110 Ma (Rizzotto, 1999; Tohver *et al.*, 2004, 2005a).

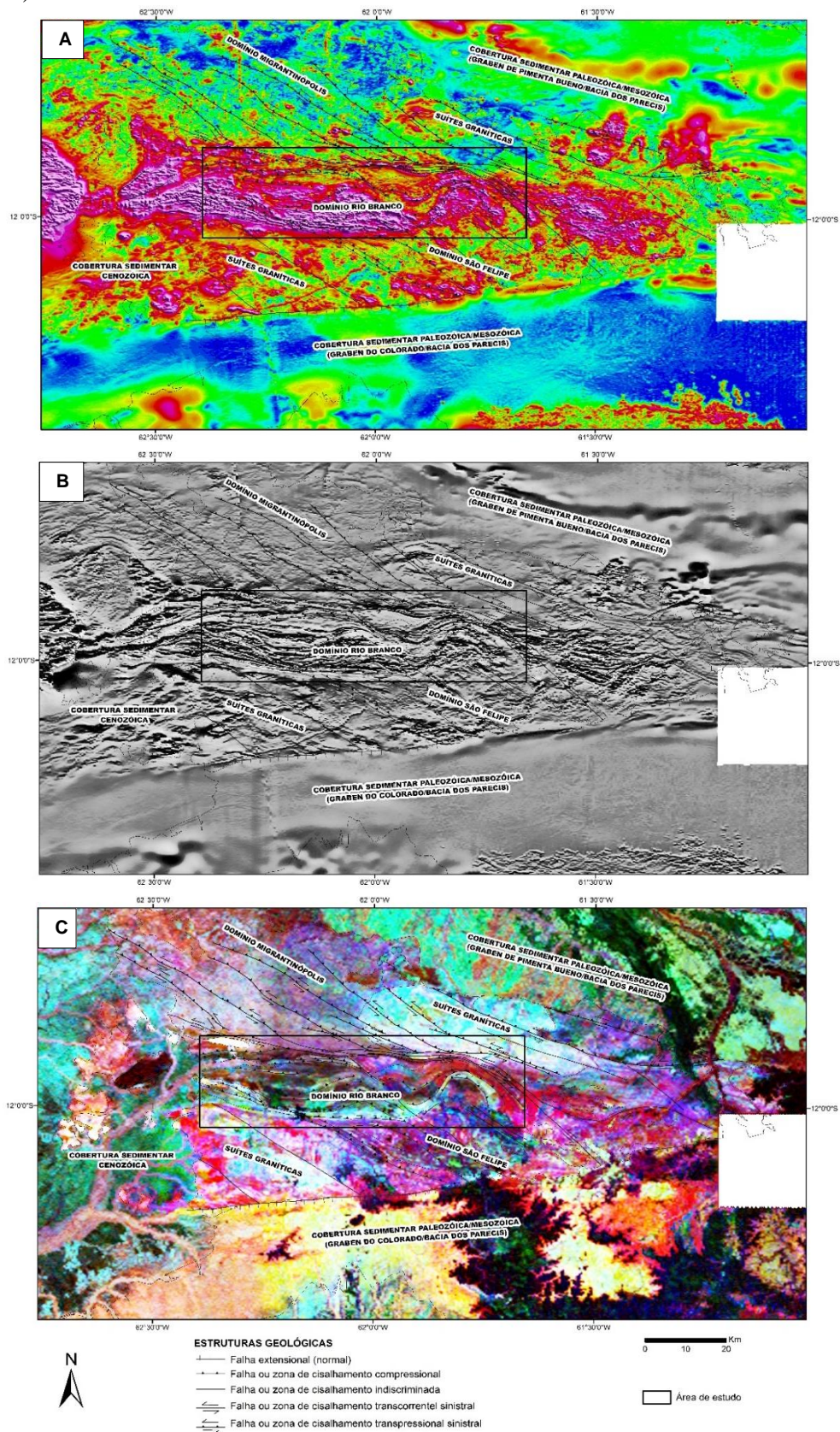
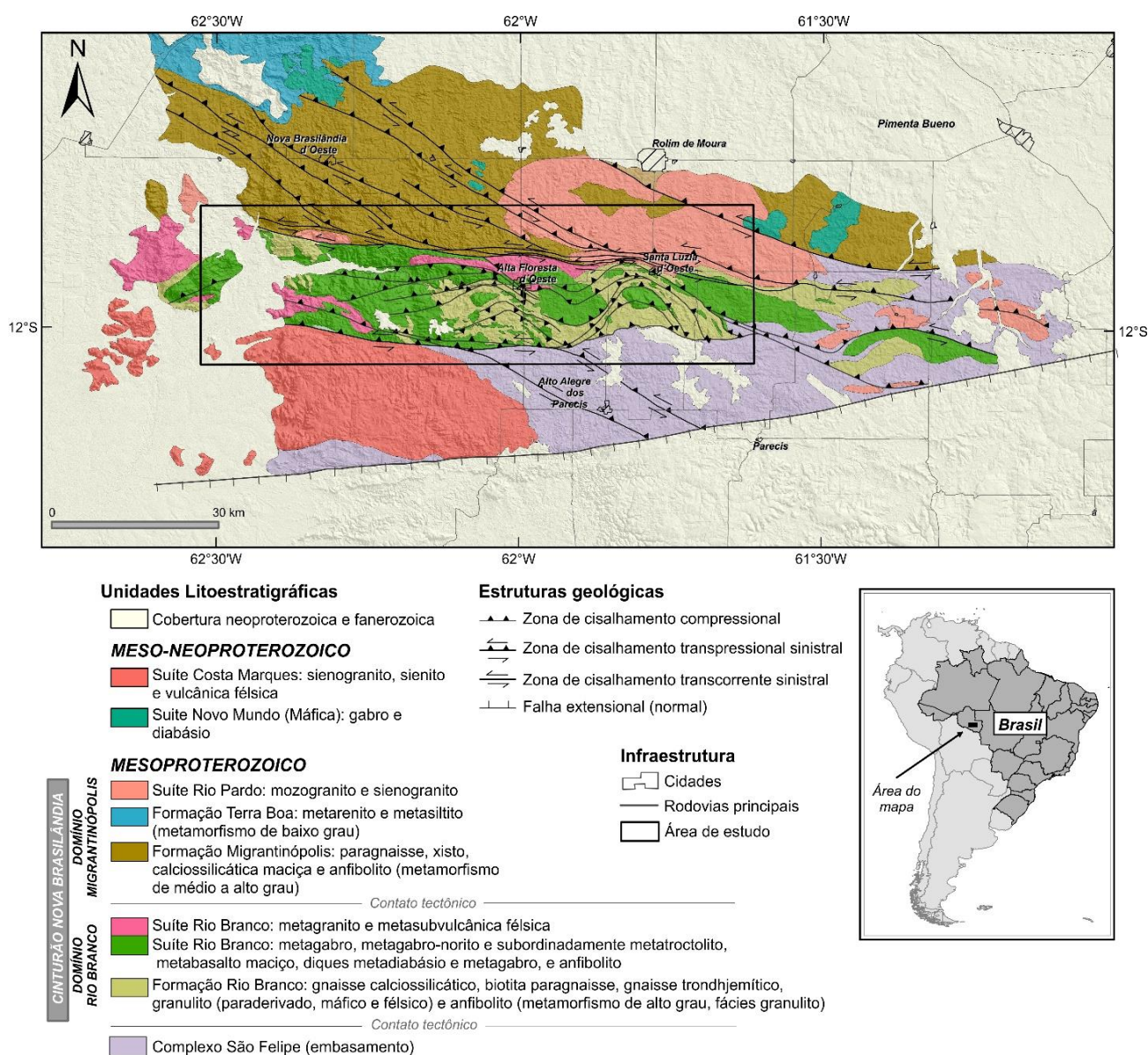


Fig. 5. Recobrimento aerogeofísico do Cinturão Nova Brasilândia e adjacências. (A) aeromagnetometria de Amplitude do Sinal Analítico (ASA), (B) aeromagnetometria primeira derivada horizontal (DZ) e (C) aerogamaespectrometria mostrando a composição ternária RGB (K, eTh, eU) (fonte: CPRM, 2014 - Projeto Aerogeofísico Sudoeste de Rondônia).

O primeiro, mais antigo, corresponde à fase de extensão continental e formação de *rift*, magmatismo intraplaca, sedimentação turbidítica e início de formação de crosta oceânica. O segundo, mais novo, refere-se à fase de colisão com transpressão e espessamento crustal, constituindo assim a orogênese Nova Brasilândia que é cronocorrelata da orogênese Shawiningan na Província Grenville (Fig. 4) (Rizzotto, 1999; Tohver *et al.*, 2004, 2005a; Santos *et al.*, 2008; Teixeira *et al.*, 2010).

Portanto, com base em nossas pesquisas, cujo conteúdo encontra-se registrado nos artigos anexados ao documento da tese, uma proposta alternativa para a evolução tectônica do Cinturão Nova Brasilândia está sendo apresentada, bem como a natureza dos estágios evolutivos e a cronologia dos eventos geológicos estão sendo definidas com mais precisão, baseados na metodologia utilizada na pesquisa.



Na região cratônica a noroeste do Cinturão Nova Brasilândia, no contexto do embasamento do Terreno Jamari, encontra-se o Sistema Transpressivo Sinistral Ji-Paraná – Cujubim (Quadros *et al.*, 2011, 2014), que consiste no prolongamento da Zona de Cisalhamento Ji-Paraná, em direção à região noroeste de Rondônia (Scandolara *et al.*, 1999; Tohver *et al.*, 2005a, 2005b), ou do Sistema Transpressivo Sinistral Ji-Paraná (Scandolara, 2006) (Fig. 1). Esse sistema corresponde a uma faixa com aproximadamente 35-80 km de largura e mais de 300 km de extensão, com *trend* geral NW-SE. Foi gerado no Esteniano (~1,13 Ga) a partir do retrabalhamento crustal das rochas que compõem a Província Rondônia-Juruena, mais especificamente o Terreno Jamari, durante uma fase específica da Orogenia Nova Brasilândia. Entretanto, seu contexto evolutivo necessita ainda de estudos adicionais para sua inserção na nova proposta de evolução do Cinturão Nova Brasilândia que está sendo apresentada nessa tese de doutorado. Adicionalmente, destacamos que o sistema transpressivo abrange várias zonas de cisalhamento dúcteis, métricas a quilométricas, subverticais, com milonitização em fácies anfibolito baixo a superior. O metamorfismo ao longo das zonas de cisalhamento na porção leste-suldeste do sistema alcançou temperaturas em torno de 450-550°C e a deformação ocorreu entre 1,18-1,15 Ga (Tohver *et al.*, 2005). Dados geocronológicos U-Pb em zircão obtidos por Quadros *et al.*, (2011, 2014) em granito anatótico (fusão de metassedimentos) gerado ao longo desse sistema transpressivo revelaram a idade de cristalização de 1138 ± 8 Ma, interpretada como idade do pico do metamorfismo ao longo do Sistema Transpressivo Sinistral Ji-Paraná –Cujubim.

Nessa mesma região cratônica, o magmatismo granítico anorogênico com idades de cristalização no intervalo entre 1082 e 950 Ma representa as manifestações magmáticas pós-evolução do orógeno Sunsás, mais especificamente pós-orogenia Nova Brasilândia (Bettencourt *et al.*, 1999; Quadros e Rizzotto, 2007). A geração mais antiga é representada pelas rochas da Suíte Intrusiva Santa Clara, designação dada por Bettencourt *et al.* (1997), que engloba dezessete maciços graníticos subcirculares a subalongados, com destaque para os maciços Oriente Novo, Oriente Velho, Santa Clara, Montenegro, Manteiga, Retiro, Jararaca, Jatuarana, Primavera, Moisés e Massaranduba (Quadros *et al.*, 2011). A Suíte Santa Clara é constituída por monzogranitos porfiríticos, sienogranitos porfiríticos, monzogranitos finos, quartzo pórfiros, traquitos, albita leucogranitos, microssienitos e, mais raramente, aplitos e pegmatitos. Apresenta idades de cristalização pelo método U-Pb em zircão e Pb-Pb entre 1080 e 1082 Ma (Bettencourt *et al.*, 1999; Quadros *et al.*, 2011). Diferentes estilos de mineralizações de cassiterita e elementos associados ocorrem nos granitos da Suíte Intrusiva Santa Clara e compreendem *stockwork* em *greisens*, *lodes* de quartzo-cassiterita e quartzo-cassiterita-wolframita, veios de quartzo-topázio-fluorita, pegmatitos com albita, microclínio, berílio, topázio, molibdenita e cassiterita. A geração mais jovem é representada pelas rochas da Suíte Intrusiva Rondônia, descrita por Kloosterman (1968) como

“*Younger Granites of Rondônia*”, que engloba diversos maciços graníticos (batólitos e *stocks*) com ampla distribuição no centro-norte de Rondônia. Essa unidade é constituída por sienogranitos equigranulares, monzogranitos porfiríticos e ortoclásio granitos, ocorrências subordinadas de topázio-albita granitos e topázio-quartzo-feldspato pórfiro, além de microssienitos e quartzo pórfiros. Corpos de granitos datados por Bettencourt *et al.* (1999), pelo método U-Pb em zircão, apresentaram idades de cristalização entre 998 e 974 Ma. Os corpos datados por Sparrenberger *et al.* (2002), pelo método U-Pb em monazita, obtiveram idades de cristalização entre 993 e 989 Ma. A maioria dos granitos das suítes intrusivas Santa Clara e Rondônia contém mineralizações de Sn, W, Nb-Ta, Be e F, em parte associadas às fases tardias do magmatismo representadas por albita-leucogranitos (p. ex. Mina de Bom Futuro).

Geology and LA-ICP-MS U-Pb geochronology of the Nova Brasilândia belt, southwest of the Amazonian Craton: New ages, re-evaluation of existing geochronological data and implications on the Sunsás orogen evolution

1 **Geology and LA-ICP-MS U-Pb geochronology of the Nova Brasilândia belt,**
2 **southwest of the Amazonian Craton: New ages, re-evaluation of existing**
3 **geochronological data and implications on the Sunsás orogen evolution**

4
5 Marcos Luiz do Espírito Santo Quadros^{a,*}, Maria Emília Schutesky Della Giustina^b, Joseneusa Brilhante
6 Rodrigues^c, Valmir da Silva Souza^b

7
8 ^a Serviço Geológico do Brasil (CPRM), Avenida Dr. Freitas, nº 3645 - Bairro do Marco, CEP 66095-110, Belém, PA, Brazil

9 ^b Instituto de Geociências, Campus Universitário Darcy Ribeiro, Universidade de Brasília (UnB), CEP 70910-900, Brasília-DF-
10 Brazil

11 ^c Serviço Geológico do Brasil (CPRM), Setor Bancário Norte, Quadra 02, AN, Bloco H, Ed. Central Brasília, CEP 70040-904,
12 Brasília, DF, Brazil

13
14 * Corresponding author (e-mail address: marcos.quadros@cprm.gov.br)

15
16
17
18 *Keywords:*

19 *Amazonian Craton*

20 *Sunsás Orogen*

21 *Nova Brasilândia belt*

22 *U-Pb geochronology*

23 *Rodinia supercontinent*

24
25
26
27
28 **ABSTRACT**

29
30
31 *New geological and LA-ICP-MS U-Pb geochronological data combined*
32 *with data compiled from previously published articles provide*
33 *information needed to characterize more precisely the tectonic evolution*
34 *timing of the Nova Brasilândia belt in southwestern Amazonian Craton,*
35 *Rondônia. The LA-ICP-MS U-Pb ages were obtained in zircon crystals*
36 *from the rocks of Rio Branco domain, southern part of the belt. Isotopic*
37 *data of the Rio Branco Formation revealed sedimentation period*
38 *between 1241 ± 7.5 Ma and 1137 ± 9 Ma and high-grade metamorphism*
39 *between 1137 ± 9 Ma and 1127.6 ± 2.3 Ma. The magmatism mafic-felsic*
40 *of the Rio Branco Suite was dated between 1119.7 ± 2.7 Ma and 1106.2*
41 *± 2.8 Ma. U-Pb ages obtained in specific groups of recrystallized zircon*
42 *(cores and rims) extracted from high-grade calc-silicate gneiss ($1019 \pm$*
43 *15 Ma), metagabbro (1016.7 ± 3.9 Ma) and anatectic granite ($1011.3 \pm$*
44 *9.6 Ma) represent possible reflections of metamorphic recrystallization*
45 *and migmatization youngest. The LA-ICP-MS U-Pb zircon ages of*
46 *sedimentation, metamorphism, migmatization and magmatism obtained*
47 *in the Rio Branco domain rocks establish the time period of two*
48 *orogenic phases recorded in the Nova Brasilândia belt between ca.*
49 *1137 Ma and 1106 Ma (accretionary phase) and between ca. 1096 Ma*
50 *and 1011 Ma (overprint metamorphic during collisional phase). Thus,*
51 *the Nova Brasilândia orogeny recorded on the southwest margin of the*
52 *Amazonian Craton is can be considered as accretionary-collisional type,*
53 *and developed between ca. 1137 and 1010 Ma.*

54
55

56 1. Introduction

57

58 The Rodinia supercontinent was formed in the late Mesoproterozoic to early Neoproterozoic
59 (ca. 1.0 Ga) as result of several collisional belts collectively referred to as the Grenville orogeny,
60 which culminated in the agglutination of cratons and blocks, including Laurentia and Amazonia.
61 Several proposals for tectonic reconstructions of Rodinia, particularly those describing the
62 agglutination of the Laurentian and Amazonian cratons, have been presented and include alternative
63 paleogeographic reconstructions for these cratons in the Mesoproterozoic (e.g. Dalziel, 1991;
64 Hoffman, 1991; Keppie and Ortega-Gutierrez, 1999; Rogers and Santosh, 2003; Loewy et al., 2003,
65 2004; Casquet et al., 2006; Li et al., 2008; Chew et al., 2011; Cawood and Pisarevsky, 2017).
66 Important revisions that address the aspects of the geological and tectonic history of the
67 Mesoproterozoic basement in the Andes region, the western part of the Amazon and of Bolivia,
68 have also been well synthesized by Cawood and Pisarevsky (2017), Ramos (2010, 2008), Cardona
69 et al. (2010), Cordani et al. (2009, 2010), Miskovic et al. (2009), Fuck et al. (2008), Li et al. (2008),
70 Cordani and Teixeira (2007), and Johansson (2009, 2014).

71 In the Amazonian Craton, the Sunsás Province (ca. 1.20-0.95 Ga), also known as the Sunsás-
72 Aguapeí Province, is a key area for studying the Rodinia supercontinent assembly. The Sunsás
73 Province is related chronologically to the Grenville Province and together they represent two of the
74 main global orogens forming Rodinia (Tohver et al., 2002, 2004; Santos et al., 2008). The geological
75 and tectonic record of the continental mass agglutination that formed Rodinia is well recorded in
76 the southwestern margin of the Amazonian Craton, in the states of Rondônia and Mato Grosso, as
77 well as in its counterparts in Bolivia. The Nova Brasilândia, Aguapeí and Sunsás orogenic belts and
78 the Ji-Paraná - Cujubim sinistral transpressive System, which includes the Ji-Paraná Shear Zone,
79 are the geotectonic units that record the mesoproterozoic orogenic activities on the southwestern
80 fringe of the Amazonian Craton associated with Rodinia assembly (see Rizzotto, 1999; Rizzotto et
81 al., 2001, 2014; Santos et al., 2003, 2008; Tohver et al., 2002, 2004, 2005a, 2005b; Boger et al.,
82 2005; Ruiz, 2005; Scandolaro, 2006; Ruiz et al., 2007; Teixeira et al., 2010; Quadros et al., 2011).

83 The term Sunsás was originally designated in Bolivia to name an orogenic belt NW-SE
84 formed in 1000 Ma (Litherland et al., 1989). The Sunsás Orogen was formed during the
85 Mesoproterozoic and comprises the western part of the Amazonian Craton in South America, and
86 is best exposed in the eastern Bolivia and western Brazil in Rondônia and Mato Grosso states
87 (Santos et al., 2008). The timing of the Sunsás orogeny was first estimate in 1100–900 Ma through
88 Rb-Sr and K-Ar isotopic studies carried out on granitic rocks and pegmatites from the Sunsás
89 collisional belt, in Bolivia (Litherland et al., 1986, 1989). The Sunsás collisional belt was correlated
90 with the Aguapeí belt in Brazil, becoming a single geotectonic unit (Tassinari et al., 1996). Recently,
91 the Nova Brasilândia, Aguapeí and Sunsás belts were grouped into a unique geotectonic unit termed
92 the Western Amazon belt (Rizzotto et al., 2014).

93 Four periods of orogenic activity are identified within the Sunsás Orogen: Santa Helena
94 orogeny (1465–1427 Ma), Candeias orogeny (1371–1319 Ma), San Andrés orogeny (ca. 1275 Ma),
95 and Nova Brasilândia orogeny (1180–1110Ma) (Rizzotto 1999; Santos et al., 2008). Bettencourt et
96 al. (2010) suggested the Rondonian-San Ignacio Orogeny as responsible for the formation of a
97 complex accretionary orogen (1556-1430 Ma) developed from the oblique collision (1370-1320
98 Ma) of the Paraguá block with the proto-Amazonian Craton. Teixeira et al. (2010) characterized the
99 Sunsás orogen with an allochthonous collisional-type belt formed between (1.11–1.00 Ga),
100 considering as the youngest of the events recorded on the southwest margin of the Amazonian
101 Craton. In our conception, based on the works of Santos et al. (2008), Teixeira et al. (2010),
102 Bettencourt et al. (2010), Rizzotto (1999), and Rizzotto et al. (2014), the Sunsás orogen comprises
103 the Nova Brasilândia, Aguapeí and Sunsás collisional belts, and the reworked craton areas
104 (transpressive or transcurrent shear zone/systems). This orogen was formed approximately between
105 1.25 and 1.00 Ga, reflection of the Nova Brasilândia orogeny (1180–1110 Ma; Rizzotto, 1999) and
106 Sunsás orogeny (1100-1000 Ma; Teixeira et al., 2010).

107 The area investigated in the present study is located in the Rio Branco domain, southern part
108 of the Nova Brasilândia belt, which represents an incomplete fragment of ocean floor added to the
109 southwest margin of the Amazonian Craton during the collisional phase of the Nova Brasilândia
110 orogeny orogen (Rizzotto, 1999; Rizzotto et al., 1999, 2001) (Fig. 1).

111 This paper presents new geological and isotopic data obtained by the method LA-ICP-MS
112 (Laser Ablation–Inductively Coupled Plasma–Mass Spectrometer) U-Pb zircon in rocks from the
113 Rio Branco domain. It also presents U-Pb, ^{40}Ar - ^{39}Ar and Sm-Nd geochronological data compiled
114 of previously published articles. Our main objective was to compose a work proposal based on the
115 new results combined with previously published information another researchers, as well as to
116 establish the chronology of sedimentation, magmatism and deformation/metamorphism events. The
117 integration and reinterpretation of geological and geochronological data provided improvements in
118 the evolution models of the Nova Brasilândia belt and provided new subsidies for the presentation
119 of alternative proposals to characterize the nature of the Nova Brasilândia orogeny. Finally, this
120 research also contributes to the discussion of the tectonic models of the Rodinia supercontinent
121 reconstruction.

122

123 **2. Geological and tectonic setting**

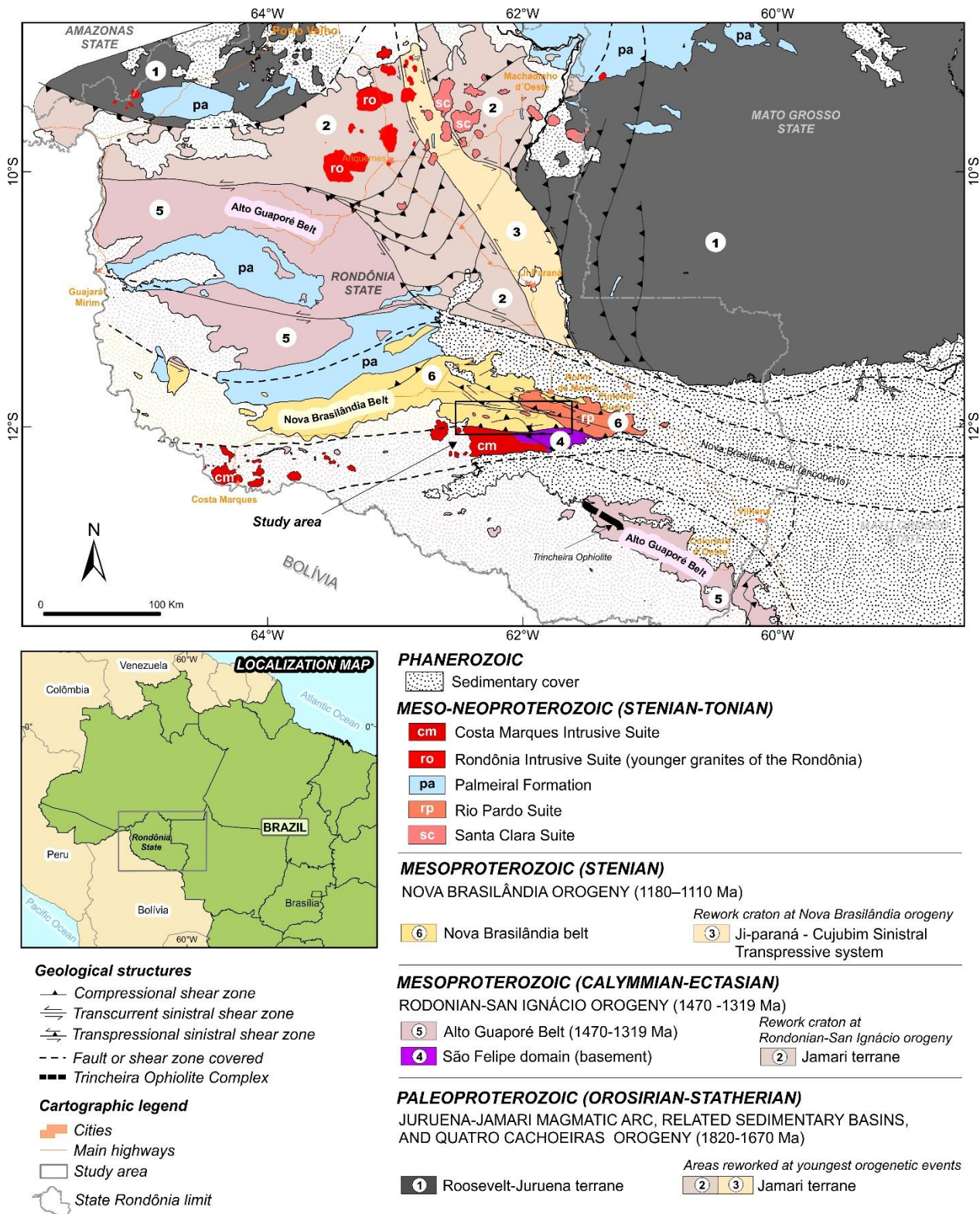
124

125 The Amazonian Craton was subdivided initially into two shields, named the Central Brazil
126 Shield in the south and the Guyana Shield in the north, separated by extensive Phanerozoic
127 sedimentary areas deposited in the Solimões and Amazon basin. Amaral (1974) subdivided the
128 craton into three geochronological provinces: Eastern Amazon, Central Amazon and Western
129 Amazon. Following, several evolutionary proposals have been suggested, improving and adapting
130 the first proposed model, mainly based on new geochronological data (e.g., Cordani et al., 1979;
131 Teixeira et al., 1989). Hasui et al. (1984) and Costa and Hasui (1991) presented models combining
132 geophysical and structural data to define twelve blocks or paleoplates ranging in age from Archean
133 to Paleoproterozoic. Accordingly, these blocks are separate by mobile belts formed dominantly by
134 continental collision, with subsequent reactivation during younger tectonic events. Tassinari and
135 Macambira (1999) reviewed the provinces concept in the subdivision of the Amazonian Craton,
136 proposing a new model supported by Sm-Nd geochronological data, in which the southwestern
137 region of the Amazonian Craton consists of the Rio Negro-Juruena Province (1.80-1.55 Ga), the
138 Rondoniana-San Ignacio Province (1.45-1.3 Ga) and the Sunsás Province (1.25-1.00 Ga). In
139 contrast, Santos et al. (2003) defined only two geochronological provinces in the southwestern
140 Amazonian Craton: the Rondônia-Juruena (1.74-1.47 Ga) and the Sunsás (1.20-0.99 Ga) provinces.

141 The structure of the southwestern sector of the craton was also initially approached in regional
142 geological mapping (Pinto Filho et al., 1977; Litherland et al., 1986, Scandolaro et al., 1999) and in
143 specific academic research (Rizzotto, 1999; Ruiz, 2005; Scandolaro, 2006), all of which with
144 lithostratigraphic connotation. Other works focused on the tectonic evolution of the Sunsás orogen,
145 i.e., the collision between the Amazonian Craton and the east and southeast edges of Laurentia (see
146 Priem et al., 1989; Sadowski and Bettencourt, 1996; Tohver et al., 2002; Rizzotto et al., 2013, 2014).
147 From the works cited above, the structural framework proposed by Tohver et al. (2005a, 2005b)
148 suggests the existence of an unexposed suture zone along which the Nova Brasilândia belt
149 developed, in relation to the collision of the Amazonian Craton with Laurentia at ca. 1.2-1.0 Ga.
150 Alternatively, Scandolaro (2006) presented a tectonostratigraphic subdivision for the southwestern
151 Amazonian Craton in Rondônia. In this proposal, each geologic terrane presents its own
152 petrographic, structural, geochemical, geophysical and geochronological characteristics and limited
153 by regional-scale fault systems or shear zones, individualized as the Jamari, Roosevelt and Nova
154 Brasilândia terranes.

155 In the Alto Guapore belt of southeastern Rondônia was characterized the ophiolitic complex
156 (1.47-1.35 Ga), represented by the Trincheira Complex rocks, showing a WNW-ESE paleo-suture
157 zone (Guapore Suture Zone) associated with the evolution of an accretionary orogen formed by
158 oceanic plate subduction between 1.47-1.43 Ga (Rizzotto and Hartmann, 2012; Rizzotto et al.,

159 2013). Rizzotto et al. (2014) suggested that the Nova Brasilândia basin was formed in the late
 160 Mesoproterozoic from the reactivation of Guaporé Suture Zone generated an intracontinental rift.
 161 Previously, Tohver et al. (2004) suggested that the Nova Brasilândia belt was formed during oblique
 162 collision followed by a strike-slip movement between the Amazonian Craton and Laurentia.
 163



164
 165
 166 **Fig. 1.** Simplified map of the southwestern Amazonian Craton in Rondônia with the approximate boundaries
 167 of the main belts, terranes, units, tectonic elements, lithologic units, and sedimentary covers. Also shown is
 168 the location of the study area. After Scandolaro et al. (1999); Scandolaro (2006), Quadros and Rizzotto
 169 (2007); Santos et al. (2000, 2008); Bettencourt et al. (2010), Quadros et al. (2011) and Rizzotto et al. (2014).

170 Recently, the mafic-felsic magmatism of the Rio Branco Suite were correlated with a LIP
171 (Large Igneous Province) event in the southwestern Amazonian Craton that took place at ca. 1.1 Ga
172 and correlated temporally to the intraplate magmatism of the Rincon Del Tigre Complex and the
173 Huanchaca sills and dikes, both in Bolivia (Teixeira et al., 2018). Article published by Quadros et
174 al. (submitted) as part of this research suggest that the medium- to low Ti tholeitic sub-alkaline
175 mafic magmatism of the Rio Branco Suite exhibits characteristic petrogenetic patterns that can be
176 associated with subduction. These rocks also present overlapping of MORB-like (mid-ocean ridge
177 basalt), IAT (island arc tholeiite) and BAB (back-arc basalt) characteristics. Therefore, these authors
178 suggest an important accretionary phase (ca. 1137 and 1106 Ma) in the evolution of the Nova
179 Brasilândia belt.

180 Finally, our simplified view of the tectonic structure of southwestern Amazonian Craton in
181 Rondônia and part of Mato Grosso, presented in this article, was elaborate from the reinterpretation
182 of geological and aerogeophysical maps previously published by CPRM-Geological Survey of
183 Brazil, articles, dissertations and theses, added to the geological and geochronological new data
184 obtained in our research (Fig. 1).

185

186 **3. Local geological and tectonic framework – previous data**

187

188 The Sunsás orogen, in our understanding, comprises the Nova Brasilândia, Aguapeí and
189 Sunsás collisional belts, and the reworked craton areas (transpressive or transcurrent shear zone or
190 systems). This orogen was formed approximately between 1.25 and 1.00 Ga, reflection of the Nova
191 Brasilândia orogeny (1180–1110 Ma) and Sunsás orogeny (1100-1000 Ma) (see Santos et al., 2008,
192 Teixeira et al., 2010; Bettencourt et al., 2010; Rizzotto et al., 2014).

193 The Nova Brasilândia belt, also known as the Nova Brasilândia metasedimentary belt, is the
194 target of our research takes place in the southwest portion of the Amazonian Craton and stretches
195 in the E-W direction to NW-SE for approximately 170 km long by 40 km wide (Fig. 2A). The belt
196 is limited to the north by the sedimentary rocks of the Pimenta Bueno graben, to the south by the
197 metamorphic rocks of the São Felipe Complex (> 1.24 Ga), to the east by the sedimentary rocks of
198 the Parecis Basin, and to the west by Cenozoic sedimentary covers (Fig. 2A). This belt was
199 subdivided into two lithostructural domains, the Migrantinópolis domain to the north and the Rio
200 Branco domain to the south, separated by the Rio Branco sinistral transcurrent shear zone (Fig. 2B).

201 The metavolcanic-sedimentary rocks were initially named as the Nova Brasilândia
202 Metavolcanic-sedimentary Sequence (Scandolara and Rizzotto, 1998), and later as the Nova
203 Brasilândia Group (Rizzotto, 1999; Rizzotto et al., 2001). It comprises two distinct units (Fig. 2A).
204 The Migrantinópolis Formation consists of a metaturbidite unit with siliciclastic-carbonate
205 composition metamorphosed under medium- to high-grade conditions, composed of quartz-
206 feldspathic gneisses, mica schists, quartzites and subordinate massive calc-silicates rocks. In
207 addition, metagabbro sills, amphibolites and, more rarely, massive metabasalts were inserted into
208 this lithostratigraphic unit. Planar structures are represented by gneissic *banding*, shistosity,
209 mylonitic foliation and asymmetric folds, as well as boudins of quartz veins. The foliation regional
210 trend is approximately N40°-50°W, with dip around 40°-60° to NE. Details of the geological-
211 structural framework of the Nova Brasilândia belt were detailed by Luft et al. (2000). The zircon U-
212 Pb (SHRIMP) age of 1122 Ma defines the maximum sedimentation age of the protoliths of the
213 Migrantinópolis Formation, considered as the opening age for the basin (Rizzotto et al., 2014).

214 The Rio Branco Formation, in the initial concept (Rizzotto, 1999; Rizzotto et al., 1999, 2001),
215 includes metamafic rocks represented by sills and stocks of metagabbro, metagabbroonorite and
216 metadiabase, with subordinate intercalations of calc-silicate gneisses and paragneisses and schists,
217 in addition to amphibolites and mafic granulites. In the mafic set, two units of magmatism were
218 identified in the Rio Branco domain. The first unit was contemporary to the sedimentation of the
219 Rio Branco Formation protoliths, occurring as elongated bodies and lenses of mafic granulites
220 originated from the high-grade metamorphism (granulite facies) of gabbros and gabbroonorites
221 (protoliths), and medium-grained amphibolites founds along of shear zones.

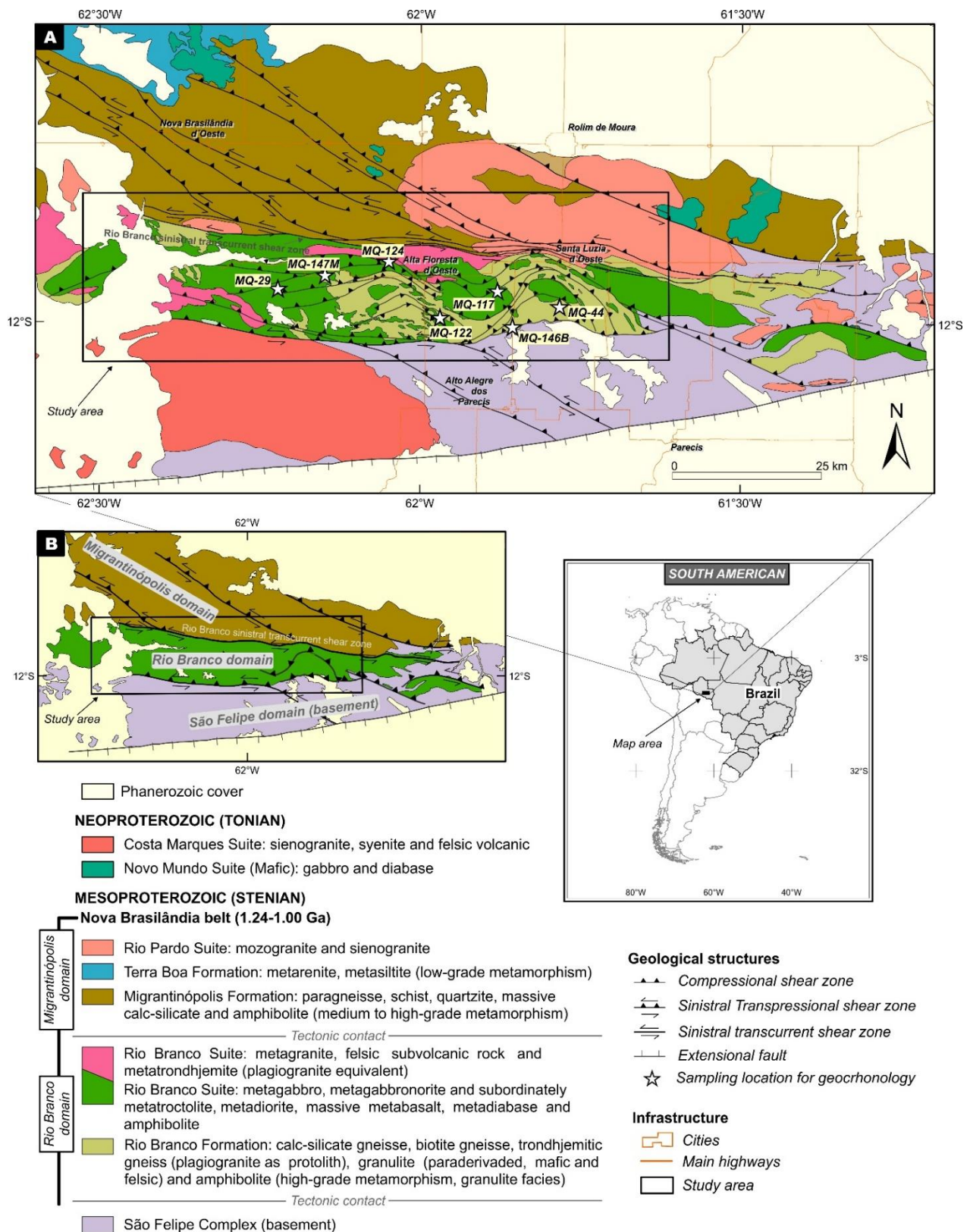


Fig. 2. Geological map of the Nova Brasilândia belt in southwestern Amazonian Craton, Rondônia. Modified after Scandolaro and Rizzotto (1998), Bahia and Silva (1998) and Bergami et al. (2018).

222
 223
 224
 225
 226
 227
 228 The second unit is composed of dykes and stocks of metagabbro and metadiabase,
 229 respectively, intrusives in high-grade metasedimentary rocks of the Rio Branco Formation. The
 230 foliation regional trend is approximately NNE and SSW, with double dips nearly to 70°-80°/NE or
 231 40°-50°/SW. These intrusions formed at shallow levels of the crust, evidenced by sub-ophytic

232 textures partially preserved in fine-grained metamafic rocks. In general, bodies have oval or tabular
233 forms, with their partially preserved igneous characteristics. In these portions of the rocks occurs
234 igneous foliation incipient defined by the alignment of amphibole prisms, pyroxene and tabular
235 crystals of plagioclase. In the deformed parts of the rock, metamorphic foliation overlaps the
236 primary igneous textures. The magmatic and metamorphic textures alternate at all scales as a
237 function of the intensity or absence of deformation, according to its location in relation to the main
238 shear zones. Part this set of metabasic rocks was metamorphosed in high-grade (see Rizzotto, 1999;
239 Rizzotto et al., 2001) and was heterogeneously deformed (mylonitized) and transformed to
240 amphibolites along transpressive and transcurrent shear zones.

241 Metagranites of monzogranitic composition included in the Rio Branco Granite unit and with
242 U-Pb age of 1113 ± 56 Ma occur as intrusions in metasedimentary rocks of the Rio Branco
243 Formation (Rizzotto, 1999). In the region southeast of Nova Brasilândia d'Oeste occur foliated
244 monzogranites and syenogranites of the Rio Pardo Suite (Silva et al., 1992) with U-Pb (zircon)
245 crystallization age of 1005 ± 41 Ma, Sm-Nd model age of 1.50 Ga, and $\epsilon_{Nd}(t) = +0.50$ (Rizzotto,
246 1999). The late emplacement of post-tectonic granites of the Rio Pardo Suite and generation of the
247 Palmeiral Formation rocks in cratonic area were associated with extensional phase and final
248 orogenic collapse between ca.1005-970 Ma (Rizzotto et al., 2001).

249 Geological structures suggest a complex history of various deformation and metamorphism
250 stages in the context of progressive deformation associated with convergence, transpression and late
251 transcurrent movements that occurred during the evolution of the Nova Brasilândia orogeny.
252 Initially, these processes formed banded gneisses and foliation with low to medium dip trending
253 NW-SE or E-W and isoclinal folds with horizontal axes as compressive tectonic products. With the
254 progression of regional deformation, transpressive shear zones became dominant, and late
255 transcurrent sinistral shear zones caused the development of high-angle mylonitic foliation,
256 subvertical to subhorizontal stretching lineations, boudins and folds, with intense transposition and
257 parallelization of structures within the shear zones (see Rizzotto, 1999; Rizzotto et al., 1999, 2001;
258 Tohver et al., 2004).

259 Previous proposals for tectonic scenarios in the Nova Brasilândia belt involve periods of
260 extension, compression, transtension and transpression, developed along a dominantly strike-slip
261 margin between the Amazônia and Laurentia. Cycles of contraction-extension and intraplate
262 magmatism during the geological evolution of the Nova Brasilândia belt were defined (Scandolaro
263 and Rizzotto, 1992; Rizzotto, 1999; Rizzotto et al., 2001). These authors proposed a first cycle by
264 continental extension marked by intraplate plutonism and turbidite sedimentation, closing with
265 transpression and crustal thickening between 1250 Ma and 1110 Ma during Nova Brasilândia
266 orogeny. The second cycle between 1005 Ma and 910 Ma comprised post-orogenic collapse forming
267 a cratonic intracontinental basin (Palmeiral Formation), accompanied by intraplate felsic
268 magmatism with metallogenetic interest for Sn, W, Nb, Ta and ETR. In this phase, lateral
269 movements of crustal blocks generated wide late transcurrent shear zones, with highlight to Rio
270 Branco sinistral transcurrent shear zone (Fig. 2).

271 The Nova Brasilândia belt was also interpreted as resulting from crustal thickening by
272 imbrication caused by transpressive suturing of the Amazonian and Paraguá Craton at ca. 1.09 Ga,
273 based on structural data, thermobarometric calculations and U-Pb (titanite and monazite) and
274 $^{40}\text{Ar}/^{39}\text{Ar}$ (biotite and hornblende) geochronology. This data revealed a long history of
275 metamorphism, tectonic exhumation and cooling in the range of 1.09 -1.06 Ga to 0.97-0.91 Ga
276 (Tohver et al., 2004, 2005a, 2006).

277 The main geochronological ages obtained in the rocks of the Nova Brasilândia belt by the U-
278 Pb methods (TIMS, SHRIMP and LA-ICP-MS) in zircon, monazite, titanite and rutile crystals, ^{40}Ar -
279 ^{39}Ar in hornblende and biotite and Sm-Nd in whole rocks are summarized in table 1.

280

Table 1.

Synthesis of U-Pb and Ar-Ar isotopic ages in metasedimentary and metaafic rocks and metagranites of the Nova Brasilândia belt, southwest of the Amazonian Craton in Rondônia.

Lithology	Location	Method	Age (Ma) or (Ga)	Interpretation of age	Reference
Rio Pardo Suite					
Monzogranite (sample GR-23)	S 11°54'19" W 62°02'11"	U-Pb SHRIMP zircon Sm-Nd (whole rock)	1005 ± 41 Ma* (n=4, upper intercept) 1,50 Ga** (TDM)	Crystallization age (*) and model age (**)	Rizzotto (1999)
Monzogranite (sample GR-345)	S 12°05'49" W 61°25'24"	U-Pb LA-ICP-MS zircon	1010 ± 15 Ma (n=10)	Crystallization age	Rizzotto et al. (2014)
Terra Boa Formation					
Metarenite (sample GB-427)	S 11°30'26" W 62°32'05"	U-Pb LA-ICP-MS zircon	Ages between 2070 and 1143 Ma. Main peaks with ages of 2031 Ma, 1536 Ma* (main peak, n=17), 1307 Ma and 1143 Ma. Peak youngest age of 1143 Ma** (n=2)	Age of the main source (*) and maximum sedimentation age in 1143 Ma (**)	Trindade Neto et al. (2018)
Migrantópolis Formation					
Fine-grained banded paragneiss (sample GR-66)	S 11°50'35" W 62°04'18"	U-Pb SHRIMP zircon Sm-Nd (whole rock)	U-Pb ages between 2090 and 1122 Ma. Ages peak of 1417 ± 35 Ma (n=3), 1320 ± 20 Ma (n=5), 1215 ± 20 Ma* (n=7) and 1122 ± 12 Ma (n=2) 1, 85 a 1, 91 Ga** (TDM)	Maximum sedimentation age in 1215 ± 20 Ma (*), first interpretation of the data by the author. Model ages (**)	Rizzotto (1999), Rizzotto et al. (2001)
Metasandstone (sample GR-66)	S 11°50'35" W 62°04'18"	U-Pb SHRIMP zircon	The ages spread from 2090 to 1103 Ma. Oldest zircons with 2090, 2020, 1904, 1748, 1716, 1546 and 1540 Ma. The younger zircons were grouped into three populations with ages of 1417 ± 35 Ma, 1320 ± 20 Ma and 1211 ± 18 Ma*	Maximum sedimentation age in 1211 ± 18 Ma (*)	Santos et al. (2000)
Fine-grained banded paragneiss (sample GR-66)	S 11°50'35" W 62°04'18"	U-Pb SHRIMP zircon	Ages between 2090 and 1122 Ma. Ages peak of 1417 ± 35 Ma (n=3), 1320 ± 20 Ma (n=5), 1215 ± 20 Ma (n=9) and 1122 ± 12 Ma* (n=2)	Maximum sedimentation age in 1122 Ma (*). Re-interpretation of data by the author	Rizzotto et al. (2014)
Anatexite Leucogranite (sample GR-20)	S 11°43'30" W 62°09'15"	U-Pb SHRIMP zircon Sm-Nd (whole rock)	1110 ± 8 Ma* (n=7) 1,66 Ga**	Crystallization age (climax age of metamorphism)* and model ages (**)	Rizzotto (1999)
Mica schist (sample 324a)	S 11°48'47" W 62°18'48"	⁴⁰ Ar- ³⁹ Ar	964 ± 1 Ma bio*	Cooling Age	Tohver et al. (2005a)
Mica schist (sample 325)	S 11°48'51" W 62°18'40"	⁴⁰ Ar- ³⁹ Ar	957 ± 2 Ma bio*	Cooling Age	Tohver et al. (2005a)
Mica schist (sample 326)	S 11°40'45" W 62°11'50"	U-Pb monazite ⁴⁰ Ar- ³⁹ Ar	1082 ± 6 Ma m 948 ± 2 bio*	Growth of the monazite below its closing temperature through dynamic recrystallization and Cooling Age	Tohver et al. (2004)
Mica schist (sample 127)	S 11°40'50" W 62°11'50"	⁴⁰ Ar- ³⁹ Ar	930 ± 3 Ma bio*, 928 ± 4 Ma bio, 923 ± 3 Ma bio*, 920 ± 3 Ma bio	Cooling Age	Tohver et al. (2005a)
Calc-silicate (sample 316)	S 11°49'20" W 61°51'05"	U-Pb monazite	1020 ± 15 Ma m	Isotopic resetting age	Tohver et al. (2005a)
Rio Branco Suite (felsic component)					
Foliated monzogranite (sample GR-10a)	S 11°55'52" W 62°09'04"	U-Pb SHRIMP zircon Sm-Nd (whole rock)	1113 ± 56 Ma* (n=5, upper intercept) 1,63 Ga** (TDM)	Crystallization age (climax age of metamorphism) (*) and model ages (**)	Rizzotto (1999)
Foliated granite dike (sample MQ-147M)	S 11°55'59" W 62°08'55"	U-Pb LA-ICP-MS zircon	1113 ± 6.7 Ma (n=15, concordia age)	Crystallization age	This work
Fine-grained metagranite subvolcanic or felsic volcanic (sample MQ-124)	S 11°54'20" W 62°02'57"	U-Pb LA-ICP-MS zircon	1112.3 ± 1.9 Ma (n=16, concordia age)	Crystallization age	This work
Rio Branco Suite (mafic component and other associated lithologies)					
Metagabbro (sample GR-05)	S 11°59'50" W 62°02'40"	U-Pb SHRIMP zircon	1110 ± 10 Ma (n=4, upper intercept)	Metamorphism age	Rizzotto (1999)
Banded leucocratic trondhjemite (sample GRT-02)	S 11°57'04" W 61°45'01"	U-Pb SHRIMP zircon and titanite	1089 ± 9 Ma* (zr, n=4) and 986 ± 6 Ma** (ti, n=5)	Metamorphism age (*) and cooling age (**)	Rizzotto et al. (2014)
Mafic granulite (sample GRT-01)	S 11°57'49" W 61°44'58"	U-Pb SHRIMP zircon	1114 ± 5 Ma* (n=4, upper intercept) and 1014 Ma** (n=1)	peak metamorphism age (*) and later metamorphic event (**)	Rizzotto et al. (2014)
Banded Trondhjemite (sample GRT-03)	S 11°53'11" W 62°29'11"	U-Pb SHRIMP zircon and titanite	1103 ± 17 Ma (zr, n=3 + ti, n=6)	Metamorphic recrystallization age	Rizzotto et al. (2014)
Fine-grained amphibolite (sample GRT-04)	S 11°53'23" W 62°29'16"	U-Pb SHRIMP zircon	1103 ± 7 Ma (n=9)	Peak metamorphism age	Rizzotto et al. (2014)
Coarse-grained amphibolite (sample GRT-05)	S 11°57'08" W 63°05'57"	U-Pb SHRIMP zircon and rutile	1103 ± 5 Ma* (zr, n=3) and 949 ± 9 Ma** (ru, n=6)	Metamorphic recrystallization age (*) another late recrystallization phase after 1.0 Ga (**)	Rizzotto et al. (2014)
Metagabbro (sample MQ-117)	S 11°57'05" W 61°52'48"	U-Pb LA-ICP-MS zircon	1119.7 ± 2.7 Ma* (n=8, concordia age), 1016 ± 3.9 Ma** (n=3, concordia age)	Inherited zircons (*) and crystallization age (**)	This work
Foliated metatrandhjemite (sample MQ-29)	S 11°56'55" W 62°13'20"	U-Pb LA-ICP-MS zircon	1106.2 ± 2.8 Ma (n=8, concordia age)	Crystallization age	This work
Rio Branco Formation					
Calc-silicate gneiss (sample 135)	S 11°55'49" W 62°02'12"	U-Pb titanite ⁴⁰ Ar- ³⁹ Ar	1061 ± 14 Ma ti (intercept) 961 ± 4 hb*, 966 ± 3 hb	Metamorphic recrystallization age and Cooling Age	Tohver et al. (2004), Tohver et al. (2005a)
Calc-silicate gneiss (sample 319)	S 11°57'29" W 61°51'11"	U-Pb monazite	993 ± 12 Ma m (intercept)	Growth of the monazite below its closing temperature through dynamic recrystallization	Tohver et al. (2004)
Metagabbro (sample 133)	S 11°54'37" W 61°46'51"	⁴⁰ Ar- ³⁹ Ar	994 ± 6 Ma hb*, 983 ± 7 Ma hb, 1005 ± 7 Ma hb*	Cooling Age	Tohver et al. (2005a)
Mylonitic paragneiss (sample 134)	S 11°54'55" W 61°46'49"	U-Pb monazite ⁴⁰ Ar- ³⁹ Ar	1096 ± 6 Ma m 912 ± 2 bio*, 910 ± 2 bio, 914 ± 2 bio*	Metamorphic recrystallization age and Cooling Age	Tohver et al. (2004), Tohver et al. (2005a)
High-grade calc-silicate gneiss (sample MQ-44)	S 11°58'30" W 61°46'59"	U-Pb LA-ICP-MS zircon	Ages between 1575 and 1012 Ma. Ages peak of 1578 Ma, 1480 Ma, 1432 Ma, 1386 Ma, 1241 ± 7.5 Ma* , 1137 ± 9 Ma** and 1019 ± 5 Ma*** . Low Th/U ratio (0,02-0,09) peak age in 1137 ± 9 Ma** (n=4, rim or overgrowth of zircon around detritic core). Youngest peak age in 1019 ± 15 Ma*** (n=5, Th/U=0,14-0,21)	Maximum sedimentation age in 1241 ± 7.5 Ma*. High-grade metamorphism age in 1137 ± 9 Ma**. Another late metamorphic recrystallization or migmatization phase in 1019 ± 5 Ma***	This work
High-grade trondhjemitic gneiss (sample MQ-122)	S 11°59'33" W 61°58'09"	U-Pb LA-ICP-MS zircon	1127.6 ± 2.3 Ma* (n=12, concordia age), 1121.6 ± 5.9 Ma (n=27, upper intercept)	Precise crystallization age (*)	This work
Anatexite granite lens in paragneiss (sample MQ-146B)	S 12°00'23" W 61°51'23"	U-Pb LA-ICP-MS zircon	Ages between 1559 and 986 Ma. Concordia age in 1137.7 ± 4.7 Ma* (n=3, Th/U=0,1-0,3) and discordia age in 1011.3 ± 9.6 Ma** (n=11, Th/U=0,01-0,03)	Inherited zircons (*) and crystallization age (**)	This work
São Felipe Complex					
Fine-grained dark banded gneiss with granitic leucosome (sample GR336)	S 12°00'23" W 61°27'29"	U-Pb LA-ICP-MS zircon	Ages peaks in 1512 Ma (n=4); 1420 Ma (n=1), 1337 Ma* (n=8) and 1068 ± 20 Ma** (n=2)	Maximum sedimentation age in 1337 Ma (*) and migmatization age (granitic leucosome) in 1068 Ma (**)	Rizzotto et al. (2014)
Migmatic gneiss (GB-611)	S 11°56'31" W 61°31'49"	U-Pb SHRIMP zircon	1552 ± 4 Ma* (n=7, concordia age), 1328 ± 12 Ma** (n=2, rim with low Th/U ratio, weighted average age)	Crystallization age (*) and Later metamorphism age	Trindade Neto et al. (2018)
Coarse-grained tonalitic orthogneiss (GR-337) with granitic dike	S 12°00'31" W 61°28'32"	U-Pb LA-ICP-MS zircon	1435 ± 2 Ma* zr (n=6, low Th/U, intercept age) and 1012 ± 22 Ma* cas (weighted average age)	Metamorphic age (*) and weighted average ²⁰⁷ Pb/ ²⁰⁶ Pb ages of granitic dike**	Rizzotto et al. (2013)

Target minerals: bio=biotite (plateau age), bio*=biotite (total gas age), hb=hornblende (plateau age), hb*=hornblende (total gas age), m=monazite, ti=titanite, ru=rutile, zr=zircon, cas=cassiterite, * and (**) = correlation of the age with interpretation, n=number of crystals or grains analyzed. SIRGAS 2000 is the reference Datum of the geographics coordinates of the samples. Ma - Millions of Years and Ga - Billions of Years.

282 4. Analytical methods

283

284 The field works consisted of systematic mapping at the 1:100,000 scale and in the field
285 detailing of areas of geological interest. Systematic profiles involving detailed description of
286 outcrops and sampling for U-Pb geochronological analysis were developed. Seven samples of the
287 Rio Branco domain were collected and analyzed (Fig. 2). The samples (~8 kg of metasedimentary
288 or felsic rock, ~20-30 kg of metamafic lithotypes) were prepared in the laboratories of CPRM-
289 Geological Survey of Brazil in Porto Velho and Belém. Samples were initially crushed, after
290 processed in the Frantz magnetic separator and subjected to densimetric separation in dense liquids.
291 Zircon crystals were separated and mounted on adhesive tape and after embedded in epoxy resin. In
292 order to identify internal structures, mounts were imaged by backscattered electrons (BSE) in the
293 scanning electron microscope (SEM) at the laboratory of the Geochronology Center of the Institute
294 of Geosciences of the University of Brasilia (Geocron-IG/UnB). The U-Pb (LA-ICP-MS) zircon
295 isotopic data were obtained at the same Center and followed the analytical procedure described by
296 Böhn et al. (2009). Before LA-ICP-MS analyses, mounts were cleaned by rinsing with dilute HNO₃
297 (2%). Once fully dry, the samples were mounted together with GJ1 standard zircon (Jackson et al.,
298 2004) in a specially adapted laser cell and loaded into a New Wave UP213 Nd:YAG laser (213 nm),
299 linked to a Thermo Finnigan Neptune Multi-collector ICP-MS. Helium was used as the carrier gas
300 and mixed with argon before entering the ICP. The laser was run at a frequency of 10 Hz. Pb isotopes
301 ²⁰⁴Pb and ²⁰⁷Pb were collected with ion counters; ²³⁸U and ²⁰⁶Pb were analyzed on a Faraday cup. The
302 content of ²⁰²Hg was monitored on an ion counter for correction of the isobaric interference between
303 ²⁰⁴Hg and ²⁰⁴Pb. The signals during ablation were taken in 40 cycles of 1 sec each. For data
304 evaluation, only coherent intervals of signal response were considered. Data reduction was
305 performed with an Excel spreadsheet developed by Geocron-IG/UnB technicians, which considers
306 blank values, zircon standards composition and error propagation. The ²⁰⁴Pb signal intensity was
307 calculated using a natural ²⁰²Hg/²⁰⁴Hg ratio of 4.346. Common-Pb correction was applied for zircon
308 grains with ²⁰⁶Pb/²⁰⁴Pb lower than 1000, applying a common lead composition following the Stacey
309 and Kramers (1975) model. Plotting of U-Pb data was performed by ISOPLOT v. 4.15 (Ludwig,
310 2003). Errors for isotopic ratios are presented at the 1σ level. For the calculation of age integrated
311 diagrams, only > 90% concordance grains or crystal to paraderived rocks and > 95% concordance
312 to orthoderived rocks were considered.

313

314 5. Results - New field geological data

315

316 5.1 The high-grade metamorphic rocks of Rio Branco Formation

317

318 In the study area, the Rio Branco Formation constitutes a high-grade metavolcanic-
319 sedimentary unit. It consists of calc-silicate gneisses, biotite paragneisses, trondhjemitic gneisses,
320 lenses of fine- to medium-grained amphibolites, as well as pelitic and mafic granulites (Fig. 3).
321 These rocks form an E-W oriented belt marked by E-W trending compositional banding dipping at
322 a high angle to N or S. Folds and late shear zones were observed in the lithological set of this
323 formation (Figs. 3A, 4A, 4B, 4C). In the outcrops, gneissic rocks are grayish-green and whitish,
324 fine- to medium-grained, non-magnetic, banded or locally massive. In the banded calc-silicate
325 gneisses, there is alternation between clear centimetric bands formed of plagioclase and subordinate
326 quartz and dark centimetric bands formed of hornblende, diopside, garnet and titanite (Figs. 3C, 3D,
327 3E). Massive calc-silicates are light green to locally white, medium-grained, and dominantly
328 composed of plagioclase, containing epidote and amphibole as varietal minerals and garnet as
329 accessory. Some calc-silicate gneisses are composed dominantly of plagioclase rimmed by garnet
330 may suggest a dehydration reaction. Porphyroblastic, symplectitic textures with intergrowths of
331 cordierite and hornblende around subhedral garnet cores and local reaction coronae between
332 diopside cores and plagioclase rims with hornblende intergrowths are common in these rocks.
333 Reaction coronas and simplectectites provide useful information about PT conditions during high-

334 grade metamorphism, however, detailed studies are necessary to understand the metamorphic
 335 conditions in which the Rio Branco Formation rocks were submitted, as well as the mineralogical
 336 reactions that occurred during the exhumation process.

337

338

339

340

341

342

343

344

345

346

347

348

349

350

351

352

353

354

355

356

357

358

359

360

361

362

363

364

365

366

367

368

369

370

371

372

373

374

375

376

377

378

379

380

381

382

383

384

385

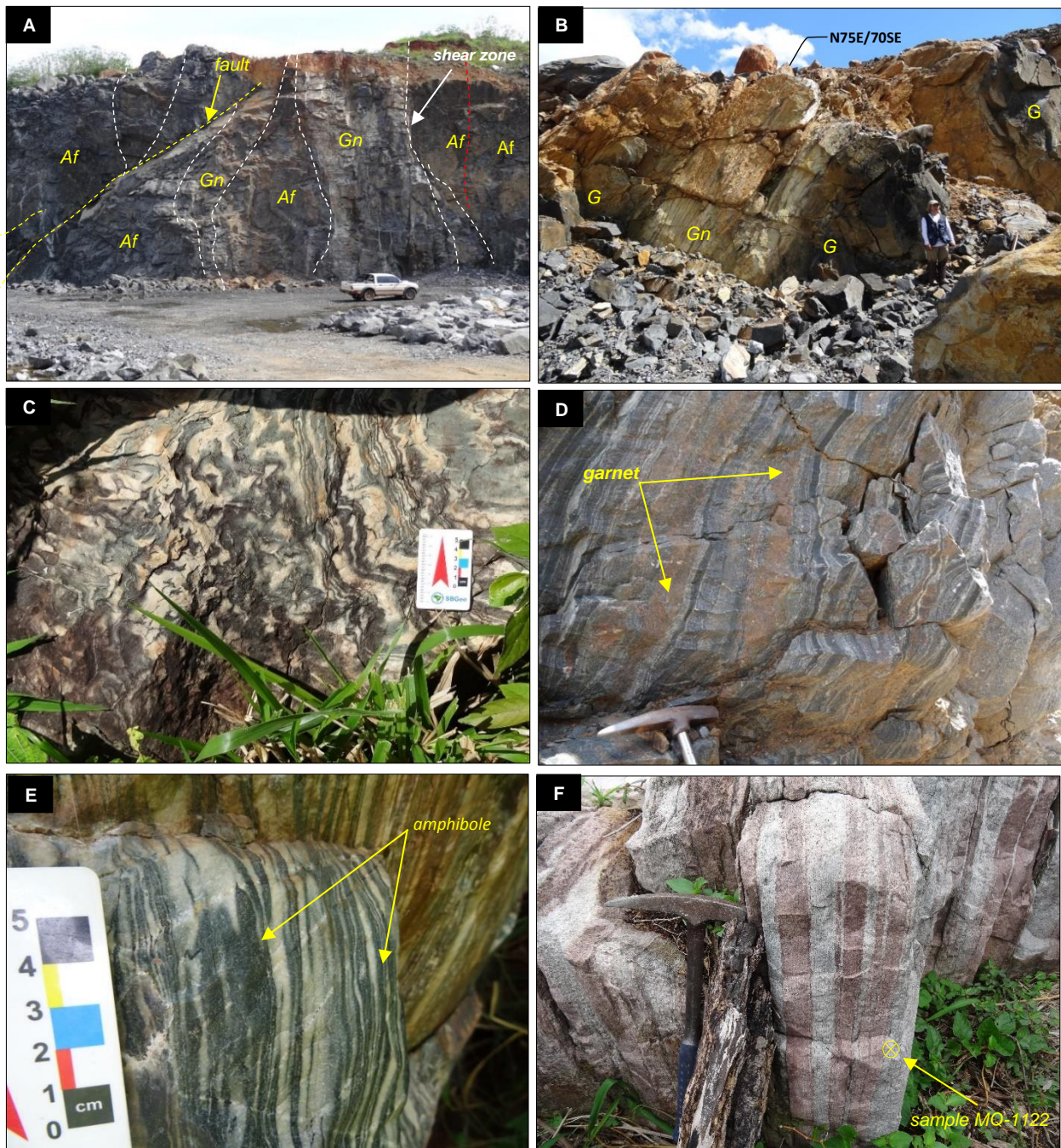
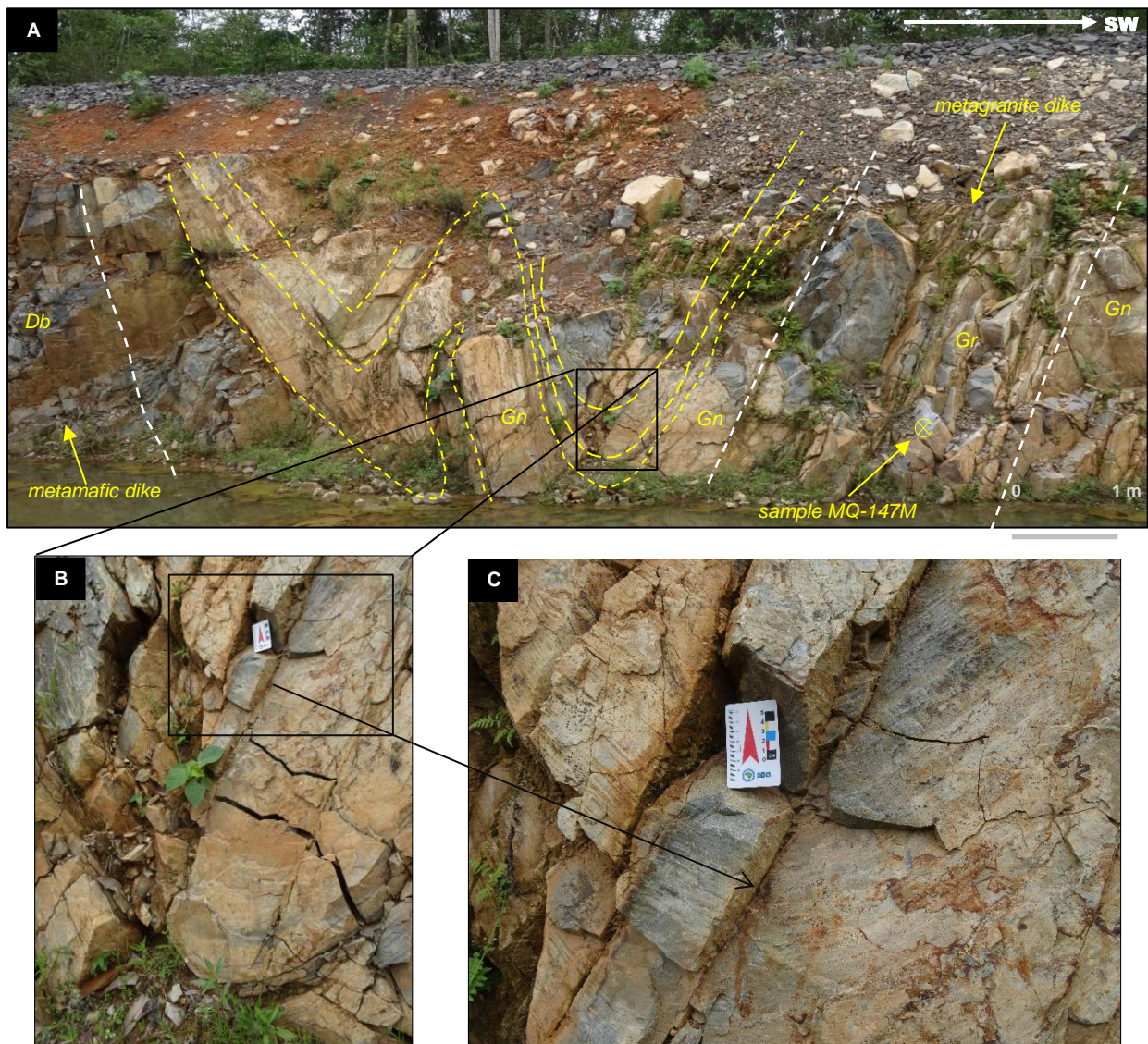


Fig. 3. Field aspect of high-grade metasedimentary rocks of the Rio Branco Formation and related metamafic rocks. (A) calc-silicate gneisses (Gn) with fine-grained amphibolite lenses (Af) in outcrop located in a quarry south of Alta Floresta d'Oeste. (B) general aspects of intercalation of calc-silicate gneisses (Gn) with granulite lens (G) in outcrop 5 km to the south of Alta Floresta d'Oeste. (C) calc-silicate gneiss (B). (D) calc-silicate gneiss with garnet-rich bands. (E) calc-silicate gneiss with intercalation of amphibole-rich bands and quartz-plagioclase-rich bands. (F) trondhjemitic gneiss (dated by U-Pb in this work).

386
387
388
389
390
391
392
393
394
395
396
397
398
399
400
401
402
403
404
405
406
407
408
409
410
411
412
413
414
415
416
417
418



419 **Fig. 4.** Outcrop located at the Cachimbo Alto Hydroelectric to the west of Alta Floresta d'Oeste. (A)
420 general aspect of calc-silicate folded gneiss (Gn) of the Rio Branco Formation, cut by metadiabase
421 dikes (Db) and metagranite dikes (Gr) of the Rio Branco Suite. (B) detail of the apical zone of the
422 largest fold in calc-silicate gneiss. (C) detail of (B). Yellow traces = banding and foliation, white
423 traces = contacts of the dikes. Sample MQ-147M of this outcrop was dated by U-Pb in this work.

424
425 Amphibolite lenses and mafic granulites bodies occur intercalated with high-grade
426 metasedimentary rocks (Figs. 3A, 3B). Amphibolites were found mainly along the shear zones and
427 are dark gray, medium- to fine-grained, and moderately to strongly magnetic, with nematoblastic,
428 foliated and mylonitic textures. The amphibolites are composed essentially of hornblende and
429 plagioclase, with diopside and orthopyroxene relics, secondary actinolite, opaque minerals and
430 titanite as accessory phases and clay minerals, chlorite and biotite as hydrothermal alteration
431 minerals. The mafic granulites occur locally in cores preserved or unaffected by shear, and are
432 composed mainly of curved plagioclase, diopside, curved orthopyroxene and opaque minerals.
433 Metamorphic history needs to be better evaluated in later studies. In some places, sulfides occur in
434 lenses and fractures filled by massive aggregates or disseminations of fine-grained sulfides

435 (pyrrhotite, pyrite, chalcopyrite and subordinate bornite) within amphibolites and calc-silicate
436 gneisses.

437 Three samples from the Rio Branco Formation were selected for LA-ICP-MS U-Pb zircon
438 dating and represent, respectively, a high-grade calc-silicate gneisses (samples MQ-44), high-grade
439 trondhjemitic gneiss (MQ-122) and anatectic granite (sample MQ-146B). Isotopic data of these
440 samples are reported in sections 6.1 and 6.4.

441

442 5.2 The Rio Branco Suite (mafic-felsic magmatism)

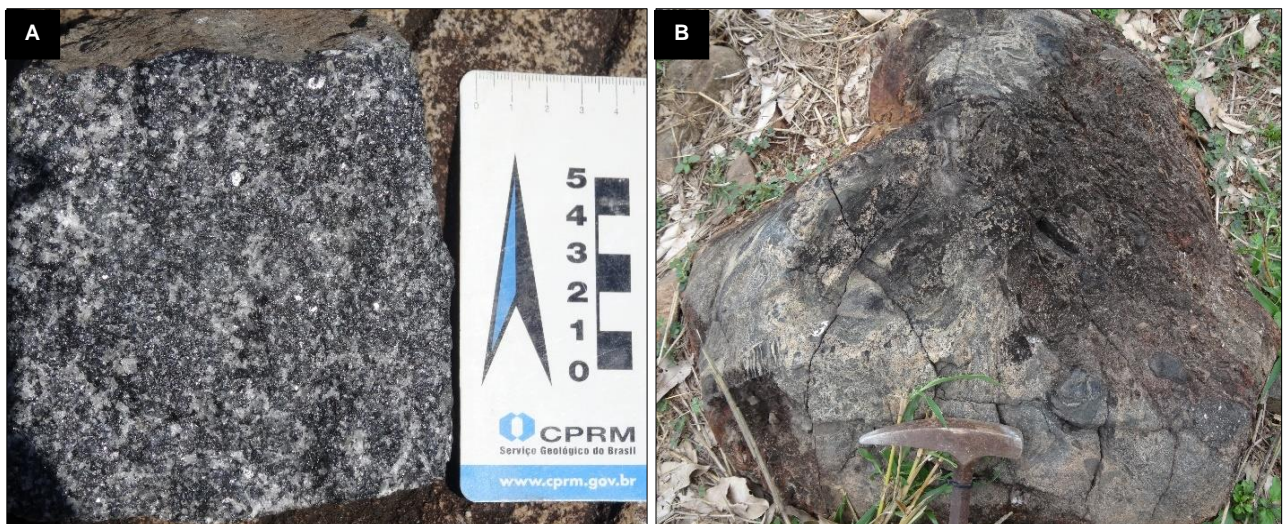
443

444 This association of igneous rocks was first named as Rio Branco Suite (Rizzotto, 1999),
445 corresponding to mafic-felsic magmatism that occurs in the form of elongated stocks and planar
446 massive bodies (sills and dike swarms), intrusive in high-grade metasedimentary rocks of the Rio
447 Branco Formation. Usually present different intensity of deformation in rocks that ranging from
448 isotropic, foliated or banded, locally migmatized.

449 The metamafic rocks of plutonic origin are locally deformed, but often exhibit preserved
450 mineralogy and igneous textures except in the portions affected by shear. Petrographic classification
451 of the Rio Branco Suite rocks revealed metagabbros, olivine metagabbros, coronitic metagabbros
452 and metagabbronorites, with subordinate metatroctolites and medium to fine-grained amphibolites
453 in the most deformed portions of bodies. Metagabbros are predominantly and exhibits dark gray
454 color, coarse- to medium-grained, moderately magnetic, and massive or slightly foliated. They are
455 formed essentially of plagioclase, clinopyroxene (diopside) and orthopyroxene, opaque minerals and
456 titanite as accessories, and clay minerals, hornblende, biotite and sericite as secondary minerals (Fig.
457 5A). At the contact between paragneisses of the Rio Branco Formation and gabbros of the Rio
458 Branco Suite hybrid rocks containing altered amphibolite xenoliths (chloritized/epidotized) occur,
459 evidencing an intrusion relationship (Fig. 5B). Locally within the metagabbros occur magmatic
460 breccias composed of angular fragments of mafic rocks surrounded by felsic materials (granitic or
461 trondhjemitic in composition) composed of feldspar, quartz and amphibole. Sample MQ-117,
462 corresponding to a metagabbro, was selected for U-Pb dating by LA-ICP-MS and the isotopic data
463 are reported in section 6.2.

464

465



466

467 **Fig. 5.** Field aspect of the rocks of Rio Branco Suite. (A) medium-grained massive metagabbro and (B)
468 metagabbro with xenoliths of calc-silicate gneiss.

469

470

471 The plutonic to subvolcanic felsic-mafic rocks (dikes, sills and elongated bodies) consist of
472 fine-grained foliated metagranites, metavolcanic felsic rocks, fine-grained metagabbros, massive
473 metabasalts, metadiabases and fine-grained amphibolites, generally trending EW, NW-SE and
474 NE-SW. The fine-grained metagabbros and metadiabases are grayish-green in color, varying from
475 fine-grained to aphanitic, representing several generations of parallel dikes, with thicknesses
476 ranging from 15 to 30 centimeters. They are magnetic to nonmagnetic and are concordant and/or
477 discordant with the regional structure. The volcanic felsic-mafic rocks consist of massive
478 metabasalts and massive fine-grained amphibolites present dark-gray color and are locally
479 magnetic. They are composed of plagioclase phenocrysts and magnetite in a fine-grained foliated
480 matrix with preserved subofitic texture. This set mafic rock occur spatially associated with felsic
481 igneous rocks of granitic and trondhjemitic composition (Rizzotto et al., 2009), with medium- to
482 fine-grained equigranular texture, foliated when deformed and pink in color. This mafic and felsic
483 set is interdigitated and mixed, suggesting temporal coexistence where the mafic and felsic bands
484 interdigitate (coeval magmatism), and their contacts are oriented according to the regional foliation
485 trend, following a N80°W trend with a high-angle to subvertical dip (Figs. 6A, B, C, D). In these
486 metamafic-metafelsic rocks, it is common the occurrence of high-angle transpressive shear zones,
487 observed mainly along the outcrops in the Cachimbo Alto Hydroelectric spillway (Fig. 6A).

488 In outcrop located at Cachimbo Alto Waterfall, three generations of metamafic dikes were
489 defined based on field relations, called M1, M2 and M3 (Fig. 7). Based on field relationships, M1
490 dike corresponds to the oldest pulse and characterized by foliated, fine-grained non-magnetic
491 amphibolites. M2 dike differs from M1 due to its magnetic signature and corresponds to an
492 intermediary pulse. M3 dike consists of a medium-grained, slightly foliated non-magnetic
493 amphibolite with plagioclase phenocrysts.

494 The elongated felsic stocks of the Rio Branco Suite are represented by gray-red porphyritic
495 biotite metagranite, which vary from protomylonites to mylonites along the shear zones (Fig. 8A,
496 B). Two samples were selected for LA-ICP-MS U-Pb zircon analysis: sample MQ-147M is from a
497 foliated granite dike intruded in high-grade calc-silicate gneiss of the Rio Branco Formation from
498 the spillway of the Cachimbo Alto hydroelectric dam (Fig. 4A, sampling location). Sample MQ-
499 124 is a fine-grained subvolcanic metagranite intruded in metamafic rocks, from an outcrop along
500 the Linha-45 road (Fig. 8C). The locations of the samples can be observe in figure 4 and the isotopic
501 data of these samples are presented in section 6.3.

502 The metatrandhjemitites occur in association with metamafic rocks and appear in the form of
503 small elongated bodies, lenses (<500 m) or dikes, sub concordant with the regional structure. They
504 are banded or foliated types, usually leucocratic and fine- to medium-grained, composed mainly of
505 quartz and saussuritized plagioclase, and subordinately of amphibole, clinopyroxene, titanite,
506 magnetite and zircon (Fig. 8D). Sample MQ-29 of medium-grained leucocratic metatrandhjemite
507 was selected for dating by the LA-ICP-MS zircon U-Pb method. The isotopic data of this sample
508 are described in section 6.3.

509

510 **5.3 Rio Pardo Suite (post-tectonic magmatism)**

511

512 In the study area, felsic rocks are represented by post-tectonic granites (ages 1.02-1.00 Ga),
513 intrusive in metasedimentary rocks of the Nova Brasilândia Group. These granites occur as elliptic
514 and elongated bodies in the direction of the regional E-W or NW-SE foliation trend. The suite
515 consists of monzogranites, syenogranites and rare aplitic dikes, as well as veins and pockets of
516 associated pegmatites. In general, they are isotropic to foliated rocks, locally mylonitized (augen
517 gneiss) and banded (gneiss).

518 These leucocratic to mesocratic rocks range from pink to gray, coarse- to medium-grained
519 showing equigranular or porphyritic textures. In the Rio Branco domain, there is an elongated body
520 of the Rio Pardo Suite intruded in calc-silicate gneiss of the Rio Branco Formation, and metamafic
521 rocks of the Rio Branco Suite.

522

523
524
525
526
527
528
529
530
531
532
533
534
535
536
537
538
539
540
541
542
543
544
545
546
547
548
549
550
551
552
553
554
555
556
557
558
559
560
561
562
563
564
565
566
567
568
569
570
571
572
573

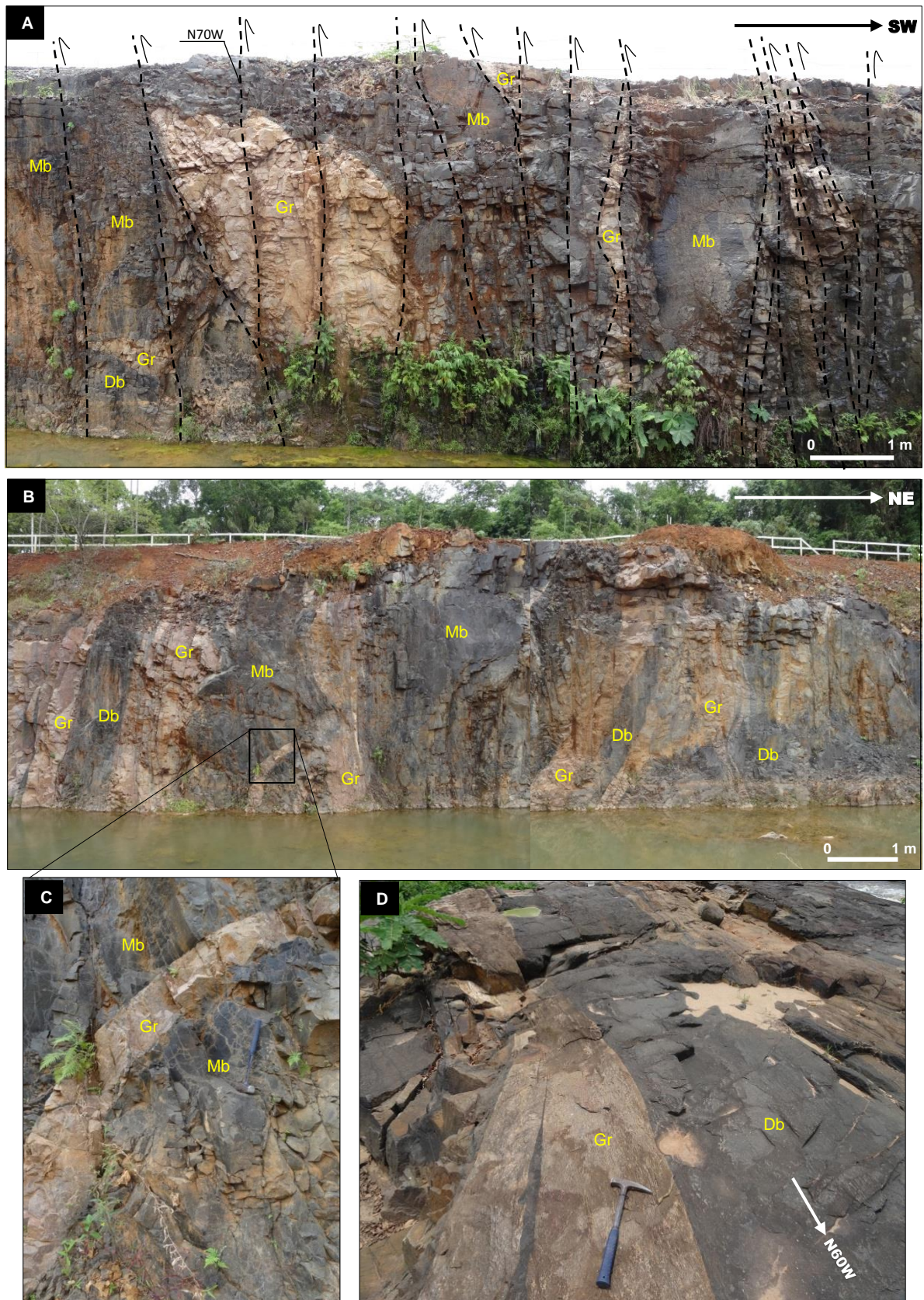
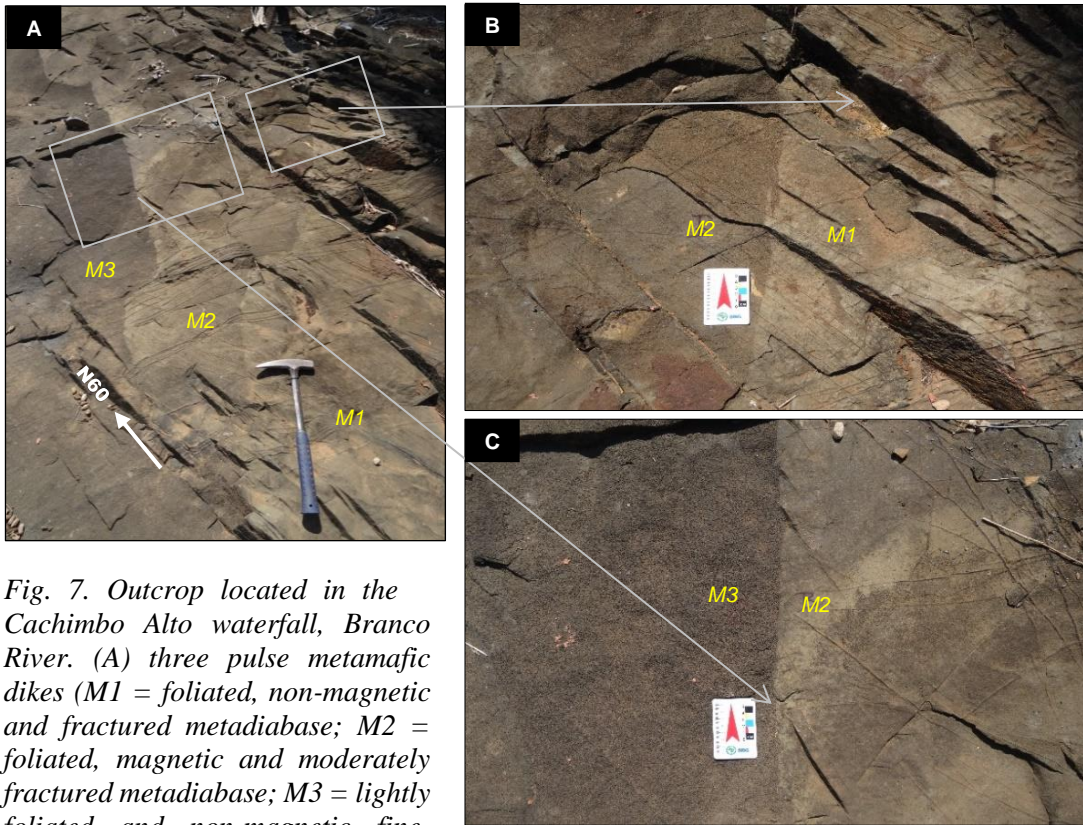


Fig. 6. (A) and (B) field general aspects of the spatial relations of multiple intrusion of dikes and coeval magmatic activity between foliated metabasalt (Mb), foliated metagranite (Gr) and metadiabase (Db), of the Rio Branco Suite. (C) detail of metagranite dike cutting metadiabase. (D) Detail in plan showing the contact relation between metadiabase and metagranite dikes. Black traces in (A) mark transpressive shear zones.



574 *Fig. 7. Outcrop located in the*
 575 *Cachimbo Alto waterfall, Branco*
 576 *River. (A) three pulse metamorphic*
 577 *dikes (M1 = foliated, non-magnetic*
 578 *and fractured metadiabase; M2 =*
 579 *foliated, magnetic and moderately*
 580 *fractured metadiabase; M3 = lightly*
 581 *foliated and non-magnetic fine-*
 582 *grained metagabbro). (B) and (C) field details of intrusive contact between dikes.*
 583

584
 585
 586
 587
 588
 589
 590
 591
 592
 593
 594
 595
 596
 597
 598
 599
 600
 601
 602
 603
 604
 605
 606
 607
 608
 609
 610
 611



Fig. 8. Field aspect in (A) porphyritic biotite metagranite, (B) intrusive contact between calc-silicate gneisse (Gn) and metagranite (Gr), (C) subvolcanic porphyritic metagranite (sample MQ-124), and (D) foliated metatrandhjemite (sample MQ-29).

612 **6. Results - LA-ICP-MS zircon U-Pb analysis**

613
614 Below, we will present zircon LA-ICP-MS U-Pb analytical results of the seven samples of
615 the Rio Branco domain from outcrops located to the south and west of Alta Floresta d'Oeste and
616 Santa Luzia d'Oeste (Table 2). The selected samples included high-grade calc-silicate gneiss
617 (sample MQ-44), high-grade trondhjemitic gneiss (sample MQ-122), metagabbro (sample MQ-
618 117), metagranite dike (sample MQ-147M), felsic subvolcanic rock/metagranite (Sample MQ-124),
619 metatrandhjemitic (sample MQ-29) and anatectic granite (sample MQ-146B) (Fig. 2).

621 **6.1 High-grade metamorphic rocks (Rio Branco Formation)**

622
623 Sample MQ-44 (S11°58'30"/W61°46'59") is a high-grade calc-silicate gneiss that occurs
624 associated with metamafic rocks. Zircon grains from this sample mostly ranges from 50 to 350 μm ,
625 some grains with core and rim features (Fig. 9). Internally, the crystals present a pattern of radial
626 and concentric fractures, where the radial fractures start at the central margin of the core and
627 propagate to the outermost layers of the grains (Fig. 9, crystal D). Based on BSE images, sixty-four
628 points located on the core and rims of zircon crystals were selected for analysis with the interest of
629 identifying the ages of the overgrowth phases. Of these, fifty-six zircon crystals (zircons data in
630 normal black font style, sample MQ-44, Table 2) were analyzed and presented concordance $> 90\%$
631 (Fig. 10A, B) and were used in the Concordia diagram and probability density plot (PDP) (Fig.
632 10B). These zircon crystals present Th/U ratios ranging from 0.02 to 0.38 and ages between 1575
633 Ma and 1012 Ma. In this sample, a group of small homogeneous zircon grains ($< 100\ \mu\text{m}$),
634 subrounded to elliptical, has Th/U ratios < 0.10 . Another group of larger zircon grains (100-270 μm)
635 presents core and rims and tends to be prismatic with smoothly rounded contours, exhibiting
636 luminescent rims and low Th/U ratios from 0.02 to 0.09. Isotopic data from the first group and rims
637 of the second group (ages 1123 to 1181 Ma, see Fig. 9A, 9G) were used to calculate the Concordia
638 age of $1137 \pm 9\ \text{Ma}$ ($n=4$, MSWD=0.61), interpreted as the age of the high-grade metamorphism
639 that affected the calc-silicate gneisses of the Rio Branco Formation (Figs. 9B, G, I, J, 10B). Zircon
640 core analyses provide Th/U ratios between 0.10 and 0.38 and $^{207}\text{Pb}/^{206}\text{Pb}$ ages that define major
641 peaks at approximately 1575, 1480 Ma, 1432 Ma, 1386 Ma and 1241 Ma (Fig. 10B). These isotopic
642 results are considered the ages of the main source areas of the Rio Branco Formation sedimentary
643 protoliths (Figs. 9A, 9B, 9C, 9D, 9E, 9F, 9G, 9H). The $^{207}\text{Pb}/^{206}\text{Pb}$ age of $1241 \pm 7.5\ \text{Ma}$ is
644 interpreted as possible maximum age of the sedimentation of the Rio Branco Formation protoliths
645 and $1137 \pm 9\ \text{Ma}$ age is interpreted as the age of high-grade metamorphism (granulitic) (Fig. 10B).
646 Detailed work is still need to define sedimentation and metamorphism precise ages.

647 In the sample MQ-44, some larger concordant zircon fragments (sizes 100-200 μm) are
648 homogeneous, locally fractured, partially recrystallized and have Th/U ratios between 0.14 and 0.21.
649 Data from these zircon fragments allowed the calculation of the Concordia age of $1019 \pm 15\ \text{Ma}$ (n
650 $= 5$), preliminarily interpreted as the age of metamorphic recrystallization or migmatization (partial
651 fusion) and possibly associated with a younger metamorphic pulse (Fig. 10A, B). Alternatively, can
652 represent an age from contamination by granitic vein injections (Fig. 9K, L, M).

653 Sample MQ-122 (S11°59'33"/W61°58'09") is a high-grade trondhjemitic gneiss light-
654 colored, fine-grained, banded, occurring in the form of lenses spatially associate with mafic
655 granulites. The essential mineralogy is saussuritized plagioclase and quartz, additionally magnetite,
656 amphibole, titanite, zircon and epidote. The texture is granoblastic with polygonal contacts. The
657 zircon crystals extracted from this sample are euhedral to subhedral short prisms with slightly
658 rounded extremities, sizes ranging from 80 to 200 μm , containing some inclusions and fractures.
659 BSE images show discrete to well-marked oscillatory zoning, but some crystals or overgrowths have
660 many irregular luminescent places, profusion of inclusions and radial or irregular fractures. From
661 sample MQ-122, thirty-six zircon crystals were analyzed (Table 2, sample MQ-122).

662
663

664
665
666
667
668

Table 2.

LA-ICP-MS U-Pb zircon isotopic data from seven rock samples of the Rio Branco domain, Nova Brasilândia belt in southwest Amazonian Craton, Rondônia.

Identifier	Th/U	f206 (%)	²⁰⁷ Pb/ ²⁰⁶ Pb	1σ %	Radiogenic ratios					Ages ⁵					% U-Pb disc ⁴	
					²⁰⁷ Pb/ ²³⁵ U	1σ %	²⁰⁶ Pb/ ²³⁸ U	1σ %	Rho	²⁰⁷ Pb/ ²⁰⁶ Pb	2σ abs	²⁰⁶ Pb/ ²³⁸ U	2σ abs	²⁰⁷ Pb/ ²³⁵ U		2σ abs
Rio Branco Formation, high-grade calc-silicate gneisse (sample MQ-44)																
047-ZR33	0.10	0.0480	0.07706	1.31	2.040	2.02	0.1919	1.50	0.74	1123	52	1132	31	1129	27	-0.81
074-ZR53B	0.08	0.0663	0.07847	1.94	2.047	3.57	0.1892	2.97	0.83	1159	76	1117	61	1131	48	3.60
065-ZR47	0.02	0.0491	0.07894	1.71	2.138	2.61	0.1964	1.93	0.74	1171	67	1156	41	1161	36	1.24
057-ZR41	0.08	0.0805	0.07934	2.56	2.051	3.70	0.1875	2.65	0.72	1181	99	1108	54	1133	50	6.18
046-ZR32B	0.08	0.0143	0.07881	0.76	2.067	1.30	0.1902	0.99	0.76	1167	30	1123	20	1138	18	3.84
006-ZR04	0.05	0.0223	0.07862	1.07	1.930	2.78	0.1780	2.54	0.91	1163	42	1056	49	1092	37	9.15
038-ZR28	0.06	0.0024	0.08127	0.62	2.346	1.07	0.2094	0.78	0.73	1228	24	1225	17	1226	15	0.20
064-ZR46	0.09	0.0080	0.08917	0.71	2.959	1.69	0.2407	1.49	0.88	1408	27	1390	37	1397	25	1.25
016-ZR11B	0.08	0.0019	0.09225	0.41	3.472	1.18	0.2730	1.05	0.89	1472	15	1556	29	1521	19	-5.67
035-ZR25	0.09	0.0206	0.09739	1.32	3.755	2.96	0.2796	2.63	0.89	1575	49	1590	74	1583	47	-0.94
023-ZR16	0.14	0.0223	0.07293	0.85	1.667	1.32	0.1658	0.93	0.71	1012	34	989	17	996	17	2.28
026-ZR18	0.19	0.0385	0.07322	1.10	1.745	1.67	0.1728	1.20	0.72	1020	44	1028	23	1025	21	-0.75
019-ZR14	0.20	0.0306	0.07364	1.08	1.754	1.81	0.1728	1.40	0.77	1032	43	1027	27	1029	23	0.41
077-ZR56	0.22	0.0366	0.07383	1.01	1.739	1.57	0.1708	1.14	0.73	1037	40	1017	22	1023	20	1.96
075-ZR54	0.22	0.0240	0.07469	0.72	1.792	1.29	0.1740	1.00	0.78	1060	29	1034	19	1043	17	2.46
040-ZR30	0.21	0.0062	0.07579	0.79	1.928	1.44	0.1844	1.14	0.79	1090	32	1091	23	1091	19	-0.15
054-ZR38	0.15	0.0296	0.07612	1.05	1.916	1.80	0.1825	1.42	0.79	1098	42	1081	28	1087	24	1.59
010-ZR08	0.13	0.0068	0.07710	0.61	2.072	1.14	0.1949	0.90	0.78	1124	24	1148	19	1140	16	-2.12
029-ZR21	0.17	0.0093	0.07764	0.79	2.056	1.21	0.1921	0.84	0.69	1138	31	1133	17	1134	16	0.45
008-ZR06	0.14	0.0096	0.07765	0.61	2.086	1.10	0.1948	0.84	0.76	1138	24	1148	18	1144	15	-0.84
066-ZR48	0.18	0.0288	0.07807	0.98	2.140	1.67	0.1988	1.30	0.78	1149	39	1169	28	1162	23	-1.77
079-ZR58	0.11	0.0514	0.08027	2.06	2.098	3.13	0.1895	2.33	0.75	1204	80	1119	48	1148	43	7.04
027-ZR19	0.15	0.0081	0.08166	0.76	2.390	1.92	0.2123	1.73	0.90	1237	30	1241	39	1240	27	-0.28
048-ZR34	0.14	0.0144	0.08192	0.74	2.399	1.28	0.2123	0.98	0.76	1244	29	1241	22	1242	18	0.18
017-ZR12	0.10	0.0192	0.08213	0.73	2.267	1.25	0.2002	0.94	0.75	1249	28	1176	20	1202	17	5.79
033-ZR23	0.11	0.0591	0.08304	1.77	2.610	2.53	0.2280	1.77	0.70	1270	68	1324	42	1304	37	-4.24
004-ZR02	0.17	0.0113	0.08417	0.73	2.496	1.17	0.2151	0.83	0.71	1296	28	1256	19	1271	17	3.14
049-ZR35	0.23	0.0282	0.08454	0.66	2.577	1.14	0.2211	0.85	0.75	1305	26	1287	20	1294	17	1.35
003-ZR01	0.13	0.0065	0.08558	0.59	2.579	1.26	0.2185	1.05	0.83	1329	23	1274	24	1295	18	4.11
056-ZR40	0.11	0.0184	0.08573	0.80	2.577	1.19	0.2180	0.80	0.67	1332	31	1271	18	1294	17	4.56
067-ZR49	0.18	0.0178	0.08631	0.74	2.668	1.42	0.2242	1.16	0.81	1345	28	1304	27	1320	21	3.08
078-ZR57	0.22	0.0021	0.08646	0.59	2.860	1.25	0.2399	1.03	0.83	1348	23	1386	26	1371	19	-2.78
014-ZR10	0.15	0.0124	0.08754	0.61	2.726	0.98	0.2258	0.68	0.69	1372	23	1312	16	1335	15	4.37
076-ZR55	0.16	0.0306	0.08782	0.87	2.865	1.70	0.2366	1.41	0.83	1379	33	1369	35	1373	25	0.71
055-ZR39	0.11	0.0173	0.08800	0.94	2.811	1.42	0.2316	1.01	0.71	1383	36	1343	24	1358	21	2.86
059-ZR43	0.13	0.0118	0.08800	0.75	2.813	1.18	0.2318	0.82	0.70	1383	29	1344	20	1359	18	2.80
013-ZR09	0.12	0.0198	0.08813	0.99	2.680	1.59	0.2206	1.19	0.75	1385	38	1285	28	1323	23	7.26
009-ZR07	0.10	0.0198	0.08825	1.06	2.936	1.69	0.2413	1.26	0.75	1388	41	1393	32	1391	25	-0.39
005-ZR03	0.19	0.0287	0.08841	0.82	2.998	1.28	0.2459	0.91	0.71	1392	31	1417	23	1407	19	-1.86
034-ZR24	0.12	0.0281	0.08873	1.07	2.760	1.64	0.2256	1.19	0.73	1398	41	1311	28	1345	24	6.23
036-ZR26	0.11	0.0169	0.08909	0.80	2.874	1.35	0.2340	1.03	0.76	1406	30	1355	25	1375	20	3.61
073-ZR53N	0.18	0.0017	0.09016	0.58	3.314	1.03	0.2665	0.77	0.74	1429	22	1523	21	1484	16	-6.59
007-ZR05	0.18	0.0028	0.09023	0.40	3.066	0.80	0.2465	0.59	0.73	1430	15	1420	15	1424	12	0.71
060-ZR44	0.28	0.0016	0.09101	0.77	3.296	1.42	0.2627	1.13	0.80	1447	29	1503	30	1480	22	-3.92
024-ZR17N	0.15	0.0062	0.09123	0.73	3.110	1.12	0.2472	0.77	0.69	1451	28	1424	20	1435	17	1.89
080-ZR59	0.38	0.0008	0.09136	0.75	3.424	1.22	0.2718	0.89	0.73	1454	28	1550	25	1510	19	-6.60
063-ZR45	0.13	0.0170	0.09254	0.98	3.162	1.62	0.2478	1.23	0.76	1478	37	1427	31	1448	25	3.48
053-ZR37	0.17	0.0031	0.09267	0.69	3.483	1.11	0.2726	0.78	0.71	1481	26	1554	22	1523	17	-4.91
043-ZR31N	0.13	0.0050	0.09267	0.62	3.317	1.24	0.2595	1.01	0.82	1481	23	1487	27	1485	19	-0.42
058-ZR42	0.19	0.0165	0.09281	0.80	3.265	1.27	0.2551	0.92	0.72	1484	30	1465	24	1473	20	1.29
028-ZR20	0.12	0.0349	0.09299	0.96	3.381	1.82	0.2637	1.51	0.83	1488	36	1509	40	1500	28	-1.43
030-ZR22	0.27	0.0035	0.09313	0.79	3.703	1.19	0.2883	0.81	0.68	1491	30	1633	23	1572	19	-9.57
018-ZR13	0.11	0.0085	0.09326	0.65	3.384	1.15	0.2632	0.88	0.76	1493	25	1506	24	1501	18	-0.86
045-ZR32N	0.13	0.0059	0.09364	0.51	3.436	1.05	0.2661	0.85	0.80	1501	19	1521	23	1513	17	-1.34
015-ZR11N	0.21	0.0041	0.09434	0.47	3.575	1.15	0.2748	0.98	0.85	1515	18	1565	27	1544	18	-3.32
020-ZR15	0.18	0.0078	0.09441	0.70	3.436	1.18	0.2639	0.88	0.74	1516	26	1510	24	1513	19	0.43
070-ZR52	0.09	0.0194	0.07686	1.00	2.243	1.51	0.2117	1.06	0.70	1118	40	1238	24	1195	21	-10.74
069-ZR51	0.13	0.0412	0.07149	1.81	1.848	2.77	0.1874	2.07	0.75	972	73	1107	42	1063	36	-13.98
068-ZR50	0.13	0.0674	0.07393	1.90	1.990	3.05	0.1952	2.36	0.77	1040	76	1149	50	1112	41	-10.57
044-ZR31B	0.28	0.0201	0.09804	0.62	2.797	1.61	0.2069	1.44	0.89	1587	23	1212	32	1355	24	23.63
039-ZR29	0.16	0.0112	0.08106	1.32	1.911	3.10	0.1710	2.78	0.90	1223	51	1017	52	1085	41	16.81
037-ZR27	0.13	0.0613	0.08775	1.65	2.459	2.80	0.2032	2.24	0.80	1377	63	1193	49	1260	40	13.39
025-ZR17B	0.13	0.0062	0.08651	0.53	2.152	1.51	0.1804	1.37	0.90	1350	20	1069	27	1166	21	20.77
060-ZR36	0.40	0.0648	0.08332	4.42	2.208	6.57	0.1022	4.86	0.74	4277	468	4433	400	4484	90	44.24

669
670
671
672
673
674
675

676
677
678

Continuation.

Identifier	Th/U	f206 (%)	²⁰⁷ Pb/ ²⁰⁶ Pb	1σ %	Radiogenic ratios					Ages ⁵					% U-Pb disc ⁴	
					²⁰⁷ Pb/ ²³⁵ U	1σ %	²⁰⁶ Pb/ ²³⁸ U	1σ %	Rho	²⁰⁷ Pb/ ²⁰⁶ Pb	2σ abs	²⁰⁶ Pb/ ²³⁸ U	2σ abs	²⁰⁷ Pb/ ²³⁵ U		2σ abs
Rio Branco Formation, high-grade trondhjemitic gneiss (sample MQ-122)																
053-ZR30	0.32	0.0376	0.07657	1.58	1.987	2.15	0.1882	1.41	0.66	1110	62	1111	29	1111	29	-0.14
016-ZR08B	0.21	0.0138	0.07768	0.63	2.023	1.08	0.1889	0.80	0.74	1139	25	1115	16	1123	15	2.06
048-ZR28B	0.17	0.0406	0.07762	0.46	2.032	0.97	0.1898	0.77	0.79	1137	18	1121	16	1126	13	1.46
009-ZR05B	0.37	0.1101	0.07733	0.46	2.027	1.23	0.1901	1.08	0.88	1130	18	1122	22	1125	17	0.70
046-ZR27	0.31	0.0401	0.07581	1.04	1.997	1.35	0.1910	0.77	0.57	1090	42	1127	16	1114	18	-3.39
018-ZR10	0.49	0.0339	0.07641	1.08	2.013	1.66	0.1911	1.20	0.73	1106	43	1127	25	1120	22	-1.94
028-ZR16	0.42	0.0185	0.07724	0.80	2.038	1.20	0.1913	0.81	0.68	1127	32	1129	17	1128	16	-0.10
029-ZR17N	0.24	0.0120	0.07617	0.71	2.010	1.15	0.1913	0.82	0.72	1099	28	1129	17	1119	16	-2.65
035-ZR20N	0.21	0.0095	0.07668	0.58	2.041	1.02	0.1930	0.76	0.74	1113	23	1138	16	1129	14	-2.22
039-ZR23	0.25	0.0077	0.07610	0.67	2.031	1.15	0.1935	0.86	0.75	1098	27	1140	18	1126	16	-3.88
068-ZR42	0.35	0.0126	0.07765	0.70	2.073	1.35	0.1937	1.09	0.81	1138	28	1141	23	1140	18	-0.28
024-ZR13	0.25	0.0137	0.07698	0.67	2.063	1.09	0.1944	0.77	0.71	1121	27	1145	16	1137	15	-2.17
037-ZR21	0.23	0.0120	0.07631	0.76	1.924	1.98	0.1829	1.79	0.91	1103	30	1083	36	1090	26	1.86
038-ZR22	0.23	0.0252	0.07726	0.65	1.973	1.08	0.1852	0.77	0.72	1128	26	1095	16	1106	14	2.90
069-ZR43	0.29	0.0131	0.07717	0.62	1.992	1.35	0.1872	1.14	0.84	1126	25	1106	23	1113	18	1.75
013-ZR07N	0.33	0.0201	0.07712	0.56	2.078	1.09	0.1954	0.85	0.78	1124	22	1151	18	1142	15	-2.36
025-ZR14	0.11	0.0090	0.07651	0.49	2.065	0.93	0.1957	0.70	0.75	1109	20	1152	15	1137	13	-3.95
060-ZR36	0.25	0.0369	0.07589	0.96	2.057	1.52	0.1966	1.12	0.74	1092	38	1157	24	1135	21	-5.92
023-ZR12B	0.37	0.0423	0.07713	1.26	2.092	1.90	0.1967	1.37	0.72	1125	50	1158	29	1146	26	-2.94
008-ZR05N	0.49	0.0088	0.07680	0.50	2.092	1.00	0.1975	0.78	0.78	1116	20	1162	17	1146	14	-4.12
065-ZR39	0.23	0.0056	0.07740	0.51	2.110	1.07	0.1976	0.87	0.81	1132	20	1163	18	1152	15	-2.74
043-ZR25N	0.28	0.0051	0.07617	0.57	2.076	1.11	0.1976	0.87	0.79	1100	23	1163	19	1141	15	-5.74
070-ZR44	0.24	0.0223	0.07628	0.76	2.091	1.15	0.1988	0.79	0.68	1103	30	1169	17	1146	16	-6.02
056-ZR33N	0.54	0.0147	0.07633	0.72	2.113	1.99	0.2008	1.82	0.91	1104	29	1180	39	1153	27	-6.88
040-ZR24	0.20	0.0115	0.07585	0.61	2.120	1.20	0.2026	0.97	0.80	1091	25	1190	21	1155	17	-9.01
057-ZR33B	0.30	0.0122	0.07685	0.37	2.169	1.07	0.2047	0.94	0.87	1117	15	1200	21	1171	15	-7.44
004-ZR02N	0.06	0.0030	0.07585	0.42	2.172	1.34	0.2077	1.22	0.91	1091	17	1217	27	1172	19	-11.49
049-ZR29N	0.15	0.0053	0.07863	0.50	2.120	1.23	0.1956	1.06	0.86	1163	20	1151	22	1155	17	0.98
047-ZR28N	0.61	0.0170	0.07879	0.74	2.116	1.52	0.1948	1.28	0.84	1167	29	1147	27	1154	21	1.66
005-ZR02B	0.07	0.0054	0.07517	0.36	1.995	0.84	0.1925	0.67	0.79	1073	14	1135	14	1114	11	-5.75
054-ZR31	0.32	0.0203	0.07521	0.73	1.834	1.29	0.1768	1.00	0.77	1074	29	1050	19	1058	17	2.28
063-ZR37	0.56	0.0609	0.07937	0.96	1.985	1.36	0.1813	0.90	0.66	1181	38	1074	18	1110	18	9.06
026-ZR15N	0.18	0.0730	0.07971	0.66	2.153	1.18	0.1958	0.90	0.76	1190	26	1153	19	1166	16	3.10
034-ZR19	0.18	0.0113	0.07381	0.62	1.890	1.16	0.1857	0.91	0.78	1036	25	1098	18	1078	15	-5.98
045-ZR26	0.34	0.0129	0.07990	0.76	2.087	1.40	0.1894	1.11	0.79	1194	30	1118	23	1144	19	6.39
030-ZR17B	0.12	0.0301	0.07993	0.77	2.179	1.27	0.1977	0.94	0.74	1195	30	1163	20	1174	18	2.69

Identifier	Th/U	f206 (%)	²⁰⁷ Pb/ ²⁰⁶ Pb	1σ %	Radiogenic ratios					Ages ⁵					% U-Pb disc ⁴	
					²⁰⁷ Pb/ ²³⁵ U	1σ %	²⁰⁶ Pb/ ²³⁸ U	1σ %	Rho	²⁰⁷ Pb/ ²⁰⁶ Pb	2σ abs	²⁰⁶ Pb/ ²³⁸ U	2σ abs	²⁰⁷ Pb/ ²³⁵ U		2σ abs
Rio Branco Suite, metagabbro (sample MQ-117)																
010-ZR08	0.16	0.0064	0.07259	0.86	1.717	1.30	0.1715	0.91	0.70	1003	35	1020	17	1015	17	-1.79
006-ZR04	0.18	0.0108	0.07272	0.56	1.729	0.96	0.1724	0.68	0.71	1006	23	1026	13	1019	12	-1.94
029-ZR23	0.28	0.0093	0.07296	0.74	1.702	1.15	0.1692	0.80	0.70	1013	30	1008	15	1009	15	0.50
015-ZR11	0.23	0.0081	0.07650	0.60	2.013	1.13	0.1908	0.88	0.78	1108	24	1126	18	1120	15	-1.59
019-ZR15	0.51	0.0024	0.07654	0.62	2.043	1.25	0.1936	1.01	0.81	1109	25	1141	21	1130	17	-2.86
037-ZR29	0.81	0.0009	0.07676	0.51	1.974	0.95	0.1865	0.71	0.75	1115	20	1103	14	1107	13	1.10
025-ZR19	0.05	0.0037	0.07693	0.46	2.048	0.97	0.1931	0.77	0.79	1119	18	1138	16	1132	13	-1.66
018-ZR14	0.13	0.0045	0.07710	0.64	2.002	1.10	0.1883	0.82	0.74	1124	25	1112	17	1116	15	1.02
038-ZR30	0.03	0.0042	0.07738	0.80	2.020	1.54	0.1893	1.27	0.82	1131	32	1118	26	1122	21	1.16
035-ZR27	0.34	0.0001	0.07742	0.53	2.002	0.96	0.1876	0.72	0.74	1132	21	1108	15	1116	13	2.10
033-ZR25	0.54	0.0088	0.07758	0.68	2.046	1.34	0.1913	1.09	0.81	1136	27	1128	23	1131	18	0.70
034-ZR26	0.06	0.0078	0.07666	0.59	1.923	1.09	0.1819	0.84	0.77	1112	24	1078	17	1089	15	3.13
004-ZR02	0.16	0.0065	0.07473	0.59	1.881	1.14	0.1825	0.90	0.79	1061	24	1081	18	1074	15	-1.83
013-ZR09	0.18	0.0124	0.07389	0.83	1.826	1.60	0.1793	1.32	0.82	1038	33	1063	26	1055	21	-2.36
027-ZR21	0.40	0.0039	0.07602	0.52	1.995	0.98	0.1903	0.75	0.76	1096	21	1123	15	1114	13	-2.50
017-ZR13	0.31	0.0056	0.07498	0.54	1.923	1.02	0.1860	0.78	0.77	1068	22	1100	16	1089	14	-2.99
039-ZR31	0.24	0.0158	0.07682	0.79	1.922	1.29	0.1814	0.95	0.73	1116	31	1075	19	1089	17	3.74
016-ZR12	0.21	0.0080	0.07660	0.58	2.357	1.56	0.2232	1.40	0.90	1111	23	1299	33	1230	22	-16.91
009-ZR07	0.13	0.0093	0.07628	1.69	2.209	2.47	0.2101	1.76	0.71	1102	67	1229	39	1184	34	-11.51
024-ZR18	0.41	0.0115	0.07453	0.62	2.001	1.52	0.1947	1.34	0.88	1056	25	1147	28	1116	20	-8.59
026-ZR20	0.19	0.0032	0.07599	0.54	2.096	1.24	0.2001	1.06	0.85	1095	21	1176	23	1148	17	-7.40
023-ZR17	0.41	0.0023	0.07618	0.54	2.073	1.35	0.1973	1.18	0.87	1100	22	1161	25	1140	18	-5.55
008-ZR06	0.20	0.0079	0.07574	0.68	2.036	1.20	0.1950	0.91	0.76	1088	27	1148	19	1128	16	-5.52
028-ZR22	0.25	0.0177	0.07403	0.97	1.892	1.91	0.1853	1.60	0.84	1042	39	1096	32	1078	25	-5.14
005-ZR03	0.27	0.0056	0.07577	0.60	2.029	1.09	0.1942	0.83	0.76	1089	24	1144	17	1125	15	-5.06
003-ZR01	0.11	0.0056	0.07719	0.61	2.134	1.10	0.2005	0.84	0.76	1126	24	1178	18	1160	15	-4.62
030-ZR24	0.17	0.0089	0.07602	0.76	1.834	1.71	0.1749	1.48	0.87	1096	30	1039	28	1058	22	5.15

679
680
681
682
683

684
685
686
687

Continuation.

Identifier	Th/U	f206 (%)	²⁰⁷ Pb/ ²⁰⁶ Pb	1σ %	Radiogenic ratios					Ages ⁵					% U-Pb disc ⁴	
					²⁰⁷ Pb/ ²³⁵ U	1σ %	²⁰⁶ Pb/ ²³⁸ U	1σ %	Rho	²⁰⁷ Pb/ ²⁰⁶ Pb	2σ abs	²⁰⁶ Pb/ ²³⁸ U	2σ abs	²⁰⁷ Pb/ ²³⁵ U		2σ abs
Rio Branco Suite, foliated granite dike (sample MQ-147M)																
004-ZR02	0.38	0.0291	0.07736	0.88	1.963	1.43	0.1840	1.07	0.75	1131	35	1089	21	1103	19	3.69
027-ZR21	0.47	0.0217	0.07809	0.70	1.983	1.53	0.1842	1.31	0.86	1149	27	1090	26	1110	21	5.18
029-ZR23	0.51	0.0223	0.07835	0.93	2.002	1.44	0.1853	1.03	0.72	1156	37	1096	21	1116	19	5.18
023-ZR17	0.33	0.0085	0.07631	0.69	1.953	1.09	0.1856	0.76	0.69	1103	28	1097	15	1099	15	0.51
016-ZR12	0.58	0.0246	0.07682	1.02	1.984	1.54	0.1873	1.10	0.71	1117	40	1107	22	1110	21	0.88
018-ZR14	0.51	0.0402	0.07737	0.82	2.001	1.56	0.1875	1.28	0.82	1131	32	1108	26	1116	21	2.03
017-ZR13	0.56	0.0224	0.07547	0.80	1.956	1.35	0.1880	1.02	0.75	1081	32	1111	21	1101	18	-2.72
019-ZR15	0.31	0.0106	0.07665	0.71	1.989	1.13	0.1882	0.80	0.71	1112	28	1112	16	1112	15	0.03
009-ZR07	0.52	0.0444	0.07838	0.79	2.037	1.70	0.1884	1.46	0.86	1156	31	1113	30	1128	23	3.77
015-ZR11	0.34	0.0072	0.07640	0.79	1.993	1.27	0.1891	0.92	0.73	1106	31	1117	19	1113	17	-1.00
028-ZR22	0.50	0.1030	0.07666	1.19	2.001	1.93	0.1893	1.48	0.76	1112	47	1118	30	1116	26	-0.47
026-ZR20	0.59	0.0150	0.07641	0.69	2.008	1.29	0.1906	1.02	0.79	1106	27	1125	21	1118	17	-1.70
030-ZR24	0.46	0.0317	0.07674	1.32	2.017	3.34	0.1906	3.04	0.91	1114	52	1125	63	1121	45	-0.94
006-ZR04	0.30	0.0134	0.07700	0.69	2.038	1.20	0.1920	0.90	0.76	1121	27	1132	19	1128	16	-0.98
038-ZR30	0.38	0.0174	0.07605	0.59	2.024	1.10	0.1930	0.85	0.78	1096	23	1138	18	1124	15	-3.77
014-ZR10	0.55	0.0135	0.07692	0.76	1.934	1.17	0.1823	0.81	0.69	1119	30	1080	16	1093	16	3.53
008-ZR06	0.54	0.0254	0.07556	1.11	1.905	1.83	0.1829	1.41	0.77	1083	44	1083	28	1083	24	0.08
005-ZR03	0.38	0.0188	0.07655	0.58	2.050	1.08	0.1942	0.83	0.77	1109	23	1144	17	1132	15	-3.13
003-ZR01	0.35	0.0156	0.07647	0.65	2.067	1.23	0.1961	0.97	0.79	1107	26	1154	21	1138	17	-4.21
010-ZR08	0.56	0.1542	0.07975	0.87	1.790	2.36	0.1628	2.16	0.92	1191	34	972	39	1042	31	18.35
037-ZR29	1.02	0.1054	0.07988	0.98	1.834	2.27	0.1665	2.01	0.89	1194	39	993	37	1058	30	16.85
036-ZR28	1.07	0.0548	0.07285	1.64	1.691	2.08	0.1683	1.23	0.59	1010	66	1003	23	1005	26	0.71
020-ZR16	0.47	0.0157	0.07897	0.66	1.838	1.81	0.1688	1.64	0.91	1171	26	1005	31	1059	24	14.18
007-ZR05	0.27	0.0427	0.07489	0.94	1.782	1.45	0.1725	1.05	0.72	1065	37	1026	20	1039	19	3.70
040-ZR32	0.28	0.0196	0.07639	0.96	1.873	1.58	0.1778	1.20	0.76	1105	38	1055	23	1072	21	4.57

Identifier	Th/U	f206 (%)	²⁰⁷ Pb/ ²⁰⁶ Pb	1σ %	Radiogenic ratios					Ages ⁵					% U-Pb disc ⁴	
					²⁰⁷ Pb/ ²³⁵ U	1σ %	²⁰⁶ Pb/ ²³⁸ U	1σ %	Rho	²⁰⁷ Pb/ ²⁰⁶ Pb	2σ abs	²⁰⁶ Pb/ ²³⁸ U	2σ abs	²⁰⁷ Pb/ ²³⁵ U		2σ abs
Rio Branco Suite, fine-grained metagranite subvolcanic (sample MQ-124)																
029-ZR23	0.18	0.0116	0.07595	0.64	1.987	1.35	0.1898	1.13	0.84	1094	26	1120	23	1111	18	-2.41
026-ZR20	0.20	0.0057	0.07601	0.79	1.957	1.19	0.1867	0.81	0.68	1095	31	1104	16	1101	16	-0.76
014-ZR10	0.31	0.0122	0.07611	0.71	1.978	1.22	0.1885	0.92	0.75	1098	28	1113	19	1108	16	-1.38
016-ZR12	0.20	0.0080	0.07613	0.62	1.957	1.01	0.1865	0.70	0.70	1098	25	1102	14	1101	14	-0.35
007-ZR05	0.17	0.0130	0.07615	0.62	1.970	1.09	0.1876	0.81	0.75	1099	25	1109	17	1105	15	-0.87
018-ZR14	0.26	0.0184	0.07620	0.53	1.962	0.98	0.1868	0.73	0.75	1100	21	1104	15	1103	13	-0.32
030-ZR24	0.23	0.0142	0.07621	0.64	1.996	1.21	0.1899	0.96	0.79	1101	26	1121	20	1114	16	-1.85
027-ZR21	0.19	0.0084	0.07644	0.50	2.019	0.92	0.1915	0.67	0.73	1107	20	1129	14	1122	12	-2.06
028-ZR22	0.24	0.0080	0.07645	0.60	1.982	1.10	0.1881	0.85	0.77	1107	24	1111	17	1110	15	-0.38
005-ZR03	0.21	0.0132	0.07650	0.61	1.990	1.13	0.1886	0.88	0.78	1108	24	1114	18	1112	15	-0.52
008-ZR06	0.25	0.0096	0.07668	0.59	1.961	1.06	0.1855	0.79	0.75	1113	24	1097	16	1102	14	1.45
004-ZR02	0.31	0.0104	0.07674	0.61	2.018	1.07	0.1907	0.80	0.75	1114	24	1125	17	1122	15	-0.99
015-ZR11	0.17	0.0169	0.07686	0.52	2.011	0.96	0.1898	0.72	0.75	1117	21	1120	15	1119	13	-0.23
006-ZR04	0.34	0.0202	0.07699	0.90	2.009	1.40	0.1892	1.01	0.72	1121	36	1117	21	1118	19	0.34
009-ZR07	0.18	0.0121	0.07717	0.64	2.009	1.08	0.1889	0.79	0.73	1125	26	1115	16	1119	15	0.92
036-ZR28	0.28	0.0181	0.07765	0.54	2.023	0.95	0.1889	0.69	0.73	1138	21	1115	14	1123	13	1.97
013-ZR09	0.53	0.0387	0.07797	0.77	2.092	1.19	0.1946	0.83	0.70	1146	30	1146	17	1146	16	0.00
024-ZR18	0.19	0.0095	0.07666	0.64	2.047	1.14	0.1936	0.86	0.76	1112	25	1141	18	1131	15	-2.58
034-ZR26	0.35	0.0126	0.07638	0.86	2.132	2.11	0.2025	1.89	0.90	1105	34	1189	41	1159	29	-7.57
020-ZR16	0.22	0.0129	0.07614	0.78	2.035	1.17	0.1938	0.79	0.68	1099	31	1142	17	1127	16	-3.91
017-ZR13	0.30	0.0720	0.08031	0.77	1.788	1.31	0.1615	0.99	0.76	1205	30	965	18	1041	17	19.90
023-ZR17	0.24	0.0148	0.09072	1.03	2.676	1.55	0.2139	1.09	0.71	1441	39	1249	25	1322	23	13.29
010-ZR08	0.46	0.1696	0.09358	1.18	2.234	2.06	0.1731	1.65	0.80	1500	44	1029	31	1192	29	31.36
037-ZR29	0.32	0.0083	0.10001	1.21	3.984	2.27	0.2889	1.89	0.83	1624	45	1636	54	1631	37	-0.72
038-ZR30	0.49	0.0099	0.11805	1.26	6.047	2.37	0.3715	1.97	0.83	1927	45	2037	69	1983	41	-5.69
033-ZR25	0.33	0.0256	0.13502	1.50	6.858	2.43	0.3684	1.87	0.77	2164	52	2022	65	2093	43	6.59

688
689
690
691
692
693
694

Continuation.

Identifier	Th/U	f206 (%)	²⁰⁷ Pb/ ²⁰⁶ Pb	1σ %	Radiogenic ratios				Ages ⁵				% U-Pb disc ⁴			
					²⁰⁷ Pb/ ²³⁵ U	1σ %	²⁰⁶ Pb/ ²³⁸ U	1σ %	Rho	²⁰⁷ Pb/ ²⁰⁶ Pb	2σ abs	²⁰⁶ Pb/ ²³⁸ U		2σ abs	²⁰⁷ Pb/ ²³⁵ U	2σ abs
Rio Branco Suite, medium-grained leucocratic metatrandhjemite (plagiogranite equivalent) (sample MQ-29)																
019-ZR15	0.47	0.0147	0.07669	0.85	1.952	1.39	0.1846	1.03	0.74	1113	34	1092	21	1099	19	1.89
003-ZR01	0.39	0.0096	0.07586	0.60	1.943	1.09	0.1858	0.83	0.76	1091	24	1098	17	1096	15	-0.65
009-ZR07	0.39	0.0118	0.07722	0.55	1.986	1.31	0.1865	1.13	0.86	1127	22	1103	23	1111	18	2.15
039-ZR31	0.55	0.0125	0.07685	0.79	1.977	1.21	0.1865	0.84	0.69	1117	31	1103	17	1108	16	1.32
005-ZR03	0.60	0.0135	0.07625	0.62	1.969	1.12	0.1873	0.85	0.76	1102	25	1107	17	1105	15	-0.45
007-ZR05	0.18	0.0067	0.07631	0.48	1.978	0.99	0.1880	0.78	0.79	1103	19	1110	16	1108	13	-0.64
023-ZR17	0.38	0.0148	0.07613	0.75	1.982	1.19	0.1888	0.84	0.71	1098	30	1115	17	1109	16	-1.50
006-ZR04	0.63	0.0197	0.07540	0.97	1.990	1.52	0.1914	1.11	0.73	1079	39	1129	23	1112	20	-4.61
010-ZR08	0.55	0.0310	0.07619	1.07	1.901	1.70	0.1810	1.26	0.74	1100	43	1072	25	1081	22	2.53
020-ZR16	0.68	0.0005	0.07691	0.88	1.919	1.61	0.1810	1.29	0.80	1119	35	1072	26	1088	21	4.17
013-ZR09	0.38	0.0192	0.07723	0.69	1.934	1.18	0.1816	0.88	0.75	1127	27	1076	17	1093	16	4.58
030-ZR24	0.17	0.0019	0.07623	0.60	1.917	1.16	0.1824	0.92	0.79	1101	24	1080	18	1087	15	1.92
024-ZR18	0.40	0.0101	0.07649	0.50	2.048	0.91	0.1942	0.67	0.73	1108	20	1144	14	1132	12	-3.25
025-ZR19	0.41	0.0472	0.07670	0.50	2.056	1.04	0.1944	0.83	0.80	1114	20	1145	17	1134	14	-2.85
034-ZR26	0.58	0.0030	0.07510	0.66	2.020	1.38	0.1950	1.15	0.84	1071	26	1149	24	1122	19	-7.23
008-ZR06	0.36	0.0363	0.07649	0.94	2.062	2.02	0.1955	1.75	0.87	1108	37	1151	37	1136	27	-3.91
038-ZR30	0.61	0.0289	0.07645	0.96	2.068	1.86	0.1962	1.54	0.83	1107	38	1155	33	1138	25	-4.32
037-ZR29	0.29	0.0218	0.07612	0.91	2.068	1.74	0.1970	1.43	0.82	1098	36	1159	30	1138	24	-5.57
035-ZR27	0.25	0.0171	0.07679	0.65	2.171	1.53	0.2051	1.33	0.87	1116	26	1203	29	1172	21	-7.78
014-ZR10	0.80	0.0456	0.07798	0.67	2.233	1.76	0.2076	1.58	0.90	1146	27	1216	35	1191	24	-6.10
040-ZR32	0.56	0.0398	0.07885	0.73	2.067	1.91	0.1901	1.72	0.90	1168	29	1122	35	1138	26	3.97
017-ZR13	0.42	0.0509	0.07876	0.73	2.055	1.60	0.1892	1.38	0.86	1166	29	1117	28	1134	22	4.18
026-ZR20	0.38	0.0259	0.07895	0.53	1.901	1.21	0.1746	1.03	0.85	1171	21	1037	20	1081	16	11.42
036-ZR28	0.36	0.0146	0.07790	1.13	2.021	1.90	0.1881	1.48	0.78	1144	45	1111	30	1123	26	2.90
015-ZR11	0.39	0.0528	0.07960	1.25	2.193	2.53	0.1998	2.17	0.86	1187	49	1174	46	1179	35	1.09

Identifier	Th/U	f206 (%)	²⁰⁷ Pb/ ²⁰⁶ Pb	1σ %	Radiogenic ratios				Ages ⁵				% U-Pb disc ⁴			
					²⁰⁷ Pb/ ²³⁵ U	1σ %	²⁰⁶ Pb/ ²³⁸ U	1σ %	Rho	²⁰⁷ Pb/ ²⁰⁶ Pb	2σ abs	²⁰⁶ Pb/ ²³⁸ U		2σ abs	²⁰⁷ Pb/ ²³⁵ U	2σ abs
Anatectic granite in paragneiss of Rio Branco Formation (sample MQ-146B)																
014-ZR09	0.02	0.0074	0.07201	0.68	1.735	1.15	0.1747	0.85	0.74	986	27	1038	16	1022	15	-5.26
027-ZR20	0.02	0.1367	0.07222	0.79	1.728	1.13	0.1735	0.72	0.63	992	32	1031	14	1019	15	-3.96
039-ZR30	0.02	0.0131	0.07237	0.67	1.640	1.15	0.1643	0.86	0.75	996	27	981	16	986	14	1.56
026-ZR19	0.02	0.0042	0.07297	0.52	1.851	1.12	0.1840	0.92	0.82	1013	21	1089	18	1064	15	-7.44
017-ZR12	0.04	0.0020	0.07306	0.53	1.814	1.03	0.1801	0.80	0.77	1016	22	1067	16	1051	13	-5.10
003-ZR01	0.02	0.0053	0.07306	0.62	1.674	0.97	0.1662	0.65	0.67	1016	25	991	12	999	12	2.44
005-ZR03	0.02	0.0045	0.07307	0.52	1.684	0.90	0.1671	0.63	0.71	1016	21	996	12	1002	11	1.95
028-ZR21	0.02	0.0073	0.07307	0.65	1.672	1.17	0.1659	0.90	0.77	1016	26	990	17	998	15	2.58
037-ZR28	0.02	0.0094	0.07313	0.50	1.772	1.04	0.1757	0.83	0.80	1018	20	1043	16	1035	13	-2.53
015-ZR10	0.03	0.0046	0.07324	0.56	1.744	1.05	0.1727	0.81	0.77	1021	23	1027	15	1025	14	-0.62
024-ZR17	0.02	0.0041	0.07327	0.59	1.754	1.11	0.1736	0.86	0.78	1021	24	1032	16	1029	14	-1.03
009-ZR06	0.17	0.0061	0.07756	0.90	2.082	1.37	0.1947	0.96	0.70	1136	36	1147	20	1143	19	-1.00
040-ZR31	0.30	0.0035	0.07800	0.77	2.044	1.17	0.1900	0.81	0.69	1147	30	1122	17	1130	16	2.21
019-ZR14	0.22	0.0075	0.07814	0.81	2.092	1.22	0.1941	0.84	0.69	1150	32	1144	18	1146	17	0.60
029-ZR22	0.02	0.0520	0.07459	0.73	1.710	1.17	0.1663	0.84	0.72	1057	29	992	15	1012	15	6.22
004-ZR02	0.36	0.0137	0.07875	0.62	2.057	0.96	0.1895	0.64	0.66	1166	24	1118	13	1135	13	4.07
033-ZR24	0.27	0.1458	0.08306	1.19	2.484	1.83	0.2169	1.34	0.73	1271	46	1265	31	1267	26	0.42
036-ZR27	0.14	0.0108	0.09078	0.69	2.954	1.37	0.2360	1.12	0.82	1442	26	1366	28	1396	21	5.29
007-ZR05N	0.25	0.0087	0.09430	0.59	3.401	1.05	0.2616	0.78	0.74	1514	22	1498	21	1505	16	1.08
020-ZR15	0.18	0.0178	0.09658	1.23	3.795	1.79	0.2849	1.25	0.70	1559	46	1616	36	1592	29	-3.65

¹ Conversion factor from mV to CPS is 62500000

² concentration uncertainty c.20%

³ not corrected for common-Pb

⁴ Discordance calculated as $(1 - ({}^{206}\text{Pb}/{}^{238}\text{U} \text{ age} / {}^{207}\text{Pb}/{}^{206}\text{Pb} \text{ age})) * 100$

Decay constants of Jaffey et al. (1971) used

Note: Zircon analysis results in italics (gray) were data not used for precise age calculations

695
696

697 In preparing the concordia diagram, we initially used isotopic data from twenty-seven zircon
698 crystals (normal black font style zircons data, sample MQ-122, Table 2). For age calculation,
699 isotopic data from twelve concordant zircon crystals (highlighted in bold in Table 2, sample MQ-
700 122) we used to calculate the Concordia age of 1127.6 ± 2.3 Ma, MSWD = 1.8, probability
701 (agreement) = 0.18 and Th / U ratios between 0.16 and 0.49, interpreted as magmatic crystallization
702 age of the protolith (Fig. 11).

703

704 6.2 Metamafic component (Rio Branco Suite)

705

706 Sample MQ-117 (S11°59'33"/W61°58'09") is a gray, foliated, not magnetic, medium-
707 grained metagabbro, with a subhedral to anhedral granular texture, composed essentially of
708 plagioclase, augite and orthopyroxene, having hornblende as a secondary mineral, on the rims of
709 pyroxene crystals. Zircon crystals extracted from this rock are generally subhedral (1:3, 1:2 and
710 1:1), rounded prismatic, ranging between 70 and 400 μm, containing fractures and inclusions. In
711 BSE images, the internal structure is dominantly homogeneous, sometimes with oscillatory
712 zonation. Eventually, zircon crystals have irregular luminescent stain with radial fracture

713 concentration. Twenty-seven zircon crystals from this sample were analyzed (Table 2). Their Th/U
 714 ratios vary between 0.03 and 0.81, present ages with low discordance, mainly around 1200-1050
 715 Ma, except three younger grains with concordant data of ~1000 Ma. The regression of the main
 716 group indicates the upper and low intercepts at 1073 ± 28 Ma and 519 ± 260 Ma, respectively
 717 (MSWD of 4.1). The selection of most concordant data (range 015-ZR11 to 033-ZR25 in Table 2,
 718 sample MQ-117) allow to calculate the Concordia age of 1119.7 ± 2.7 Ma, interpreted as the best
 719 estimate of the magmatic crystallization age of the rock (Fig. 12). Age possibility reinforced by the
 720 field geological relations that suggest contemporaneity between the metamafic and metafelsic
 721 components of the Rio Branco Suite (see sections 5.2 and 6.3). The set of three zircon crystals
 722 (grains ZR04, ZR08 and ZR23) was used for calculation of the Concordia age of 1016.7 ± 3.9 Ma
 723 (MSWD = 0.29), interpreted as record of the possible youngest metamorphic pulse (Fig. 12).

724

725 6.3 Metafelsic component (Rio Branco Suite)

726

727 Sample MQ-147M (S11°55'59"/W62°08'55") is from a foliated granitic dike intrusive in
 728 high-grade calc-silicate gneiss and biotite paragneiss of the Rio Branco Formation (Figs. 4A, 6A,
 729 6B, 6C). It is a medium to fine-grained equigranular, leucocratic, foliated metagranite, composed of
 730 plagioclase, k-feldspar and quartz, and present hornblende, biotite, titanite, allanite, zircon and
 731 opaque minerals as accessories and secondary minerals are represented by white mica, epidote and
 732 iron oxides. The foliation is marked by stretched quartz and feldspar crystals and by the orientation
 733 of mafic minerals, concentrated along the more deformed portions of the rock. Only twenty-five
 734 zircon crystals could be extracted from this rock and they were analysed for LA-ICP-MS U-Pb
 735 (Table 2). They are prismatic crystals, euhedral to subhedral, 1:2 and 1:3 ratios, between 100 and
 736 300 μm long, and exhibiting some fractures. The BSE images show well-marked oscillatory
 737 zonation and irregular areas with high luminescence, especially in the rims of the crystals. Among
 738 the data of the analyzed twenty-five spots, only the analytical result of fifteen more concordant
 739 crystals (range 004-ZR02 to 038-ZR30 in Table 2, sample MQ-147M) were used in the calculations.
 740 They present Th/U between 0.29 and 0.59 and their isotopic data indicates the of the Concordia age
 741 of 1113 ± 6.7 Ma (MSWD = 1.4), which represents the age of magmatic crystallization of the felsic
 742 dyke (Fig. 13A).

743

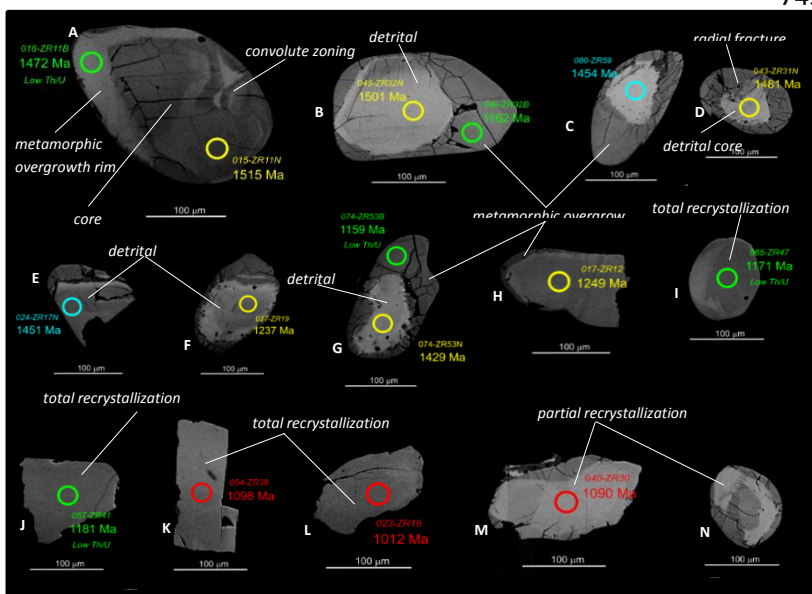
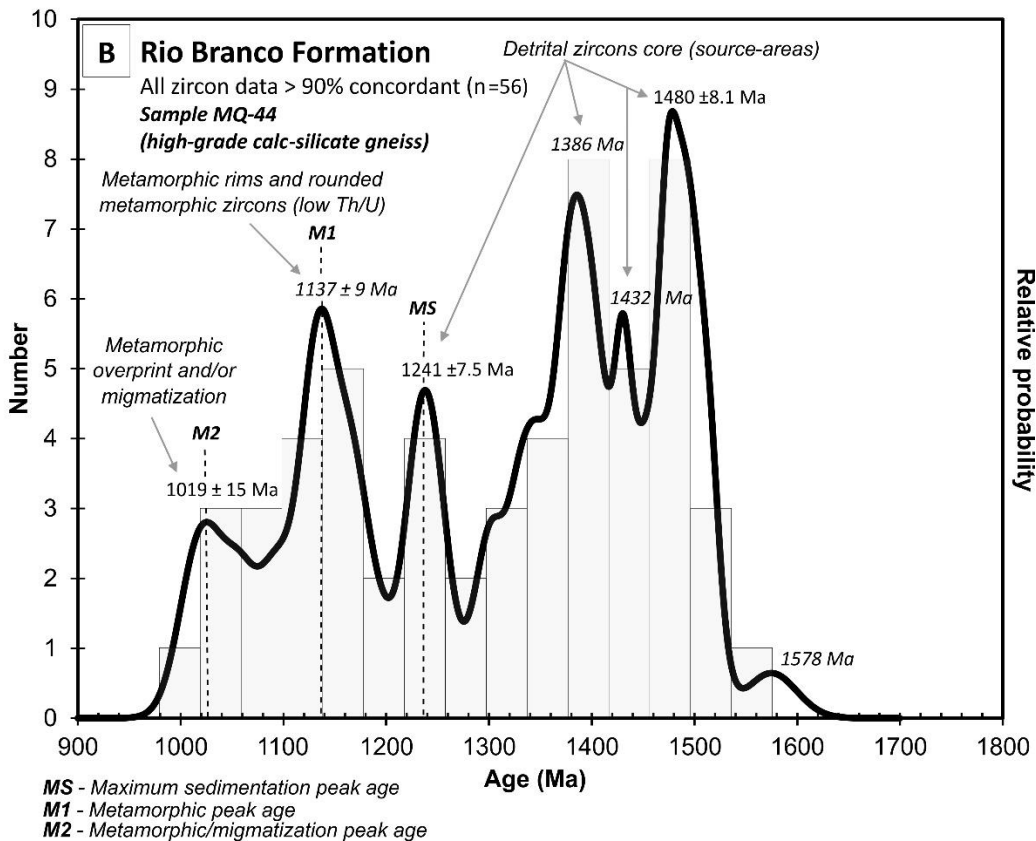
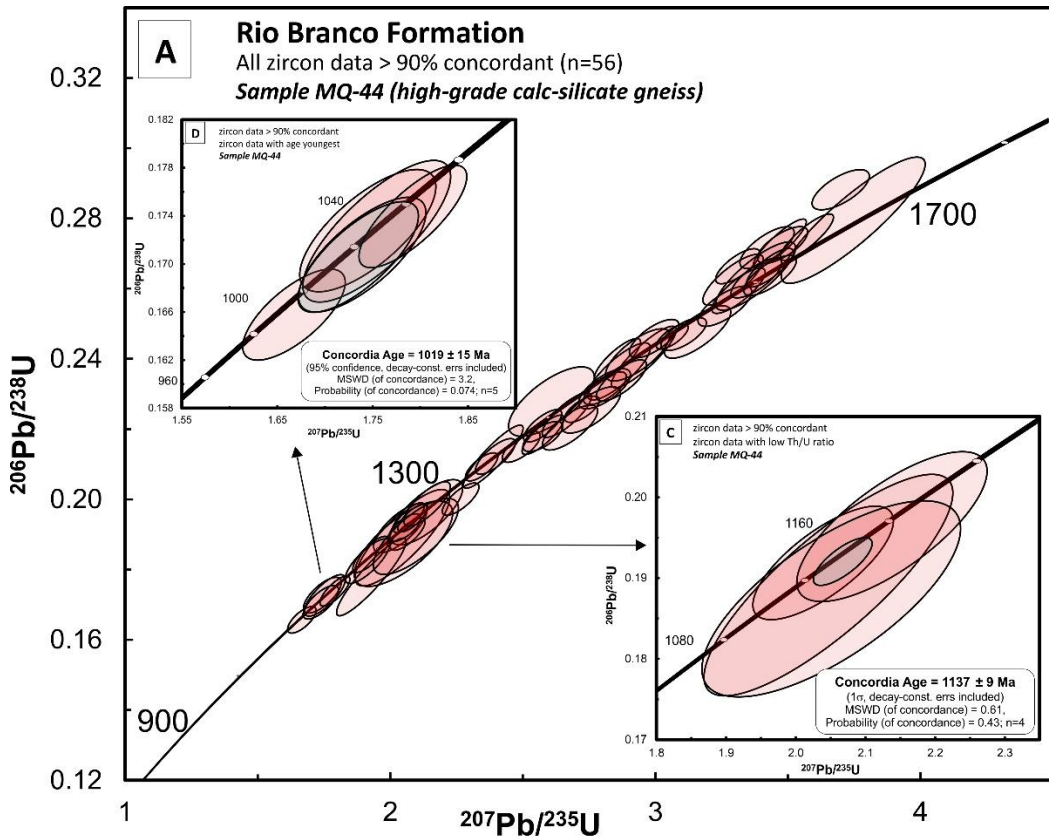


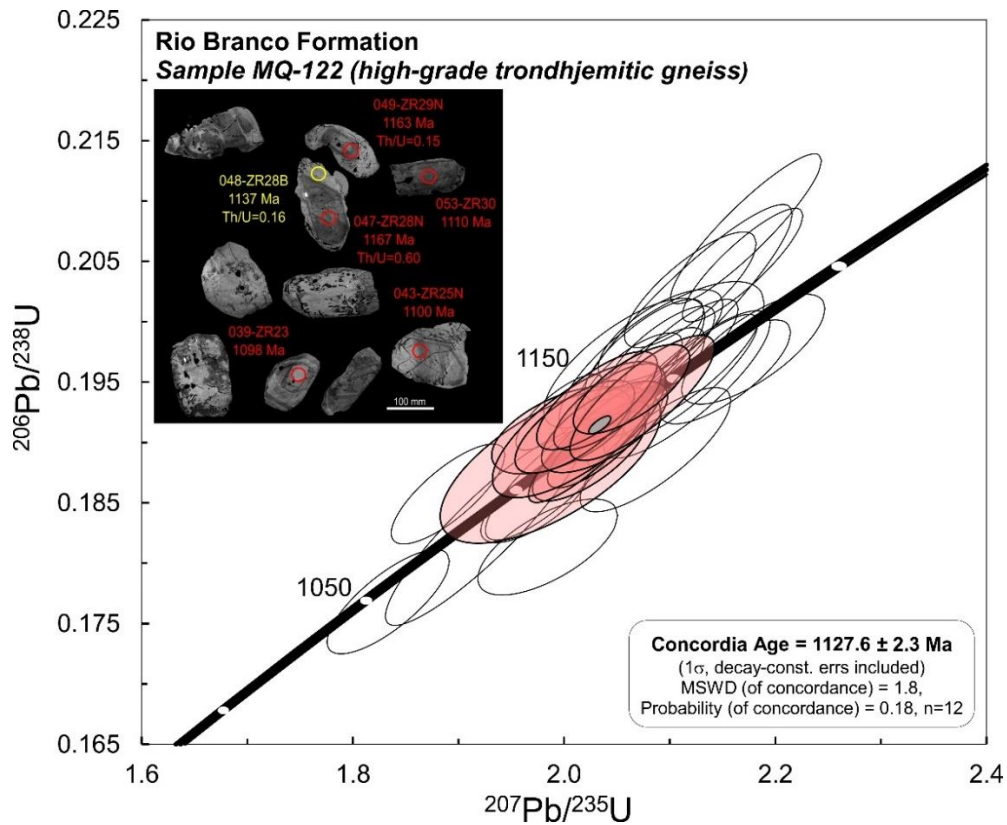
Fig. 9. BSE (Backscattered Electron) images of selected zircon grains of sample MQ-44 (calc-silicate gneiss of the Rio Branco Formation) showing usually recrystallized forms and varied internal morphologies. (A) zircon presenting core with high Th/U ratio, convolute zoning and overgrowth with low Th/U ratio (metamorphic rim). (B), (C), (D), (E), (F), (G) and (H) homogeneous and partially recrystallized zircon grains showing detrital core and metamorphic rims with low Th/U ratio and radial fractures. (I) sub-rounded and homogeneous zircon with low Th/U ratio. (J) homogeneous zircon fragment with

762 low Th/U ratio. (K), (L) homogeneous and fractured zircon fragments. (M), (N) zircon with features of partial
 763 recrystallization. Circles indicate the analyzed spot location. Numbers represent $^{207}\text{Pb}/^{206}\text{Pb}$ ages and the
 764 color circles mean yellow=crystallization, green=overgrowth or metamorphic recrystallization, red=
 765 metamorphic recrystallization and/or migmatization. Based on Corfu et al. (2003) and Harley et al. (2007).



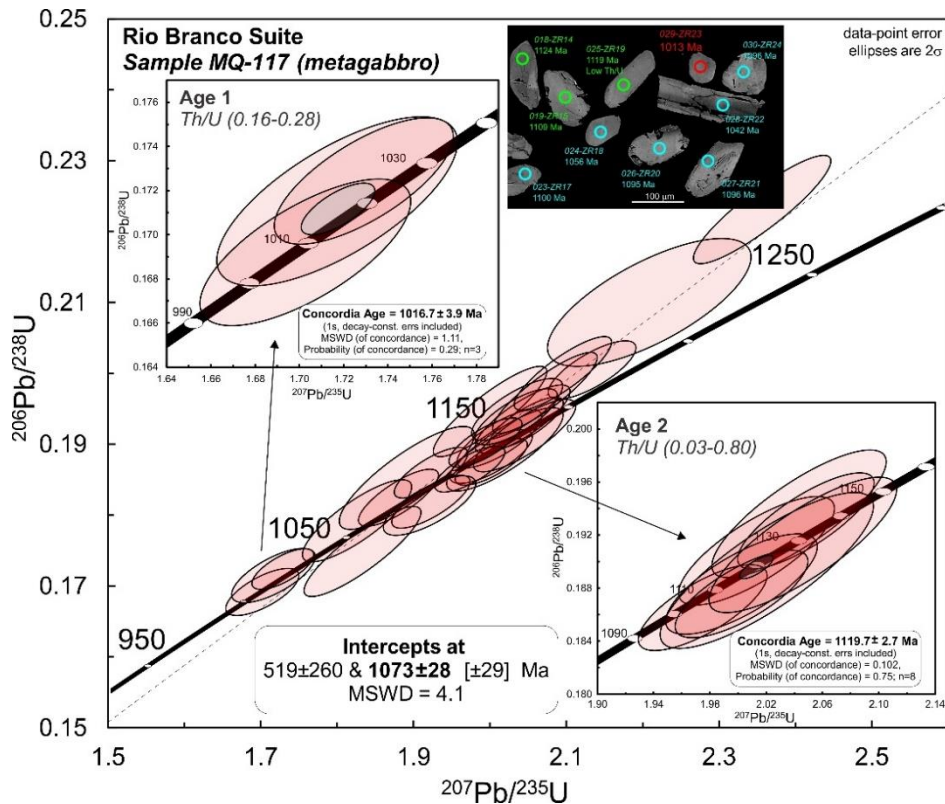
766
767
768
769
770
771
772
773

Fig. 10. (A) U-Pb (LA-ICP-MS) Concordia diagram and (B) relative probability histogram for $^{207}\text{Pb}/^{206}\text{Pb}$ ages of the detrital zircon grains of high-grade calc-silicate gneiss of the Rio Branco Formation (sample MQ-44). (D) Concordia age of high-grade metamorphism age in 1137 ± 9 Ma (M1) and (D) another late metamorphic recrystallization or migmatization phase in 1019 ± 15 Ma (M2). The Maximum sedimentation age in 1241 ± 7.5 Ma (MS).



774
 775
 776
 777

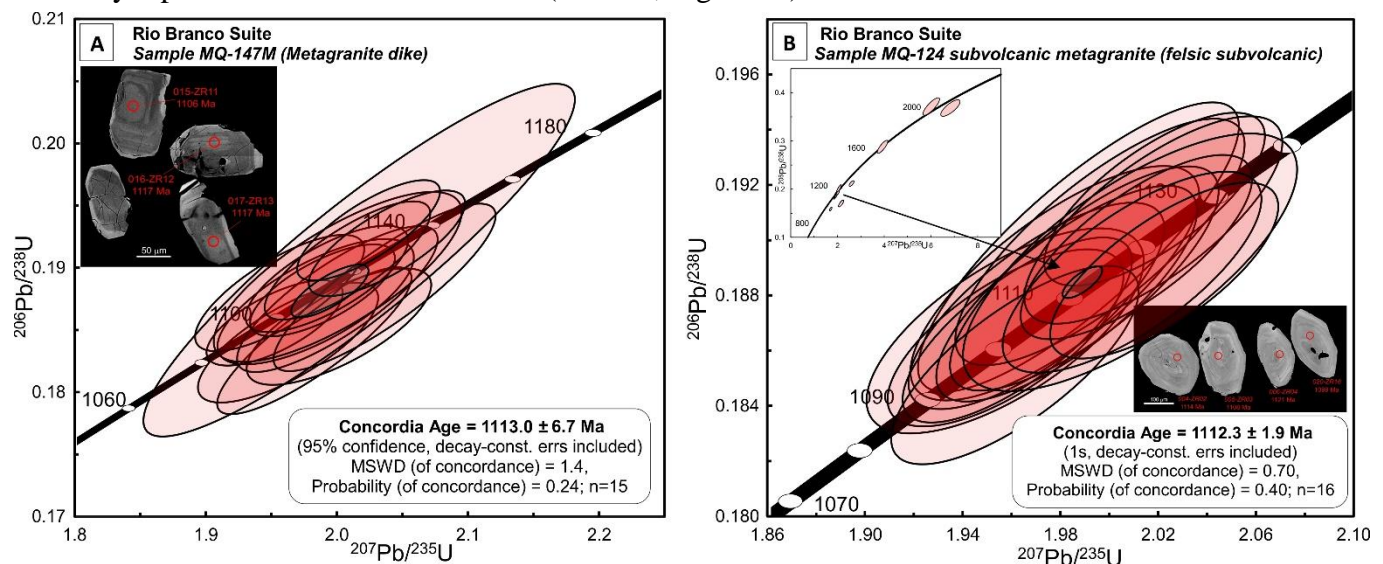
Fig. 11. U-Pb Concordia diagram of concordant zircon of high-grade trondhjemitic gneiss (sample MQ-22) from the Rio Branco Domain, Nova Brasilândia belt.



778
 779
 780
 781
 782

Fig. 12. U-Pb Discordia and Concordia diagrams of metagabbro (sample MQ-117) from the Rio Branco domain, displaying primary population of zircon (zoned core and light rim) with Concordia age of 1120±3 Ma (n=8), low-high Th/U ratios (0.03-0.80), and second population of zircon (rounded and homogeneous) with Concordia age of 1017±4 Ma (n=3), Th/U (0.16-0.28).

783 Sample MQ-124 (S11°54'20"/W62°02'57") is a fine-grained subvolcanic metagranite
 784 (metafelsic subvolcanic), which occurs in the form of a body elongated in the E-W direction,
 785 measuring approximately 16 km x 1.6 km. The metagranite intruded fine-grained amphibolite. It is
 786 a porphyritic felsic rock with fine-grained to aphanitic matrix, containing stretched porphyroclasts
 787 of k-feldspar and xenoliths of foliated metamafic rocks (Fig. 8C). From this sample, twenty-six
 788 zircon crystals were extracted and classified into two groups based on their morphology and internal
 789 structure, observed on BSE images (Table 2). The first group consists of small zircon grains (25-
 790 110 μm), usually prismatic or rounded, homogenous or with concentric zoning and micro fractures.
 791 Subordinately in this group occur round crystals exhibiting characteristics of light gray core and
 792 thin dark gray rims and crystals with bipyramidal forms. The second zircon group consists of large,
 793 prismatic and elongated crystals with bipyramidal terminations, measuring 150-400 μm , internally
 794 exhibiting concentric or oscillatory zoning. Analyzes of the first group revealed a wide dispersion
 795 of ages, with $^{207}\text{Pb}/^{206}\text{Pb}$ Paleoproterozoic ages of 2164 Ma, 1927 Ma and 1624 Ma. Sixteen zircon
 796 crystals of the second group were analysed and proved to be the most concordant and with Th/U
 797 ratios ranging from 0.16 to 0.34 (range 029-ZR23 to 036-ZR28 in Table 2, sample MQ-124), were
 798 used in the calculation of the Concordia age of 1112.3 ± 1.9 Ma (MSWD = 0.70), interpreted as the
 799 magmatic crystallization age of the rock (Fig. 13B). The oldest ages up to 1624 Ma and 2164 Ma
 800 may represent crustal contamination (Table 2, Fig. 13 B).



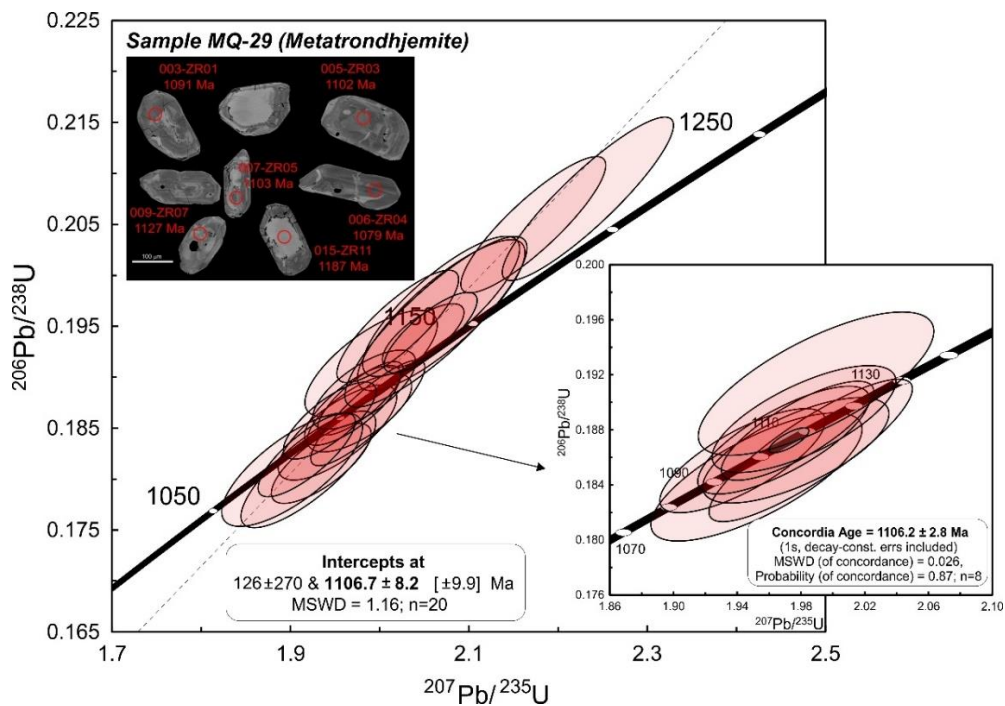
801 **Fig. 13 .** U-Pb Concordia diagrams of concordant zircon from samples from the Rio Branco Domain, Nova
 802 *Brasilândia* belt. (A) metagranite dike intrusive in folded high-grade calc-silicate gneisses of the Rio Branco
 803 *Formation*. (B) felsic metasubvolcanic rock of the Rio Branco Suite, intrusive in metamafic rocks.

804
 805 Sample MQ-29 (S11°56'55"/W62°13'20") is a medium-grained leucocratic
 806 metatrandhjemite (plagiogranite equivalent), which occurs in the form of lenses within metamafic
 807 rocks, with about 400 m length and 80 m width, spatially associated with metagabbros (Fig. 8D). It
 808 consists essentially of quartz and generally saussuritized plagioclase, containing approximately 10
 809 % of interstitial mafic minerals (amphibole and clinopyroxene), with titanite, magnetite and zircon
 810 traces. From this sample were extracted and analyzed twenty-five zircon crystals (Table 2). They
 811 are prismatic crystals from euhedral to subhedral, with rounded ends, sizes varying between 40 and
 812 350 μm and with frequent inclusions (Fig. 15). The BSE images exhibit crystals oscillatory zoning
 813 remnants and abundant irregular dark and luminescent areas. Areas with oscillatory zoning are more
 814 common in larger crystals. In general, zircon of the MQ-29 sample presents Th/U ratios between
 815 0.16 and 0.79, compatible with those of zircon of magmatic origin. The regression of all data
 816 indicates the upper intercept of 1106.7 ± 8.2 Ma (MSWD=1.16, n=20) (Fig. 14). In order to obtain
 817 a more accurate age, the most concordant data (> 95 % concordance, Table 2), were used in the
 818 calculation of Concordia age of 1106.2 ± 2.8 Ma (MSWD = 0.026 and probability = 0.87, n=8),
 819 interpreted as the age of magmatic crystallization (Fig. 14).

820 **6.4 Anatectic granite (in Rio Branco Formation)**

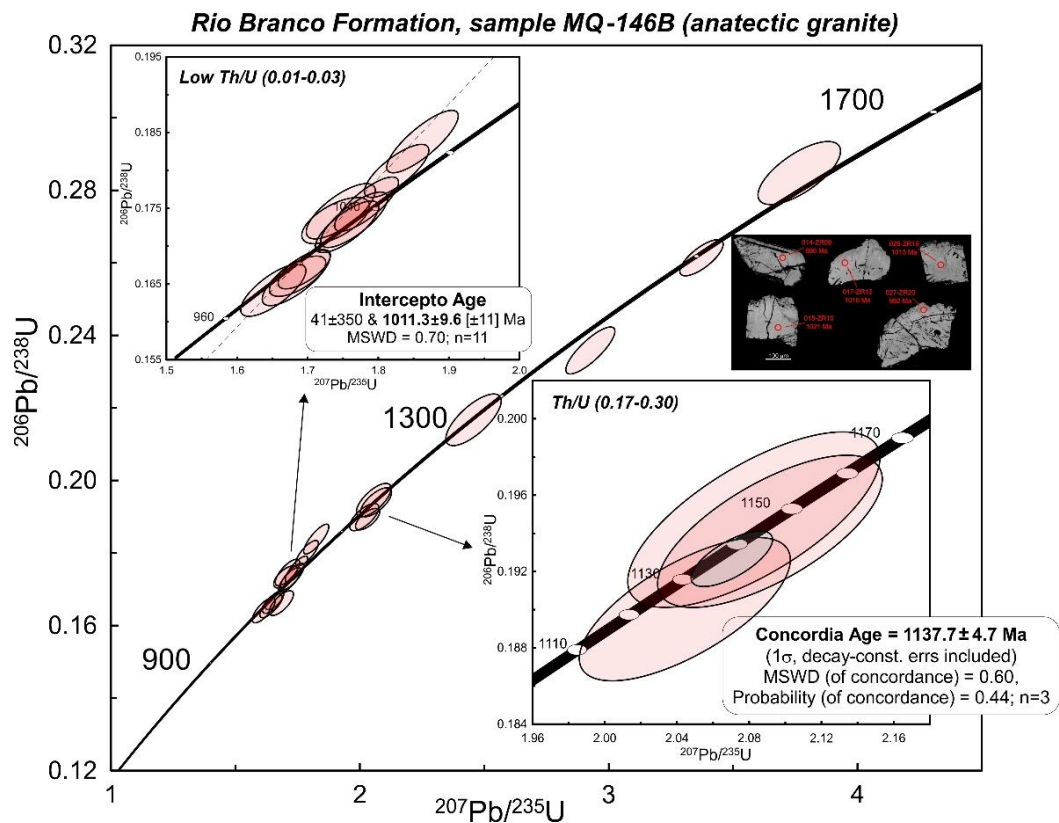
821
 822 Sample MQ-146B (S12°00'23"/W61°51'23") is from a weathered white anatectic granite
 823 lens in paragneiss. This sample was selected for dating by the LA-ICP-MS U-Pb zircon method in
 824 an attempt to characterize the age of deformation and metamorphism that generated partial melting
 825 (or migmatization) of the metasedimentary component of the Rio Branco Formation, during the
 826 climax of metamorphism. The twenty zircon crystals extracted from this sample were classified into
 827 three morphologically distinct groups. The main group consists dominantly of large (435-260 μm),
 828 homogeneous or zoned, fractured subhedral crystals, with 1:3 and 1:2 proportions. The analysis of
 829 these crystals (n=20) shows a wide dispersion of Mesoproterozoic ages, associated with Th/U ratios
 830 between 0.01 and 0.03 (Fig. 15). Among them, a set of eleven points analyzed showed some
 831 alignment (range 014-ZR09 to 024-ZR17 in Table 2, sample MQ-146B) that allowed the calculation
 832 of the regression, whose upper intercept is 1011.3 ± 9.6 Ma MSWD=0.70 (Fig. 15). The second
 833 zircon set consisting of three rounded and homogeneous crystals (1:1 and 1:2), sizes between 230
 834 and 130 μm and Th/U ratios between 0,17 and 0,30 (crystals 009- ZR06, 040-ZR31 and 019-ZR14
 835 in Table 2) furnished the Concordia age of 1137.7 ± 4.7 Ma (MSWD=0.6) (Fig. 15). The third group
 836 of zircon grains is represented by small rounded crystals (100-50 μm) presenting core and rims,
 837 radial fractures and ratio width vs. length of 1:1 to 1:2. The third zircon group presented cores with
 838 Mesoproterozoic $^{207}\text{Pb}/^{206}\text{Pb}$ ages in 1559 Ma, 1514 Ma, 1442 Ma, 1271 Ma, 1166 Ma and 1057
 839 Ma, not used for calculation of age rock (Fig. 15). Thus, we interpret the upper intercept of 1011.3
 840 ± 9.6 Ma as the crystallization age of the anatectic granite originate from partial fusion (or
 841 migmatization) of the metasedimentary rocks of the Rio Branco Formation during the climax of a
 842 possible second metamorphic pulse. In the sample MQ-146B, the U-Pb ages of 1137.7 ± 4.7 Ma
 843 interpreted as inheritance and 1011.3 ± 9.6 Ma interpreted as migmatization (Fig. 15) are identical
 844 or very close to the metamorphic U-Pb ages found in the MQ-44 (paragneiss) and MQ-117
 845 (metagabbro) samples (Figs. 10A, 12).

846
 847



848
 849
 850
 851

Fig. 14. U-Pb (LA-ICP-MS) Concordia diagram of concordant zircon grains from metatrandhjemite sample of the Rio Branco Domain, Nova Brasilândia belt.



852 **Fig. 15.** U-Pb (LA-ICP-MS) Discordia and Concordia diagrams showing zircon
 853 ages of the two main populations of anatectic granite (sample MQ-146B) in
 854 paragneiss of the Rio Branco Formation. The age range of 1150-1136 Ma (n=3)
 855 includes metamorphic and magmatic zircon grains based on BSE images and Th/U
 856 ratios and provides an age of 1137.7 ± 4.7 Ma. The range of 1021-986 Ma (n=11)
 857 includes zircon grains with low Th/U ratio (0.01-0.03), rendering an intercept age
 858 of 1011.3 ± 9.6 Ma on the Discordia diagram.

859
 860 **7. Discussion**

861
 862 The association of high-grade metavolcanic-sedimentary rocks (calc-silicate gneisses, biotite
 863 paragneisses and granulites paraderived, mafic or felsic) with mafic-felsic metagneous rocks
 864 (metagabbros, massive metabasalts, metadiabases, amphibolites, metatrandhjemites massive or
 865 banded and metagranites) at Rio Branco domain in the southern portion of the Nova Brasilândia belt
 866 was initially interpreted as an incomplete fragment of seafloor (Rizzotto, 1999). These rocks were
 867 folded, sheared and metamorphosed in high-grade (amphibolite- to granulite-facies). Field features
 868 demonstrate that the metamafic and metafelsic components present intrusion relations with high-
 869 grade metasedimentary rocks, in the form of stocks, small elongate bodies, sills and dikes.

870 The evaluation of field geological data and LA-ICP-MS U-Pb zircon geochronological
 871 analyzes obtained in our research, combined with the re-interpretation of previously published U-
 872 Pb, ^{40}Ar - ^{39}Ar and Sm-Nd geochronological data (Table 1) provided a temporal understanding of the
 873 geological events recorded in the Nova Brasilândia belt occurred during the Mesoproterozoic
 874 (Stenian) and early Neoproterozoic (Tonian). The timing of sedimentation, magmatism,
 875 deformation and metamorphism episodes provided a better understanding of the geological
 876 evolution of the Nova Brasilândia belt, during the Nova Brasilândia orogeny (Table 3). The use of
 877 different isotopic systems, analytical methods and analyzed materials provided ages with different
 878 meanings, which were used to establish the of crystallization, deposition, deformation,
 879 metamorphism and cooling ages of the rocks, as well as identifying sources-areas.

880 Accordingly, the new isotopic data of the Rio Branco domain described in section 4.2 with
 881 those available in literature were used to support our interpretations in relation of the progression of
 882 Nova Brasilândia belt geological events over time.

883 **7.1 Maximum sedimentation ages**

884
885 U-Pb detrital zircon ages from the northern portion of the Nova Brasilândia Belt indicate
886 maximum depositional ages of 1122 ± 12 Ma (Rizzotto et al., 2014) for Migrantinópolis Formation
887 and 1143 Ma for Terra Boa Formation (Trindade Neto et al., 2018). These studies identified source
888 ages compatible with the rocks of the Jamari Complex (~ 1174 Ma) and Serra da Providência Suite
889 (~ 1554 Ma) located north of the Nova Brasilândia belt, and also with rocks from the Rio Branco
890 domain, southern portion of the Nova Brasilândia belt. Therefore, they presented zircon contribution
891 from oldest units located north of the Nova Brasilândia belt.

892 The new U-Pb LA-ICP-MS data presented in this article reveal the maximum sedimentation
893 age of 1241 ± 7.5 Ma, obtained in detrital zircon from high-grade calc-silicate gneiss (sample MQ-
894 44) from the Rio Branco Formation in the southern portion of the Nova Brasilândia belt (Rio Branco
895 domain). The other analyzed zircon grains presented $^{207}\text{Pb}/^{206}\text{Pb}$ ages distributed into three peaks
896 with approximately 1480 Ma, 1432 Ma and 1386 Ma. These ages are compatible with source areas
897 located south of the Nova Brasilândia belt composed of rocks from the Colorado and Trincheira
898 complexes (Rizzotto et al., 2013, 2014).

899

900 **7.2 Magmatic crystallization ages**

901
902 The previously published U-Pb magmatic crystallization ages (Table 1) include data of: a)
903 The Rio Branco Suite – a foliated monzogranite of 1113 ± 56 Ma (Rizzotto, 1999); b) The
904 Migrantinópolis Formation – an anatectic leucogranite of 1110 ± 8 M derived from paragneiss
905 (Rizzotto, 1999); and, c) Rio Pardo Suite – two samples of monzogranite of 1005 ± 41 Ma (Rizzotto,
906 1999) and 1010 ± 15 Ma (Rizzotto et al., 2014). These ages, according to the authors cited above,
907 were interpreted as marking the peak of a metamorphism of the Nova Brasilândia belt (ca. 1113-
908 1110 Ma), as well as the post-tectonic granitic magmatism represented by the Rio Pardo Suite (1010-
909 1005 Ma). We would like to point out that despite the reasonable number of analyzes, some of them
910 are inaccurate, as they are associated with high errors.

911 In our research, new magmatic crystallization U-Pb zircon ages were obtained by LA-ICP-
912 MS for Rio Branco Suite. These results present low errors and MSWD, providing more accuracy in
913 the chronology of geological events: a) Medium-grained metagabbro (sample MQ-117) intrusive in
914 high-grade calc-silicate gneiss and biotite paragneiss of the Rio Branco Formation of 1119.7 ± 2.7
915 Ma; b) Foliated metagranite dike (sample MQ-147M) intrusive in high-grade calc-silicate gneiss of
916 the Rio Branco Formation of 1113 ± 6.7 Ma; c) Fine-grained subvolcanic metagranite (sample MQ-
917 124) coeval with massive metabasalt of the Rio Branco Suite of 1112.3 ± 1.9 Ma; d)
918 Metatrandhjemite (sample MQ-29) that occurs as lens inside metagabbro of the Rio Branco Suite
919 of 1106.2 ± 2.8 Ma. High-grade metatrandhjemitic gneiss (sample MQ-122) spatially associated
920 with Rio Branco Formation presented Concordia age of 1127.6 ± 2.3 Ma. These ages of Rio Branco
921 Suite define the timing of mafic-felsic magmatic event between 1119.7 ± 2.7 Ma and 1106.2 ± 2.8
922 Ma. The age of 1127.6 ± 2.3 Ma obtained from trondhjemitic gneiss approximates the high-grade
923 metamorphic age of 1137 ± 9 Ma, considering the dating method used error. Therefore, the age of
924 1127.6 ± 2.3 Ma was preliminarily interpreted in this paper as possible magmatic crystallization age
925 that may represent the fusion of mafic rock during the orogenetic event and very close to the peak
926 of high-grade metamorphism. However, further studies are needed to confirm this hypothesis.

927

928 **7.3 Metamorphism and cooling ages**

929
930 U-Pb (TIMS and SHRIMP) ages of metamorphic recrystallization or metamorphism
931 obtained in zircon, monazite, titanite and rutile crystals of rocks from the Nova Brasilândia belt
932 were compiled from previously published articles (Table 1). Of these published ages, we highlight
933 the metamorphic recrystallization age of 1096 ± 6 Ma (monazite in mylonitic paragneiss), $1089 \pm$
934 9 Ma (titanite in banded leucocratic trondhjemite), 1082 ± 6 Ma (monazite in mica schist), $1061 \pm$

935 14 Ma (intercept age in titanite of the calc-silicate gneiss), 1020 ± 15 Ma (monazite in calc-silicate)
936 (Tohver et al., 2004, 2005a; Rizzotto et al., 2014). A high-grade metamorphic pulse accompanied
937 by low pressure (3.1 Kb) and high temperature migmatization was characterized with U-Pb age
938 (SHRIMP) of 1110 ± 8 Ma obtained in zircon crystal from a granitic leucosome sample and age of
939 1110 ± 10 Ma of a metagabbro of the Nova Brasilândia Group (see Rizzotto, 1999).

940 During our research, new U-Pb ages (LA-ICP-MS) obtained from specific groups of zircon
941 crystals from the Rio Branco domain rocks also revealed metamorphic recrystallization and
942 migmatization ages: a) The $^{207}\text{Pb}/^{206}\text{Pb}$ peak age of 1137 ± 9 Ma and peak age of 1019 ± 15 Ma in
943 calc-silicate gneiss (sample MQ-44); b) Concordia age of 1016.7 ± 3.9 Ma in metagabbro (sample
944 MQ-117); and, c) Upper intercept age of 1011.3 ± 9.6 Ma in anatectic granite (sample MQ-146B)
945 in biotite paragneiss of the Rio Branco Formation.

946 Two main high-grade metamorphic pulse were identified based on the new U-Pb zircon
947 dating (LA-ICP-MS) and the reinterpretation of previously published geochronological data (see
948 Table 1). The geological field relations of rocks reinforce the identification and timing of distinct
949 metamorphic pulses. The oldest metamorphic pulse (amphibolite- to granulite-facies) was recorded
950 in high-grade gneisses and granulite of Rio Branco Formation in the Rio Branco domain between
951 approximately 1138 and 1128 Ma, therefore developed prior to the emplacement of Suite Rio
952 Branco mafic-felsic magmatism. The varying conditions of P-T for oldest metamorphic pulse were
953 initially established based on the paragneisses. High-temperature metamorphic conditions between
954 $670^\circ - 800^\circ \text{C}$ and low-pressure around 3.1 kbars (Rizzotto, 1999). In the southern part of the belt,
955 peak T-conditions of maximum 750°C and maximum P of 7.9 kbars for granulitic paragenesis
956 (Tohver et al., 2004, 2005a). Low-grade ranges (*greenschist facies*) occur locally along shear zones
957 and in the occurrence regions of the Migrantinópolis Formation rocks especially in the northern part
958 of the Nova Brasilândia Belt (Scandolaro and Rizzotto, 1998; Quadros and Rizzotto, 2007). These
959 varied P-T conditions suggest juxtaposition of high-temperature/low-pressure (HT/LP) and high-
960 temperature/high-pressure (HT/HP) metamorphic domains, where metamorphism has reached
961 amphibolite- to granulite-facies conditions. Additionally, the age of 1110 ± 8 Ma of the anatectic
962 leucogranite in Migrantinópolis Formation paragneisses (sample GR-20) was also interpreted as the
963 record of regional metamorphic peak that affected the Migrantinópolis Formation rocks (Rizzotto,
964 1999).

965 The second and youngest metamorphic pulse between 1096 ± 6 Ma and 1011.3 ± 9.6 Ma
966 was recorded in high-grade gneisses of Rio Branco Formation and the metamafic component of Rio
967 Branco Suite. This had been characterized in previous studies involving geological characterization
968 in the field, petrography and geochronology (Rizzotto, 1999; Tohver et al., 2004, 2005a; Rizzotto
969 et al., 2014). This second pulse possibly corresponds to the high-grade metamorphism (amphibolite-
970 facies) from crustal thickening that partially marks the suturing of the Paraguá block to the southern
971 margin of the Amazonian proto-Craton in latest Mesoproterozoic times (Tohver et al., 2004). U-Pb
972 monazite ages of 1090 Ma and titanite ages of approximately 1060 Ma record cooling from the peak
973 metamorphic conditions (Tohver et al., 2004). The published $^{40}\text{Ar}-^{39}\text{Ar}$ data clearly show the age
974 range of cooling episodes that occurred in the Nova Brasilândia belt between 1005 ± 7 Ma (in
975 hornblende from metagabbro) and 910 ± 2 Ma (in biotite from mylonitic paragneiss) (Tohver et al.,
976 2004, 2005a, 2005b).

977

978 **7.4 Tectonic evolution**

979

980 The geological and geochronological data available in the literature on the Nova Brasilândia
981 belt, in association with the new geological field data and U-Pb zircon (LA-ICP-MS) data for the
982 Rio Branco domain presented in this paper, suggest that the tectonic evolution of this belt occurred
983 diachronically in the Mesoproterozoic (Stenian) and early Neoproterozoic (Tonian). We propose
984 that the Nova Brasilândia belt records three evolutionary phases (pre-orogenic, orogenic and post-
985 orogenic) occurred between ca. 1241 Ma and 910 Ma. These phases resulting from the

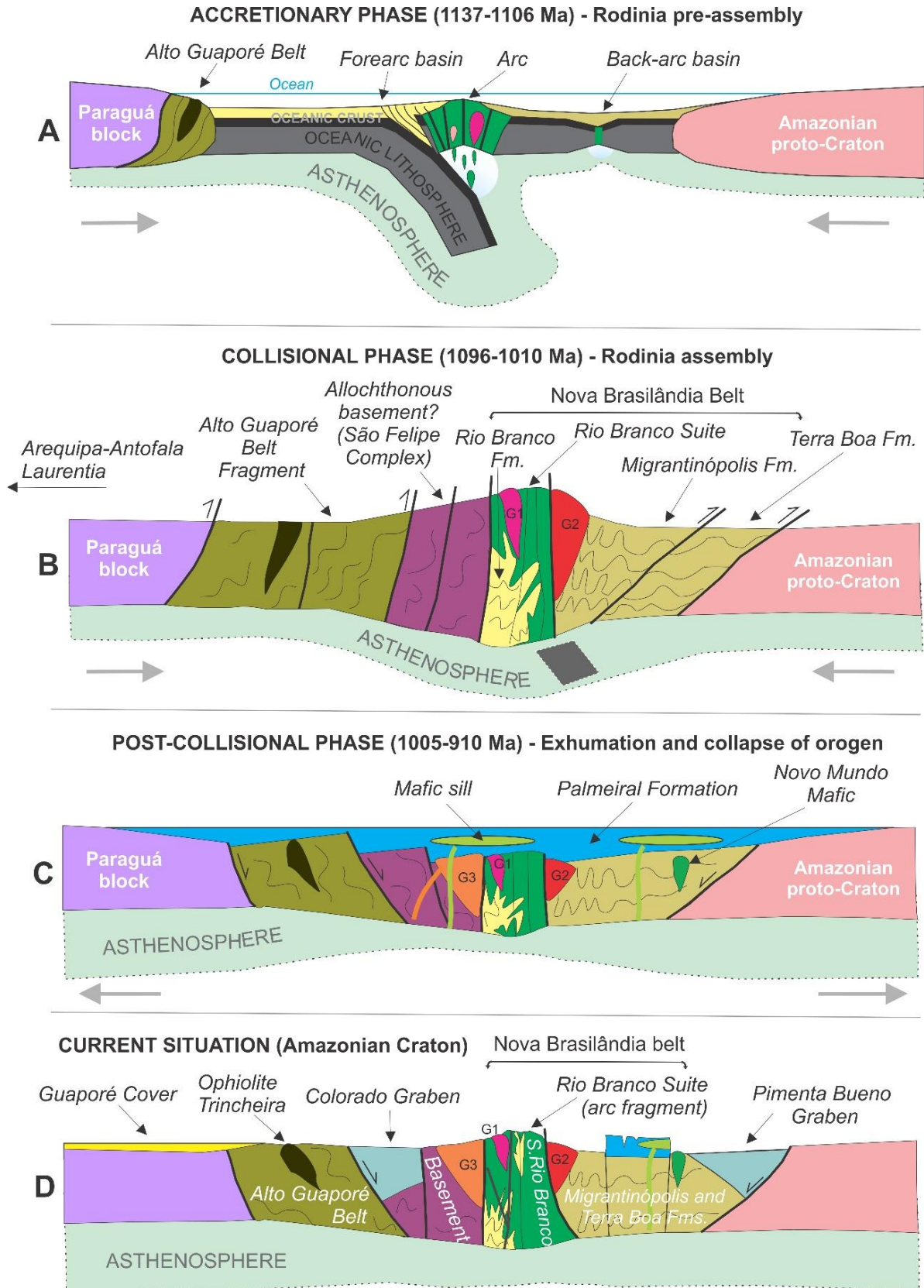
986 fragmentation and agglutination of crustal masses associated with final Rodinia assembly, followed
987 by the subsequent final exhumation and orogenic collapse (Fig. 16, Table 3).

988 Pre-orogenic phase (ca. < 1241 and 1137 Ma) corresponds to extension (rift, rift-drift and
989 drift) with formation of passive margin and proto-ocean (Rizzotto, 1999). The first orogenic phase
990 (ca. 1137 and 1106 Ma) mark the oldest event of the Nova Brasilândia orogeny. It is being proposed
991 in this paper based on geological and geochronological new data, adding to the information and
992 interpretations initially presented by Rizzotto (1999), Rizzotto et al. (2001, 2014) and Tohver et al.
993 (2004, 2005a, 2005b, 2006). It possibly corresponds to the beginning of subduction and closure of
994 a pre-existing ocean, associated with the initial phase of an accretionary orogeny (Fig. 16A),
995 according to Quadros et al. (submitted). An intra-oceanic subduction environment is being attributed
996 to this phase of the Nova Brasilândia orogeny and may be the key to explaining the deformation and
997 metamorphism of high-grade that occurred prior to mafic-felsic magmatism (Rio Branco Suite), as
998 well the positioning of the high-grade metamorphic rocks below the Rio Branco Suite metamafic
999 rocks (Quadros et al., submitted). Another features to be highlighted are the episodes of
1000 sedimentation, metamorphism, deformation and magmatism between ca. 1137 and 1106 Ma,
1001 therefore, with very close ages and associated with a short time for developed of the geological
1002 episodes during the Nova Brasilândia belt tectonic evolution. The presence of metatrandhjemites
1003 (plagiogranites equivalent) with crystallization ages very close to high-grade metamorphism
1004 reinforces the thesis of the intra-oceanic subduction between two oceanic plates.

1005 During the first orogenic phase (ca. 1137 and 1106 Ma), there were a series of magmatic
1006 pulses of mafic and mafic-felsic nature (Rio Branco Suite) intruding high-grade metasedimentary
1007 rocks of the Rio Branco Formation, but with crystallization age very close to that of high-grade
1008 metamorphism. Emplacement of the Rio Branco Suite rocks occurred between 1119.7 ± 2.7 Ma and
1009 1106.2 ± 2.8 Ma (according to the ages of samples MQ-117, MQ-147M, MQ-124 and MQ-29) and
1010 lasted approximately between 19 Ma and 8 Ma considering analysis error (Table 3). Field relations
1011 and isotopic data suggest that this mafic-felsic magmatism occurred in three distinct pulse. The first
1012 pulse had a predominantly mafic nature, represented by metagabbro, with emplacement at deeper
1013 crustal levels at 1119.7 ± 2.7 Ma (sample MQ-117) and under high-temperature conditions, as
1014 evidenced by olivine reaction coronae with plagioclase in metagabbro and metatroctolite. The
1015 second pulse was mafic-felsic, the mafic component represented by sills and dikes of fine-grained
1016 metagabbros (preserved subophitic textures), fine-grained amphibolites (basalt and diabase
1017 protoliths), metadiabases and massive metabasalts, with emplacement at shallow crustal levels at up
1018 to surface overflow. The felsic component of the second pulse is represented by elongated bodies
1019 and dikes of metagranites (porphyritic or fine-grained equigranular) and felsic metavolcanic rocks
1020 with ages of 1113 ± 6.7 Ma (sample MQ-147M), 1112.3 ± 1.9 Ma (sample MQ-124). The third
1021 pulse of magmatism, the youngest associated with first orogenic phase, corresponds to the
1022 generation of lenses and dikes of metatrandhjemites occurring at approximately of 1106.2 ± 2.8 Ma
1023 (sample MQ-29) and corresponding to small volumes of residual magmas probably formed during
1024 fractional crystallization processes or from the fusion of mafic rocks.

1025
1026
1027
1028
1029
1030
1031
1032
1033
1034
1035
1036
1037

1038
1039



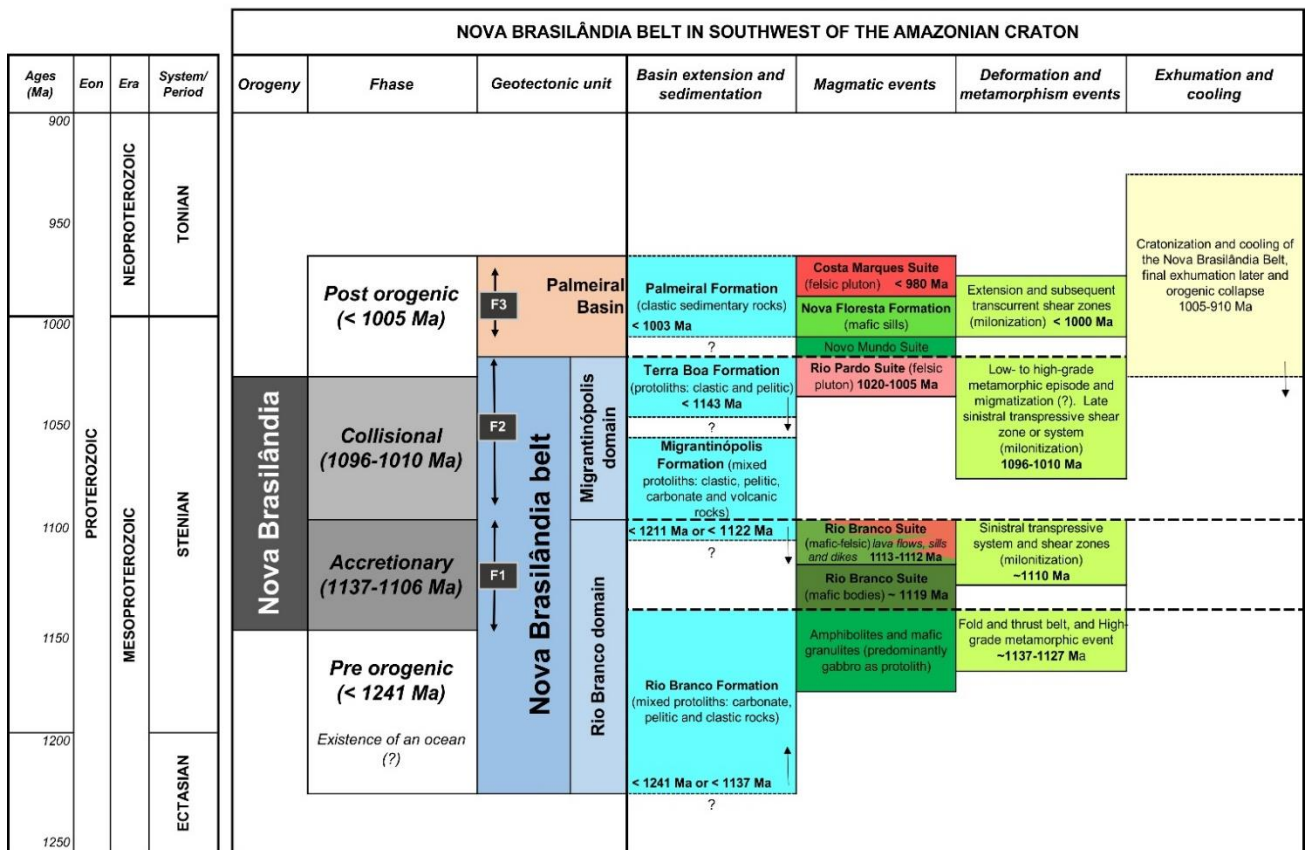
1040
1041
1042
1043
1044
1045

Fig. 16. Simplified model for the Mesoproterozoic (Stenian-Tonian) tectonic evolution proposed for the Nova Brasilândia belt of the southwestern part of the Amazonian Craton, Rondônia.

1046 Second orogenetic phase (about 1096 and 1010 Ma) was presumably evidenced from
 1047 younger U-Pb (LA-ICP-MS) ages obtained from recrystallized zircon crystals, suggesting
 1048 metamorphic overprint between 1019 ± 15 Ma and 1011.3 ± 9.6 Ma. In this context, calc-silicate
 1049 gneiss (sample MQ-44) from the Rio Branco Formation provides a peak $^{207}\text{Pb}/^{206}\text{Pb}$ age of $1019 \pm$
 1050 15 Ma, interpreted as metamorphic recrystallization associated with the younger event. The U-Pb
 1051 age of 1011.3 ± 9.6 Ma (upper intercept) recorded in an anatectic granite (sample MQ-145B)
 1052 occurring as a lens within the paragneiss of the Rio Branco Formation is considered the melt
 1053 crystallization age during the peak of the second metamorphic pulse. Among the recovered zircon
 1054 populations from a metagabbro (sample MQ-117) of the Rio Branco Suite, one of them provides
 1055 the Concordia age of 1016 ± 3.9 Ma, interpreted as the isotopic record of the younger metamorphic
 1056 pulse. However, this youngest age set is still insufficient for accurately demonstrate the participation
 1057 of an event of deformation and metamorphism that generated partial melting (or migmatization) of
 1058 the metasedimentary component of the Rio Branco Formation when analyzed in isolation.
 1059

Table 3.

Time-stratigraphy of Mesoproterozoic (Stenian-Tonian) geological events in the southwest Amazonian Craton recorded in the rocks of the Nova Brasilândia belt, in Rondônia. F1, F2 and F3 are phases of evolution. Arrows indicate change at the beginning of sedimentation and cooling (after Rizzotto, 1999; Scandolaro and Rizzotto, 1998; Rizzotto et al., 2001, 2014; Santos et al., 2003, 2008; Tohver et al., 2002, 2004, 2005a; Teixeira et al., 2010, 2018).



1060
 1061
 1062

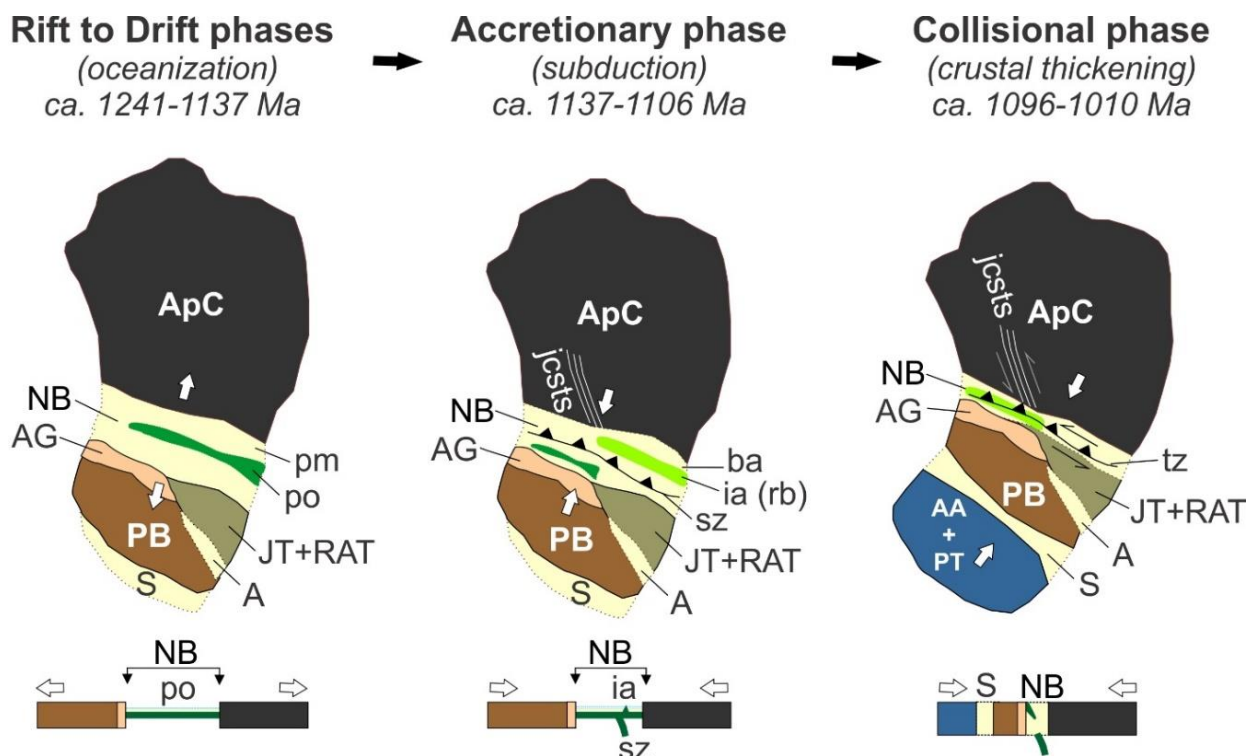
1063 A high-grade metamorphic episode in the Nova Brasilândia belt was previously characterized
 1064 by Rizzotto (1999). The author obtained the age of 1110 ± 8 Ma (zircon U-Pb, SHRIMP) in an
 1065 anatectic leucogranite (GR-20) originating from the Migrantinópolis Formation metatubirdite
 1066 fusion, generated at the metamorphic peak. Additional, ages of 1096 Ma, 1080 Ma and 1085 Ma,
 1067 and 1020 Ma obtained from metamorphic monazite and titanite, respectively, by the U-Pb TIMS
 1068 method in metasedimentary rocks of the Migrantinópolis and Rio Branco formations constrain the
 1069 time of deformation transpressive and metamorphism (Tohver et al., 2004). These ages possibly
 1070 represent younger metamorphism that occurred after the emplacement of the Rio Branco Suite
 1071 rocks. A brief analysis together with the new ages presented in this paper and the U-Pb ages of

1072 previous works (Rizzotto, 1999; Tohver et al., 2004, 2005a; Santos et al., 2008; Rizzotto et al.,
1073 2014) reinforces the characterization of a youngest metamorphism between 1096 ± 5 Ma and 1011.3
1074 ± 9.6 Ma. We suggest that the youngest metamorphism may be associated with the collisional phase
1075 of the Nova Brasilândia orogeny (Fig. 16B), as a reflection of the interactions between Laurentian
1076 and Amazonian cratons, as well as, participation of other cratons, fragments and smaller blocks
1077 (e.g., the Arequipa-Antofala basement, Paraguá block, Alto Guaporé belt fragment and São Felipe
1078 basement). The felsic magmatism of the Rio Pardo Suite at ca. 1005 ± 41 Ma (see Rizzotto, 1999)
1079 registers the beginning of post-tectonic stage of this second orogenetic evolutionary phase in the
1080 Nova Brasilândia belt.

1081 In order to improve the tectonic models of joints between craton, block or terraine fragments
1082 during the development of Mesoproterozoic mobile belts of southwestern Amazonian Craton (Nova
1083 Brasilândia, Sunsás and Aguapeí belts), we present a simplified scenario that demonstrates the
1084 possible cratonic masses involved during the evolution of the Nova Brasilândia belt (Fig. 17).
1085 Complex interactions occurred between Amazonian proto-Craton, Paraguá block, Arequipa-
1086 Antofala basement and allochthonous terrane fragments that need to be better understood. Our
1087 proposal is partly according to the models proposed by Tohver et al. (2002, 2004, 2005b), Loewy
1088 et al. (2004), Boger et al. (2005) and Rizzotto et al. (2014), however, inserted an intra-oceanic
1089 subduction phase in the evolution of the Nova Brasilândia belt (see Quadros et al., submitted).

1090 The post-orogenic phase (<1005 Ma) was not evaluated in this research. It was, developed
1091 in the interval between 1005 and 910 Ma has been recorded in the northern portion of the Nova
1092 Brasilândia belt, reworked cratonic areas (Fig. 16C, Table 3), and marks the collapse of part of
1093 Sunsás orogen (based in Santos et al., 2008). Corresponds to an extensional phase (~ 980 -910 Ma)
1094 post-convergence and exhumation of the orogen, with basin formation and continental siliciclastic
1095 sedimentation (Palmeiral Formation), anorogenic felsic alkaline intrusions (Costa Marques Suite),
1096 and mafic dikes, sills and stocks (Nova Floresta Formation and Novo Mundo Suite). Important
1097 sinistral transcurrent shear zones (e.g., Rio Branco shear zone) were generated at this phase. In the
1098 cratonic area northwest of the study area, several anorogenic granite bodies with Sn-polymetallic
1099 mineralizations (~ 1.08 -0.98 Ga), called Santa Clara Suite and Rondônia Suite were generated
1100 during this extensional phase (see Rizzotto, 1999; Santos et al., 2000, 2008; Rizzotto et al., 2001,
1101 2014; Tohver et al., 2005b, 2006; Quadros and Rizzotto, 2007). Studies by Tohver et al. (2004,
1102 2006) showed U-Pb (titanite and monazite) and $^{40}\text{Ar}/^{39}\text{Ar}$ (amphibole and biotite) metamorphic ages
1103 at time intervals between 1.09-1.06 Ga and 0.97-0.91 Ga, suggesting a long history of
1104 metamorphism, tectonic exhumation and cooling (Table 1). The indication of the minimum
1105 metamorphism age and deformation (shear) at 970-966 Ma and 965 ± 23 Ma, respectively, were
1106 determined by $^{40}\text{Ar}/^{39}\text{Ar}$ and K-Ar (amphibole) analyses of amphibolites (Tohver et al., 2004).

1107 The transtension-transpression recorded by the shear zones that affect the rocks of the Nova
1108 Brasilândia belt may be related to late tectonic extrusion associated with movements and mass
1109 escapes in the late phases of the oblique collisional orogeny. It is possible to establish based on the
1110 available field geological, U-Pb and $^{40}\text{Ar}/^{39}\text{Ar}$ geochronological data (Table 1), that there are at least
1111 three shear phases involving transtension-transpression developed at approximately 1110 Ma and
1112 1010 Ma. These periods of transtension-transpression occurred after the accretionary phase identified
1113 in our research in the Rio Branco domain. These possibilities mentioned above need to be better
1114 evaluated in future studies. Finally, the Figure 16D represents the current stage of the Nova
1115 Brasilândia belt after tectonic reactivations, grabens formation, sedimentation, and erosion along
1116 the Phanerozoic.



Symbology: **ApC**-Amazonian proto-Craton; **PB**-Paraguá block; **AA**-Arequipa-Antofala basement; **JT**-Jauru terrane; **RAT**-Rio Alegre terrane; **PT**-Pampia terrane; **AG**-Alto Guaporé belt; **NB**-Nova Brasilândia belt; **S**-Sunsas belt; **A**-Aguapeí belt/aulacogen; **po**-proto-ocean; **ia**-island arc; **sz**-subduction zone; **pm**-passive margin; **ba**-back-arc; **rb**-Rio Branco Suite; **jcsts**-Ji-Paraná - Cujubim Sinistral Transpressive system; **tz**-transpression zone

1117

1118

1119

1120

1121

1122

1123

1124 8. Conclusion

1125

1126

1127

1128

1129

1130

1131

1132

1133

1134

1135

1136

1137

1138

1139

1140

1141

1142

1143

Fig. 17. Schematic tectonic scenarios of the late Mesoproterozoic (Stenian) with the phase of evolution of the Nova Brasilândia belt involving the break-up of the Amazonian proto-Craton, followed by the accretion of the Paraguá block and the Arequipa-Antofala basement to the western margin of the Amazonian proto-Craton (modified from Boger et al., 2005; Rizzotto et al., 2014).

- The new ages LA-ICP-MS U-Pb obtained in zircon crystals from the Rio Branco domain, southern part of the Nova Brasilândia belt restricted the deposition period of the Rio Branco Formation sedimentary protoliths between 1241 Ma and 1137 Ma. The study of metamorphic zircon grains (cores and rims) suggest a high-grade metamorphism between 1137 ± 9 Ma and 1127.6 ± 2.3 Ma, before the onset of mafic-felsic magmatism of the Rio Branco Suite generated between 1119.7 ± 2.7 Ma and 1106.2 ± 2.8 Ma. Therefore, ages close between high-grade metamorphism and mafic magmatism of Suite Rio Branco suggest an orogenic tectonic environment for the formation of the studied rocks.
- We also identified recrystallized zircon crystals from rocks of the Rio Branco Formation and the Rio Branco Suite with ages U-Pb that possibly represent the record of an episode of youngest metamorphism and migmatization in the evolution of the Nova Brasilândia belt, occurred between 1019 ± 15 Ma and 1011.3 ± 9.6 Ma.

- 1144 • The time interval of the two orogenic phases developed during the Nova Brasilândia orogeny
1145 was identified. The first phase mark an accretionary orogenetic event occurred between ca.
1146 1137 Ma and 1106 Ma comprises a tectonic scenario involving intra-oceanic subduction and
1147 magmatic arc formation and back-arc basin. Our proposal implies in the existence of a small
1148 ocean between the Paraguá block (added of allochthonous terranes fragments) and the
1149 Amazonian proto-Craton in the period between ca. 1241 Ma and 1137 Ma, formed prior to
1150 the accretionary phase proposed in this article. The second phase corresponds to the
1151 subsequent collision of the Amazonian proto-Craton with the Paraguá block (added of
1152 allochthonous terranes) which conditioned the crustal thickening and youngest high-grade
1153 metamorphism in the Nova Brasilia belt at about 1096 Ma as previously proposed by Tohver
1154 et al. (2004). In addition, the youngest zircon U-Pb ages obtained in our research between
1155 1019 ± 15 Ma and 1011.3 ± 9.6 Ma, associated with the U-Pb and K-Ar ages obtained by
1156 Rizzotto (1999), Rizzotto et al. (2014) and Tohver et al. (2004, 2005b, 2006), suggest the
1157 time interval between ca. 1096 and 1010 Ma for the collisional phase, second episode of
1158 metamorphism and inception of orogen cooling.
1159
- 1160 • This new compressional tectonic scenario involving intra-oceanic subduction is different
1161 from those previously proposed involving alternating of transpression and transtension
1162 episodes that conditioned the opening of an intracontinental rift, evolution to passive margin,
1163 proto-ocean formation and basin closure (Rizzotto, 1999; Rizzotto et al., 1999; Tohver et
1164 al., 2004). Therefore, the data from our research presented in this article and those published
1165 by Quadros et al. (submitted) suggest that the nature of the Nova Brasilândia orogeny is
1166 accretionary-collisional type, developed between ca. 1137 and 1010 Ma.
1167

1168 **Acknowledgments**

1169
1170 This work was financed by UnB and by the ARIM Nova Brasilândia Project of CPRM-
1171 Geological Survey of Brazil. The authors are grateful to CPRM-Geological Survey of Brazil in Porto
1172 Velho, Rondônia and Belém, Pará, Brazil for assistance in fieldwork and access to laboratories for
1173 the preparation of samples collected in the field. We also thank Anderson Alves de Souza, Luciano
1174 Castro da Silva and Lívio Wagner Chaves Correa for the geological discussions during field
1175 activities and office work. We thank Maria Rosalva Campos Coelho for the help in the preparation
1176 of the samples for U-Pb zircon geochronological analyses. We thank CPRM and UnB technicians
1177 for their support and performing U-Pb zircon geochronological analyses in the laboratory of the
1178 Geochronology Center of the Institute of Geosciences of the University of Brasilia (Geocron-
1179 IG/UnB). Constructive reviews of this manuscript by anonymous reviewers are gratefully
1180 acknowledged.
1181

1183 **References**

- 1184
1185 Amaral, G. 1974. *Geologia Pré-Cambriana da Região Amazônica* (Tese de doutorado). Instituto de
1186 Geociências, Universidade de São Paulo, São Paulo, SP, Brasil.
1187
- 1188 Bahia, R.B.C., Silva, C.R. da. (Orgs.). 1998. Rio Pardo Folha SC.20-Z-C-VI, Estado de Rondônia. Brasília:
1189 CPRM, 1998. Escala 1:100.000. *Programa levantamentos geológicos básicos do Brasil*. Convênio
1190 DNPM/CPRM.
1191
- 1192 Bergami, G.N., Prado, E.M.G, Souza, A.A de, Oliveira, C.E.S., Guerra, G.I.T., Silva, G.F. da, Corrêa,
1193 L.W.C., Silva, L.C. da; Quadros, M.L. do E.S., Graça, M.C., Adorno, R.R., Rodrigues, T.R., Ribeiro,
1194 T. de J., Oliveira Neto, W.L. de, Silva, D.R.V. da. 2018. *Mapa geológico integrado da ARIM Nova*
1195 *Brasilândia. Porto Velho: CPRM, 2018. Escala 1:150.000. (Projeto Evolução Crustal e Metalogenia da*
1196 *Faixa Nova Brasilândia).*

- 1197
1198 Bettencourt, J. S., Leite Jr., W. B., Ruiz, A. S., Matos, R., Payolla, B. L., Tosdal, R. M. 2010. The
1199 Rondonian-San Ignacio Province in the SW Amazonian Craton: an overview. *Journal of South*
1200 *American Earth Sciences*, 29, 28-46.
1201
- 1202 Boger, S. D., Raetz, M., Giles, D., Etchart, E., Fanning, C. M. 2005. U-Pb age data from the Sunsás region
1203 of eastern Bolivia, evidence for the allochthonous origin of the Paraguá Block. *Precambrian Research*,
1204 139, 121-146.
- 1205 Bühn, B., Pimentel, M. M., Matteini, M., Dantas, E. L. 2009. High spatial resolution analysis of Pb and U
1206 isotopes for geochronology by laser ablation multi-collector inductively coupled plasma spectroetry
1207 (L-C-ICPMS). *An. Acad. Bras. Cienc.*, 81, 99-114.
- 1208 Cardona, A., Chew, D., Valencia, V. A., Bayona, G., Miskovic, A., Ibanez-Mejia, M. 2010. Grenvillian
1209 remnants in the Northern Andes: Rodinian and Phanerozoic paleogeographic perspectives. *Journal of*
1210 *South American Earth Sciences*, 29, 92–104.
- 1211 Casquet, C., Pankhurs, R. J., Fanning, M., Baldo, E., Galindo, C., Rapela, C. W., Casado, J. G., Dahlquist,
1212 J. A. 2006. U-Pb SHRIMP zircon dating of Grenvillian metamorphism in Western Sierras Pampeanas
1213 (Argentina): correlation with the Arequipa-Antofalla Craton and constraints on the extent of the
1214 Precordillera Terrane. *Gondwana Research*, 9(4), 524-529.
- 1215 Cawood, P. A. and Pisarevsky, S. A. 2017. Laurentia-Baltica-Amazonia relations during Rodinia assembly.
1216 *Precambrian Research*, 292, 386-397. <https://doi.org/10.1016/j.precamres.2017.01.031>.
- 1217 Chew, D. M., Cardona, A., and Miskovic, A. 2011. Tectonic evolution of western Amazonia from the
1218 assembly of Rodinia to its break-up. *International Geology Review*, 53, 11-12, 1280-1296.
- 1219 Cordani, U. G., Tassinari, C. C. G., Teixeira, W., Basei, M. A. S., Kawashita, K. 1979. Evolução tectônica
1220 da Amazônia com base nos dados geocronológicos. *Anais do Congresso Geológico Chileno*, Arica,
1221 China, 2.
- 1222 Cordani, U. G., and Teixeira, W. 2007. Proterozoic accretionary belts in the Amazonian Craton. In: Hatcher,
1223 R. D. J., Carlson, M. P., McBride, J. H., Martínez, C. J. R. (Ed.). 4-D framework of continental crust:
1224 boulder, Colorado. *Geological Society of America Memoir*, 200, 297–320.
- 1225 Cordani, U. G., Teixeira, W., D'Agrella-Filho, M. S., Trindade, R. I. 2009. The position of the Amazonian
1226 Craton in supercontinents. *Gondwana Research*, 15, 396–407.
- 1227 Corfu, F., Hanchar, J. M., Hoskin, P. W. O., Kinny, P. 2003. Atlas of Zircon Textures. In Hanchar, J. M.,
1228 and Hoskin, W. O. (Ed.). *Zircon. Reviews in Mineralogy and Geochemistry*, 53.
- 1229 Cordani, U. G., Fraga, L. M., Reis, N. J., Tassinari, C. C. G., Brito-Neves, B. B. 2010. On the origin and
1230 tectonic significance of the intra-plate events of Grenvillian-type age in South America: a discussion.
1231 *Journal of South American Earth Sciences*, 29, 143–159.
- 1232 Costa, J. B. S. and Hasui, Y. 1991. O quadro geral da evolução tectônica da Amazônia. In: *Anais do*
1233 *Simpósio Nacional de Estudos Tectônicos*, Rio Claro, São Paulo, 3.
- 1234 Dalziel, I. W. D. 1991. Pacific margins of Laurentia and East Antarctica-Australia as a conjugate rift pair:
1235 Evidence and implications for an Eocambrian supercontinent. *Geology*, 19, 598 – 601.
- 1236 Fuck, R. A., Neves, B. B. B., Schobbenhaus, C. 2008. Rodinia descendants in South America. *Precambrian*
1237 *Research*, 160(1–2), 108–126.
- 1238 Harley, S. L. Kelly, N.M., Möller, A. 2007. Zircon Behaviour and the Thermal Histories of Mountain
1239 Chains. *Elements*, 3 (1): 25–30. doi: <https://doi.org/10.2113/gselements.3.1.25>

- 1240 Hasui, Y., Haralyi, N. L. E., Schobbenhaus, C. 1984. Elementos geofísicos e geológicos da Região
1241 Amazônica: subsídios para o modelo geotectônico. *Anais do Sumposium Amazonico*, Manaus, Brasil,
1242 2.
- 1243 Hoffman, P. F. 1991. Did the breakout of Laurentia turn Gondwana inside out? *Science*, 252, 1409-1412.
- 1244 Jackson, S., Pearson, N. J., Griffin, W. L., Belousova, E. A. 2004. The application of laser ablation-
1245 inductively coupled plasma-mass spectrometry to in situ U–Pb zircon geochronology. *Chem. Geol.*,
1246 211, 47-69.
- 1247 Johansson, A., 2009. Baltica, Amazonia and the SAMBA connection — 1000 million years of
1248 neighbourhood during the Proterozoic? *Precamb. Res.* 175, 221–234.
- 1249 Johansson, A., 2014. From Rodinia to Gondwana with the “SAMBA” model - a distant view from Baltica
1250 towards Amazonia and beyond. *Precamb. Res.* 244, 226–235.
- 1251 Keppie, J. D. and Ortega-Gutierrez, F. O. 1999. Middle American Precambrian basement: a missing piece
1252 of the reconstructed 1 Ga orogen. *Geol. Soc. of Am., Spec. Paper 336*, 199-210.
- 1253 Li, Z. X., Bogdanova, S. V., Collins, A. S., Davidson, A., De Waele, B., Ernst, R. E., Fitzsimons, I. C. W.,
1254 Fuck, R. A., Gladkochub, D. P., Jacobs, J., Karlstrom, K. E., Lu, S., Natapov, L. M., Pease, V.,
1255 Pisarevsky, S. A., Thrane, K., Vernikovskiy, V. 2008. Assembly, configuration, and break-up history
1256 of Rodinia: a synthesis. *Precam. Res.* 160, 179-210.
- 1257 Litherland, M., Annels, R. N., Appleton, J., Berrange, J., Bloomfield, K., Burton, C., Darbyshire, D. P. F.,
1258 Fletcher, C. J. N., Hawkins, M. P., Klink, B. A., Llanos, A., Mitchell, W. I., O'Connor, E. A., Pitfield,
1259 P. E. J., Power, G., Webb, B. C. 1986. The geology and mineral resources of the Bolivian Precambrian
1260 shield. *Overseas Memoir. British Geological Survey Paper 9*.
- 1261 Litherland, M., Annels, R.N., Darbyshire, D.P.F., Fletcher, C.J.N., Hawkins, M.P., Klink, B.A., Mitchell,
1262 W.I., O'Connor, E.A., Pitfield, P.E.J., Power, G., Webb, B.C. 1989. The Proterozoic of eastern Bolivia
1263 and its relationship to the Andean mobile belt. *Precambrian Research* 43, 157–174.
- 1264 Loewy, S., Connelly, J. N., Dalziel, I. W. 2004. An orphaned basement block: the Arequipa-Antofalla
1265 Basement of the central Andean margin of South America. *Geol. Soc. Am. Bull.*, 116, 171-187.
- 1266 Loewy, S., Connelly, J. N., Dalziel, I. W., Gower, C. F. 2003. Eastern Laurentia in Rodinia: Constraints
1267 from wholerock Pb and U-Pb geochronology. In Sircombe, K. N. and McElhinny, M. W. (Ed.).
1268 Orogenic belts, regional and global tectonics: a memorial volume to Chris McAulay Powell.
1269 *Tectonophys* 375, 169-197.
- 1270 Ludwig, K. R. 2003. User’s manual for Isoplot 3.00 (pp. 74). *BerkeleyGeochronology Center*, 4.
- 1271 Luft Jr., J. L., G. Rizzotto, F. Chemale Jr., E. F. Lima. 2000. Análise geológico-estrutural do Cinturão
1272 Sunsás na região de Nova Brasilândia, sudeste de Rondônia. *Rev. Pesq. Geocienc.*, 2, p. 65-78.
- 1273 Miskovic, A., Schaltegger, U., Spikings, R. A., Chew, D. M., Kosler, J. 2009. Tectono-magmatic evolution
1274 of Western Amazonia: geochemical characterisation and zircon U-Pb geochronologic constraints from
1275 the Peruvian Eastern Cordilleran granitoids. *Geological Society of America Bulletin*, 121, 1298–1324.
- 1276 Pinto Filho, F. P., Freitas, A. F. de, Melo, C. F., Romanini, S. J. 1977. *Projeto Sudeste de Rondônia:
1277 relatório final*. Porto Velho: CPRM.
- 1278 Priem, H. N. A., Bon, E. H., Verdumen, E. A. Th., Bettencourt, J. S. 1989. Rb-Sr chronology of
1279 Precambrian crustal evolution in Rondonia (Western margin Brazilian Craton). *Journal of South
1280 American Earth Sciences*, 2, 163-170.

- 1281 Quadros, M. L. do E. S. and Rizzotto, G. J. (Org.). 2007. *Geologia e recursos minerais do Estado de*
1282 *Rondônia: texto explicativo do mapa geológico e de recursos minerais do Estado de Rondônia*. Escala
1283 1:1.000.000. Porto Velho: CPRM.
- 1284 Quadros, M. L., Palmeira, L. C., Castro, C. C. 2011. *Geologia e Recursos Minerais da Folha Rio*
1285 *Machadinho: SC.20-X-C, escala 1:250.000* (pp. 203). Porto Velho: CPRM.
- 1286 Quadros, M.L. do E.S.; Giustina, M.E.S.D.; Souza, V.S. Geology, petrology and Sr-Nd isotopes of the Rio
1287 Branco Suite, Nova Brasilândia belt in southwest of the Amazonian Craton: Evidence of a pre-Rodinia
1288 island arc (ca. 1137-1106 Ma) (submitted).
- 1289 Ramos, V. A. 2008. The basement of the Central Andes: the Arequipa and related terranes. *Annual Review*
1290 *Earth and Planetary Sciences*, 36, 289–324.
- 1291 Ramos, V. A. 2010. The Grenville-age basement of the Andes. *Journal of South American Earth Sciences*,
1292 29, 77–91.
- 1293 Rizzotto, G. J. 1999. *Petrologia e Geotectônica do Grupo Nova Brasilândia, Rondônia* (Dissertação de
1294 mestrado). Federal University of Rio Grande do Sul, Porto Alegre, Brazil.
- 1295 Rizzotto, G. J., Lima, E. F., and Chemale Jr., F. 1999. Geologia e geoquímica das rochas metabásicas da
1296 sequência metavulcano-sedimentar Nova Brasilândia – sudoeste de RO. *Revista Brasileira de*
1297 *Geociências*, 29(2), 119-128.
- 1298 Rizzotto, G. J., Lima, E. F., and Chemale Jr., F. 2001. Geologia do Grupo Nova Brasilândia, sudeste de
1299 Rondônia, acreção continental e implicações geotectônicas. In Reis, N. J., and Monteiro, M. A. S.
1300 (Coord.). *Contribuições à Geologia da Amazônia. Sociedade Brasileira de Geologia*, 2, 342–442.
- 1301 Rizzotto, G. J., and Hartmann, L. A. 2012. Geological and geochemical evolution of the Trincheira
1302 Complex, a Mesoproterozoic ophiolite in the southwestern Amazon craton, Brazil. *Lithos*, 148, 277-
1303 295.
- 1304 Rizzotto, G. J., Santos, J. O. S., Hartmann, L. A., Tohver, E., Pimentel, M. M., and Mcnaughton, N. J. 2013.
1305 The Mesoproterozoic Guaporé suture in the SW Amazonian craton: geotectonic implications based on
1306 field geology, zircon geochronology and Nd-Sr isotopic geochemistry. *J. South. Am. Ear. Sci.*, 48,
1307 271-295.
- 1308 Rizzotto, G. J., Hartmann, L. A., Santos, J. O. S., and Mcnaughton, N. J. 2014. Tectonic evolution of the
1309 southern margin of the Amazonian craton in the late Mesoproterozoic based on field relationships and
1310 zircon U-Pb geochronology. *Anais da Academia Brasileira de Ciências*, 86(1), 57-84.
- 1311 Rogers, J. J., and Santosh, M. 2003. Supercontinents in Earth history. *Gond. Res.*, 6, 357-368.
- 1312 Ruiz. A. S. 2005. *Evolução geológica do sudoeste do Cráton Amazônico, região limítrofe Brasil-Bolívia,*
1313 *Mato Grosso* (Tese de doutorado). Universidade Estadual Paulista, Rio Claro, São Paulo, Brasil.
- 1314 Ruiz A. S., Simões L. S., Araujo L. M., Godoy A. M., Matos J. B., Souza M. Z. 2007. Cinturão Orogênico
1315 Aguapeí (1025-900 Ma): um exemplo de faixa móvel intracontinental no SW do Cráton Amazônico.
1316 *Anais do Simpósio Nacional de Estudos Tectônicos*, Natal, Brasil, 11.
- 1317 Sadowski, G. R., and Bettencourt, J. S. 1996. Mesoproterozoic tectonic correlations between eastern
1318 Laurentia and western border of the Amazon Craton. *Precam. Res.*, 76, 213-227.
- 1319 Santos, J. O., Hartmann, L. A., Gaudette, H. E., Groves, D. I., Mcnaughton, N. J., Fletcher, I. R. 2000. A
1320 new understanding of the provinces of the Amazon Craton based on integration of field mapping and
1321 U-Pb and Sm-Nd geochronology. *Gond. Res.*, 3, 453-488.

- 1322 Santos, J. O. S., Rizzotto, G. J., Chemale, F., Hartmann, L. A., Quadros, M. L. do E.S., Mcnaughton, N. J.
1323 2003. Três orogêneses colisionais do Sudoeste do Cráton Amazonas: evidências com base em
1324 geocronologia U-Pb. *Resumos do Simpósio Brasileiro de Geologia do Centro-Oeste*, Cuiabá, Brasil,
1325 8.
- 1326 Santos, J. O., Rizzotto, G. J., Potter, P., Mcnaughton, N., Matos, R., Hartmann, L. A., Chemale, J. R.,
1327 Quadros, M. L. 2008. Age and autochthonous evolution of the Sunsás Orogen in West Amazon Craton
1328 based on mapping and U Pb geochronology. *Precam. Res.*, 165, *An. Acad. Bras. Cienc.*, 86 (1), 120-
1329 152.
- 1330 Scandolaro, J. E. 2006. *Geologia e evolução do terreno Jamari, embasamento da faixa Sunsás/Aguapeí,*
1331 *centro-leste de Rondônia, sudoeste do Cráton Amazônico* (Tese de doutorado). Instituto de
1332 Geociências, Universidade de Brasília, Brasília, Brasil.
- 1333 Scandolaro, J. E. and Rizzotto, G. J. (Org.). 1998. *Paulo Saldanha, Folha SC.20-Z-C-V. Estado de*
1334 *Rondônia, escala 1:100.000*. Brasília: CPRM.
- 1335 Scandolaro, J. E., Rizzotto, G. J., Bahia, R. B. C., Quadros, M. L. do E. S., Silva, C. R. da, Amorim, J. L.
1336 de. 1999. *Mapa geológico do Estado de Rondônia, escala 1:1.000.000*. Porto Velho: CPRM.
- 1337 Scandolaro, J. E., Rizzotto, G. J., Silva, L. C. 1992. Geologia da Região de Nova Brasilândia, Sudeste de
1338 Rondônia. *Resumos do Congresso Brasileiro De Geologia*, São Paulo, Brasil, 37.
- 1339 Stacey, J. S, and Kramers, Jan. 1975. Approximation of Terrestrial Lead Isotope Evolution by a 2-Stage
1340 Model. *Earth and Planetary Science Letters*, 26(2), 207-221. [https://doi.org/10.1016/0012-](https://doi.org/10.1016/0012-821X(75)90088-6)
1341 [821X\(75\)90088-6](https://doi.org/10.1016/0012-821X(75)90088-6).
- 1342 Silva, C.R.; Bahia, R.B.C.; Silva, L.C. 1992. Geologia da região de Rolim de Moura – sudeste de Rondônia.
1343 In: *Congr. Bras. Geol.*, 37. São Paulo, 1992. Boletim de resumos expandidos. São Paulo, SBG. 1: 152-
1344 153.
- 1345 Tassinari, C. C. G., Cordani, U. G., Nutman, A. P., Van Schmus, W. R., Bettencourt, J.S., Taylor, P. N.
1346 1996. Geochronological systematics on basement rocks from the Rio Negro-Juruena Province
1347 (Amazonian Craton) and tectonic implications. *Int. Geol. Rev.* 38, 161-175.
- 1348 Tassinari, C. C. G. and Macambira, M. J. B. 1999. *Geochronological provinces of the Amazonian Craton.*
1349 *Episodes*, 22(3), 174-182.
- 1350 Teixeira, W., Geraldes, M. C., Matos, R., Ruiz, A. S., Saes, G., Vargas-Mattos, G. 2010. A review of the
1351 tectonic evolution of the Sunsás belt, SW Amazonian Craton. *Journ. of South Am. Earth Sci.*, 29(1),
1352 47-60.
- 1353 Teixeira, W., and Tassinari, C. C. G. 1984. Caracterização geocronológica da Província Rondoniana e suas
1354 implicações geotectônicas. *Anais do Symposium Amazonico*, Manaus, Brasil, 2.
- 1355 Teixeira, W., Tassinari, C. C. G., Cordani, U. G., Kawashita, K. 1989. A review of the geochronology of
1356 the Amazonian Craton: tectonic implications. *Precambrian Research*, 42, 213-227.
- 1357 Teixeira, W., Hamilton, M. A., Lima, G. A., Ruiz, A. S., Matos, R., Ernst, R. E. 2015. Precise ID-TIMS
1358 U–Pb baddeleyite ages (1110–1112 Ma) for the Rincón del Tigre-Huanchaca large igneous province
1359 (LIP) of the Amazonian Craton: implications for the Rodinia supercontinent. *Precambrian Research*,
1360 265, 273-285.
- 1361 Teixeira, W., Hamilton, M. A., Girardi, V. A. V., Faleiros, F. M., Emst, R. E. 2018. U-Pb baddeleyite ages
1362 of key dyke swarms in the Amazonian Craton (Carajás/Rio Maria and Rio Apa areas): tectonic
1363 implications for events at 1880, 1110 Ma, 535 Ma and 200 Ma. *Precambrian Research*.
1364 doi:10.1016/j.precamres.2018.02.008

- 1365 Tohver, E., Van Der Pluijm, B. A., Mezger, K., Essene, E., Scandolaro, J. E., Rizzotto, G. J. 2004.
1366 Significance of the Nova Brasilândia metasedimentary belt in western Brazil: redefining the
1367 Mesoproterozoic boundary of the Amazon Craton. *Tectonics*, 23. doi:10.1029/2003TC001563
1368 (TC6004).
- 1369 Tohver, E., Van Der Pluijm, B. A., Mezger, K., Scandolaro, J. E., Essene, E. J. 2005a. Two stage tectonic
1370 history of the SW Amazon craton in the late Mesoproterozoic: identifying a cryptic suture zone.
1371 *Precamb. Res.*, 137, 35-59.
- 1372 Tohver, E., Van Der Pluijm, B. A., Scandolaro, J. E., Essene, E. 2005b. Late mesoproterozoic deformation
1373 of SW Amazonia (Rondonia, Brazil): geochronological and structural evidence for collision with
1374 Southern Laurentia. *J. Geol.*, 113, 309-323. doi: 10.1086/428807.
- 1375 Tohver, E., Van Der Pluijm, B. A., Van Der Voo, R., Rizzotto, G. J., Scandolaro, J. E. 2002.
1376 Paleogeography of the Amazon Craton at 1.2 Ga: early grenvillian collision with the llano segment of
1377 Laurentia. *Earth and Planetary Science Letters*, 199, 185-200.
- 1378 Tohver, E., Teixeira, W., Van Der Pluijm, B., Geraldes, M., Bettencourt, J. S., Rizzotto, G. J. 2006.
1379 Restored transect across the exhumed Grenville orogen of Laurentia and Amazonia, with implications
1380 for crustal architecture. *Geology*, 34, 669-672.
- 1381 Touret, J. L. R., Santosh, M., and Huizenga, J. M. 2016. High-temperature granulites and supercontinents.
1382 *Geoscience Frontiers*, 7, 101-113.
- 1383 Trindade Netto, G.B., Lima, A.F., Oliveira, W.L. 2018. *Geologia e recursos minerais da Folha Presidente*
1384 *Médici SC.20-Z-C: escala 1:250.000, Estado de Rondônia*. Programa Geologia do Brasil (PGB):
1385 CPRM, Porto Velho. 156 p. il.

Geology, geochemistry and Sr-Nd isotopes of the Rio Branco Suite, Nova Brasilândia belt in southwest of the Amazonian Craton: Evidence of a Rodinia pre-assembly accretionary phase (ca. 1137 and 1106 Ma) during the evolution of the Nova Brasilândia orogeny

1 **Geology, geochemistry and Sr-Nd isotopes of the Rio Branco Suite, Nova**
2 **Brasilândia belt in southwest of the Amazonian Craton: Evidence of a Rodinia**
3 **pre-assembly accretionary phase (ca. 1137 and 1106 Ma) during the evolution of**
4 **the Nova Brasilândia orogeny**

5
6 Marcos Luiz do Espírito Santo Quadros^{a,*}, Maria Emília Schutesky Della Giustina^b, Valmir da Silva Souza^b,
7 Jaime Estevão Scandola^c

8
9 ^a Serviço Geológico do Brasil (CPRM), Avenida Dr. Freitas, nº 3645 - Bairro do Marco, CEP 66095-110, Belém, PA, Brazil

10 ^b Instituto de Geociências, Campus Universitário Darcy Ribeiro, Universidade de Brasília (UnB), CEP 70910-900, Brasília-DF-Brazil

11 ^c Serviço Geológico do Brasil (CPRM), Setor Bancário Norte, Quadra 02, AN, Bloco H, Ed. Central Brasília, CEP 70040-904, Brasília, DF, Brazil

12
13 * Corresponding author (e-mail address: marcos.quadros@cprm.gov.br)
14
15

17 **ARTICLE INFO**

18 *keywords:*

19 Rio Branco Suite
20 Nova Brasilândia belt
21 Amazonian Craton
22 Sunsás orogen
23 Geochemistry

17 **ABSTRACT**

18
19 *The tectonic affinity of the Rio Branco Suite magmatism in the Nova Brasilândia*
20 *belt, southwest of the Amazonian Craton, Rondônia, is important for*
21 *understanding the role of the Rio Branco domain in the identification of the*
22 *Mesoproterozoic orogenetic events associated the Rodinia supercontinent pre-*
23 *assembly. The regional country rocks (Rio Branco Formation) is composed of*
24 *calc-silicate gneiss, biotite paragneiss, amphibolite and granulite with ages of*
25 *provenacne between ca. 1241-1137 Ma submitted to high-grade metamorphism*
26 *between ca. 1137-1127 Ma. The Rio Branco Suite (ca. 1119-1106 Ma) is*
27 *composed of coeval mafic-felsic rocks classified as metagabbro, metatroctolite,*
28 *massive metabasalt, metadiabase, amphibolite, metagranite, felsic*
29 *metavolcanic rocks and metatrandhjemite, exposed as rounded or oval*
30 *intrusions, sills and dykes. Whole-rock geochemical data show that the*
31 *metamafic rocks of the Rio Branco Suite are of sub-alkaline medium- to low Ti*
32 *tholeiitic with composition and signature of overlapping of MORB-like (mid-*
33 *ocean ridge basalt), IAT (island arc tholeiite) and BAB (back-arc basalt). In*
34 *multi-element diagrams of the metamafic rocks show negative anomalies of Nb*
35 *and Ta, positive of Pb, and gradual enrichment in Th relative to Nb and Ta. On*
36 *the other hand, features $Ti/V=10-50$, $La/Yb=1.74-12.33$ and $Th/Yb=0.10-3.56$,*
37 *low to high Ce/Y (4.12-24.67) ratios and low-ratios Ce/Pb (3.3-20.5), Nb/U*
38 *(3.2-16.25) and Th/La (0.01-0.30), are subduction environment characteristics.*
39 *Sr-Nd isotope composition showed ϵNd with slightly negative to positive values*
40 *between -2.89 and +1.66 ($t=1120$ Ma) close to CHUR and varied $^{87}Sr/^{86}Sr$*
41 *ratios (0.702-0.713) and low $^{143}Nd/^{144}Nd$ ratios (~ 0.512) suggests crustal*
42 *contamination. The geological data, geochemical and isotopic signatures of the*
43 *Rio Branco Suite metamafic component shown in discriminated tectonic*
44 *diagrams and trace elements diagrams are considered effective in the*
45 *diagnostic of subduction environment. Results presented here demonstrate that*
46 *the collisional orogenetic phase of the Nova Brasilândia orogeny associated*
47 *with assembly of Rodinia were preceded by a Mesoproterozoic accretionary*
48 *phase between ca. 1137 and 1106 Ma that provided the development of arc -*
49 *back-arc system. Closure of an ocean prior to the amalgamation of Rodinia*
50 *occurred through intra-oceanic subduction between of Paraguá block (with*
51 *allochthonous terranes accreted) and Amazonian proto-Craton during oblique*
52 *or frontal tectonic interactions between large crustal masses represented by*
53 *Laurentia and Amazon.*
54
55
56
57
58

59 **1. Introduction**

60

61 The geological events of the late Mesoproterozoic and Neoproterozoic (ca. 1241-910 Ma)
62 recorded on the southwestern margin of the Amazonian Craton, in the Brazilian states of Rondônia
63 and Mato Grosso and in Bolivia, are generally referred to as Sunsás Province or Sunsás-Aguapeí
64 Province (Tassinari and Macambira, 1999; Santos *et al.*, 2000, Teixeira *et al.*, 2010). Local
65 denominations have been assigned such as Nova Brasilândia, Sunsás-Nova Brasilândia, Sunsás,
66 Sunsás-Aguapeí or Aguapeí, as names to define provinces, mobile belts, orogen or orogenies
67 (Tassinari and Macambira, 1999; Santos *et al.*, 2000, 2008; Teixeira *et al.*, 2010). Globally, Sunsás
68 Orogen is the representative of the Supercontinent Rodinia assembly event in the Amazon, along
69 with Grenville orogen that extends from Labrador in northeastern Canada to the Adirondack
70 Mountains and southwestward under the coastal plain of the eastern United States, as well as several
71 orogens correlated from others parts of the earth. The first proposals of Rodinia assembly
72 demonstrated that it was evident that western South America was part of the supercontinent Rodinia
73 (Hoffman, 1991; Dalziel, 1997). Sadowski and Bettencourt (1996) introduced the tectonic scenario
74 that Grenville front in North America and Canada was consequence of the collision between
75 Laurentia and Amazon. Paleogeographic reconstructions for the Mesoproterozoic have suggested a
76 long period of interaction between large crustal masses of North and South America, known as
77 Laurentia and Amazonia, respectively.

78 The recognition of the geological similarities between the Grenville and Sunsás provinces
79 as the end products of continent-continent collision during the consolidation of Rodinia led to the
80 proposal of the juxtaposition of the grenvillian mobile belts in Laurentia with those of the
81 southwestern region of the Amazonian Craton (Sunsás, Aguapeí and Nova Brasilândia belts) (see
82 Tohver *et al.*, 2002, 2004, 2005a, 2005b, 2006; Santos *et al.*, 2008; Teixeira *et al.*, 2010; Rizzotto *et al.*,
83 2014).

84 This paper presents new field geological data and a detailed geochemical and isotopic Sr-Nd
85 assessment performed on the Rio Branco Suite metamafic rocks. The objective is contributing to
86 the discussion of the Rio Branco Suite meaning in the tectonic evolution of Nova Brasilândia belt
87 and Sunsás Orogen in the southwest of the Amazonian Craton, Rondônia (Fig. 1). New field
88 geological data provided and allow a better definition of the spatial and temporal relationships
89 between the lithological units. The geochemical and isotopic signatures of the mafic magmatism
90 were investigated to unravel the magma sources, nature of the mantle reservoirs and tectonic
91 affinity. In addition, this paper it presents new information that can use to improve the global
92 geotectonic models that try to explain the Rodinia supercontinent assembly.

93

94

95 **2. Geological background**

96

97 **2.1 Regional context**

98

99 The Amazonian Craton is one of the principal Precambrian geotectonic units of South
100 America. It is exposed mainly in Brazil, but extends into Guyana, Suriname, Venezuela, Colombia
101 and Bolivia. It is one of the world's largest cratonic areas covering about 5,600,000 km², of which
102 about 4,400,000 km² are in Brazil. The Amazonian Craton is tectonically limited by the Araguaia
103 belt to the E, and by the Paraguay Belt to the S and SE. A large part of the Amazonian Craton is
104 covered by Phanerozoic sedimentary sequences of the Parnaíba Basin, to the E; by the Xingu and
105 Alto Tapajós basins to the S, and by those of the Parecis Basin to the SW. To the W, the Amazonian
106 Craton is covered by the Solimões Basin, and to the N by the Tacutu Basin. In the central region of
107 the Craton the overlying sediments are those of the Amazonas Basin. The basement of the
108 Amazonian Craton extends under Cenozoic deposits up to the Andean pre-Cordillera, where
109 Mesoproterozoic are exposed (Kroonenberg, 1982; Priem *et al.*, 1989).

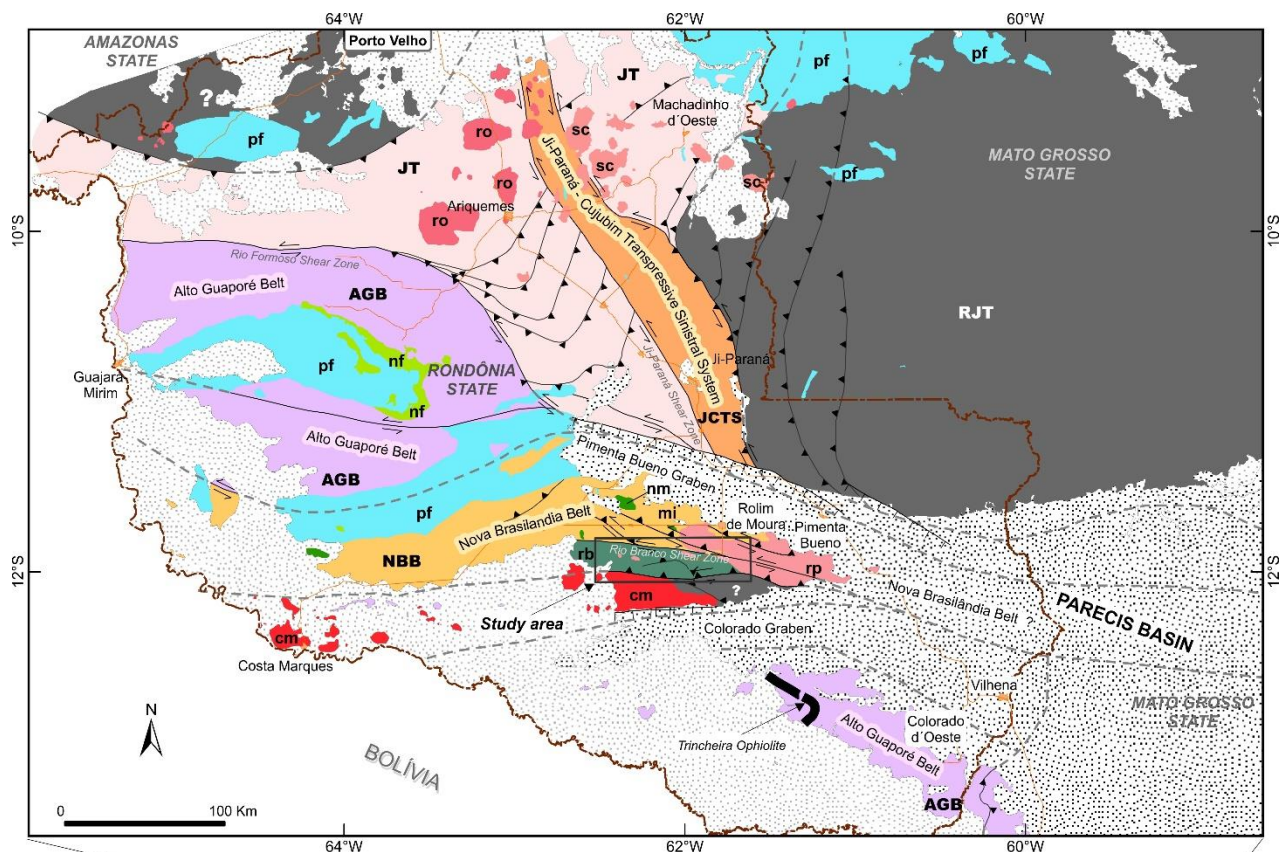
110 The Amazonian Craton was initially subdivided into two shield areas, known as southern
111 Central Brazil and northern Guiana Shield, separated by extensive sedimentary cover of the
112 Amazonas Syncline. Several evolutionary models have been proposed based on geochronological
113 data (eg, Cordani et al., 1979; Teixeira et al., 1989) or on geophysical and structural data (Hasui et
114 al., 1984; Costa and Hasui, 1997). However, Tassinari and Macambira (1999) returned to the
115 concept of provinces in the sub-division of the Amazonian Craton, suggesting a new model based
116 on Sm-Nd geochronological data. In this work, the southwestern region of the Amazonian Craton
117 was referred to as the Rio Negro-Juruena (1.80-1.55 Ga), Rondonian-San Ignacio (1.45-1.3 Ga) and
118 Sunsás provinces (1.25-1.00 Ga). In the model proposed by Santos et al. (2000), however, the same
119 area consists of only two geochronological provinces referred to as Rondônia-Juruena (1.74-1.47
120 Ga) and Sunsás provinces (1.20-0.99 Ga).

121 Alternatively, Scandolaro (2006) proposed a tectono-stratigraphic compartmentation of the
122 southwestern Amazonian Craton in Rondônia. The subdivision in terranes was defined based on the
123 descriptive aspects of geological units of regional extent, including their petrological, structural,
124 geochemical, geophysical and geochronological characteristics, and divided by faults or shear
125 zones. These terranes are known as the Jamari, Roosevelt and Nova Brasilândia terranes.

126 Southwestern of Amazonian Craton and its surroundings have also been the main target in
127 regional and local geological mapping projects carried out by researchers from various government
128 and research institutions, with emphasis on lithostratigraphy and crustal evolution (Litherland and
129 Bloomfield, 1981; Litherland et al., 1986; Scandolaro et al., 1999; Rizzotto, 1999; Santos et al.,
130 2002; Ruiz, 2005; Scandolaro, 2006; Quadros and Rizzotto, 2007; Ruiz et al., 2007; Salinas, 2010).
131 Other studies on the Amazonian Craton related the tectonic evolution of the Sunsás Orogen to the
132 collision between the Amazonian Craton and the eastern and southeast margins of Laurentia
133 (Sadowski and Bettencourt, 1996; Tohver et al., 2002, 2005b; Santos et al., 2008; Bettencourt et al.,
134 2010; Teixeira et al., 2010; Ramos, 2010; Rizzotto et al., 2013, 2014; Cawood and Pisarevsky,
135 2017).

136 Three important metasedimentary belts on the southwest border of the Amazonian craton
137 called Nova Brasilândia, Aguapeí and Sunsás are considered key areas for understanding the late
138 Mesoproterozoic (Stenian) orogenetic events that make them important records in the Amazon of
139 orogenetic activities resulting from the assembly of supercontinent Rodinia. Table 1 shows the main
140 geological and tectonic characteristics of the orogenies recorded in southwestern of the Amazonian
141 Craton in Rondônia, Mato Grosso and Bolivia associated with the evolution of the Sunsás orogen,
142 with emphasis on the comparison between the Sunsás, Aguapeí and Nova Brasilândia belts. The
143 Nova Brasilândia belt stands out for its important phase of oceanization after the break-up of the
144 Amazonian proto-Craton in the Stenian (< 1241 Ma) and for presenting a complex tectonic history
145 in relation to other late Mesoproterozoic mobile belts, according to data presented in this article.
146 These are important areas for establishing a correlation between the Sunsás Province, in the
147 Amazonian Craton, and the Grenville Province, in southern Laurentia. The Nova Brasilândia and
148 Aguapeí belts are exposed along the Bolivia-Brazil border and Sunsás belt in Bolivia, all positioned
149 at the rims of the Paraguá block.

150 The Nova Brasilândia belt positioned between the northwest margin of the Paraguá block and
151 the southwestern Amazonian proto-Craton was previously considered to originate from the opening
152 and closing of an intracontinental rift with formation of a proto-ocean in the opening phase
153 (Rizzotto, 1999). It is also representative of a crypt suture zone developed during the collision of
154 the Amazonian Craton with Laurentia in ca. 1.2-1.0 Ga (Tohver et al., 2005a). This belt is
155 constituted by the Nova Brasilândia Group (ca. 1215-1122 Ma; Rizzotto, 1999; Rizzotto et al., 2014)
156 which is composed of the Migrantinópolis and Rio Branco formation considered originally of a
157 supracrustal unit of deep sea turbidites of siliceous-clastic-to-carbonatic composition and
158 metamorphosed in upper amphibolite to granulite facies during Nova Brasilândia orogeny (ca. 1180-
159 1110 Ma; Santos et al., 2008). Metamafic and metafelsic rocks of the Rio Branco Granite and
160 metagranites Rio Pardo Suite are the magmatic representatives in the belt (Rizzotto, 1999; Rizzotto
161 et al., 2009, 2001, 2014; Quadros et al., submitted) (Fig. 1).



SUNSÁS PROVINCE (1250-950 Ma)

- NBB** Nova Brasilândia belt: formed from the opening and closing of the oceanic basin during the Nova Brasilândia orogeny (1180-1100 Ma). Part of a arc - back-arc system
- JCTS** Ji-paraná - Cujubim Sinistral Transpressive System: zone of deformation and metamorphism, with crustal reworking of pre-existing rocks, formed during Nova Brasilândia orogeny (1180-1100 Ma)

RODONIAN-SAN IGNÁCIO PROVINCE (1470 -1319 Ma)

- JT** Jamari terrane: portion of the Rio Negro-Juruena Province, reworked during Quatro Cachoeiras orogeny (1670-1630 Ma), collisional phase of Rondonian-San Ignácio orogeny (1371-1319 Ma) and Nova Brasilândia orogeny (1180-1100 Ma)
- AGB** Alto Guaporé belt: formed during accretion and collision associated with Rondonian-San Ignácio orogeny (1470-1319 Ma). Ophiolitic complex and A-type granites (post-orogenic) and I-type (1370-1320 Ma)

RIO NEGRO-JURUENA PROVINCE (1840-1554 Ma)

- RJT** Roosevelt-Juruena terrane: magmatic arc and associated metavolcanosedimentary basins (1840-1740 Ma), deformed and metamorphosed during Quatro Cachoeiras orogeny (1670-1630 Ma). Intruded by A-type granites and charnockites of Serra da Providência Suite (1570-1540 Ma)

Nova Brasilândia post-orogeny units (1.00-0.91 Ga)

Phanerozoic cover

- Guaporé cover (Neogene)
- Parecis cover (Paleozoic and Mesozoic)

Anorogenic A-type granites (Neoproterozoic)

- cm** Costa Marques Suite
- ro** Rondônia Suite (Younger granites of Rondônia)

Siliciclastic sedimentary cover (Meso-Neoproterozoic)

- pf** Palmeiral Formation
- sc** Santa Clara Suite

Post orogenic granites (Mesoproterozoic)

- rp** Rio Branco and Rio Pardo suites

Nova Brasilândia orogeny units (1.24-1.00 Ga)

Late- to post-orogenic granites (Mesoproterozoic)

- mi** Migrantinópolis and Terra Boa formations (metasedimentary rocks and associated metamafic)

Metavolcanosedimentary units (Mesoproterozoic)

- rb** Rio Branco Formation (metasedimentary rocks) and Rio Branco Suite (associated metamafic stocks, sills and dikes)

Nova Brasilândia pre-orogeny units (> 1.24 Ga)

- Basement** (< 1.84 Ga and > 1.24 Ga)

- Mafic sills**
- nf** Nova Floresta Formation
- Mafic stock**
- nm** Novo Mundo Suite

Geological structures

- Compressional shear zone
- Transcurrent sinistral shear zone
- Transpressional sinistral shear zone
- Extensional fault (normal)
- Fault or shear zone covered
- Trincheira Ophiolite Complex

Cartographic legend

- Cities
- Main highways
- Study area
- Rondônia State limit



162
163

164 **Fig. 1.** Simplified map of the southwestern Amazonian Craton in Rondônia and adjacent areas, showing the
165 boundaries of the main tectono-stratigraphic terranes and of the geochronological provinces (modified after
166 Tassinari e Macambira, 1999, Santos et al., 2003; Scandolaro, 2006; Bettencourt et al., 2010; Quadros et
167 al., 2011; Rizzotto et al., 2014).

168

169 The metasedimentary Aguapeí belt is an aulacogen or aborted rift developed in the eastern
 170 borders of the Paraguá block in the southwestern of Mato Grosso. This one comprises a folded
 171 metasedimentary unit called the Aguapeí Group (ca. 1167 and 1149 Ma) that represent a thick
 172 sequence of silicy rocks composed of the Fortuna, Promise Valley and Crystalline formations
 173 deposited in marine environment, exhibits only localized deformation and low-grade metamorphism
 174 between ca. 960–910 Ma, late reflexes of the Sunsás orogeny (Geraldés et al., 1997, 2001; Saes
 175 1999; Saes et al., 1992; Santos et al., 2005; Fernandes et al., 2006; Ruiz et al., 2005, 2007; Teixeira
 176 et al., 2010).

177 The Sunsás belt (ca. 1100–900 Ma) is structurally marked by extensive fronts of sinistral shear
 178 zones (or mylonitization zones), denominated Santa Catalina, Rio Negro and San Diablo tectonic
 179 fronts that developed low grade metamorphism during tectonic active along the southern margin of
 180 the Paraguá block between ca. 1080 and 1050 Ma, associated with Sunsás orogeny (Litherland et
 181 al., 1986; Saes et al., 1992; Teixeira et al., 2010). The belt is comprised by the metamorphosed
 182 Sunsás and Vibosi sequences deposited in an alluvial to deltaic system in an intracontinental rift
 183 environment also by the Rincón del Tigre mafic–ultramafic Complex and granitic intrusive suites
 184 (Litherland and Bloomfield, 1981; Saes et al., 1992; Boger et al., 2005; Teixeira, et al., 2010, 2015).

185
 186 **Table 1.**
 187 *Main geological and tectonic characteristics of the orogenies recorded in southwestern Amazonian Craton*
 188 *in Rodônia, Mato Grosso and Bolivia (compiled from Litherland et al., 1986; Rizzotto, 1999; Sadowski and*
 189 *Bettencourt, 1996; Boger et al., 2005; Ruiz, 2005; Tohver et al., 2004, 2005a; Santos et al., 2008; Rizzotto*
 190 *et al. 2014; Teixeira et al., 2010, 2015, Lima et al., 2017).*

Orogen	Orogeny	Nature of orogeny	Período	Tectonic unit	Main tectonic characteristics	Regional unit	Mafic or felsic magmatism. Pre-orogenic ¹ , orogenic ² , post-orogenic ³ and anorogenic ⁴ intrusions in region
Sunsás	Sunsás	Reflection of the Sunsás orogeny (deformation/metamorphism) Pre-orogenic phase (rift)	1030-910 Ma < 1260 Ma (1167-1149 Ma)	Aguapeí aulacogen or belt	Aborted intracontinental rift (aulacogen) in Paraguá block, later deformed (folds, thrust and extensional shear zones-SZ, such as: Indiavaí-Lucialva SZ and Pirantina SZ). Low-grade metamorphism (greenschist facies)	Pre-orogenic platform covers: Aguapeí Groups (Fortuna, Vale da Promissão and Morro Cristalina Formations)	Guapé ⁴ , São domingos ⁴ and Saracé ⁴ suites (939-917 Ma) Huanchaca mafic sills ¹ (1111 Ma)
	Sunsás	Collisional Pre-orogenic phase (passive margin)	1100-1000 Ma < 1200 Ma	Sunsás belt: Rio Negro, Santa Catalina and San Diablo fronts	Collisional type, on the south border of the Paraguá block, effects of crustal rework on craton areas (sinistral transcurrent shear systems or zones) and contemporary rifts. Low-grade metamorphism (greenschist facies)	Passive margin sequence: Sunsás and Vibosi Groups	Felsic intrusions (Sunsás Intrusive Suite ^{2,3,4}): Casa de Piedra ^{3,4} (1005 Ma), Don Mario ^{2,3} (1014 Ma), Taperas ^{3,4} (1076 Ma), Naranjito ^{3,4} (1070 Ma), Primavera ^{3,4} (~1090 Ma) and El Carmen ^{3,4} (1092 Ma) and Santa Teresa ^{2,3} (1105 Ma). Rincon del Tigre Complex ¹ (1110 Ma)
	Nova Brasilândia	Collisional (contemporary of the Sunsás orogeny) Accretionary Pre-orogenic phase (rift, rift-drift and drift phases: ocean formation and passive margin. Oceanization phase)	1096-1010 Ma 1137-1106 Ma < 1241 Ma	Nova Brasilândia belt: Migrantinópolis and Rio Branco domains, Ji-Paraná - Cujubim Sinistral Tranpressive System	Accretionary-collisional type on the southwestern margin of the Amazonian proto-Craton and rework effects on craton areas (systems and shear zones). Low (greenschist facies)- to high-grade metamorphism (amphibolite- to granulite-facies). Early phase of oceanization followed by arc - back-arc system in the subduction phase	Pos-orogenic platform covers: Palmeiral Formation (Vila Palmeiral, Pacaás Novos and Uopianes ridge). Pre-orogenic covers: Terra Boa Formation and Nova Brasilândia Group (Rio Branco and Migrantinópolis Formations)	Mafic sills (Nova Floresta) associated with platform covers. Anorogenic felsic magmatism in cratonic areas: Rondônia Intrusive Suite/Younger Granites of Rondônia ⁴ (0.95-0.96 Ga), Costa Marques ⁴ (0.98-0.96 Ga) and Santa Clara ⁴ (1.08–1.07 Ga) intrusive Suites. Orogenic and post-orogenic magmatism in the belt: Rio Pardo Suite ³ (1.05 Ga) and mafic-felsic magmatism of the Rio Branco Suite ² (1.11-1.10 Ga)

192
 193
 194 Recently, the Nova Brasilândia, Aguapeí and Sunsás belts were considered to belong to a
 195 single geotectonic unit, called the Western Amazon Mobile Belt, developed at the late
 196 Mesoproterozoic in intracontinental rift environment from by reactivating of the Guaporé suture
 197 zone (Rizzotto et al., 2014).

198 **2.2. The Nova Brasilândia belt**

199

200 Consists of metavolcanic-sedimentary rocks displayed in an E-W to NW-SE elongated belt
201 that strikes approximately 170 km long by 40 km as a window in Phanerozoic sediments. The Nova
202 Brasilândia belt is tectonically limited to the north by the Pimenta Bueno Graben, and by the São
203 Felipe (> 1.23 Ga) basement rocks to the south. To the east, it is cover by the Parecis Basin sediments
204 and to the west by sediments and extensive weathering profiles of the Guaporé cover (Figs. 2, 3).
205 Strong magnetic anomalies observed in the southern part of the belt with an E-W trend show that it
206 extends to E and SW beyond the exposure limits (Figs. 1, 2).

207 The Nova Brasilândia belt comprises migmatized quartz-feldspathic paragneiss, schist, calc-
208 silicate gneiss, quartzite, amphibolite, granulite, metamafic rocks and metagranite (Fig. 2). Previous
209 studies by Rizzotto (1999) defined the Nova Brasilândia Group as consisting of two distinct units:
210 the first of metavolcanic-sedimentary origin represented by the Migrantinópolis Formation,
211 consisting of a medium- to high-grade turbiditic unit of siliclastic to carbonatic composition,
212 consisting of gneiss, quartz-feldspar mica schist and subordinate calc-silicate gneiss, in addition to
213 sills of metagabbro and amphibolite (Fig. 2A, 2C). The second unit, known as the Rio Branco
214 Formation, consists of metamafic rocks, showing geochemical affinities with P-MORB, and felsic
215 rocks, trondhjemites, and, locally, metabasalt with subordinate intercalations of calc-silicate gneiss,
216 biotite-garnet paragneiss and fine-grained schist (see Scandola and Rizzotto, 1998; Rizzotto,
217 1999; Rizzotto *et al.*, 1999, 2001). In this paper, the association of intrusive mafic-felsic rocks from
218 the southern portion of the belt that were initially incorporated into the Rio Branco Formation and
219 Rio Branco Granite became part of the Rio Branco Suite (Fig. 2D). The Nova Brasilândia belt is
220 subdivided in lithostructural domains called of Rio Branco Domain (southern part), which is noted
221 for the strong magnetic anomalies, and Migrantinópolis Domain (northern part) with lower magnetic
222 anomalies except at specific locations within this domain. These two domains are tectonically
223 separated from each other or with the São Felipe Domain rocks by regional scale shear zones (Figs.
224 2C, 2D). Therefore, two episodes of mafic magmatism were described in the Nova Brasilândia belt
225 (Rizzotto, 1999). The first consists of sills coeval to the deposition of the paragneiss protoliths. The
226 second episode is manifested in the form of intrusive bodies (dykes and stocks) within the turbiditic
227 deposits, as well as in the previous mafic sills. These bodies are located in shallow crustal levels, as
228 evidenced by the ophitic textures and the fine-grained granulation. Generally, the intrusive bodies
229 are oval in shape, but rarely layered and showing partially preserved igneous textures. These mafic
230 rocks were subsequently deformed and metamorphosed in amphibolite facies, locally granulite
231 facies. The incipient foliation is observe by the alignment of amphibole, plagioclase and pyroxene
232 crystals, although the superimposed metamorphic textures alternate at all scales (Rizzotto, 1999;
233 Rizzotto *et al.*, 2001). Also in the Nova Brasilândia belt, several pulse of felsic magmatisms are
234 observed. These rocks are monzogranite to syenogranite in composition and vary from isotropic to
235 foliated. The first generation (ca. 1113-1112 Ma) was called the Rio Branco Granite (Rizzotto, 1999;
236 Rizzotto *et al.*, 2001), and the second generation (ca. 1005 Ma) of the Rio Pardo Suite (Silva *et al.*,
237 1992; Rizzotto, 1999). In addition, small lenticular bodies (5 to 60 meters) of high-silica
238 metatondhjemites occur spatially associated with mafic rocks (Rizzotto, 1999).

239 The first model for the tectonic evolution of the Nova Brasilândia belt suggested the opening
240 of an intracontinental rift, which evolved to a passive margin with the formation of a proto-ocean
241 (Rizzotto, 1999). This model would involve a complete Wilson Cycle over a period of about 40 Ma.
242 More recently, Rizzotto and Hartmann (2012) considered that the Nova Brasilândia rift developed
243 as the result of the reactivation along the Guaporé suture zone, a mega-structure that marked the
244 collage of the Paraguá block with the proto-Amazonian Craton at the Late Calymmian to Early
245 Ectasian (ca. 1470 and 1320 Ma). In this sense, the Rio Branco and Migrantinópolis formations
246 were interpreted, by these authors, as a relict section of a fossil oceanic crust part incorporated to
247 the margins of the Amazonian Craton during continent-continent collision associated with the final
248 phase of the evolution of the Sunsás Orogen in the Meoproterozoic (ca. 1.10-1.00 Ga).

249

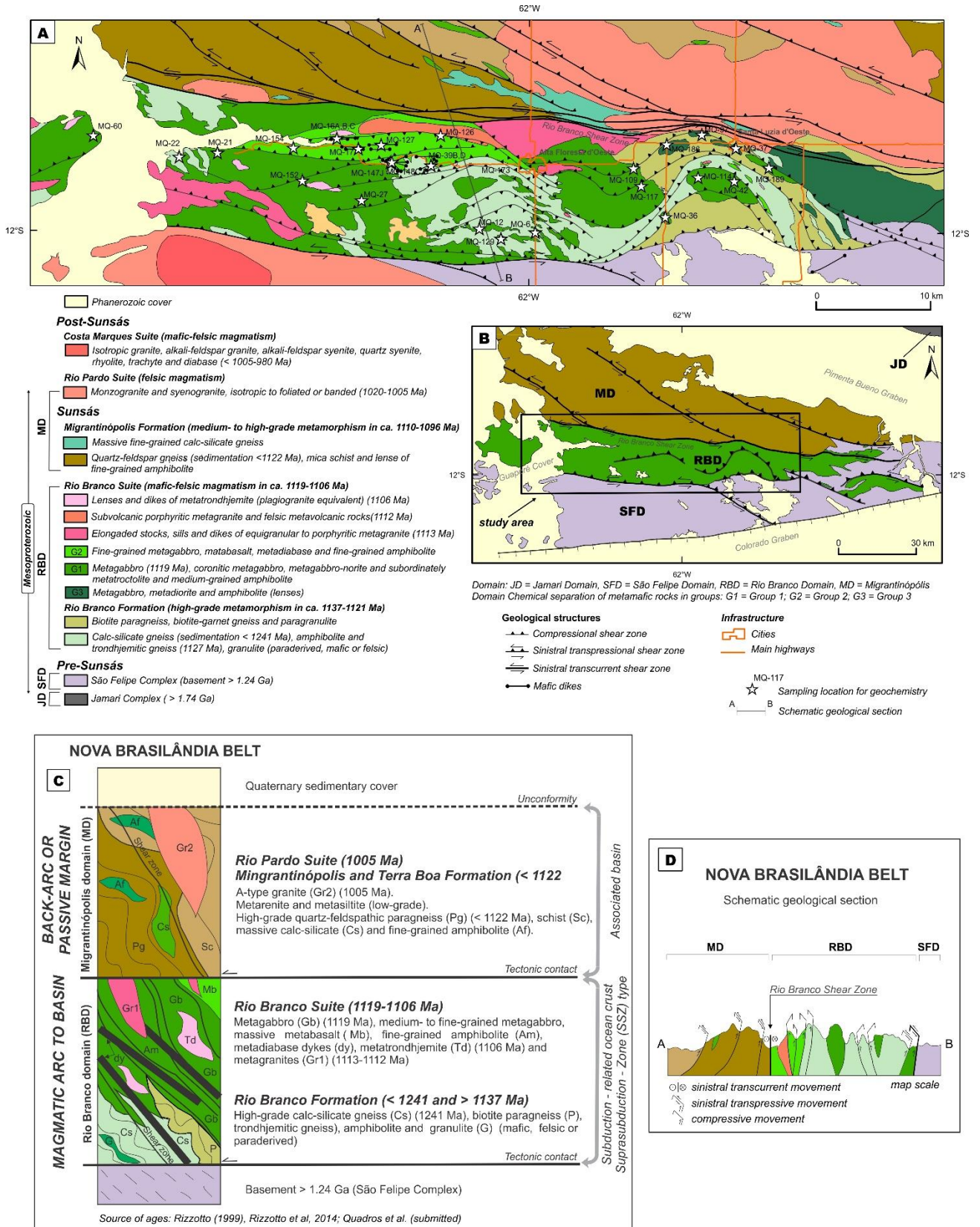


Fig. 2. (A) geological map of the study area in the Nova Brasilândia belt, southwestern Amazonian Craton. (B) subdivision of Nova Brasilândia belt in domain. (C) section showing the stratigraphy of the Nova Brasilândia belt with their respective domains and tectonic environments. (D) schematic geological section and subdivision into domains.

259 3. Analytical methods

260

261 3.1 Whole-rock geochemistry (major and trace elements)

262

263 The analyses of the whole-rock geochemistry (major and trace elements) of the samples of
264 metamafic rocks collected from the Rio Branco Suite were carried out at the ALS Laboratory
265 (certificate BH17273983). The analytical methods included ICP-AES and ICP-MS for the main
266 oxides and trace elements. The analytical work requested preparation package (PREP-31), with ALS
267 preparation codes CRU-31 (fine crushing – 70% < 2 mm), LOG-22 (sample login – red w/o
268 BarCode), PUL-31 (pulverize split to 85% < 75 µm), SPL-21 (Split sample-riffle splitter) and WEI-
269 21 (received sample weight). The analytical package requested was ME-4ACD81 (Base metals by
270 4-acid dig., instrument ICP-AES) for the analysis of elements Ag, As, Cd, Co, Cu, Li, Mo, Ni, Pb,
271 Sc, Tl and Zn, ME-ICP06 (whole-rock package-ICP-AES) for the analysis of oxides Al₂O₃, BaO,
272 CaO, Cr₂O₃, Fe₂O₃, K₂O, MgO, MnO, Na₂O, P₂O₅, SiO₂, SrO and TiO₂; packet ME-MS81 (Lithium
273 borate Fusion ICP-MS) for the analysis of elements Ba, Ce, Cr, Cs, Dy, Er, Eu, Ga, Gd, Hf, Ho, La,
274 Lu, Nb, Nd, Pr, Rb, Sm, Sn, Sr, Ta, Tb, Th, Tm, U, V, W, Y, Yb and Zr; and the preparation
275 package OA-GRA05 (Loss on ignition at 1000°C, instrument ICP-MS) for the calculation of LOI;
276 and preparation packet TOT-ICP06/ME-MS81D (Total calculation for ICP06, instrument ICP-
277 AES) for the total closure calculation for the sample. Detailed descriptions of the methods and the
278 ALS packages used may be consulted, or obtained, from the ALS Home Page (www.alsglobal.com).
279 For analysis of the major elements we proceeded with the recalculation for the anhydrous base,
280 followed by the usage of classification diagrams using AFM graphs (Irvine and Baragar, 1971) and
281 TAS (Cox *et al.*, 1979). The differentiation index chosen, this is to say the element that varied the
282 most within the series or suite was MgO and Zr. For the elaboration of the discrimination diagrams
283 for the series we used REE diagrams chondrite-normalized (CNb) (Boynton, 1984) and multi-
284 element diagrams (spidergrams) primitive mantle-normalized (PMN) (McDonough and Sun, 1995).
285 For the classification of the tectonic environment we used the discriminant tectonic diagrams
286 applied to mafic rocks and compared these with their applications in the definition of ancient
287 tectonic environments as well as with modern Phanerozoic environments (see Pearce, 1982, 2008;
288 Pearce *et al.*, 1984; Shervais, 1982; Wood, 1980; Cabanis and Lecolle, 1989; Dilek and Furnes,
289 2011; Saccani *et al.*, 2013, 2014; Dey *et al.* 2018, Chen *et al.*, 2014; Xia and Li, 2019).

290

291 3.2 Sm-Nd and Sr isotopic analyses

292

293 Most of the metamafic rocks collected from the Rio Branco Suite were in general, not
294 affected by post-magmatic alteration processes such as metamorphism, hydrothermal alteration and
295 weathering. All are processes that frequently change the composition of the mobile and trace
296 elements, leading to imprecise calculations of the initial isotope ratios, and particularly the Sr
297 isotopes. However, in an attempt to minimize the impact of post-magmatic alteration of the selected
298 samples for Sm-Nd and Sr (whole-rock) isotope analysis, the samples were carefully selected for
299 petrographic and chemical analysis with the objective of eliminating samples that were altered or
300 significantly deformed, and principally those samples collected along the shear zones.

301

302 Sm-Nd and Sr isotope analyses followed the method described by Gioia and Pimentel
303 (2000), and were carried out at the Geochronology Laboratory of the University of Brasília. Whole-
304 rock powders (ca. 50 mg) were mixed with ¹⁴⁹Sm-¹⁵⁰Nd spike solution and dissolved in Savillex
305 capsules. Sm and Nd extraction of whole-rock samples followed conventional cation exchange
306 techniques, using Teflon columns containing LN-Spec resin (HDEHP – diethylhexil phosphoric
307 acid supported on PTFE powder). Sm and Nd samples were loaded on re-evaporation filaments of
308 double filament assemblies and the isotope measurements were carried out on a multi-collector
309 Finnigan MAT 262 mass spectrometer in static mode. Uncertainties for Sm/Nd and ¹⁴³Nd/¹⁴⁴Nd
310 ratios are better than +0.5% (2σ) and +0.005% (2σ), respectively, based on repeated analyses of
international rock standards BHVO-1 and BCR-1. The ¹⁴³Nd/¹⁴⁴Nd ratios were normalized to

311 $^{146}\text{Nd}/^{144}\text{Nd}$ of 0.7219, and the decay constant used was $6.54 \times 10^{-12} \text{ a}^{-1}$. The TDM values were
312 calculated using the model of De Paolo (1981).

313 The Sr-Sr isotopic analyzes were performed using Thermo Scientific TRITON™ Plus
314 Thermal Ionization Mass Spectrometry (TIMS) at the Geodynamic, Geochronological and
315 Environmental Laboratory of the Institute of Geosciences of the University of Brasília (UnB).
316 Samples were deposited with 50% HNO₃ on double-array Re filaments. The Sr was analyzed in
317 multi-dynamic rotational mode, where the isotopic ratios are composed of 10 blocks of 15 cycles
318 each, with integration time of 17 seconds per cycle, totaling about 40 minutes of analysis for each
319 sample. The mass fractionation of the instrument for Sr isotope ratios was corrected by the $^{88}\text{Sr}/^{86}\text{Sr}$
320 ratio to 8.375209 (equivalent to $^{86}\text{Sr}/^{88}\text{Sr}$ ratio of 0.1194) employing an exponential law.

321

322

323 4. Results

324

325 The Nova Brasilândia belt is subdivided, in this work, in lithostructural domains called of
326 Rio Branco Domain (southern part), which is noted for the strong magnetic anomalies, and
327 Migrantinópolis Domain (northern part) with lower magnetic anomalies except at specific locations
328 within this domain. These two domains are tectonically separated from each other or with the São
329 Felipe Domain rocks by regional scale shear zones (Fig. 2C).

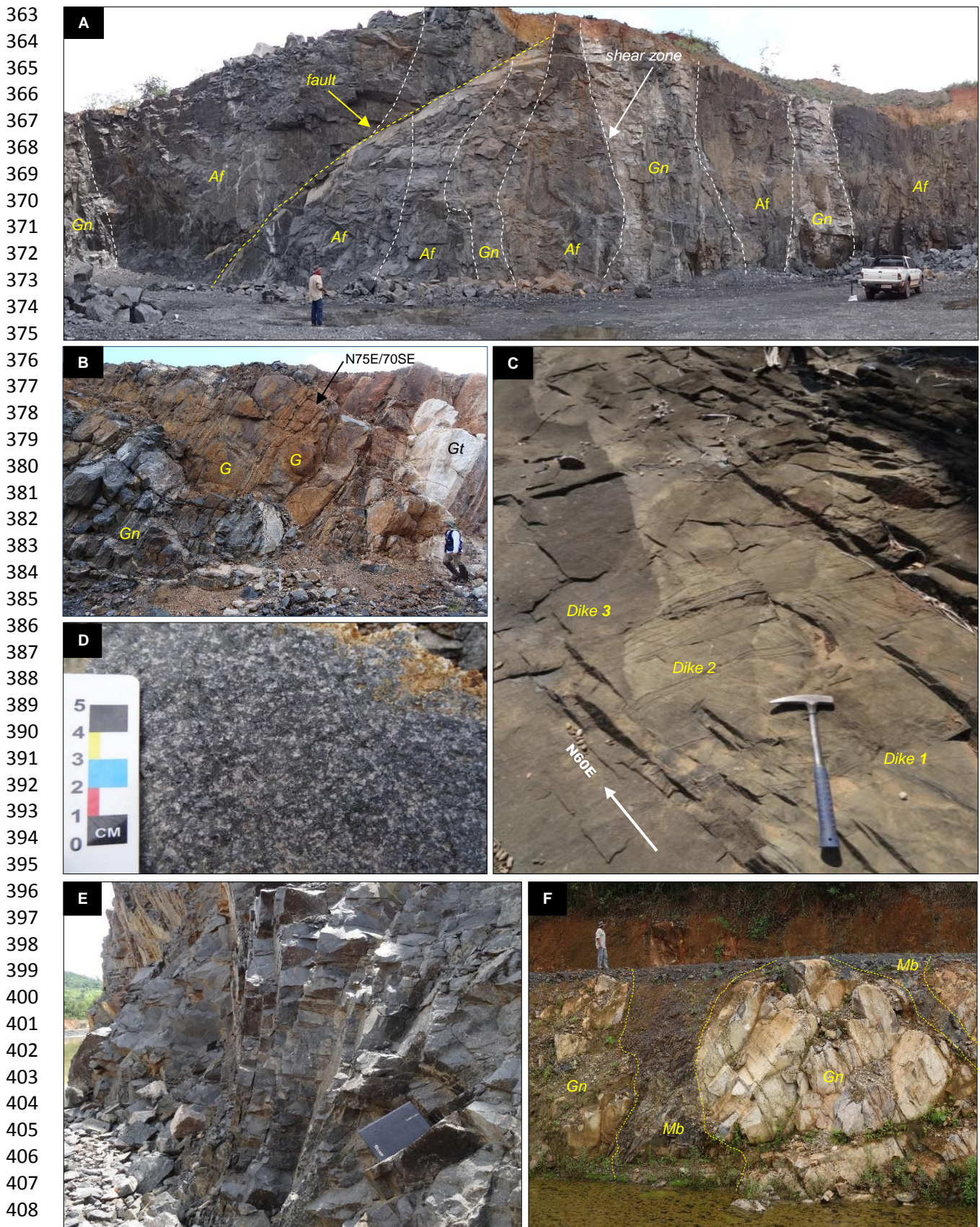
330 Our field investigations in an area in the Rio Branco domain (vertex polygon: S 11° 48'
331 55"/W 61° 41' 25", S 12° 02' 51"/W 61° 41' 25", S 12° 02' 51"/W 62° 26' 55" and S 11° 48' 55"/W
332 62° 26' 55") revealed an incomplete sequence of a possible magmatic arc and related basins partially
333 preserved in the Nova Floresta d'Oeste, Rondônia (Fig. 2A). During our study of the Rio Branco
334 Domain, in the southern part of the Nova Brasilândia belt, we found high-grade metavolcanic-
335 sedimentary rocks consisting of calc-silicate gneiss, biotite paragneiss and lenses of fine- to
336 medium-grained amphibolite, trondhjemitic gneiss (trondhjemite as protolith) and paraderived
337 granulite (pelitic protolith) and mafic granulite (gabbroic rocks as protoliths) (Figs. 3A, 3B). We
338 kept this rock association under the name of Rio Branco Formation (sedimentation between ca. 1241
339 Ma and 1137 Ma; Quadros et al., submitted). The intrusive mafic and felsic rocks within the Rio
340 Branco Formation are describe in this article under the name of Rio Branco Suite. The mafic
341 component (~ 80% of the suite) occurs as semi-circular or elliptical plutons of metagabbros (ca.
342 1119 Ma), metagabbronorites, and metatroctolites and their deformed and transformed varieties to
343 amphibolites, or as sills and dykes of fine-grained metagabbros, massive metabasalts and
344 metadiabases (Figs. 3C, 3D, 3F). The felsic component of the Rio Branco Suite (~20%) includes
345 dykes of metagranites (ca. 1113 Ma) and metatrandhjemites (plagiogranite equivalent), and elongate
346 bodies of porphyritic metagranites and subvolvanic metagranites (ca. 1112 Ma), spatially associated
347 with fine-grained metamafic dykes (Fig. 3C). This felsic assemblage was maintain in the Rio Branco
348 Suite according to the initial definition of Rizzotto (1999).

349 New geological field observations have shown that Rio Branco Suite mafic-felsic rocks are
350 clearly intrusive on the high-grade metamorphic rocks principally in calc-silicate gneiss and biotite
351 paragneiss of the Rio Branco Formation. Mafic granulite (orthopyroxene+clinopyroxene+
352 plagioclase±amphibole±biotite±opaque minerals) and some of the amphibolites (amphibole+
353 plagioclase+ biotite± opaque minerals) occur as lenses or as intercalations in metasedimentary rocks
354 of the Rio Branco Formation (Figs. 4A, 4B, 4C). Evidence for intrusion was observed in the contact
355 zone between the metagabbros and their host rocks, where hybrids containing xenoliths of altered
356 amphibolite (chloritization/epidotization) and calc-silicate gneiss are observed. Presence of dyke
357 swarms intrusive in high-grade metasedimentary rocks (Fig. 4D, 4E). Magmatic breccia may occur,
358 locally, composed of angular mafic rock fragments surrounded by leucogranite with quartz, feldspar
359 and amphibole forming pockets in outcrops of mafic rocks (Fig. 4F).

360

361

362



410 **Fig. 3.** Field aspects of calc-silicate gneisses of the Rio Branco Formation and metamafic rocks of the Rio
411 Branco Suite. (A) calc-silicate gneiss (Gn) with fine-grained amphibolite lenses (Af). (B) calc-silicate gneiss
412 (Gn) with lenses of trondhjemitic gneiss (Gt) and mafic granulite (G) in outcrops situated in a quarry south
413 of Alta Floresta d'Oeste. (C) medium-grained metagabbro. (D) three generations of mafic dykes (dykes 1, 2
414 and 3), (E) fine-grained amphibolite (massive basalt as protolith) and (F) dykes of metabasalt (Mb) intrusive
in calc-silicate gneiss (Gn) in outcrops situated at the Cachimbo Alto Hydroelectric installation situated
to the west of Alta Floresta d'Oeste.



417
418 **Fig. 4.** (A), (B) and (C) general field aspects of the spatial relationships of coeval mafic-felsic magmatism of
419 the Rio Branco Suite. (D) detail in plan view showing the contact relationships between metamafic and
420 metafelsic rocks. (E) monzogranite dike in amphibolite (F) Magmatic breccia. Outcrops of the Rio Branco Suite
421 at the Cachimbo Alto Hydroelectric installation and in a quarry located, respectively, to the west and in the
422 south of Alta Floresta d'Oeste (Gn-Calc-silicate gneiss; Af- amphibolite; Mb-foliated fine-grained
423 metagabbro/massive metabasalt; g-granulite; Mgr-foliated fine-grained metagranite).

427 4.1 Petrography

428

429 The main petrographic characteristics of the metamafic rocks of the Rio Branco Suite
430 described in this article are summarized in Table 2. With respect to the crustal level in which these
431 rocks crystallized we observed one group formed at deeper levels (plutonic rocks), consisting of
432 medium to fine-grained gabbroid rocks, and a second group consisting of metamafic rocks emplaced
433 at shallow depths (subvolcanic rocks), consisting of fine-grained metagabbro, massive metabasalt
434 and metadiabase (sills and dykes) in addition to fine-grained amphibolite. In general, these rocks
435 were exposed to varying intensities of deformation and metamorphism, with mineralogical and
436 textural transformations forming massive amphibolite and foliated and/or mylonitized amphibolite,
437 principally along shear zones (Fig. 5).

438 However, the occurrence of mafic rocks with mineralogical assemblages and preserved
439 primary igneous textures is very common, including deformed/sheared intervals with important
440 textural and mineralogical transformations, with wedging and curving of the plagioclase twinning,
441 sub-grain formation on the rims of plagioclase and pyroxene crystals, mineral orientation and
442 alteration products of pyroxene to hornblende (Figs. 5C, 5G, 5H). Petrographically, these rocks are
443 fine- to medium-grained metagabbro and subordinately metatroctolite, in addition to massive
444 metabasalt and metadiabase.

445 Metagabbro and metagabbro are the main rock-types. They are dark grey in colour,
446 and medium to fine-grained, locally coarse-grained. They may be moderately magnetic, slightly
447 foliated, and composed mainly of plagioclase, diopside and small amounts of orthopyroxene.
448 Hornblende is present in variable quantities, along with titanite, apatite and opaque minerals.
449 Magnetite and ilmenite are accessory and biotite and sericite are secondary minerals. Textures are
450 ophitic to sub-ophitic (Fig. 5A, 5D). Locally, reaction coronas (coronitic texture) between olivine
451 and plagioclase consisting of amphibole and pyroxene (orthopyroxene and clinopyroxene) are still
452 preserved. Olivine crystals are frequently serpentinized (Fig. 5B).

453 Metadiabase, massive metabasalt and fine-grained metagabbro are grey-green in colour, and
454 vary from fine-grained to aphanitic. They represent several generations of parallel dykes, with
455 thickness from 15-30 cm to several meters. These dykes may be magnetic or non-magnetic. They
456 are concordant and/or discordant with the regional trend of foliation. Sub-ophitic textures
457 predominate.

458 Medium-grained metamafic granulite (gabbro protolith) is grey in colour, foliated, non-
459 magnetic, and has a granular subhedral to anhedral texture. It is composed essentially of plagioclase,
460 clinopyroxene (augite) and orthopyroxene that shows exsolution of augite. Hornblende is a
461 secondary mineral. Deformation microtextures are characterized by flame-shaped or wedge
462 twinning, undulatory extinction, curving of the plagioclase twinning, and subgrains formation in
463 plagioclase (Figs. 5C, 5G, 5H). Subgrains formation in clinopyroxene rims and granoblastic textures
464 predominate. Orthopyroxene with kink bands (curved), undulatory extinction and subgrains rims
465 are considered indicative of granulite facies conditions (additional information in Rizzotto, 1999).
466 Superimposed mylonitic textures are common along the shear zones (Fig. 5H). However, relict
467 igneous textures are observed locally in high-grade metamafic rocks.

468 Amphibolite is fine-grained (basalt and fine-grained gabbro protolith). These rocks are dark
469 grey in colour, magnetic and composed of phenocrystals of plagioclase and magnetite in a foliated
470 aphanitic matrix. They are spatially associated with felsic equigranular igneous rocks that are fine
471 to medium-grained, pink in colour and foliated.

472

473 4.2. Geochemistry

474

475 The following results are those of 34 samples of metamafic rocks collected within the Rio
476 Branco Domain in the southern part of the Nova Brasilândia belt (Figs. 2A, 2B). Included in these
477 geochemical analyses are samples of metagabbro, metagabbro, metatroctolite, fine-grained
478 massive metabasalt and amphibolite, massive metabasalt and dykes of fine-grained metagabbro,

479 metabasalt and metadiabase (Table 3). Most samples analyzed showed low loss on ignition (L.O.I.),
 480 between -0.06 % and 0.84 % Wt (weight percent), suggesting that they were little affected by
 481 metamorphism and superimposed alteration. However, the values of the major elements (oxides)
 482 obtained were recalculated to 100 % Wt in a volatile free base (anhydrous base) and values of trace
 483 elements in ppm (parts per million) were chondrite-normalized (CN) and primitive mantle-
 484 normalized (PMN). These were the values used in the elaboration of the diagrams of correlation,
 485 classification, discriminants of the series, REE (rare-earth elements), multi-element (spidergram)
 486 and in the definition of the tectonic environment. The results of the geochemical analysis of the Rio
 487 Branco domain metamafic rocks shown in the table 3, with original values of the laboratory analysis
 488 and without recalculation or normalization.

489

490 **Table 2**

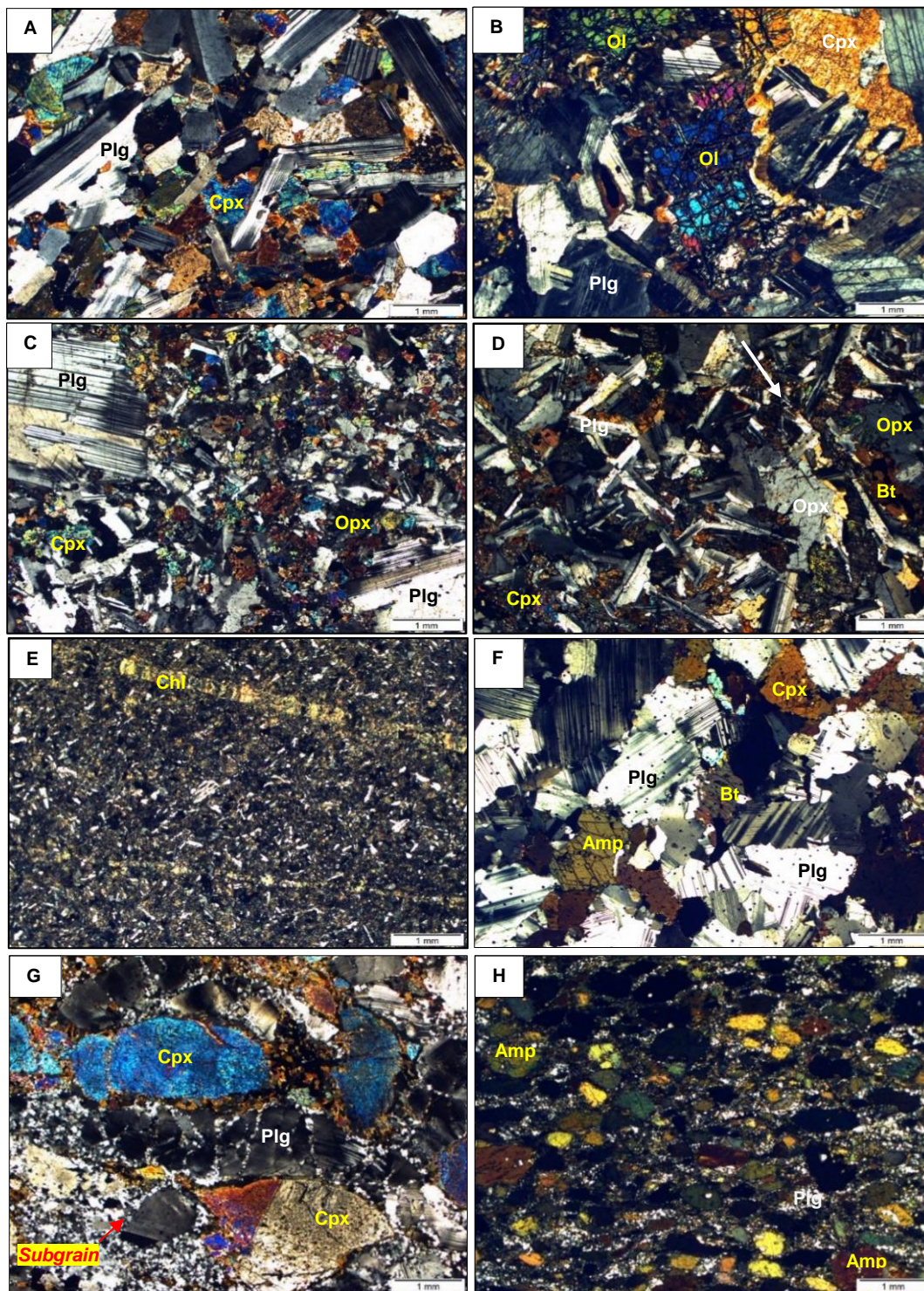
491 *Summary of the main petrographic characteristics of the Rio Branco Suite (metamafic rocks), Nova*
 492 *Brasilândia Belt. Abbreviations, ol: olivine; cpx: clinopyroxene; opx: orthopyroxene; pl: plagioclase; ap:*
 493 *apatite; Ti-py: titanite pyrite; Sp: sphene; op: opaque minerals; serp: serpentine; Fe-ox: Fe-oxides; amp:*
 494 *amphibole; bt: biotite; cl: chlorite.*

Rock	Texture	Mineral assemblage
Metagabbro	Ophitic to sub-ophitic, cumulate and interstitial, porphyritic. Granuloblastic when deformed and metamorphosed. Amphibole crystals surrounding pyroxene	cpx (augite)+opx+pl (anortite-bytonite)±anp (hornblende)±bt±ap±op±Fe-ox
Metagabbronorite	Ophitic to sub-ophitic, cumulate and interstitial. Granuloblastic when deformed and metamorphosed	cpx (augite)+opx+pl±op±Fe-ox
Metatroctolite	Porphyritic, interstitial and reaction corona (coronitic texture)	pl (anortite-bytonite)+ol (Mg-fosterite)+cpx (augite)+Ti-py+amp(Mg-hornblende/tschemakite)±serp±op±Fe-ox (ilmenite)
Metabasalt and metadiabase dikes	Sub-ophitic and aphanitic predominantly, granoblastic when deformed and metamorphosed	cpx+pl+amp (hornblende)±bt±sp±op±Fe-ox (ilmenite and magnetite)±cl
Massive metabasalt	Aphanitic and sub-ophitic predominantly. Porphyritic or/and aphyric	pl+cpx+amp (hornblende)±bt±sp±op±Fe-ox +cl
Amphibolite (gabbro protolith)	Porfiroblastic, porfiroclastic, granoblastic (mylonitic terms) and granonematoblastic. Foliated (mylonitic) or microbended	amp (hornblende)+plg+bt+op±Fe-ox±cl
Mafic granulite (protolith is gabbro). <i>Associated with the rocks of Rio Branco Formation</i>	Granoblastic predominantly. Plagioclase with flame-shaped or wedge twinning, undulatory extinction, curving of the twinning, and subgrain. Orthopyroxene with kink bands, undulating extinction and subgrain rims	plg+opx+Cpx (diopside)±amp (hornblende as a mineral of alteration in the pyroxene rims)±op

495

496

497 The geochemical characteristics of the metamafic rocks studied are described using the
 498 major elements and trace elements that are considered immobile during low temperature alteration
 499 processes or during metamorphism (see Pearce and Norry, 1979). These include many incompatible
 500 trace elements such as Ti, P, Zr, Y, Sc, Nb, Ta, Hf, Th, and medium rare earth elements (MREE),
 501 heavy rare earth elements (HREE), as well as some transition metals such as Ni, Co, Cr, V. In
 502 general, the metamafic rocks of the Rio Branco Suite contain SiO₂ (45.40-52.95 Wt. %) and
 503 moderate amounts of MgO (2.45-11.44 Wt. %), Al₂O₃ (12.42-24.83 Wt. %), Fe₂O₃ (3.78-17.22 Wt.
 504 %), Na₂O (2.33-2.92 Wt. %), K₂O (0.18-1.09 Wt. %), low values of TiO₂ (0.34-3.16 Wt %) and
 505 CaO concentrations (9.15-13.27 Wt. %) (Table 3).



506
 507 **Fig. 5.** Photomicrographs of metamafic rocks from the Rio Branco Suite. (A) medium-grained metagabbro
 508 composed of plagioclase, clinopyroxene, orthopyroxene, amphibole and biotite. (B) medium-grained
 509 metatroctolite with corona texture composed of olivine (fosterite), plagioclase and clinopyroxene (augite).
 510 The reaction rims around the olivine are formed of amphibole (tschermakite), ilmenite and Ti-pyrite. (C)
 511 medium-grained metagabbro composed of phenocrysts of plagioclase surrounded by a matrix containing
 512 plagioclase, clinopyroxene, orthopyroxene, amphibole and biotite. (D) medium-grained metagabbro
 513 composed of plagioclase, clinopyroxene, orthopyroxene, amphibole (hornblende) and biotite, with sub-
 514 ophitic texture. (E) metabasalt dyke with sub-ophitic texture and chlorite+epidote veins. (F) medium-grained
 515 metagabbro composed of plagioclase, clinopyroxene, amphibole and biotite. (G) foliated metagabbro with
 516 plagioclase sub-grains. (H) mylonitic amphibolite in of shear zone. Symbols: Plg, plagioclase; Amp,
 517 amphibole; Chl, chlorite; Cpx, clinopyroxene; Opx, orthopyroxene; Bt, biotite; epd, epidote.

518 Values of Mg# in the metamafic rocks vary from 33.8 to 71.6 Wt %. According to the
519 patterns of the major elements (oxides) and trace elements observed in the diagrams of the
520 classification, variation, rare earth element (REE) and multi-elements chondrite-normalized or
521 primitive mantle-normalized, the Rio Branco Suite comprise an evolved mafic magmatic series
522 without hiatus with LREE enrichment and variable Eu anomaly (positive to negative with magmatic
523 fractionation). Three groups were individualized based on lithological data, crustal level of the rocks
524 cristalization and geochemical trends, and denominated of the Group 1, Group 2 and Group 3. On
525 the oxide variation diagrams for Al₂O₃ vs. MgO, CaO vs. MgO, TiO₂ vs. MgO, K₂O vs. MgO and
526 FeOt vs. MgO, the samples of the metamafic rocks of Groups 1 and 2 showed a good correlation.
527 Al₂O₃ and CaO show a positive correlation, following a tendency for the fractionation of olivine,
528 orthopyroxene clinopyroxene, plagioclase and apatite, with a trend suggesting an evolved mafic
529 series (Fig. 6). In the TiO₂ vs. MgO, FeOt vs. MgO and K₂O vs. MgO diagrams the samples of
530 groups 1 and 2 show a negative correlation in respect to MgO, with an increase in Ti, K and Fe in
531 function of the fractionation of biotite, magnetite and Ti-sulphides (eg. pyrite), chiefly in the
532 samples of Group 2, which are the most fractionated rocks of the suite. The binary diagrams for Zr
533 vs. Ti, Nb, Nd, Th, La, Y and Yb show a good correlation, and the chemical variation between the
534 samples display a positive linear trend of magmatic fractionation without a hiatus (Fig. 6). The
535 relations La versus La/Yb and La versus La/Sm suggest that the compositions of the rocks of the
536 Rio Branco Suite (particularly Group 1 and Group 2) were mainly generated by fractional
537 crystallization. The samples of Group 3 do not show a defined correlation in the variation diagrams.

538 Group 1 (seven samples) consists of metagabbro, metagabbronorite, and medium-grained
539 amphibolite present as intrusive bodies occurring in the form of sub-rounded to elongate stocks
540 varying from 5 to 10 km across. This group consists of sub-alkaline tholeiitic metamafic rocks with
541 SiO₂=47.95-51.59 Wt. %, TiO₂=0.70-1.87 Wt. % (low Ti), MgO=6.84-11.44 Wt. %, P₂O₅=0.04-
542 0.10 Wt. %, V=182-569 ppm, Zr=37-106 ppm, Ni=59-199 ppm (sample MQ-129 with 199 ppm
543 Ni), Cr=240-690 ppm (sample MQ-114 with 690 ppm Cr), Cu=21-68 ppm, Nb=1.0-2.7 ppm (low
544 Nb) and Mg#=51.31-71.62. Trace element ratios are Ti/V=19.71-29.81, Ti/Y=191.84-531.56 (low),
545 Nb/Y=0.07-0.12 (low), La/Yb=1.74-3.32 (low), Ce/Y=4.07-7.75 (low), Th/Yb =0.07-0.43,
546 Ce/Pb=3.55-8.6 (low), Nb/U=3.2-16.25 (low), Th/La=0.03-0.15 (low), Ta/Yb=0.03-0.09 (low),
547 Zr/Y=2.14-3.98 (high) and Zr/Nb=25.45-46-15 (high) (Figs. 7, 8, 9).

548 Group 2 (twenty-three samples) consists of mafic to metamafic bodies hosted in shallow
549 crust levels, in the form of sills or dyke swarms, has lenticular shape (stretched) when deformed.
550 They have metric to kilometer thicknesses are relate to fractures, failures or other weaknesses in
551 calc-silicate gneisses and biotite paragneisses of the Rio Branco Formation, and in Group 1
552 metamafic rocks. Part of this magmatism possibly crystallized over or near the surface. Twenty-
553 three rock samples analyzed characterize group 2 that similarly to the Group 1, correspond to sub-
554 alkaline tholeiitic mafic rocks with SiO₂=46.68-50.83 Wt. %, TiO₂=1.09-3.16 Wt. % (medium- to
555 low Ti), MgO=4.45-7.70 Wt. %, P₂O₅=0.10-0.41 Wt. %, V=246-488 ppm, Zr=93-273 ppm, Ni=25-
556 121 ppm, Cr=90-360 ppm, Cu=3-106 ppm, Nb = 3.0-9.8 ppm (low Nb) and Mg#=33.88-58.82.
557 Trace element ratios are Ti/V=20-50, Ti/Y= 175.88-343.95 (low), Nb/Y=0.06-0.12 (low),
558 Nb/La=0.08-0.53 (low), La/Yb=1.95-3.56 (low); Ce/Y=4.12-8.07 (low), Ce/Pb=3.6-20.5 (low),
559 Nb/U=3.9-13.04 (low), Th/La=0.05-0.30 (low), Th/Yb =0.17-1.05, Ta/Yb=0.03-0.09 (low),
560 Zr/Y=1.91-3.58 (high) and Zr/Nb=21.52-36.00 (high) (Figs. 7, 8, 9).

561 Group 3 (four samples) consist of metagabbro and subordinate fine-grained amphibolite.
562 They form discordant intrusive, lenticular, elliptical or irregular bodies, which geometry is
563 controlled by the regional structures. These bodies are generally less than 30 km² and are referred
564 to as elongated stocks intruded into calc-silicate gneiss, biotite paragneiss, and granulite of the Rio
565 Branco Formation. This group consists of sub-alkaline tholeiitic metamafic rocks having much
566 lower quantities of Th, Nb, Zr, Hf, high K in relation to group 1 and group 2, and very high and
567 anomalous contents of Sr between 1680 and 1285 ppm. This group of rocks is represented by four
568 samples with SiO₂=45.40-52.95 Wt. %, TiO₂=0.34-1.61 Wt. % (medium- to low Ti), MgO=2.48-
569 5.16 Wt. %, P₂O₅=0.04-0.99 Wt. %, V=92-623 ppm, Zr=6-13 ppm (low Zr), Ni=10-43 ppm (low),

570 Cr=30-160 ppm (low), Cu=4-496 ppm (sample MQ-37 with 496 ppm de Cu), Nb = 0.3-0.9 ppm
 571 (very low Nb) and Mg#=44.89-56-55. This group shows element ratios Ti/V=13.51-20.55, Ti/Y=
 572 495.73-887.74 (high), Nb/Y=0.06-0.09 (low), La/Yb=6.33-12.33 (high), Ce/Y=13.47-24.67 (high),
 573 Ce/Pb=3.3-9.7 (low), Nb/U=6.0-12.85 (low), Th/La=0.01 (low), Th/Yb=0.10-0.17, Ta/Yb=0.11-
 574 0.33 (high), Zr/Y=0.90-1.46 (low) and Zr/Nb=14.44-20.00 (low) (Figs. 7, 8, 9).

575
 576
 577
 578

579 **Table 3.**

580 *Chemical compositions (major and trace elements) of the metamafic rocks of the Rio Branco Suite, Nova*
 581 *Brasilândia belt, southwest of the Amazonian Craton. The table contains of original data of the analyses,*
 582 *values of REE not normalized and of non-recalculated oxides for anhydrous basis.*

Sample Rock Group	MQ-97 mgmg 3	MQ-186 mgn 3	MQ-37 mg 3	MQ-109 mg 3	MQ-129 mg 1	MQ-36 mg 1	MQ-117 mgmg 1	MQ-42 mgmg 1	MQ-114 mg (p) 1	MQ-60 mg 1	MQ-189 mg 1	MQ-27 mg 2
SiO ₂	53.1	48.7	45.2	48.8	46.3	50.6	50.3	51.5	49	49.1	47	50.5
Al ₂ O ₃	24.9	23.6	19.1	24	14.9	15.25	17.7	15.35	16.15	14.8	14.25	15.75
Fe ₂ O ₃ t	3.79	6.19	12.5	6.31	9.31	10.35	9.07	7.36	7.56	14.4	12.45	10.65
CaO	10.4	11.5	11	11.2	10.6	11.25	10.8	13.25	13.1	10.65	11.85	10.9
MgO	2.49	2.55	5.14	2.94	11.05	7.46	6.8	8.56	9.63	7.66	7.76	7.68
Na ₂ O	4.63	4.04	3.36	3.9	2.79	3.48	3.03	2.61	2.3	2.45	2.55	2.25
K ₂ O	0.33	0.32	0.38	0.29	0.54	0.49	0.41	0.19	0.18	0.23	0.67	0.62
TiO ₂	0.34	0.74	1.6	0.77	0.76	1.31	1.06	0.77	0.69	1.9	1.08	1.09
MnO	0.06	0.07	0.13	0.07	0.14	0.16	0.14	0.13	0.13	0.19	0.18	0.16
P ₂ O ₅	0.04	0.04	0.99	0.04	0.04	0.1	0.08	0.06	0.05	0.09	0.08	0.11
LOI	0.56	0.51	0.64	0.53	0.73	0.52	0.51	0.49	0.47	0.37	0.72	0.2
Total	100.85	98.5	100.2	99.06	97.28	101.08	99.96	100.32	99.38	101.93	98.67	99.98
Ba	114	204	129	128	108	98.8	106	48.2	65.3	111	79.1	100.5
Ce	7.4	6.6	19.4	6.8	19.6	17.2	13.3	7.2	7.1	11.4	13.2	25.7
Cr	160	40	30	50	680	510	260	240	690	360	390	330
Cs	0.45	0.05	0.07	0.02	0.46	0.13	0.17	0.19	0.34	0.67	0.06	0.95
Dy	0.81	1.12	2.54	1.01	4.22	4.9	3.81	2.85	2.66	3.65	4.75	6
Er	0.34	0.62	1.29	0.7	2.4	3.13	2.57	1.8	1.64	2.36	2.98	3.48
Eu	1.08	0.87	1.15	0.85	1.09	1.34	1.08	0.73	0.66	1.11	1.28	1.15
Ga	25.8	26.6	25.7	27.1	16.8	21.4	19.6	17.8	17.3	21.8	19.5	19.7
Gd	0.84	1.34	3.51	1.09	3.9	4.91	3.6	2.8	2.65	3.27	4.08	5.59
Hf	0.2	0.2	0.5	0.3	1.8	3	2.4	1.3	1.2	1.7	1.8	3
Ho	0.15	0.22	0.48	0.22	0.81	1	0.77	0.65	0.55	0.71	1.04	1.18
La	3.7	3.1	8.7	3.5	8.4	7.9	5.9	3.3	2.6	4.8	5	11.7
Lu	0.04	0.06	0.13	0.06	0.37	0.37	0.38	0.22	0.2	0.32	0.43	0.54
Nb	0.3	0.3	0.9	0.5	1.8	2.4	2.7	1.3	1	2.2	1.3	4
Nd	3.3	4	13.8	4.1	11.2	11.6	8.5	5.8	5	7.6	9.6	14.4
Pr	0.85	0.74	2.83	0.89	2.64	2.43	1.82	1.13	0.97	1.59	1.73	3.25
Rb	2.2	2.2	2.8	0.9	14.5	14.9	9.7	5.1	8.3	3.5	8.9	31.7
Sm	0.81	0.99	2.95	0.93	2.86	3.44	2.43	1.94	1.53	2.21	2.89	3.86
Sn	1	1	1	1	2	2	1	1	1	1	3	2
Sr	1475	1680	1285	1475	108.5	232	200	166	172.5	206	128	130
Ta	0.1	0.1	0.1	0.1	0.1	0.2	0.2	0.1	0.1	0.2	0.1	0.3
Tb	0.14	0.18	0.51	0.18	0.73	0.87	0.61	0.49	0.45	0.58	0.74	0.94
Th	0.05	0.05	0.1	0.05	1.08	1.23	0.9	0.45	0.23	0.2	0.19	3.52
Tm	0.09	0.08	0.2	0.1	0.38	0.42	0.36	0.27	0.25	0.35	0.44	0.59
U	0.05	0.05	0.07	0.05	0.56	0.73	0.54	0.28	0.17	0.17	0.08	1.05
V	92	335	623	228	182	262	245	217	193	569	300	246
W	1	1	1	1	1	1	1	1	1	1	1	1
Y	4.1	5.1	14.4	5.6	24.6	26.6	23.0	17.5	15.6	21.1	28.0	33.4
Yb	0.3	0.49	0.95	0.45	2.53	2.87	2.5	1.77	1.48	2.23	2.87	3.36
Zr	6	6	13	8	56	106	88	44	37	56	60	101
Co	13	15	38	18	48	41	34	35	41	52	47	44
Cu	17	279	496	4	31	21	31	68	61	58	49	75
Mo	<1	<1	<1	<1	<1	<1	<1	<1	<1	<1	<1	1
Ni	43	10	13	12	199	59	70	59	114	103	78	121
Pb	3	2	2	2	4	2	2	2	2	2	2	2
Sc	6	11	18	11	35	43	33	50	43	41	46	38
Zn	35	41	91	47	59	56	58	39	46	91	69	71

Symbols of rock types: mn - metagabbro, mg - metagabbro, mg (p) - metagabbro (parental), mt - metatrolite, mgmg - medium-grained metagabbro, fgmg - fine-grained metagabbro, fga - fine-grained amphibolite, fgmgd - fine-grained metagabbro dike, mmb - massive metabasalt, mmbd - massive metabasalt dike and mdd - metadiabase dike. Fe₂O₃t = Fe₂O₃ total.

583
 584
 585
 586
 587
 588
 589
 590

591
592
593
594
595
596
597
598
599
600

Table 3 (continuation)

Sample Rock Group	MQ-152 mt 2	MQ-118D mdd 2	MQ-17 fgmg 2	MQ-22 mgmg 2	MQ-126 mmb 2	MQ-21 mgmg 2	MQ-6 fga 2	MQ-16C mdd 2	MQ-147J mmb 2	MQ-147B mmb 2	MQ-154 fgmg 2	MQ-148B fgmgd 2
SiO ₂	50.7	49.1	49.8	51	49.5	50.4	48.9	49.9	48	48.1	50.1	48.6
Al ₂ O ₃	16.3	13.35	15.1	15.25	14.05	15.05	12.8	12.55	12.6	12.9	13.3	12.7
Fe ₂ O _{3t}	10.8	14.5	11.6	11.75	12.95	12.2	13.45	17.4	16.1	14.95	14.25	16.3
CaO	12.55	10.25	11.25	10.85	10.8	11.55	9.25	9.24	9.94	9.79	11.15	10.05
MgO	7.09	6.69	6.86	7.06	6.77	7.75	5.52	4.5	5.64	6.56	6.56	5.76
Na ₂ O	2.23	2.91	3.54	2.2	2.28	2.28	3.85	2.56	2.83	2.88	2.66	2.66
K ₂ O	0.41	1.04	0.51	0.5	0.61	0.4	0.67	0.93	0.54	1.07	0.42	0.52
TiO ₂	1.11	1.65	1.49	1.32	1.43	1.38	2.36	3.19	2.48	1.81	1.61	2.34
MnO	0.17	0.2	0.16	0.17	0.16	0.18	0.14	0.29	0.25	0.2	0.23	0.25
P ₂ O ₅	0.1	0.14	0.14	0.16	0.15	0.14	0.21	0.41	0.26	0.2	0.17	0.28
LOI	0.25	0.7	0.67	0.08	0.69	0.1	0.8	0.35	0.32	0.8	0.26	-0.06
Total	101.79	100.6	101.17	100.41	99.46	101.51	98	101.37	99.01	99.32	100.76	99.44
Ba	72	112.5	85.2	131	62.7	94.8	110.5	221	147.5	118	107	122
Ce	20.7	33.7	41	26.7	25.3	25.9	31.9	53.2	42.6	29.6	25.2	35.9
Cr	350	300	150	330	300	360	130	110	150	210	170	90
Cs	0.44	0.09	4.09	0.8	0.42	0.46	0.07	1.28	1.12	0.31	0.82	0.53
Dy	5.17	9.08	8.8	5.76	6.68	6.78	8.76	14.15	11.15	7.43	7.44	10
Er	3.37	5.99	5.16	3.46	4.23	4.18	5.33	8.53	6.69	5	4.78	6.04
Eu	1.14	1.52	1.57	1.28	1.5	1.36	1.83	2.68	2.31	1.79	1.55	1.95
Ga	20.7	24.7	20.6	20.7	21.2	21.1	23.1	25.1	24.4	22.4	22.3	21.6
Gd	5.18	8.35	7.93	5.51	6.43	6.06	8.48	12.9	10	7.45	7.18	8.95
Hf	2.7	3.9	2.6	2.9	3.5	3.9	4.4	7.6	6.4	4.1	3.6	5.8
Ho	1.1	1.98	1.66	1.25	1.36	1.44	1.8	2.9	2.23	1.6	1.54	2.01
La	9.4	12.4	15.2	12.2	11.2	11.7	12.6	22	18.1	11.6	10.3	15
Lu	0.47	0.88	0.77	0.5	0.58	0.57	0.76	1.33	0.95	0.68	0.64	0.84
Nb	3.3	6.6	4.2	4.2	3.8	4.2	4.7	9.8	6.8	4.3	4.5	6
Nd	12.6	22.4	27.6	15.7	16.1	16	23	35.9	26.4	19.1	16.5	24.4
Pr	2.86	4.95	6.83	3.6	3.45	3.63	5.19	8.41	5.65	4.16	3.54	5
Rb	16.5	14.7	18.9	15.5	13.9	16.1	7.4	37.4	21.5	23.8	16	14.6
Sm	3.47	6.47	7.11	4.29	4.52	4.4	6.97	9.64	7.51	5.11	5.08	6.39
Sn	2	3	2	1	5	2	4	4	3	3	2	2
Sr	147	126	175.5	146	137	129	154.5	140	140	120	137.5	129
Ta	0.3	0.4	0.3	0.3	0.3	0.3	0.4	0.7	0.4	0.3	0.3	0.4
Tb	0.88	1.51	1.41	0.95	1.09	1.11	1.49	2.28	1.78	1.3	1.26	1.65
Th	2.2	3.06	1.82	1.94	2.3	2.23	2.46	4.05	3.28	2.07	1.66	2.56
Tm	0.5	0.9	0.81	0.55	0.64	0.64	0.85	1.3	0.98	0.72	0.69	0.9
U	0.64	1.93	0.78	0.56	0.75	0.71	0.92	1.14	0.87	1.42	0.59	0.72
V	258	377	310	299	321	307	431	387	488	403	357	420
W	1	1	1	1	2	1	1	2	1	1	1	1
Y	32.2	56.3	48.7	34.4	39.6	39.9	52.2	82.8	64.5	45.2	43.6	57.3
Yb	3.61	5.98	5.08	3.53	4.14	4.18	5.5	8.82	6.71	4.69	4.39	6.02
Zr	94	142	93	102	123	143	158	273	219	141	127	206
Co	42	43	34	42	45	48	44	44	46	48	52	51
Cu	84	36	3	88	91	80	31	42	56	65	83	66
Mo	<1	<1	<1	1	<1	1	1	1	<1	<1	<1	<1
Ni	65	49	44	77	50	112	33	25	46	62	52	42
Pb	2	2	2	2	2	2	2	9	10	5	7	3
Sc	42	50	43	44	44	43	49	46	49	49	51	50
Zn	69	99	67	83	50	82	33	204	112	94	105	136

Symbol of rock types: mn - metagabbro, mg - metagabbro, mg (p) - metagabbro (parental), mt - metatrolite, mgmg - medium-grained metagabbro, fgmg - fine-grained metagabbro, fga - fine-grained amphibolite, fgmgd - fine-grained metagabbro dike, mmb - massive metabasalt, mmbd - massive metabasalt dike and mdd - metadiabase dike. Fe₂O_{3t} = Fe₂O₃ total.

601
602
603
604
605
606
607
608
609
610
611
612
613
614
615

616
617
618
619
620

Table 3 (continuation)

Sample Rock Group	MQ-20 fgmg 2	MQ-118E mmb 2	MQ-118A mmb 2	MQ-16A fgmg 2	MQ-148A mmbd 2	MQ-148C fgmgd 2	MQ-16B fgmg 2	MQ-12 fgmg 2	MQ-39B fgmg 2	MQ-127 mmb 2
SiO ₂	47.8	49	48.9	48.4	48.7	48.7	48.4	46.8	49.1	48.6
Al ₂ O ₃	14.2	12.6	12.5	12.65	13.15	13.05	15	13.9	13.75	12.7
Fe ₂ O ₃ t	12.7	15.5	16.2	15.5	13.55	15.55	12.15	15.3	13	14.5
CaO	9.78	10.5	10.1	9.99	11.45	10.35	11.05	10.45	11.75	10.3
MgO	6.75	6.12	5.85	5.6	6.87	6.64	7.14	6.63	7.16	6.14
Na ₂ O	3.56	2.65	2.52	2.8	2.44	2.58	2.6	3.33	2.45	2.58
K ₂ O	0.72	0.67	0.52	0.46	0.36	0.35	0.37	0.44	0.34	0.53
TiO ₂	1.42	2.09	2.39	2.13	1.7	2.17	1.42	2.83	1.46	1.72
MnO	0.19	0.23	0.24	0.25	0.24	0.22	0.2	0.24	0.22	0.21
P ₂ O ₅	0.17	0.23	0.24	0.22	0.16	0.2	0.17	0.28	0.15	0.15
LOI	0.79	0.55	0.01	0.29	0.38	0.14	0.29	0.16	0.37	0.84
Total	98.15	100.2	99.53	98.34	99.08	100.01	98.86	100.42	99.83	98.33
Ba	120.5	114	144.5	115	150	93.8	119	129	94.9	165
Ce	26.1	34.4	36.3	28.3	24.6	32.7	22.7	30.4	19.2	24.2
Cr	260	250	150	130	300	210	330	170	350	160
Cs	0.72	0.19	0.72	1.05	1.41	1.35	0.88	0.49	0.59	0.7
Dy	6.28	8.96	10.25	9.12	7.36	9.3	6.36	8.62	6.39	10.15
Er	3.87	5.8	6.53	5.62	4.59	5.79	3.67	4.77	4.35	6.07
Eu	1.53	1.84	2	1.85	1.47	1.66	1.49	1.99	1.41	2.35
Ga	20.3	23.4	23	21.8	21.3	23.2	20.5	24.5	22	21.7
Gd	5.75	9.07	9.8	8.21	6.71	8.46	5.95	8.21	5.94	9.88
Hf	3	5.1	5.9	4.5	3.7	5.2	3.1	4.6	3.1	3.6
Ho	1.31	1.91	2.11	1.92	1.54	1.87	1.25	1.75	1.37	2.02
La	11.3	14.4	15	12	10.2	13.3	9.6	12.3	7.5	18.9
Lu	0.62	0.75	0.89	0.91	0.66	0.83	0.53	0.69	0.53	0.83
Nb	3.9	5.9	5.9	5.1	4.2	5.1	3.5	5.2	3	3.6
Nd	17.4	22.1	23.6	19.6	16.5	21.8	15.1	22.4	14.4	32.4
Pr	4.4	4.85	5.11	4.7	3.53	4.86	3.63	5.03	2.61	7.59
Rb	28.6	15.1	14.8	17.5	23.2	13	12.3	13.7	11.9	14.9
Sm	4.72	6.63	6.6	5.76	5.06	6.23	4.25	6.41	4.48	8.65
Sn	5	2	3	2	1	2	1	2	2	3
Sr	154.5	140	140.5	138	142	145	147.5	183.5	139	122
Ta	0.2	0.4	0.4	0.4	0.3	0.3	0.3	0.4	0.2	0.2
Tb	0.99	1.6	1.65	1.53	1.21	1.52	1.03	1.43	1.01	1.83
Th	1.32	2.21	2.46	1.87	1.52	2.08	1.07	1.47	0.99	1.02
Tm	0.57	0.82	0.91	0.87	0.65	0.83	0.56	0.74	0.58	0.86
U	1	0.71	0.7	0.59	0.33	0.71	0.31	0.58	0.23	0.48
V	313	431	487	459	378	442	321	452	353	424
W	1	2	1	1	2	1	1	1	3	1
Y	37.8	54.3	60.2	52.9	43.7	54.4	35.5	49.2	37.8	57.5
Yb	4.17	5.71	6.42	5.74	4.36	5.45	3.76	4.54	3.85	5.87
Zr	115	177	203	156	138	180	115	172	108	124
Co	41	47	48	47	45	44	46	49	49	57
Cu	9	74	62	63	87	36	80	40	106	55
Mo	<1	1	1	1	<1	<1	<1	<1	<1	1
Ni	66	44	55	44	55	74	82	58	64	58
Pb	4	2	4	5	14	7	4	2	3	2
Sc	43	49	49	49	50	49	45	48	49	50
Zn	75	107	117	116	144	72	118	91	137	97

Symbol of rock types: mn - metagabbronite, mg - metagabbro, mg (p) - metagabbro (parental), mt - metatroctolite, mgmg - medium-grained metagabbro, fgmg - fine-grained metagabbro, fga - fine-grained amphibolite, fgmgd - fine-grained metagabbro dike, mmb - massive metabasalt, mmbd - massive metabasalt dike and mdd - metadiabase dike. Fe₂O₃t = Fe₂O₃ total.

621
622
623

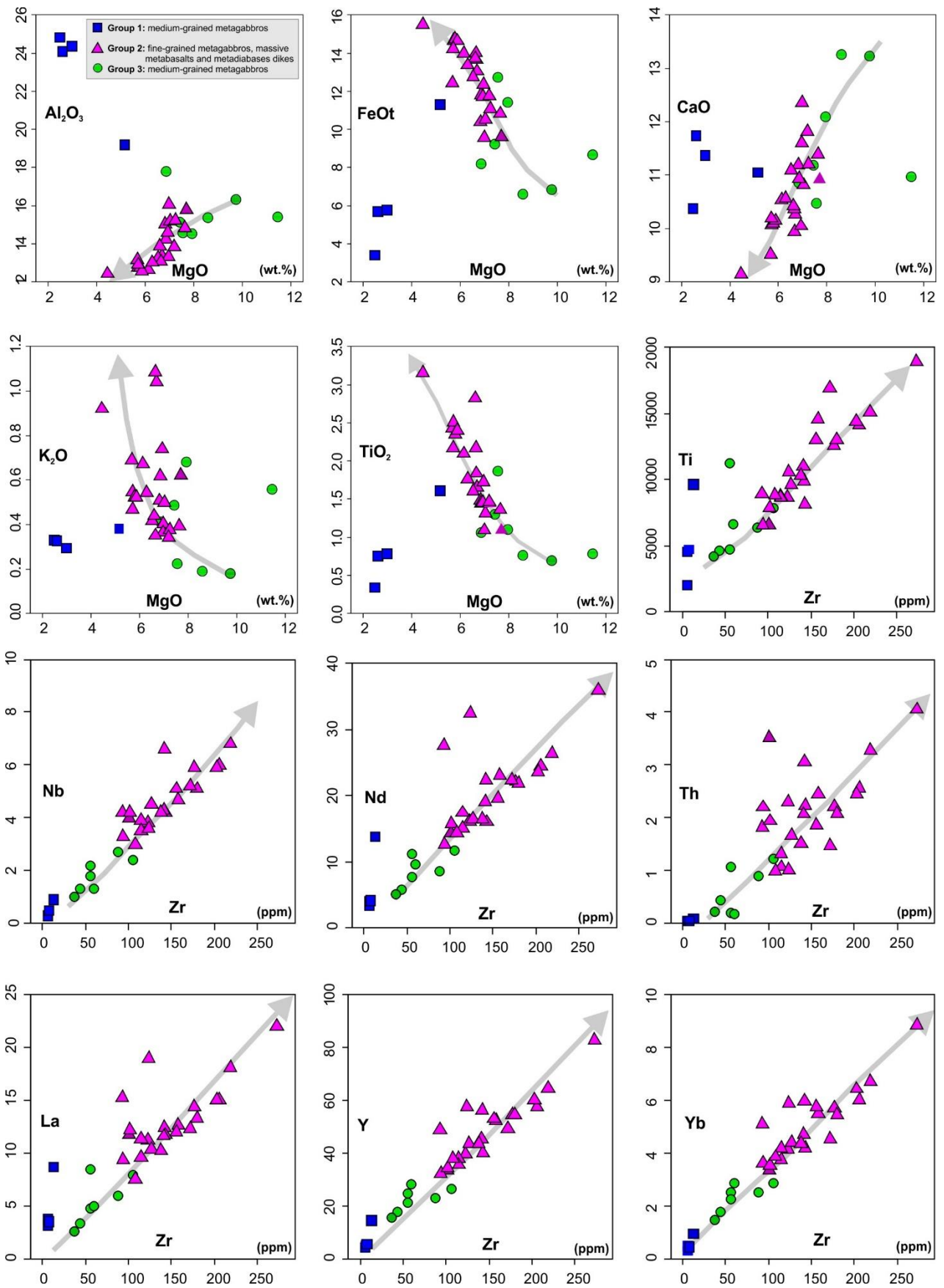
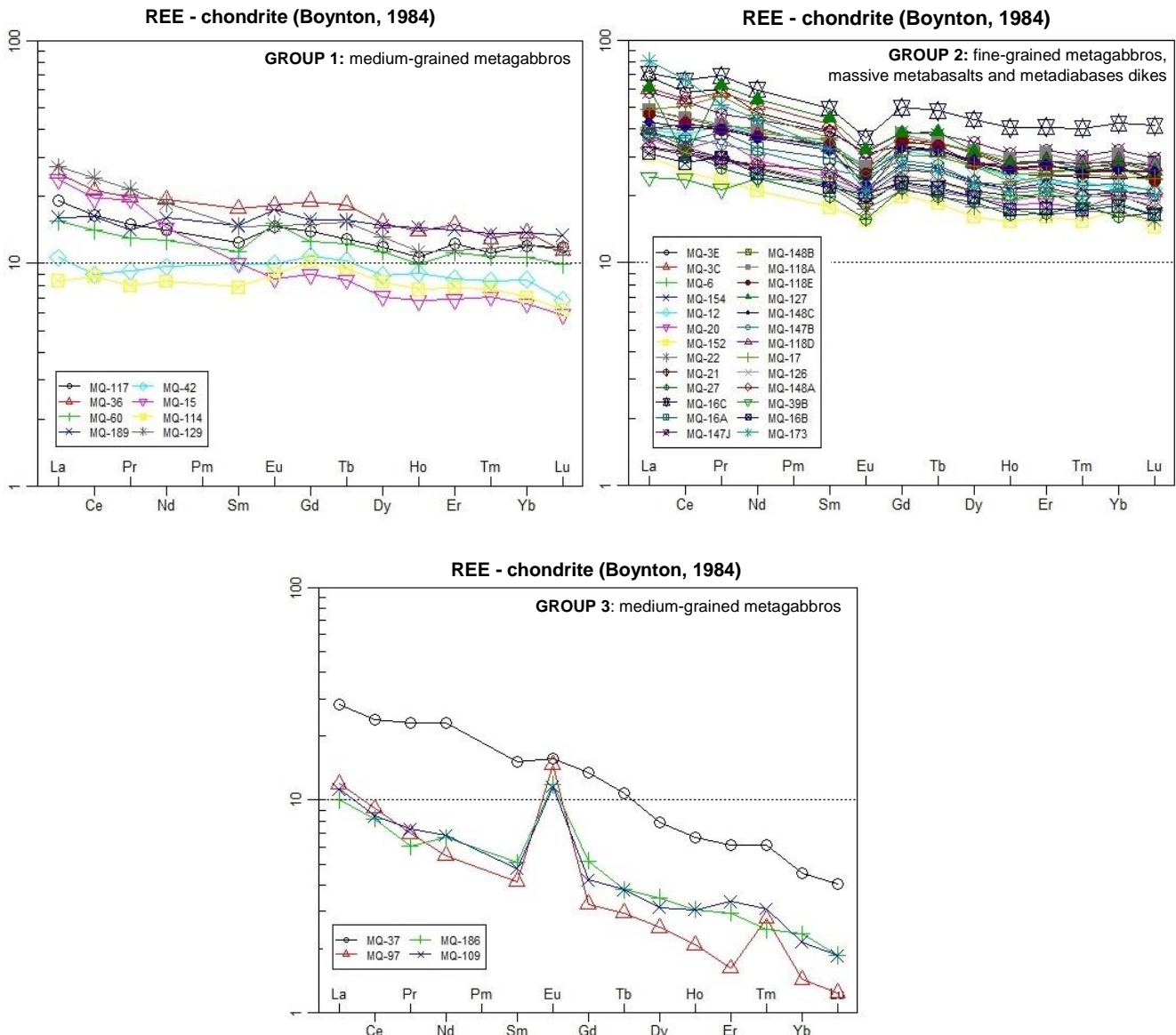


Fig. 6. Variation diagrams of selected major and trace elements vs. MgO and Zr, respectively, for metamafic rocks from the Rio Branco Suite. Oxides were recalculated on anhydrous bases. Grey arrows indicate inferred magmatic fractionation trends for different groups of metamafic rocks.

625 The mafic samples from the Rio Branco Suite plot in the field of the tholeiitic series on the
 626 AFM classification diagrams of Irvine and Baragar (1971) (Fig. 10A). On the classification diagram
 627 TAS (SiO_2 vs. $\text{Na}_2\text{O}+\text{K}_2\text{O}$) of Cox et al. (1979) the samples plot in the gabbro/basalt field defining
 628 a sub-alkaline tholeiitic series (Fig. 10B). The chondrite-normalized EER diagrams (Boynton, 1984)
 629 and primitive mantle-normalized multi-elements diagrams (McDonough and Sun, 1989) show
 630 specific characteristics in relation to the behavior of trace elements allowing the separation of the
 631 analyzed rocks into groups (Group 1, Group and Group 3). These groups with characteristic patterns
 632 allow for the identification of different degrees of fractionation, as well as enrichment and depletion
 633 in certain trace elements which that are indicators of geological processes that can assist in the
 634 identification of the tectonic environment (Figs. 7, 8, 9).

635
 636
 637
 638

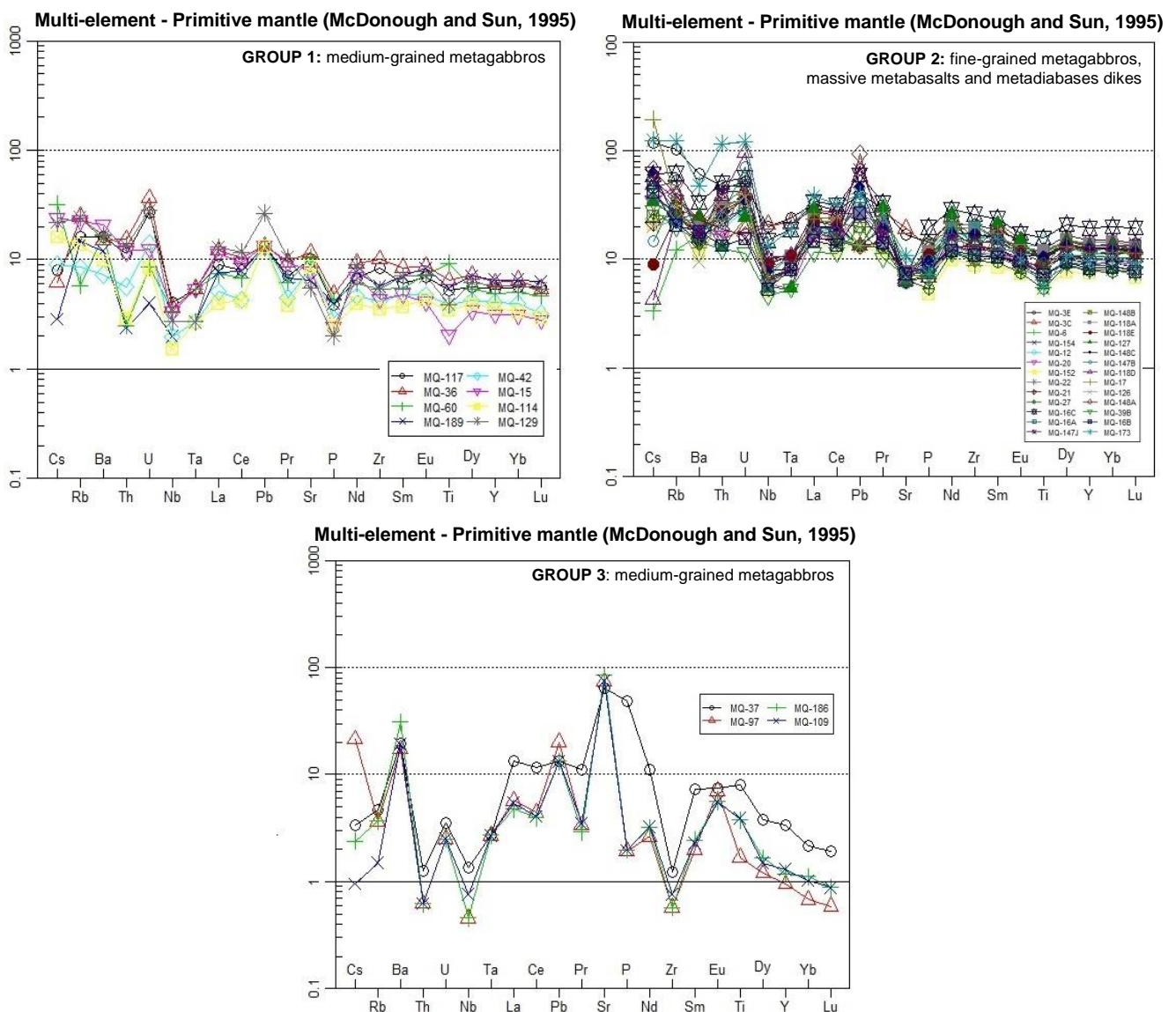


639
 640
 641
 642
 643

Fig. 7. Chondrite-normalized REE patterns presented by the metamafic rocks from the Rio Branco Suite.

644 The rocks of Group 1 and Group 2 have broad similar geochemical signatures, with
 645 pronounced negative anomalies of Nb and Ta, negative anomalies of Th, Ti and P, enrichment in
 646 large ion lithophile elements (LILE) (Ba, Rb, Sr), pronounced positive anomalies of Pb and U and
 647 discrete positive anomalies for Sr and K. These same rocks show enrichment in Ce, La, K, Rb and
 648 Cs, with discrete enrichment in incompatible elements. The high field strength elements (HFSE)
 649 (Zr, Nb, Ti) have a sub-horizontal pattern. The main difference resides in the Eu negative anomaly,
 650 only observed in rocks from Group 2. The Group 3 show pronounced negative anomalies of Zr, Nb,
 651 Th and Hf, enrichment in LILE (Ba, Rb, K, Ce and Sr), pronounced positive anomalies of Eu, Sr
 652 (anomalous), Pb, K, U and Ba, enrichment in La and P and depletion in HFSE (Y, Zr, Nb, Ti). In
 653 Group 3, positive Sr anomalies are considered very high (anomalous), but were presented by the
 654 four analyzed samples of this group. In all three groups is clear the LILE enrichment and HFSE
 655 depletion with respect to REE concentrations.

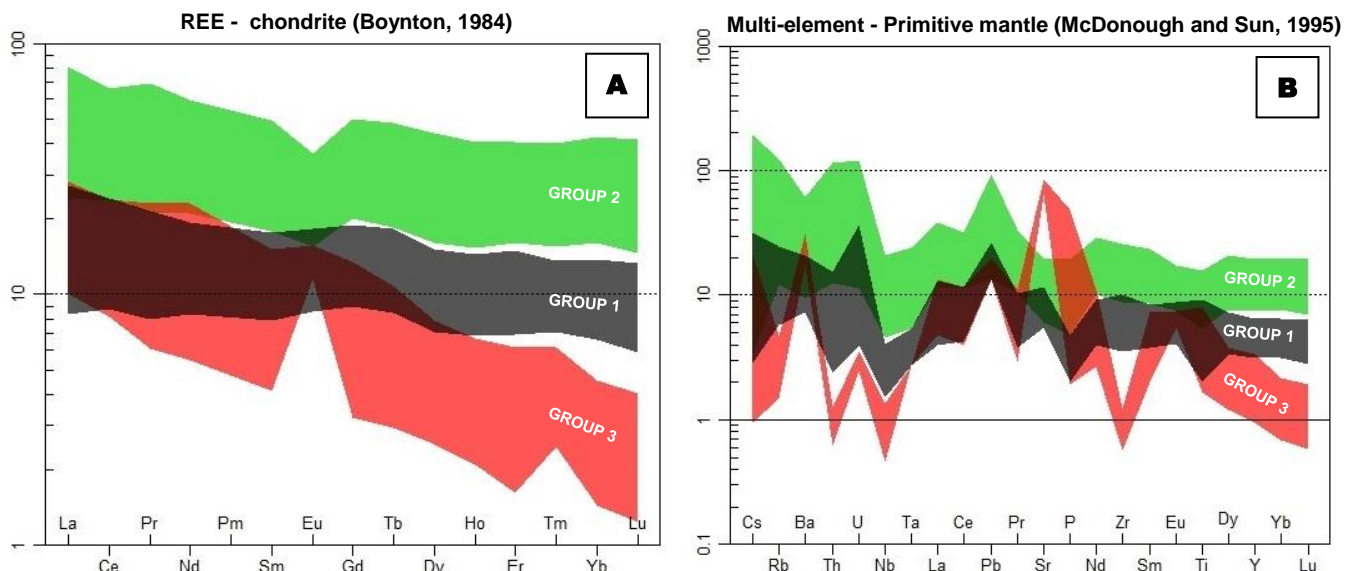
656
 657
 658



659
 660
 661
 662

Fig. 8. Primitive mantle-normalized multi-element patterns presented by the metamafic rocks from the Rio Branco Suite.

663 The metamafic rocks of the Rio Branco Suite still show chondrite-normalized (CN) REE
664 patterns, enriched in LREE ((La/Sm)_{CN} = 1.05-2.87, and (La/Yb)_{CN} = 1.17-8.32), suggesting a
665 IAT-type signature. Additionally, this is confirmed by the primitive mantle-normalized (PMN)
666 spidergrams (McDonough and Sun, 1995), where the arc signature is reinforced by the negative Nb
667 anomalies (Groups 1, 2, 3), Ta (Groups 1, 2, 3), Zr (Groups 1, 3) and Hf (Group 3), positive Pb
668 anomalies (in all groups) and low grades of Ti. The geochemical behaviour of Th, Nb, Ta and Pb is
669 fundamental for the understanding of the tectonic environment because of the gradual enrichment
670 in Th in relation to Nb and Ta, in the metamafic rock of Groups 1, 2 and 3 is indicative of a supra-
671 subduction zone (Dilek and Furnes 2014; Pearce, 2014; Saccani, 2015). The positive anomalies of
672 Pb reinforce the geochemical signature associated with subduction zones, and the elevated values
673 for K and increased values for La suggest the participation of a crustal contamination component.
674 The Ce/Pb, Nb/U and Th/La ratios are particularly useful in identifying differences in magma
675 sources because they are sensitive indicators of crustal contamination of mantle-derived mafic
676 magmas indicated either crustal contamination during stagnation in the crust, or contribution by the
677 upper oceanic crust and overlying sediments that make up the subducting slab (Kessel et al., 2005;
678 Xu et al., 2017). We highlight that in all groups of the Rio Branco Suite metamafic rocks, low-ratios
679 Ce/Pb (3.3-20.5), Nb/U (3.2-16.25) and Th/La (0.01-0.30) is also consider effective in interpretation
680 of mafic-felsic magmatism of the Rio Branco Suite as subduction-related.
681



682 **Fig. 9.** (A) chondrite-normalized REE envelope patterns presented by the metamafic rocks groups from the
683 Rio Branco Suite. (B) primitive mantle-normalized multi-elements envelope patterns presented by the
684 metamafic rocks groups from the Rio Branco Suite.

685
686
687 **4.3. Sr-Nd isotopes**
688

689 The most of the metamafic rocks collected from the Rio Branco Suite were generally little
690 affected by post-magmatic alteration processes such as metamorphism, hydrothermalism and
691 weathering. They are all processes that frequently alter the composition of the mobile and trace
692 elements, leading to imprecise calculations of the initial isotope ratios, and particularly the Sr
693 isotopes, considering that Rb and Sr are mobile large ion lithophile elements. However, in an attempt
694 to minimize the impact of post-magmatic alteration of the selected samples for Sm-Nd and Sr
695 (whole-rock) isotope analysis, the samples were carefully selected for petrographic and chemical
696 analysis with the objective of eliminating samples that were altered or significantly deformed, and
697 principally those associated with zones of high strain. The Sr and Nd isotope data were obtained
698 from fourteen samples of metamafic rock of the Rio Branco Suite (metagabbro, metadiabase and
699 fine-grained amphibolite) and are listed on Table 4. The interval of the Sr and Nd isotope

700 composition show varied values (from high to low) of $^{87}\text{Sr}/^{86}\text{Sr}$ ratios between 0.702 and 0.714,
 701 low $^{143}\text{Nd}/^{144}\text{Nd}$ ratios of 0.512, and Sm/Nd ratios < 2 .

702 Specifically, the interval of the Sr and Nd isotope composition of samples of the metamafic
 703 rocks of the Rio Branco Suite by group when compared to present mantle reservoirs, allow us to
 704 infer some considerations, although with some caution. Group 1 have average $^{87}\text{Sr}/^{86}\text{Sr}$ ratios of
 705 0.705-0.706 and average $^{143}\text{Nd}/^{144}\text{Nd}$ ratios of 0.512, thus corresponding to a set of rocks that best
 706 approximate those of the mantle. Group 2 shows medium to high $^{87}\text{Sr}/^{86}\text{Sr}$ ratios of 0.708-0.714 and
 707 average $^{143}\text{Nd}/^{144}\text{Nd}$ ratios of 0.512. Group 3 shows average $^{87}\text{Sr}/^{86}\text{Sr}$ ratios of about 0.702, and
 708 average $^{143}\text{Nd}/^{144}\text{Nd}$ ratios of 0.512. Group 3 presents a negative correlation between Sr and Nd that
 709 deviates from the usual pattern for this rock type, based on the contrasting geochemical behavior of
 710 the Rb and Sm antecedents, which makes this group highly suspicious and without a well-defined
 711 geochemical pattern. If the Nd isotope composition ratio were expressed using the notation ϵNd , the
 712 ϵNd was calculated on only five samples of fourteen analyzed from of Rio Branco Suite,
 713 recalculated for $T=1120$ Ma (age of crystallization obtained from Group 2 metagabbro, sample MQ-
 714 117), come to between -2.89 and +1.66, suggesting mantle source and crustal contamination.

715

716 **Table 4**

717 *Sm–Nd and Sr isotopic compositions of the metamafic rocks of Rio Branco Suite.*

Sample	Group	Rock	Sm (ppm)	Nd (ppm)	$\frac{^{147}\text{Sm}}{^{144}\text{Nd}}$	$^{143}\text{Nd}/^{144}\text{Nd}$	$\epsilon\text{Nd} (0)$	T_{DM} (Ga)	Time (t)	$\epsilon\text{Nd} (1120 \text{ Ma})$	$^{87}\text{Sr}/^{86}\text{Sr}$
MQ-117	1	Medium-grained metagabbro	2.77	9.03	0.1853	0.5127	1.08		1120		0.706
MQ-158	1	Metatroctolite	0.81	4.82	0.1011	0.5126	-1.04		1120		0.705
MQ-15	2	Metagabbro	1.98	8.25	0.1448	0.5121	-10.33	2.05	1120	-2.89	0.714
MQ-21	2	Metagabbro	4.83	17.25	0.1694	0.5125	-2.38		1120		0.711
MQ-118A	2	Massive metabasalt	7.82	26.53	0.1781	0.5127	0.51		1120		0.709
MQ-118D	2	Metagabbro	3.49	17.17	0.1229	0.5121	-9.81	1.51	1120	0.77	0.711
MQ-118E	2	Fine-grained metagabbro	7.16	24.71	0.1752	0.5126	-0.32		1120		0.709
MQ-147B	2	Fine-grained metagabbro	6.32	23.15	0.1651	0.5123	-7.34		1120		0.714
MQ-148A	2	Massive metabasalt dike	5.49	18.17	0.1826	0.5127	0.71		1120		0.710
MQ-148B	2	Fine-grained metagabbro dike	7.81	23.64	0.1998	0.5126	-0.85		1120		0.708
MQ-148C	2	Fine-grained metagabbro dike	7.14	1.93	2.2335	0.5120	-12.30		1120		0.709
MQ-176B	2	Fine-grained metagabbro	4.85	17.73	0.1654	0.5125	-2.83	1.71	1120	1.66	0.711
MQ-37	3	Metagabbro	3.49	14.71	0.1435	0.5123	-6.26	1.56	1120	1.37	0.702
MQ-97	3	Medium-grained metagabbro	1.01	3.77	0.1625	0.5122	-8.76		1120		0.702

718

719

720

721 **5. Discussion**

722

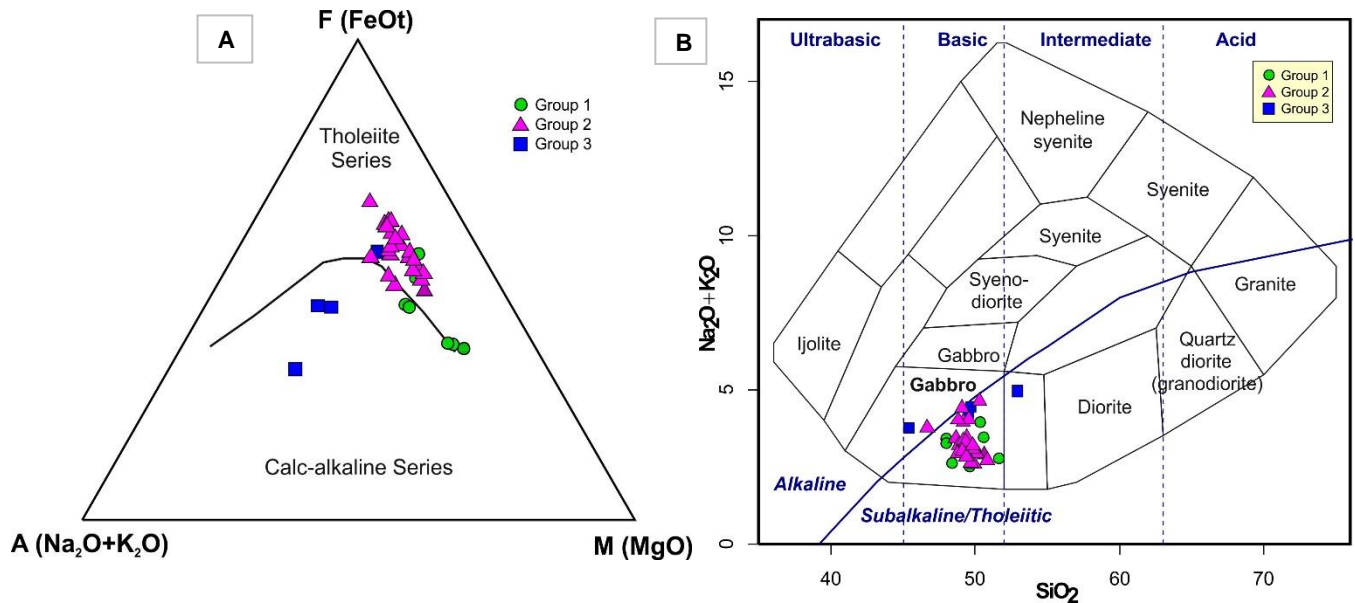
723 **5.1 Tectonic Setting**

724

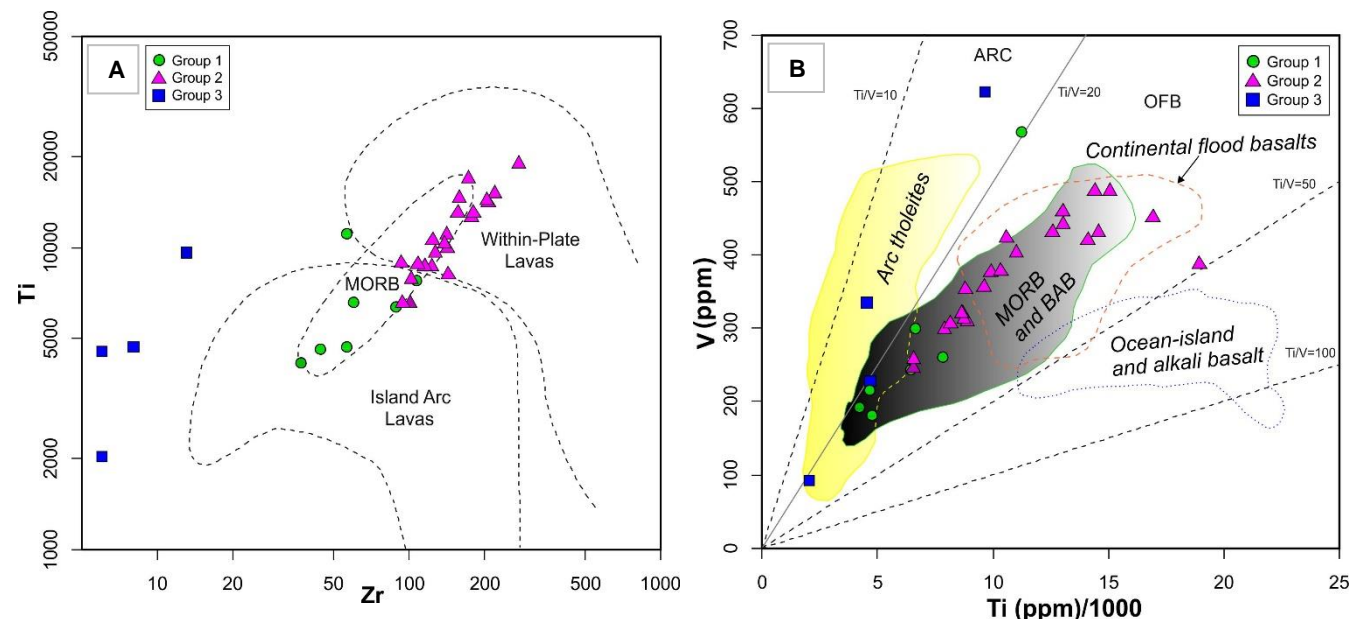
725 A wider geochemical examination of the involvement of other magma reservoirs and
 726 geodynamic setting, together with the behaviour of Sr-Nd isotopic systems in the metamafic rocks
 727 of the Rio Branco Suite provide important clues to elucidate the tectonic environment and better
 728 understanding of the geochemical signatures of the Rio Branco Suite. Since these rocks have been
 729 subjected to high-grade metamorphism, trace elements, especially those considered immobile, were
 730 applied in discriminant diagrams, which will be discussed below.

731 The mafic samples from the Rio Branco Suite plot predominantly in the tholeiite field on the
 732 AFM diagram of Irvine and Baragar, except two samples that plot in the calc-alkaline field because
 733 they are enriched in alkalis. We highlight that sample position that represents the less evolved
 734 magma of suite (sample MQ-114), having a tholeiitic affinity (Fig. 10A). On the classification
 735 diagram, more specifically on the TAS graph (SiO_2 vs. $\text{Na}_2\text{O}+\text{K}_2\text{O}$) of Cox et al. (1979), the samples
 736 plot in the gabbro/basalt field defining a sub-alkaline tholeiitic series (Fig. 10B). In the Ti vs. Zr
 737 graphic (after Pearce, 1982) the metamafic rocks of the Rio Branco Suite show a clear trend formed
 738 by samples from Groups 1 and 2, defining fractionation due to the crystallization of olivine,

739 clinopyroxene, orthopyroxene and plagioclase resulting in an increase in Ti and Zr, while the
 740 fractionation of magnetite causes a diminution of Ti, and the fractionation of amphibole or biotite
 741 may bring about a depletion in Ti and Zr (Murphy, 2007) (Fig. 11A). This relative enrichment in Ti
 742 and Zr in the more evolved rocks of the Rio Branco Suite might have been influenced by the
 743 participation of a contaminant component during magma-crust interactions (Fig. 11A). In the
 744 Ti/1000 vs. V diagram of Shervais (1982), the magmatic differentiation trend displayed by the rocks
 745 of the Rio Branco Suite may coincide with the ARC (arc tholeiitic), MORB (mid-ocean ridge basalt)
 746 and BAB (back-arc basalt) fields (relation $Ti/V > 10$ and $Ti/V < 50$), as a function of the relative
 747 increase in Ti in the more evolved rocks (Fig. 11B).
 748
 749



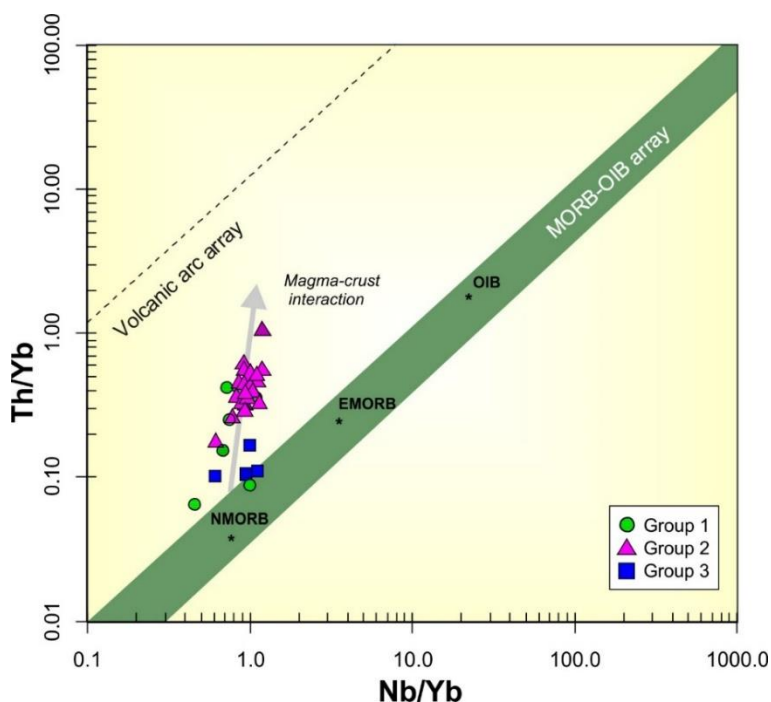
750
 751 **Fig. 10.** Classification diagrams of the series. (A) AFM diagram (Irvine and Baragar, 1971) and (B) TAS
 752 (SiO_2 vs. Na_2O+K_2O) diagram of Cox et al. (1979).
 753
 754



755 **Fig. 11.** (A) Ti vs. Zr diagram (Pearce, 1982) and (B) Ti/1000 vs. V (Shervais, 1982), showing the
 756 fractionation trends observed in the metamafic rocks of the Rio Branco Suite (ARC-arc; MORB-mid-ocean
 757 ridge basalt; BAB-back-arc basalt; OFB-ocean floor basalt).

758 In the diagram Th/Yb vs. Nb/Yb (Pearce, 2008), the Rio Branco Suite samples show an
 759 almost vertical trend from the N-MORB source towards the volcanic arc array suggesting the
 760 geochemical influence of contamination components that increased Zr/Nb and Zr/Y ratios (Group
 761 1 and Group 2) relative to a less contaminated mantle source (Group 3). This chart shows a gradual
 762 enrichment of Th in relation to Nb (Fig. 12). Accordingly, the samples from Group 1, Group 2 and
 763 Group 3 show characteristics typical of subduction zones. Notwithstanding, those of Groups 1 and
 764 2 display more significant evidence for magma-crust interactions, whereas those of Group 3 have,
 765 for the best part, preserved evidence for the magma source with less evidence for magma-crust
 766 interaction. However, these are characteristics associated with an oceanic arc formed in the
 767 environment of a supra-subduction zone, with the formation of rocks from different sources with
 768 the participation of a contamination component. A question to consider is the possibility that the
 769 negative Nb anomalies may have resulted from a process other than subduction. However, according
 770 to Pearce (2008), it is possible to distinguish genuine subduction anomalies from false ones created
 771 by contamination processes from the fractionation trend showed by the rocks analysed, and plotted
 772 on Th/Yb vs. Nb/Yb diagram (Fig. 12). In this diagram, the diagonal (inclined) magmatic
 773 fractionation trends with variable enrichment in Th, may be better explained by variable amounts
 774 of crustal contamination. On the other hand, the sub-vertical trends indicating variable enrichment
 775 of Th, in relation to Nb, from the N-MORB font may be associated with a subduction component
 776 (Pearce, 2008).

777 Therefore, the metamafic rocks of the Rio Branco Suite may have formed from the partial
 778 melting of a depleted mantle wedge, in which the upward moving magma may have partially
 779 assimilated the country rocks. This may have occurred during the magmatic evolution or during
 780 magma-crust interactions leading to the formation of an island arc, the rocks of which are typically
 781 enriched in Ce, La, K, Th, Rb. However, the influence of a subducted plate of deep oceanic origin
 782 along with sea water with strong contaminants cannot be discarded.



783
 784
 785
 786
 787
 788
 789

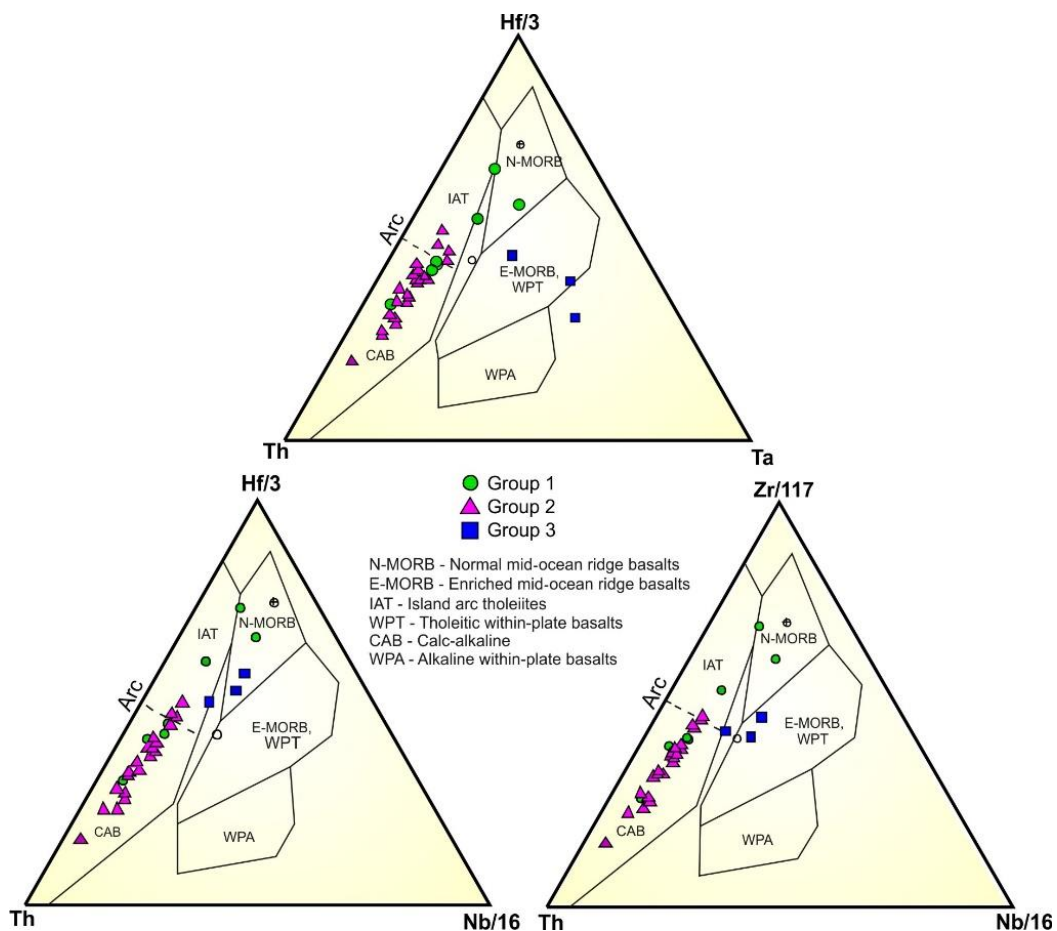
Fig. 12. Nb/Yb vs. Th/Yb diagram (after Pearce, 2008) for metamafic rocks from the Rio Branco Suite (NMORB: normal (depleted) mid-ocean ridge basalts; EMORB: enriched mid-ocean ridge basalts; OIB: oceanic island basalts). The grey arrow indicates the inferred petrogenetic trend.

790 The use of trace elements (Th, Hf, Zr, La, Y, Ta and Nb) from the Rio Branco Suite samples
 791 (Groups 1, 2 and 3) in Wood (1980) and Cabanis and Lecolle (1989) diagrams revealed geochemical
 792 signatures compatible with compressive orogenic environment dominantly, although these diagrams
 793 demonstrate also compatibility with back-arc basin basalts and MORB-like chemistry (Figs. 13, 14).
 794 A large part of the samples of the Rio Branco Suite plot both in the island arc tholeiite (IAT) and
 795 calc-alkaline basalt field (CAB) of the Wood (1980) diagrams, which occurs in function of the
 796 gradual enrichment in Th with respect to Hf, Nb and Zr possibly during subduction (Fig. 13).
 797 However, these diagrams also reveal the influence of the supra-subduction components (subduction
 798 zone enrichment) with petrogenetic trend characteristic of the enrichment in supra-subduction zone
 799 (SSZ) in the chemistry of the trace elements of the mafic rocks of the Rio Branco Suite (Fig. 14).

800 Also, in the Cabanis and Lecolle (1989) diagrams, part of the rocks of Groups 1 and 2 plot
 801 in the island arc tholeiite field (arc field), whereas the samples from Group 3 fall in the calc-alkaline
 802 field (Fig. 14). The samples of the island arc tholeiite (IAT) that fall in the calc-alkaline field are
 803 the result of enrichment or contamination in La during subduction and the magma-crust interaction,
 804 which implies an interpretation that these samples are not necessarily calc-alkaline mafic rocks but
 805 crustal contaminated tholeiite, as previously suggested in figure 14.

806 Finally, in the tectonic discriminant diagrams presented in this paper, the metamafic rocks
 807 of Suite Rio Branco also present overlapping geochemical signature features that mainly suggest
 808 IAT (island arc tholeiite) and BAB (back-arc basalt) affinities. Our preferred hypothesis for the
 809 origin of Rio Branco Suite (metamafic rocks) and of Rio Branco and Migrantinópolis formations
 810 (high-grade metavolcanic-sedimentary rocks) is that they were formed in a transition of the arc -
 811 back-arc environments. Geotectonic configurations developed in response to a subduction during
 812 the Mesoproterozoic (Stenian), between ca. 1137 Ma and 1106 Ma.

813

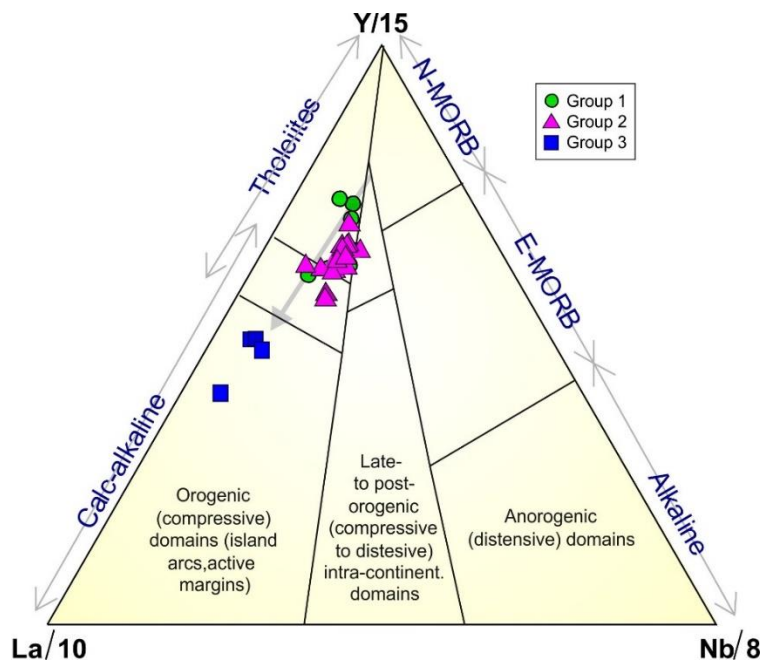


814

815

816

Fig. 13. Triangular diagrams of the Th-Hf-Ta-Zr-Nb system (Wood, 1980) used to identify the subduction components of the metamafic rocks from the Rio Branco Suite.



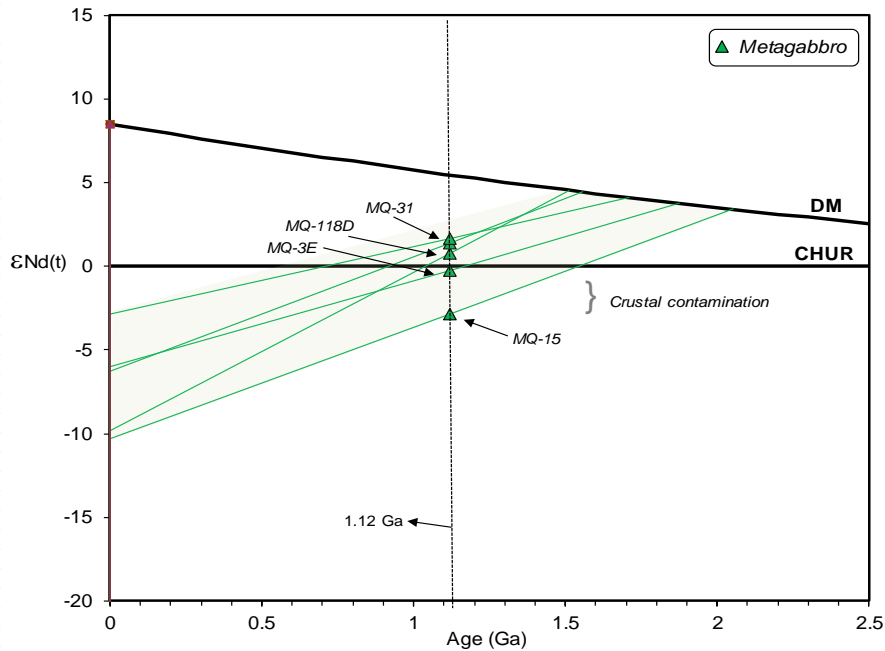
817
818 **Fig. 14.** *La/10 (ppm) vs. Y/15 (ppm) vs. Nb/8 (ppm) diagram of Cabanis*
819 *and Lecolle (1989) for metamafic rocks from the Rio Branco Suite. The*
820 *grey arrow indicates the inferred petrogenetic trend, characteristic of*
821 *the enrichment in supra-subduction zone (SSZ).*
822

823
824 **5.2 Nd-Sr isotopic constraints and the source of mafic magmas**

825
826 The association of the Sr and Nd isotopic composition of rocks from the Rio Branco Suite
827 by group, when compared to present mantle reservoirs, allow us to infer that the metamafic rocks
828 are compatible with mantle magmatism in arc environment with the participation of an important
829 contaminant, which carried an enriched or contaminated mantle reservoir signature. The ϵ_{Nd}
830 obtained in mafic rock of the Rio Branco Suite, recalculated for $t=1120$ Ma, come to slightly
831 negative to positive (-2.89 and +1.66) values near CHUR, suggesting crustal contamination or
832 metasomatic fluids that may be associated with subduction (Figs. 15, 16B). The model ages of the
833 depleted mantle (TDM) of the metamafic rock samples from the Rio Branco Suite were between
834 2.05 Ga and 1.51 Ga (Table 4, Fig. 15). The mafic magma of the Rio Branco Suite may have been
835 submitted to varying degrees of crustal contamination, partially from magma-crust interaction, from
836 an enriched reservoir or from the interaction of the subducted oceanic plate with the mantle wedge.
837 Additionally, the source is indicated by the low La/Ta ratios (between 24.00 and 94.50) vs. ϵ_{Nd}
838 ($T=1120$ Ma, between +1.66 and -2.89) and the low La/Yb vs. Nb/La ratios, between approximately
839 0.52 and 4 for the rocks of Group 1 and Group 2, and between 0.13 and 12.3 for the rocks of Group
840 3. These isotopic and geochemical signatures of the Rio Branco Suite rocks identified in this
841 research are similar in value to those previously observed in several melts derived from lithospheric
842 mantle (see Watson, 1993; Lawton and McMillan, 1999; Chen et al., 2014).

843 Combined Nd and Sr isotopic data (Fig. 16) reveal that rocks from Group 1 best approximate
844 the isotopic composition of those of the Bulk Silicate Earth (BSE), extending towards the lower end
845 of the mantle array. This suggests a degree of mixing of depleted mantle magmas and enriched
846 reservoirs (Fig. 16A). Moreover, from the diagram rocks from Group 2 and Group 3 might be
847 interpreted as evolutionary trend indicating the mixing between magmas with a signature similar to
848 Group 1 (BSE signature) with different enriched sources (EM I and EM II). However, two samples
849 from Group 3 with low $^{87}\text{Sr}/^{86}\text{Sr}$ ratios, low $^{143}\text{Nd}/^{144}\text{Nd}$ ratios and high Sr (ppm) content
850 (considered anomalous) fall into the “forbidden zone field” in $^{87}\text{Sr}/^{86}\text{Sr}$ vs. $^{143}\text{Nd}/^{144}\text{Nd}$ diagram,

851 which should be better evaluated in future studies within the context of a subduction environment
 852 and the P and T conditions involved during metamorphism.
 853



854 **Fig. 15.** Plots of whole-rock $\epsilon Nd(t)$ versus age for the metamafic
 855 rocks in the Rio Branco Suite. The $\epsilon Nd(t)$ values of the
 856 Mesoproterozoic metamafic rocks were re-calculated to $t=1120$ Ma.
 857

858
 859 **5.3. The evolution of the Rio Branco Suite in the context of the Rodinia supercontinent**
 860 **assembly**

861 Available literature has shown that some mafic suites are formed in supra-subduction zones,
 862 and which evolve to form island arcs or volcanic arcs. In the initial phase of subduction and the
 863 formation of a proto-island arc, we usually observe a sequential geochemical evolution with
 864 components having the characteristics of MORB, IAT (tholeiitic island arc) and even boninites that
 865 occur vertically or laterally in complete magmatic sequences, principally in younger (Phanerozoic)
 866 tectonic oceanic environments, where their structure is well preserved and more complete (see Dilek
 867 and Furnes, 2009, 2011; Reagan et al., 2010). In this type of subduction environment (associated
 868 with a supra-subduction zone or a volcanic arc), the mafic magmatism occurs in the initial stages of
 869 arc formation. In this setting, an older pre-existing piece of oceanic crust of MORB-type is necessary
 870 to serve as the host for gabbroic plutonic bodies, basalt dykes and diabase in the lower part of the
 871 crust, as well as serving as a substrate for basalt flows, principally for the types associated with
 872 supra-subduction zones. Depending on the evolution and maturation of the arc, and the subduction
 873 progress, there exists the possibility for the formation of trondhjemite, tonalite and even granite
 874 bodies in the middle zone of the crust, in addition to andesite volcanos, rhyolite flows and dyke
 875 intrusions in the upper crust. Additionally, there may occur flows (massive mafic flows and pillow
 876 lava), volcanoclastic and pyroclastic rocks the surface (see Dilek and Furnes, 2011). In general, the
 877 formation of a volcanic arc is the result of prolonged subduction (~ 20-40 Ma) that may not evolve
 878 to a continent-continent collision phase in the same event of arc formation (Dilek and Flower, 2003).
 879
 880

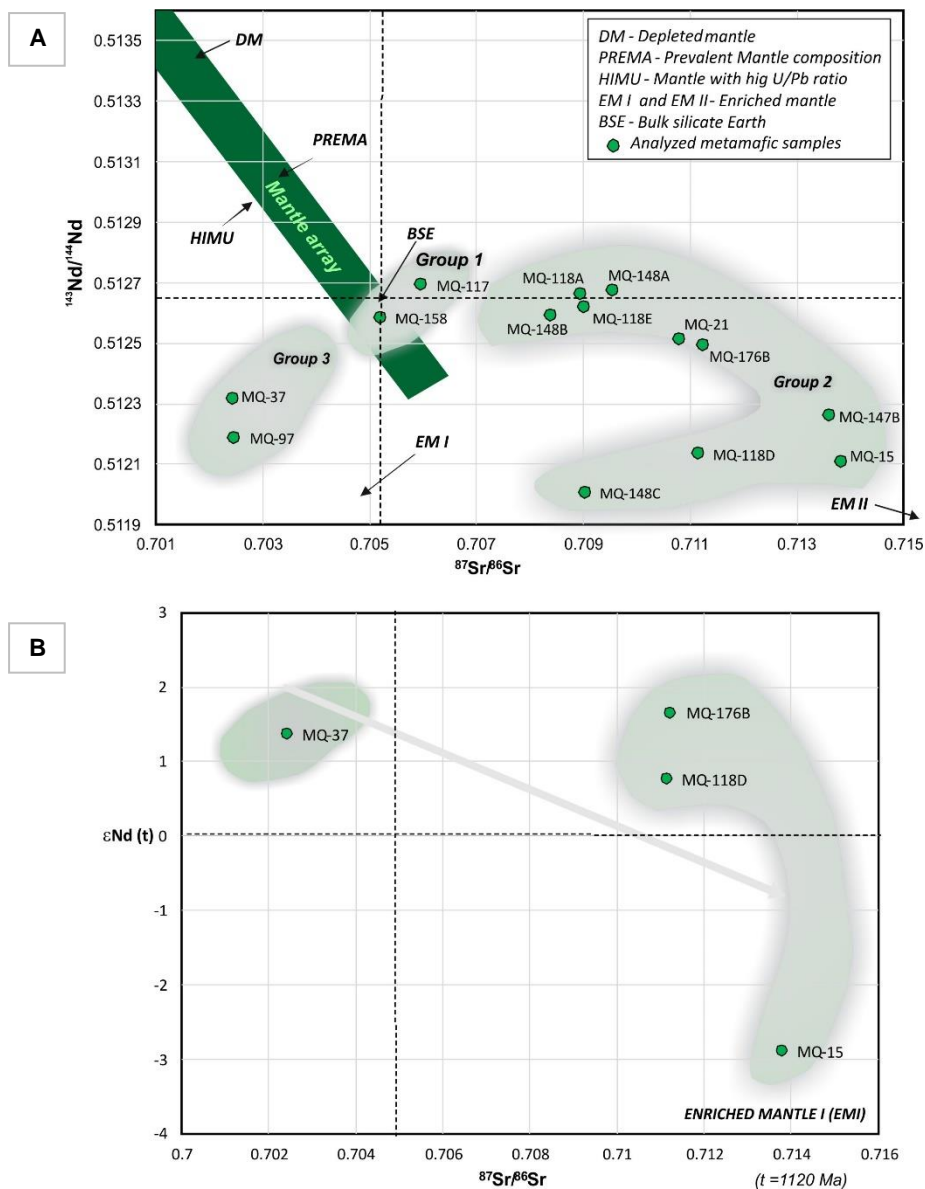


Fig. 16. (A) isotope correlation diagram of $^{143}\text{Nd}/^{144}\text{Nd}$ vs. $^{87}\text{Sr}/^{86}\text{Sr}$ of the metamafic rock samples of the Rio Branco Suite and their positions in relation to the main oceanic mantle reservoirs according to Zindler and Hart (1986). (B) correlation diagram of ϵNd vs. $^{87}\text{Sr}/^{86}\text{Sr}$ for time $t=1120 \text{ Ma}$.

881
882
883
884
885
886
887
888 Based on our study, we chose to consider it as the first possibility of mafic sub-alkaline
889 tholeiitic medium- to low Ti magmatism of the Rio Branco Suite was generated by intra-oceanic
890 subduction between ca. 1137 Ma and 1106 Ma, with peak of high-grade metamorphism at ca. 1137
891 Ma and 1127 Ma probably related to the initial phase of the subduction (see Wakabayashi *et al.*,
892 2010). Our first suggestion involves magmatic arc formation magmatic (possible island arc)
893 between ca. 1119 Ma and 1106 Ma, which we named of Rio Branco arc, after the high-grade
894 metamorphism recorded in the metavolcanic-sedimentary rocks of the Rio Branco Formation, but
895 of very close ages and possibly associated with the same tectonic event. The second possibility is
896 suggest due to the overlapping of IAT and BAB geochemical signatures in the tectonic discriminant
897 diagrams presented in this paper, leading to the interpretation that the Rio Branco Suite rocks were
898 formed in an arc - back-arc environment (Fig. 16).

899 This scenario observed in Rio Branco domain, southern part of the Nova Brasilândia belt,
900 suggests Rodinia pre-assembly accretionary phase on the border of the Amazonian proto-Craton

901 between ca. 1137 Ma and 1106 Ma. As proposed above, we suggest the possibility that during the
902 formation of the Rio Branco magmatic arc at ca. 1119 Ma and 1106 Ma, local extensions might
903 have been active during the early phase of intra-oceanic subduction, causing the rise of the *mantle*
904 *wedge* and partial melting. Therefore, this close association between the high-grade metamorphism
905 and the voluminous mafic magmatism may be interpreted, provisionally, as being associated with
906 the evolution of a “hot orogen” (see Wakabayashi *et al.*, 2010). In this context, at about 1137 Ma,
907 the margins of the Laurentia and Amazonian cratons were dominated by the convergent interaction
908 between two plates and blocks associated with the beginning of the closure of a pre-existing ocean
909 that was formed approximately between ca. 1241 and 1137 Ma.

910 The Paraguá block and Amazonian proto-Craton was amalgamated during the Rondonian-
911 San Ignacio Orogeny between 1470 and 1350 Ma (Boger *et al.*, 2005; Bettencourt *et al.*, 2010;
912 Rizzotto *et al.*, 2013). The scenario of intra-oceanic subduction proposed in our research suggests
913 the existence of an ocean formed between the Amazonian proto-Craton and a block (composed by
914 the Paraguá block, fragments of the Alto Guaporé belt, São Felipe basement and other allochthonous
915 terranes located in Bolivia and the Mato Grosso territory). The formation of this ocean occurred
916 possibly after ca. 1241 Ma and before ca. 1137 Ma, during the rift-to-drift phases originated as from
917 reactivation of EW structures pre-existing along the Guaporé suture, promoting the break-up of the
918 Amazonian proto-Craton that had been assembled during the Rondonian-San Ignacio orogeny (ca.
919 1350 Ma). This possibility of the existence of this block (Rio Guaporé block as a suggested name)
920 needs to be better evaluated in later studies.

921 In our proposal, the Nova Brasilândia orogeny begins with subduction and formation of an
922 arc - back-arc system between ca. 1137 and 1106 Ma (accretionary phase), originated from of re-
923 approximation of the Paraguá block and Amazonian proto-Craton after the break-up of the
924 Amazonian proto-Craton and oceanization between ca. 1241 and 1137 Ma. The final collision and
925 crustal thickening (collisional phase) occurred only between ca. 1096 and 1010 Ma, presumably
926 driven by the collision and accretion of the Arequipa-Antofalla Basement to the western margin of
927 the Paraguá block, reflecting in the rocks inside the Nova Brasilândia belt (Loewy *et al.*, 2004;
928 Tohver *et al.*, 2004; Quadros *et al.*, submitted).

929 In this same period or near to it, magmatic arcs and metavolcanic-sedimentary belts was
930 formed along of cratons margins, such as the Composite Metasedimentary belt of northern
931 Grenville, Nova Brasilândia belt in the southwestern of the Amazonian Craton, Coal Creek Arc of
932 the Llano uplift, and basement inliers in the Andean Cordillera such as the Arequipa-Antofala
933 basement (Cawood and Pisarevsky, 2017). Orogenic events of this period (ca. 1.2 and 1.1 Ga) are
934 known of Nova Brasilândia orogeny at the Sunsás Province and Shawinigan orogeny at the
935 Grenville Province.

936 Finally, based on geological, geochemical and Sr-Nd isotope new data obtained during this
937 study and the reinterpretation of data previously published by Rizzotto (1999), Rizzotto *et al.* (2001,
938 2014), Tohver *et al.* (2002, 2004, 2005a, 2005b, 2006 and references therein), we propose in this
939 article a new scenario for the tectonic evolution of the Nova Brasilândia orogeny, with emphasis on
940 the Rio Branco domain on the southern part of the Nova Brasilândia belt. In general terms, our
941 proposal centers around the Mesoproterozoic evolution of the Nova Brasilândia belt, which is part
942 of the Sunsás Orogen. We suggest a Rodinia pre-assembly accretionary phase between ca. 1137 and
943 1106 Ma (Fig. 17) and we associate the Nova Brasilândia orogeny that was initially named by
944 Rizzotto (1999). At this stage there was an intra-oceanic subduction event and formation of a
945 magmatic arc and arc-related basins, as the start of the closure of the ocean that formed between ca.
946 1241 and 1137 Ma (Fig. 17). This accretionary phase (ca. 1137 and 1106 Ma) recorded in the Nova
947 Brasilândia belt was not recorded in the Aguapeí and Sunsás belts suggesting that only the Nova
948 Brasilândia belt underwent an oceanization phase between ca. 1241 and 1137 Ma.

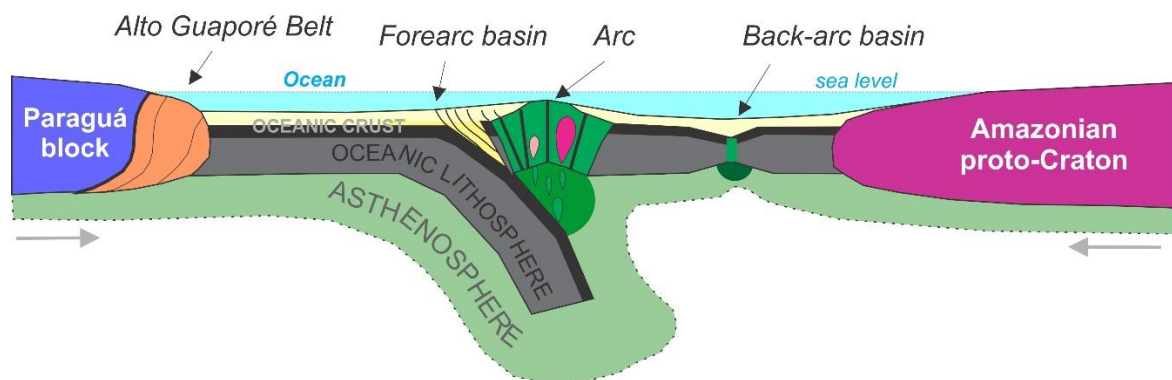
949 This new compressive scenario involving subduction contrast with the one previously
950 defined for the Nova Brasília belt as a product of intracratonic reactivations that occurred during the
951 development of the Sunsás orogen, involving opening and closing an intracontinental rift (Rizzotto,
952 1999; Teixeira *et al.*, 2010; D'Agrella-Filho *et al.*, 2012; Rizzotto *et al.*, 2014). This partially

953 contrasts with the proposed scenario of collision and suture between the Amazonian proto-Craton
 954 and Paraguá block (Tohver et al., 2004), as it presents a new scenario involving the break-up of the
 955 Amazonian proto-Craton into two blocks after its consolidation during the last Rondonian-San
 956 Ignácio orogeny (ca. 1350 Ma). Consequently occurred the opening of an ocean between ca. 1241
 957 and 1137 Ma, followed by an accretionary-collisional orogenetic phase between ca. 1137 and 1010
 958 Ma (Nova Brasilândia orogeny). In addition, there is possibility that part intraplate mafic
 959 magmatism (gabbro) associated with the Nova Floresta Fomation, Rondônia, dated by the K-Ar
 960 (biotite and plagioclase) method in ca. 1201 and 1196 Ma (Tohver et al., 2002) may be associated
 961 to the break-up between Amazonian proto-Craton and Paraguá block by the relative rotation
 962 between Amazon and Laurentia (see Johansson , 2009). This rotation may have provided continental
 963 rifting and oceanization between 1241 and 1137 Ma, followed by the beginning of the ocean closure
 964 and intra-oceanic subduction between 1137 and 1106 Ma.

965 At this phase, finally there was a second accretion of the Paraguá block, together with the
 966 Arequipa-Antofala basement and smaller fragments (Alto Guaporé belt fragment, São Felipe
 967 basement, Rio Branco arc and related-basins), to the Amazonian proto-Craton for Rodinia
 968 supercontinent assembly at the late Mesoproterozoic. Reworked craton portions on the basement to
 969 the north and northwest of the Nova Brasilândia belt well record two Mesoproterozoic collisional
 970 phases (Ectasian-Stenian) of crustal mass accretion to the Amazonian proto-Craton, in regions along
 971 of the Jamari domain and Ji-Parana - Cujubim sinistral transpressive system at approximately 1350
 972 Ma and 1110 Ma, respectively (Fig. 1).

973

**ACCRETIONARY PHASE (1137-1106 Ma)
 Rodinia pre-assembly**



974

975

976 *Fig. 17. Simplified new scenario accretionary proposed for the evolution of the Nova Brasilândia*
 977 *belt in southwestern Amazonian Craton, Rondonia, during the Mesoproterozoic (Stenian).*

978

979

980 The insertion of an accretionary phase in the evolution of the Nova Brasilândia belt generates
 981 several implications that with the advancement of research promoted the improvement of the
 982 previously proposed model involving transtension/transpression, formation of intracontinental rift,
 983 passive margin and proto-ocean, and deformation/high-grade metamorphisms during subduction
 984 and collision. Based on this new proposal presented in this paper, new tectonic models of
 985 paleogeographic reconstitution of paleocontinents in Mesoproterozoic may be suggest by involving
 986 data from this southwestern portion of the Amazonian Craton, an important area of the Amazon for
 987 understanding the geological processes of the assembly of Rodinia.

988

989 **6. Conclusion**

990

991 New geological, geochemical (whole-rock) and isotopic (Sm-Nd and Sr) data of the Rio
 992 Branco Suite metamafic rocks presented in this paper led to the proposal of a new evolutionary

993 geotectonic scenario for the Nova Brasilândia belt in the southwest region of the Amazonian Craton
994 in Rondônia, and its significance in evolution Mesoproterozoic (Stenian) of the Sunsás orogen. The
995 main conclusions of our work are summarize as follows:

996

997 1. The metamafic component of the Rio Branco Suite (ca. 1119 and 1106 Ma) show of a
998 tholeiitic sub-alkaline composition with intermediate- to low Ti and geochemical signature
999 overlay that suggest MORB-like (mid-ocean ridge basalt), IAT (island arc tholeiite) and
1000 BAB (back-arc basalt) affinities. The identified groups of metamafic rock (Group 1, 2, 3)
1001 show negative anomalies of Nb and Ta, gradually enriched in Th relative to Nb and Ta,
1002 positive anomalies of Pb, and positive anomalies of K. Besides Ti/V ratios (10 and 50),
1003 La/Yb ratios (between 1.74 and 12.33), Th/Yb ratios (between 0.10 and 3.56), and low-
1004 ratios Ce/Pb (3.3 and 20.5), Nb/U (3.2 and 16.25), and Th/La (0.01 and 0.30). The ϵ_{Nd}
1005 (recalculated for $t = 1120$ Ma) of the metamafic rocks of Rio Branco Suite with slightly
1006 negative to positive values (between -2.89 and +1.66) close to CHUR suggests crustal
1007 contamination that may be associated with subduction. Sr-Nd isotopic compositions
1008 demonstrate that in Group 1 average $^{87}\text{Sr}/^{86}\text{Sr}$ ratios of 0.705-0.706 and average
1009 $^{143}\text{Nd}/^{144}\text{Nd}$ ratios of 0.512, Group 2 shows medium to high $^{87}\text{Sr}/^{86}\text{Sr}$ ratios of 0.708-0.714
1010 and average $^{143}\text{Nd}/^{144}\text{Nd}$ ratios of 0.512, and Group 3 (anomalous considered) shows
1011 $^{87}\text{Sr}/^{86}\text{Sr}$ low ratios of about 0.702, and $^{143}\text{Nd}/^{144}\text{Nd}$ low ratios of 0.512. All these
1012 geochemical and isotopic characteristics considered effective in interpreting the subduction
1013 tectonic environment for the generation of mafic magmatism of the Rio Branco Suite.

1014

1015 2. Geochemical, isotopic and geological evidence recorded in the Rio Branco domain
1016 suggests that tholeiitic mafic magmatism with low to medium titanium of the Suite Rio
1017 Branco (ca. 1119 and 1106 Ma) was generated during intra-oceanic subduction, possibly
1018 in a tectonic environment associated with the arc - back-arc system (Fig. 17). Additionally,
1019 in this scenario, the metatrandhjemites spatially associated with metamafic rocks are
1020 probably of the oceanic arc-type and reinforced the tectonic environment of subduction
1021 proposed in this article. Therefore, the Rio Branco Suite represents an incomplete fragment
1022 of magmatic arc (island arc) associated with ocean-ocean subduction.

1023

1024 3. Based on our research we suggest that the southern part of the Nova Brasilândia belt (Rio
1025 Branco domain) is the record of an important Mesoproterozoic (Stenian) activity
1026 convergent accretionary that occur between ca. 1137 and 1106 Ma. The high-grade
1027 metavolcanic-sedimentary (Rio Branco Formation) and metamafic-metafelsic (Rio Branco
1028 Suite) rocks are products of this event of subduction (Fig. 17).

1029

1030 4. This accretionary phase in the Nova Brasilândia belt marks the beginning of the closure of
1031 an existing ocean between the a large block consisting of the Paraguá block and smaller
1032 blocks or terrane fragments (such as Alto Guaporé belt fragment, São Felipe basement and
1033 others on the Bolivia and Brazil). We associate this accretionary phase with the beginning
1034 of the Nova Brasilândia orogeny (Table 1).

1035

1036

1037 *Acknowledgements*

1038

1039 This work was financed by the UNB and by the ARIM Nova Brasilândia Project of CPRM-
1040 Geological Survey of Brazil. The authors are grateful to the CPRM-Geological Survey of Brazil in
1041 Porto Velho, Rondônia and in Belém, Pará, Brazil for assistance in fieldwork and access to
1042 laboratories for the preparation of the samples collected in the field. We also thank the geologists
1043 Luciano Castro da Silva, Anderson Alves de Souza, Jaime Estevão Scandola and Livio Wagner
1044 Chaves Correa for the geological discussions during field activities and office work. We thank the

1045 mining technician Maria Rosalva Campos Coelho for her help in the preparation of the samples for
1046 Sm-Nd and Sr analysis. We thank the CPRM and UnB technicians for their support and performing
1047 Sm-Nd and Sr analyses in the laboratory of the Geochronology Centre of the Institute of
1048 Geosciences of the University of Brasilia (Geocron-IG/UnB). Constructive revisions of this
1049 manuscript by reviewers were acknowledged with thanks.

1050

1051

1052 **References**

1053

1054 Amaral, G. 1974. *Geologia Pré-Cambriana da Região Amazônica* (Tese de doutorado). Instituto
1055 de Geociências, Universidade de São Paulo, São Paulo, SP, Brasil.

1056 Bettencourt, J. S., Leite, W. B., Ruiz, A. S., Matos, R., Payolla, B. L., Tosdal, R. M. 2010. The
1057 Rondonian-San Ignacio Province in the SW Amazonian Craton: An overview (Vol. 29).
1058 *Journal of South American Earth Sciences*, pp. 28–46.

1059 Boger, S.D., Raetz, M., Giles, D., Etchart, E., Fanning, C.M., 2005. U–Pb age from the Sunsás
1060 region of eastern Bolivia, evidence for allochthonous origin of the Paraguá Block. *Precambrian*
1061 *Research* 139, 121–146.

1062 Boynton, W. V. 1985. Cosmochemistry of the rare earth elements: meteorite studies, In P.
1063 Henderson, (Ed.), *Rare Earth Element Geochemistry* (pp. 115-1522). Elsevier, Amsterdam.
1064 (Developments in Geochemistry 2).

1065 Cabanis, B., and Lecolle, M. 1989. Le diagramme La/10–Y/15–Nb/8: Unoutil pour la
1066 discrimination des series volcaniques et la mise en evidence des processus de mélange et/ou
1067 de contamination crustale. *Comptes Rendus de l'Académie des Sciences-Series II*, 309, 2023–
1068 2029.

1069 Cawood, P. A., and Pisarevsky, S. A. 2017. Laurentia-Baltica-Amaozonia relations during Rodinia
1070 assembly. *Precambrian Research*. doi: <http://dx.doi.org/10.1016/j.precamres.2017.01.031>.

1071 Chen, W. T., Sun, W., Wang, W., Zhao, J., Zhou, M. 2014. “Grenvillian” intra-plate mafic
1072 magmatism in the southwestern Yangtze Block, SW China. *Precambrian Research*, 242. 138–
1073 153.

1074 Coleman, R. G. 1977. *Ophiolites*. New York: Springer-Verlag.

1075 Cordani, U. G., Tassinari, C. C. G., Teixeira, W., Basei, M. A. S., Kawashita, K. 1979. Evolução
1076 Tectônica da Amazônia com base nos dados geocronológicos. *Anais do Congresso Geológico*
1077 *Chileno*, Arica, China, 2.

1078 Costa, J. B. S., and Hasuy, Y. H. 1997. Evolução Geológica da Amazônia. In: Costa, M. L. C. and
1079 Angélica, R. S. (Coord.). *Contribuições à Geologia da Amazônia* (pp. 15-90). Belém: FINEP;
1080 SBG-NO.

1081 Cox, K. G., Bell, J. D., Pankhurst, R. J. 1979. *The Interpretation of Igneous Rocks*. London:
1082 George Allen & Unwin.

1083 D'Agrella-Filho, M.S., Trindade, R.I.F., Elming, S.-Å., Teixeira, W., Yokoyama, E., Tohver, E.,
1084 Geraldés, M.C., Pacca, I.I.G., Silva, J.A., Barros, M.A.S., Ruiz, A.S., 2012. The 1420 Ma
1085 Indiavaí Mafic Intrusion (SW Amazonian Craton): Paleomagnetic results and implications for
1086 the Columbia Supercontinent. *Gondwana Res.* 22, 956–973.

1087 Dalziel, I.W.D. 1997. Overview: Neoproterozoic–Paleozoic geography and tectonics: review,
1088 hypothesis, environmental speculations. *Bull. Geol. Soc. Am.* 109:16–42

1089 De Paolo, D. J. 1981. Trace Element and Isotopic Effects of Combined Wallrock Assimilation and
1090 Fractional Crystallization. *Earth and Planetary Science Letters*, 53, 189-202. Recuperado de
1091 [http://dx.doi.org/10.1016/0012-821X\(81\)90153-9](http://dx.doi.org/10.1016/0012-821X(81)90153-9)

1092 Dey, A., Hussain, M. F., Barman, M. N. 2018. Geochemical characteristics of mafic and ultramafic
1093 rocks from the Naga Hills Ophiolite, India: implications for petrogenesis. *Geoscience*
1094 *Frontiers*, 9, 517-529.

- 1095 Dilek, Y. and Flower, M. F. J. 2003. Arc-trench roll-back and forearc accretion: 2. In Albania, C.,
1096 Oman in Dilek, Y. and Robinson, P.T. (Eds.). A model template for ophiolites Ophiolites in
1097 Earth History. *Geological Society of London Special Publication*, 218, 43–68.
- 1098 Dilek, Y. and Furnes, H. 2009. Structure and geochemistry of Tethyan ophiolites and their
1099 petrogenesis. In subduction rollback systems. *Lithos*, 113, 1–20. doi:
1100 10.1016/j.lithos.2009.04.022.
- 1101 Dilek, Y. and Furnes, H. 2011. Ophiolite genesis and global tectonics: geochemical and tectonic
1102 fingerprinting of ancient oceanic lithosphere. *GSA Bulletin*, 123(3/4), 387–411. doi:
1103 10.1130/B30446.10.
- 1104 Dilek, Y. and Furnes, H. 2014. Ophiolites and Their Origins. *Elements*, 10, 93–100.
- 1105 Fernandes, C.J., Kuyumjian, R.M., Pulz, G.M., Geraldés, M.C., Pinho, F.E.C., 2006. Geologia
1106 estrutural e idade $^{40}\text{Ar}/^{39}\text{Ar}$ do depósito de ouro Pau-a-Pique, Faixa Móvel Aguapeí, sudoeste
1107 do Estado do Mato Grosso. *Revista Brasileira de Geociências* 36, 3–15.
- 1108 Geraldés, M.C., Figueiredo, B.R., Tassinari, C.C., Ebert, H.D. 1997. Middle Proterozoic vein-
1109 hosted gold deposits in the Pontes e Lacerda region, southwestern Amazonian Craton, Brazil.
1110 *Int Geol Rev* 39: 438-448.
- 1111 Geraldés, M.C., Van Schmus, W.R., Condie, K.C., Bell, S., Teixeira, W., Babinski, M. 2001.
1112 Proterozoic Geologic Evolution of the SW part of the Amazonian Craton in Mato Grosso
1113 State, Brazil. *Precam Res* 111: 91-128.
- 1114 Hastie, A. R., Fitton, J. G., Mitchell, S. F., Neill, I., Nowell, G. M., Millar, I. L. 2015. Can Fractional
1115 Crystallization, Mixing and Assimilation Processes be Responsible for Jamaican-type
1116 Adakites? Implications for Generating Eoarchean Continental Crust. *Journal of Petrology*,
1117 56(7), 1251–1284. doi: 10.1093/petrology/egv029.
- 1118 Hasui, Y., Haralyi, N. L. E., Schobbenhaus, C. 1984. Elementos geofísicos e geológicos da Região
1119 Amazônica: subsídios para o modelo geotectônico. *Anais do Symposium Amazonico*, Manaus,
1120 Brasil, 2.
- 1121 Hoffmann, P.F. 1991. Did the breakout of Laurentia turn Gondwanaland inside-out? *Science*
1122 252:1409–12
- 1123 Irvine, T. N. and Baragar, W. R. A. 1971. A guide to the chemical classification of the common
1124 volcanic rocks. *Canadian Journal of Earth Sciences*, 8(5), 523-548.
- 1125 Johansson, A., 2009. Baltica, Amazonia and the SAMBA connection — 1000 million years of
1126 neighbourhood during the Proterozoic? *Precambr. Res.* 175, 221–234.
- 1127 Kessel, R., Schmidt, M.W., Ulmer, P., Pettke, T., 2005. Trace element signature of subduction-
1128 zone fluids, melts and supercritical liquids at 120–180 km depth. *Nature* 437, 724-727.
- 1129 Kroonenberg, S. B. 1982. A Grenvillian granulite belt in the Colombian Andes and its relation to
1130 the Guiana Shield. *Geologie en Mijnbouw*, 61, 325-333.
- 1131 Lawton, T. F. and McMillan, N. J. 1999. Arc abandonment as a cause for passive continental
1132 rifting: comparison of the Jurassic Borderland rift and the Cenozoic Rio Grande rift. *Geology*,
1133 27, 779-782.
- 1134 Lima, G., Macambira, M., Sousa, M. Z., Ruiz, A. 2017. Suíte Intrusiva Rio Perdido: magmatismo
1135 intraplaca no sul do Cráton Amazônico – Bloco Rio Apa. *Geologia USP. Série Científica*. 17.
1136 79. 10.11606/issn.2316-9095.v17-454.
- 1137 Litherland, M. and Bloomfield, K. 1981. The Proterozoic History of Eastern Bolivia. *Precambrian*
1138 *Res.*, 15, 157-179.
- 1139 Litherland, M., Annells, R. N., Appleton, J. D., Berrange, J. P.; Bloomfield, K., Burton, C. C. J.,
1140 Darbyshire, D. P. F., Fletcher, C. J. N. Hawkins, M. P., Klinck, B. A., Llands, A., Mitchell,
1141 W. I., O'Connor, E. A., Pitfield, P. E. J., Power, G., Weeb. B. C. 1986. *The Geology and*
1142 *Mineral Resources of the Bolivian Precambrian Shield*. London: Brit. Geol. Surv. 153 p.
1143 (Overseas Memoir 9).
- 1144 Lister, G. and Forster, M. 2009. Tectonic mode switches and the nature of orogenesis. *Lithos*, 113,
1145 274–291. doi:10.1016/j.lithos.2008.10.024.

- 1146 Loewy, S., Connelly, J. N., Dalziel, I. W. 2004. An orphaned basement block: the Arequipa-
1147 Antofalla Basement of the central Andean margin of South America. *Geol. Soc. Am. Bull.*,
1148 *116*, 171-187.
- 1149 McDonough W. F. and Sun S. 1995. "The composition of the Earth" *Chemical Geology* 120, p.
1150 223–253.
- 1151 Murphy, J. B. 2007. Igneous Rock Associations 8. Arc Magmatism II: geochemical and isotopic
1152 characteristics. *Geoscience Canada*, *34(1)*, 7-35.
- 1153 Pearce, J. A. 1982. Trace element characteristics of lavas from destructive plate boundaries. In
1154 Thorps, R. S. (Ed.), *Andesites* (pp. 525–548). New York: John Wiley and Sons.
- 1155 Pearce, J. 1996. A User's Guide to Basalt Discrimination Diagrams. *Geol. Assoc. Canada Short*
1156 *Course Notes*, *12*, 79-113.
- 1157 Pearce, J. A. 2008. Geochemical fingerprinting of oceanic basalts with applications to ophiolite
1158 classification and the search for Archean oceanic crust. *Lithos*, *100*, 14–48.
- 1159 Pearce, J. A. 2014. Immobile elements fingerprinting of ophiolites. *Elements*, *10*, 101–108.
- 1160 Pearce, J. A. and Norry, M. J. 1979. Petrogenetic implications of Ti, Zr, Y and Nb variations in
1161 volcanic rocks. *Contributions to Mineralogy and Petrology*, *69*, 33–47.
- 1162 Pearce, J. A., Lippard, S. J., Roberts, S. 1984. *Characteristics and tectonic significance of supra-*
1163 *subduction zone ophiolites* (pp. 77-94). London: Geological Society, (Special Publications,
1164 16).
- 1165 Pinto Filho, F. P., Freitas, A. F. de, Melo, C. F., Romanini, S. J. 1977. *Projeto Sudeste de*
1166 *Rondônia: Relatório Final* (Vol. 4). Porto Velho: CPRM.
- 1167 Priem, H. N. A., Bon, E. H., Verdumen, E. A. Th., Bettencourt, J. S. 1989. Rb-Sr chronology of
1168 Precambrian crustal evolution in Rondonia (Western margin Brazilian Craton). *Journal of*
1169 *South American Earth Sciences*, *2*, 163-170.
- 1170 Quadros, M. L. do E. S. and Rizzotto, G. J. (Org.). 2007. *Geologia e recursos minerais do Estado*
1171 *de Rondônia: texto explicativo do mapa geológico e de recursos minerais do Estado de*
1172 *Rondônia* (pp. 116). Escala 1:1.000.000. Porto Velho: CPRM.
- 1173 Quadros, M. L. do E.S., Palmeira, L. C., Castro, C. C. 2011. Geologia e Recursos Minerais da
1174 Folha Rio Machadinho: SC.20-X-C, escala 1:250.000 (pp. 203). Porto Velho: CPRM.
- 1175 Quadros, M. L. do E.S., Giustina, M.E.S.D., Rodrigues, J. B. R., Souza, V. da S. Geology and LA-
1176 ICP-MS U-Pb zircon geochronology of the Rio Branco domain, Nova Brasilândia belt,
1177 southwest Amazonian Craton: new data, reinterpretation of compiled geochronological data
1178 and implications on the evolution of the Sunsás orogen (submitted).
- 1179 Ramos, V. A. 2010. The Grenville-age basement of the Andes. *Journal of South American Earth*
1180 *Sciences*, *29*, 77–91.
- 1181 Reagan, M. K., Ishizuka, O., Stern, R. J., Kelley, K. A., Ohara, Y., Blichert-Toft, J., Bloomer, S.
1182 H., Cash, J., Fryer, P., Hanan, B. B., Hickey-Vargas, R., Ishii, T., Kimura, J. I., Peate, D. W.,
1183 Rowe, M. C., Woods, M. 2010. Fore-arc basalts and subduction initiation in the Izu-Bonin-
1184 Mariana system. *Geochemistry, Geophysics, Geosystems*, *11(3)*. doi:
1185 10.1029/2009GC002871.
- 1186 Rizzotto, G. J. 1999. *Petrologia e Geotectônica do Grupo Nova Brasilândia: Rondônia*
1187 *(Dissertação de mestrado)*. Federal University of Rio Grande do Sul, Porto Alegre, Brazil.
- 1188 Rizzotto, G. J. 2001. Reavaliação do Ciclo Orogênico Sunsas/Aguapeí no Sudoeste do Amazonian
1189 Craton. *Abstracts Workshop on Geology of the SW Amazonian Craton: state of the art, IGC*
1190 *Project 426* (pp. 66-67).
- 1191 Rizzotto, G. J. and Hartmann, L. A. 2012. Geological and geochemical evolution of the Trincheira
1192 Complex, a Mesoproterozoic ophiolite in the southwestern Amazon craton, Brazil. *Lithos*,
1193 *148*, 277-295.
- 1194 Rizzotto, G. J., Lima, E. F., Chemale Jr., F. 1999. Geologia e geoquímica das rochas metabásicas
1195 da sequência metavulcano-sedimentar Nova Brasilândia – sudoeste de RO. *Revista Brasileira*
1196 *de Geociências*, *29(2)*, 119-128.

- 1197 Rizzotto, G. J., Lima, E. F., Chemale Jr., F. 2001. Geologia do Grupo Nova Brasilândia, sudeste
1198 de Rondônia, acreção continental e implicações geotectônicas. In Reis, N. J., Monteiro, M.
1199 A. S. (Coord.). *Contribuições à Geologia da Amazônia*, 2, 342–442.
- 1200 Rizzotto, G. J., Santos, J. O. S., Hartmann, L. A., Tohver, E., Pimentel, M. M., McNaughton, N. J.
1201 2013. The Mesoproterozoic Guaporé suture in the SW Amazonian craton: geotectonic
1202 implications based on field geology, zircon geochronology and Nd-Sr isotopic geochemistry.
1203 *J South Am Ear Sci* 48, 271-295.
- 1204 Rizzotto, G. J., Hartmann, L. A., Santos, J. O. S., McNaughton, N. J. 2014. Tectonic evolution of
1205 the southern margin of the Amazonian craton in the late Mesoproterozoic based on field
1206 relationships and zircon U-Pb geochronology. *Anais da Academia Brasileira de Ciências*, 86
1207 (1), 57-84.
- 1208 Ruiz. A. S. 2005. *Evolução geológica do sudoeste do Amazonian Craton, região limítrofe Brasil-*
1209 *Bolívia, Mato Grosso* (Tese de doutorado). Universidade Estadual Paulista, Rio Claro, São
1210 Paulo, Brasil.
- 1211 Ruiz, A. S., Simões, L. S., Araujo, L. M., Godoy, A. M., Matos, J. B., Souza, M. Z. 2007. Cinturão
1212 Orogênico Aguapeí (1025-900 Ma): um exemplo de Faixa Móvel Intracontinental no SW do
1213 Amazonian Craton (pp. 116-118). *Anais do Simpósio Nacional de Estudos Tectônicos*, Natal,
1214 Brasil, 11.
- 1215 Saccani, E. 2015. A new method of discriminating different types of post-Archean ophiolitic
1216 basalts and their tectonic significance using Th-Nb and Ce-Dy-Yb systematics. *Geoscience*
1217 *Frontiers*, 6, 481-501.
- 1218 Saccani, E., Allahyari, K., Beccaluva, L., Bianchini, G. 2013. Geochemistry and petrology of the
1219 Kermanshah ophiolites (Iran): Implication for the interaction between passive rifting, oceanic
1220 accretion, and OIB-type components in the Southern Neo-Tethys Ocean. *Gondwana*
1221 *Research*, 24, 392–411.
- 1222 Saccani, E., Allahyari, K., Rahimzadeh, B. 2014. Petrology and geochemistry of mafic magmatic
1223 rocks from the Sarve-Abad ophiolites (Kurdistan region, Iran): Evidence for interaction
1224 between MORB-type asthenosphere and OIB-type components in the southern Neo-Tethys
1225 Ocean. *Tectonophysics*, 621.
- 1226 Sadowski, G. R. and Bettencourt, J. S. 1996. Mesoproterozoic tectonic correlations between
1227 eastern Laurentia and western border of the Amazon Craton. *Precam. Res.*, 76, 213-227.
- 1228 Saes, G.S., 1999. Evolução tectônica e paleogeográfica do Aulacógeno Aguapeí (1.2–1.0 Ga) e
1229 dos terrenos do seu embasamento na porção sul do Craton Amazônico. Doctoral thesis,
1230 Institute of Geociences, University of São Paulo, São Paulo, Brazil, p. 135.
- 1231 Saes, G.S., Leite, J.A.D., Alvarenga, C.J.S., 1992. Evolução tectono-sedimentar do Grupo
1232 Aguapeí, Proterozóico Médio na porção meridional do Cráton Amazônico: Mato Grosso e
1233 Oriente Boliviano. *Revista Brasileira de Geociências* 23 (1), 31–37.
- 1234 Salinas, G.R.M., 2010. Geocronologia e evolução tectônica paleo-mesoproterozóica do oriente
1235 boliviano - região sudoeste do cráton amazônico. Tese de Doutorado, Instituto de Geociências,
1236 Universidade de São Paulo, São Paulo. 52 p. doi:10.11606/T.44.2010.tde-23012011-170732.
- 1237 Santos, J. O., Hartmann, L., Gaudette, H. E., Groves, D. I., McNaughton, N. J., Fletcher, I. R.
1238 2000. A new understanding of the provinces of the Amazon Craton based on integration of
1239 field mapping and U-Pb and Sm-Nd geochronology. *Gond. Res.*, 3, 453-488.
- 1240 Santos, J. O., Rizzotto, G. J., Easton, M. R., Potter, P. E., Hartmann, L. A., McNaughton, N. J.
1241 2002. The Sunsás Orogen in Western Amazon Craton, South America and correlation with
1242 the Grenville Orogen of Laurentia, based on U-Pb isotopic study of detrital and igneous
1243 zircons. In Geological Society of America, 2002 Denver Annual Meeting (October 27-30,
1244 2002). *Precam. Geol.*, 122-128.
- 1245 Santos, J.O.S., McNaughton, N.J., Hatmann, L.A., Fletcher, I.R., Salinas, R.M., 2005. The age of
1246 the deposition of the Aguapeí Group, Western Amazon Craton, based on U–Pb study on
1247 diagenetic xenotime and detrital zircon. In: Latin American Congress, Quito, Equador,
1248 extended abstracts, pp. 1–4.

- 1249 Santos, J. O., Rizzotto, G. J., Potter, P., Mcnaughton, N., Matos, R., Hartmann, L. A., Chemale, J.
1250 R., Quadros, M. L. 2008. Age and autochthonous evolution of the Sunsás Orogen in West
1251 Amazon Craton based on mapping and U Pb geochronology. *Precam. Res.*, 165, An. Acad.
1252 Bras. Cienc., 86 (1), 120-152.
- 1253 Scandolaro, J. E. 2006. *Geologia e evolução do terreno Jamari, embasamento da faixa*
1254 *Sunsás/Aguapeí, centro-leste de Rondônia, sudoeste do Amazonian Craton* (Tese de
1255 doutorado). Instituto de Geociências, Universidade de Brasília, Brasília, Brasil.
- 1256 Scandolaro, J. E., Amorim, J. L. de, Rizzotto, G. J., Quadros, M. L. do E. S., Bahia, R. B. C. 1999.
1257 Compartimentação tectono-estratigráfica pré-cambriana de Rondônia: subsídios para os
1258 modelos evolutivos (pp. 282-285). *Resumos do Simpósio de Geologia da Amazônia*, Manaus,
1259 Brasil, 6.
- 1260 Scandolaro, J. E. and Rizzotto, G. J. (Org.). 1998. *Programa Levantamentos Geológicos Básicos*
1261 *do Brasil, Paulo Saldanha Folha SC.20-Z-C-V, Estado de Rondônia: Escala 1:100.000.*
1262 Brasília: CPRM.
- 1263 Shervais, J. W., 1982. Ti–V plots and the petrogenesis of ophiolitic lavas. *Earth and Planetary*
1264 *Science Letters*, 59, 101–118.
- 1265 Silva, C.R.; Bahia, R.B.C.; Silva, L.C. 1992. Geologia da região de Rolim de Moura – sudeste de
1266 Rondônia. In: Congr. Bras. Geol., 37. São Paulo, 1992. Boletim de resumos expandidos. São
1267 Paulo, SBG. 1: 152-153.
- 1268 Tassinari, C. C. G. and Macambira, M. J. B. 1999. Geochronological provinces of the Amazonian
1269 Craton. *Episodes*, 22 (3), 174-182.
- 1270 Teixeira, W., Tassinari, C. C. G., Cordani, U. G., Kawashita, K. 1989. A review of the
1271 geochronology of the Amazonian Craton: tectonic implications. *Precambrian Research*, 42,
1272 213-227.
- 1273 Teixeira, W., Geraldés, M. C., Matos, R., Ruiz, A. S., Saes, G., Vargas-Mattos, G. 2010. A review
1274 of the tectonic evolution of the Sunsás belt, SW Amazonian Craton. *Journal of South*
1275 *American Earth Sciences*, 29, 47–60.
- 1276 Teixeira, W., Hamilton, M.A., Lima, G.A., Ruiz, A.S., Matos, R., Ernst, R.E., 2015. Precise ID-
1277 TIMS U-Pb baddeleyite ages (1110–1112 Ma) for the Rincón del Tigre-Huanchaca large
1278 igneous province (LIP) of the Amazonian Craton: implications for the Rodinia supercontinent.
1279 *Precamb. Res.* 265, 273–285.
- 1280 Tohver, E., Van Der Pluijm, B. A., Mezger, K., Essene, E., Scandolaro, J. E., Rizzotto, G. J. 2004.
1281 Significance of the Nova Brasilândia metasedimentary belt in western Brazil: redefining the
1282 Mesoproterozoic boundary of the Amazon Craton. *Tectonics*, 23(6).
1283 doi:10.1029/2003TC001563.
- 1284 Tohver, E., Van Der Pluijm, B. A., Scandolaro, J. E., Essene, E. 2005a. Late mesoproterozoic
1285 deformation of SW Amazonia (Rondonia, Brazil): geochronological and structural evidence
1286 for collision with Southern Laurentia. *J. Geol.*, 113, 309-323. doi: 10.1086/428807.
- 1287 Tohver, E., Van Der Pluijm, B. A., Mezger, K., Scandolaro, J. E., Essene, E. J. 2005b. Two stage
1288 tectonic history of the SW Amazon craton in the late Mesoproterozoic: identifying a cryptic
1289 suture zone. *Precam. Res.*, 137, 35-59.
- 1290 Tohver, E., Van Der Pluijm, B. A., Van Der Voo, R., Rizzotto, G. J., Scandolaro, J. E. 2002.
1291 Paleogeography of the Amazon Craton at 1.2 Ga: early grenvillian collision with the llano
1292 segment of Laurentia. *Earth and Planetary Science Letters*, 199, 185-200.
- 1293 Tohver, E., Teixeira, W., Van Der Pluijm, B., Geraldés, M., Bettencourt, J. S., Rizzotto, G. J. 2006.
1294 Restored transect across the exhumed Grenville orogen of Laurentia and Amazonia, with
1295 implications for crustal architecture. *Geology*, 34, 669-672.
- 1296 Touret, J. L. R., Santosh, M., Huizenga, J. M. 2016. High-temperature granulites and
1297 supercontinents. *Geoscience Frontiers*, 7, 101-113.
- 1298 Wakabayashi, J., Basu, A., Ghatak, A. 2010. Supra-subduction zone ophiolite generation,
1299 emplacement, and initiation of subduction: A perspective from geochemistry, metamorphism,

1300 geochronology, and regional geology. *Geological Society of America Bulletin*, 122(9/10),
1301 1548–1568. doi: 10.1130/B30017.1.

1302 Watson, S. 1993. Rare earth element inversions and percolation models for Hawaii. *Journal of*
1303 *Petrology*, 34(4), 763-783.

1304 Wood, D. A. 1980. The application of a Th–Hf–Ta diagram to problems of tectonomagmatic
1305 classification and to establishing the nature of crustal contaminations of basaltic lavas of
1306 British tertiary volcanic province. *Earth and Planetary Science Letters*, 56, 11–30.

1307 Xia, L. and Li, X. 2019. Basalt geochemistry as a diagnostic indicator of tectonic setting.
1308 *Gondwana Research*, 65, 43–67. <https://doi.org/10.1016/j.gr.2018.08.006>

1309 Xu, W., Xu, X., Zeng, G. 2017. Crustal contamination versus an enriched mantle source for
1310 intracontinental mafic rocks: Insights from early Paleozoic mafic rocks of the South China
1311 Block. *Lithos*. 286. 10.1016/j.lithos.2017.06.023.

1312 Zindler, A. and Hart, S.R. 1986. Chemical geodynamics. *Ann. Rev. Earth Planet. Sci.*, 14, 493-
1313 571.

5. Discussões e conclusões

Os novos dados geológicos, geoquímicos (rocha total), geocronológicos U-Pb em zircão (LA-ICP-MS) e isotópicos Sr-Nd (rocha total) apresentados nesta tese de doutorado, intitulada “**Geologia, geoquímica e geocronologia das rochas da Suíte Rio Branco, Cinturão Nova Brasilândia e implicações na evolução do orógeno Sunsás no sudoeste do Cráton Amazônico**”, atingiram os objetivos principais propostos inicialmente no plano de pesquisa, tais como a obtenção das idades de máxima sedimentação e do metamorfismo de alto-grau das rochas metassedimentares da Formação Rio Branco, idades de cristalização do magmatismo máfico-félsico da Suíte Rio Branco e idades de *overprint* metamórfico, caracterização da afinidade química e fonte do magmatismo máfico da Suíte Rio Branco e definição do ambiente tectônico. Os dados obtidos nessa pesquisa servem, também, de base científica para estabelecer a cronologia dos estágios ou fases de evolução tectônica mesoproterozoica (esteniana) nas quais as rochas do Cinturão Nova Brasilândia foram submetidas, durante a orogenia Nova Brasilândia (Tabela 1, Fig. 7).

Os dados obtidos proporcionaram a concepção de um novo cenário tectônico alternativo para o Cinturão Nova Brasilândia, envolvendo subducção intraoceânica e colisão de massas cratônicas continentais. Elucidaram também o significado do magmatismo máfico da Suíte Rio Branco na evolução mesoproterozoica do Cinturão Nova Brasilândia e, conseqüentemente, do orógeno Sunsás. As principais discussões e conclusões desta pesquisa constam nos artigos e estão apresentadas de forma resumida nas seções seguintes:

5.1 Fase pré-orogênica (< 1241 Ma)

O cenário tectônico compressivo (margem ativa) envolvendo subducção intraoceânica proposto nesta tese de doutorado contrasta, em parte, do modelo anteriormente definido para o Cinturão Nova Brasilândia envolvendo reativações tectônicas ao longo da zona de sutura Guaporé, abertura e fechamento de *rift* intracontinental e formação de proto-oceano (Rizzotto, 1999; Rizzotto *et al.*, 1999, 2001, 2014). Contrasta parcialmente também do modelo tectônico de colisão e suturamento entre o proto-Cráton Amazônico e o Bloco Paraguá entre 1096 e 1000 Ma (Tohver *et al.*, 2004). Entretanto, as fases *rift*, *rift-drift* e *drift* proposta inicialmente por Rizzotto (1999), envolvendo episódios de transtensão que condicionaram a abertura de *rift* intracontinental, que evoluiu para margem passiva, não é totalmente inviabilizada e continua sendo considerada para explicar a existência de um proto-oceano no Esteniano, muito embora na parte sul do Cinturão Nova Brasilândia os registros geológicos dessa fase não claramente evidenciados. A existência desta fase extensional que proporcionou a abertura de um oceano se torna necessário para que a subsequente

subducção intraoceânica possa ter sido desenvolvida, entretanto, ainda não existem dados e informações geológicas suficientes que possam sugerir a dimensão desse oceano e sua idade precisa, mas provavelmente tratava-se de um oceano relativamente pouco desenvolvido, possivelmente um proto-oceano, em função do curto período de tempo para sua abertura e o fechamento. O curto período de tempo para o desenvolvimento deste oceano e bem evidenciado nas idades U-Pb em zircão provenientes das rochas da parte sul do Cinturão Nova Brasilândia (ver artigo 1, submetido).

Tabela 1. Principais características geológicas e tectônicas do Cinturão Nova Brasilândia no sudoeste do Cráton Amazônico em Rondônia (após Scandolaro e Rizzotto, 1998; Bahia e Silva, 1998; Rizzotto, 1999; Tohver et al., 2004, 2005a; Santos et al., 2008; Rizzotto et al., 2014).

Orógeno	Orogenia	Natureza da orogenia ^{1,2}	Período	Unidade tectônica	Principais características tectônicas	Unidade regional	Magmatismo máfico e félsico na região. Intrusões orogênicas ¹ , pós-orogênicas ² e anorogênicas ³
Sunsás	Nova Brasilândia	Colisional (contemporânea da orogenia Sunsás)	1096-1010 Ma	Cinturão Nova Brasilândia: domínios Migrantinópolis e Rio Branco. No cráton:	Tipo acrecionário-colisional na margem sudoeste do proto-Cráton Amazônico e efeitos de retrabalhamento crustal sobre as áreas do cráton (sistemas e zonas de cisalhamento). Metamorfismo variando de baixo grau (fácies xisto-verde) até alto grau (fácies anfíbolito a granulito). Fase inicial de oceanização. Sistema <i>arc - back-arc</i> na fase acrecionária (subducção)	Cobertura de plataforma pós-colisional: Formação Palmeiral (Vila Palmeiral, serras do Pacaás Novos e Uopianes).	Sills máficos (Nova Floresta ³) associados as coberturas plataformais.
		Acrecionária	1137-1106 Ma	Sistema Tranpressivo Sinistral Ji-Paraná - Cujubim			Magmatismo félsico anorogênico em áreas cratônicas: suítes intrusivas Rondônia ³ (<i>Younger Granites of Rondônia</i>) (0,98-0,95 Ga), Costa Marques ³ (0,98-0,96 Ga) e Santa Clara ³ (1,08–1,07 Ga).
		Fase pré-orogênica (<i>rift, rift-drift e drift</i>): formação de oceano e margem passiva. Fase de oceanização	< 1241 Ma			Coberturas pré-colisionais: Formação Terra boa e Grupo Nova Brasilândia (formações Rio Branco e Migrantinópolis)	Magmatismo orogênico a pós-orogênico no cinturão: Suíte Intrusiva Rio Pardo ² (1,05 Ga), magmatismo máfico-félsico da Suíte Rio Branco ^{1,2} (1,11-1,10 Ga)

No cenário pré-orogenia Nova Brasilândia, a fusão inicial do Bloco Paraguá com o proto-Cráton Amazônico (parte que corresponde a Província Rio Negro-Juruena ou Província Rondônia-Juruena) ocorreu aproximadamente entre 1350 e 1320 Ma, ao final da orogenia Rondôniana-San Ignácio, conforme registros geológicos contidos principalmente nas rochas do Cinturão Alto Guaporé (Scandolaro, 2006; Bettencourt *et al.*, 2010; Rizzotto *et al.*, 2013). Entretanto, a fase pré-orogênica na evolução do Cinturão Nova Brasilândia sugere a existência de um oceano entre aproximadamente 1241 e 1137 Ma, situado entre o proto-Cráton Amazônico e um novo bloco composto pelo Bloco Paraguá, acrescido de terrenos alóctones e faixas móveis (p.ex. embasamento São Felipe e Cinturão Alto Guaporé). Portanto, este oceano Esteniano pode ter sido formado por consequência da quebra de segmento crustal composto pelo Bloco Paraguá, Cinturão Alto Guaporé e parte da Província Rio Negro-Juruena, após sua cratonização inicial ocorrida no Ectasiano (1350 Ma), ao final da orogenia Rondoniana-San Ignácio.

A dinâmica para explicar sucessivas fases de aglutinação e quebra de massas cratônicas envolve a rotação relativa entre a Amazônia e Laurentia, conforme postulado por Johansson (2009).

Essa rotação pode ter proporcionado a formação de *rifts* intracontinentais na borda sudoeste do proto-Cráton Amazônico e blocos adjacentes, que podem ter sido abortados (p. ex. *rift* Aguapeí) ou que evoluíram para formação de oceano (p. ex. Nova Brasilândia) (Tabela 1, Fig. 7).

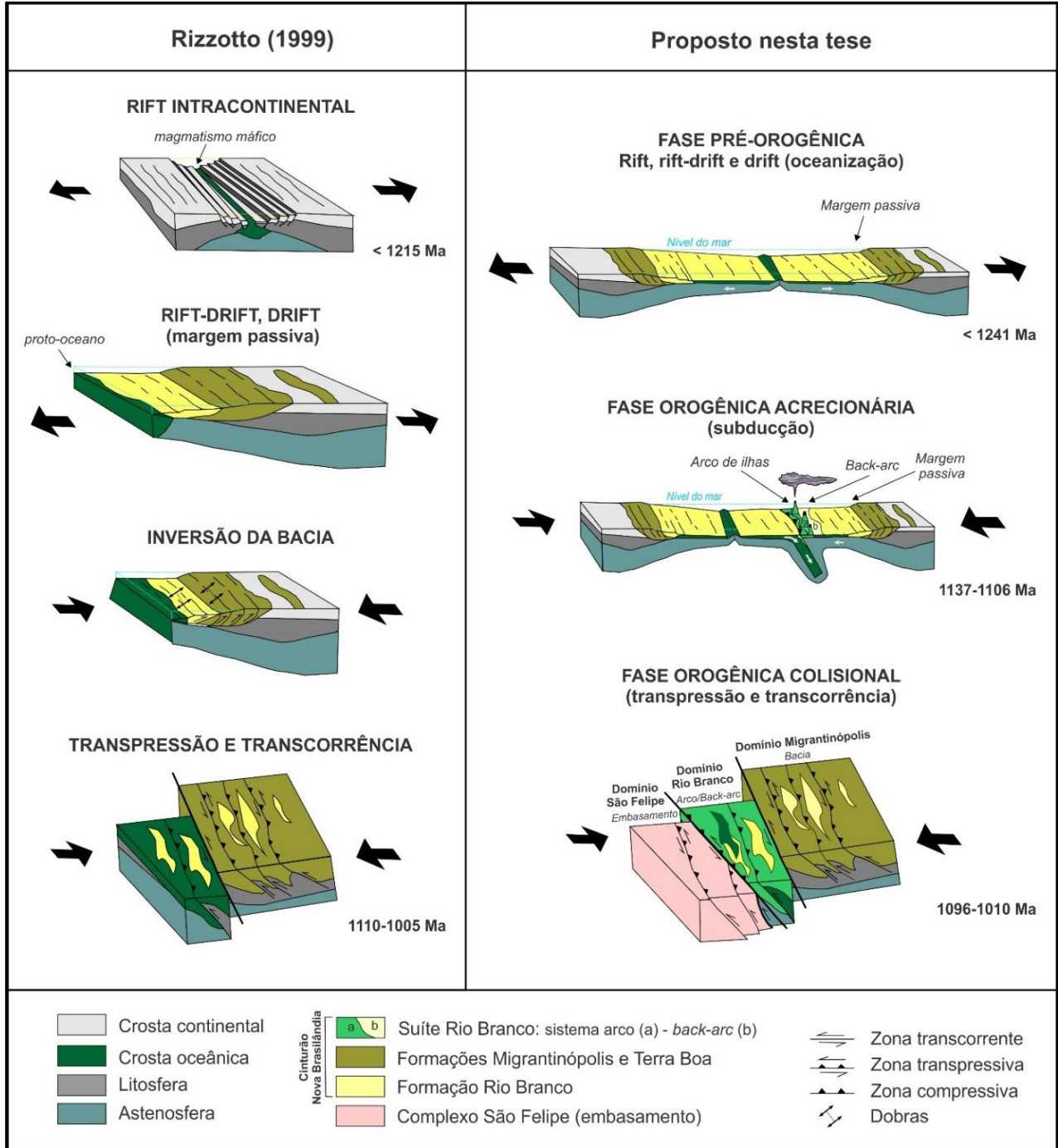


Fig. 7. Quadro comparativo com os cenários de evolução tectônica propostos para o Cinturão Nova Brasilândia, sudoeste do Cráton Amazônico, Rondônia, no Mesoproterozoico (Esteniano).

5.2 Fase orogênica acrecionária (1137-1106 Ma)

A fase acrecionária ocorrida entre 1137 e 1106 Ma, proposta pela primeira vez nesta tese de doutorado e artigos relacionados, corresponde a cenário tectônico compressional que envolve subducção intraoceânica, formação de arco de ilhas e bacias relacionadas a arco (*forearc* ou *back-arc*) (Tabela 1, Fig. 7). Esta proposta alternativa de subducção difere do modelo anteriormente definido para o cinturão de Nova Brasília como produto de reativações intracratônicas, abertura e o fechamento de *rift* intracontinental (Rizzotto, 1999; Rizzotto *et al.*, 1999, 2014). Para explicar o condicionamento de um ambiente tectônico envolvendo subducção, considera-se também as prováveis rotações relativas entre a Amazônia e Laurentia proposta por Johansson (2009) para explicar nova abertura e fechamento de um oceano, envolvendo subducção intraoceânica entre 1137 e 1106 Ma.

O cenário de subducção identificado nas rochas parte sul do Cinturão Nova Brasilândia foi diagnosticado com base nos dados geoquímicos e de isótopos de Sr-Nd. O contexto geológico e geocronológico U-Pb demonstram que o metamorfismo de alto grau (fácies granulito) ocorreu aproximadamente entre 1137 e 1127 Ma e o magmatismo máfico-félsico toleítico de médio a baixo Ti da Suíte Rio Branco foi gerado aproximadamente entre 1119 e 1106 Ma (ver artigo1). Portanto, a constatação de episódios geológicos com idades de metamorfismo de alto grau e de magmatismo máfico muito próximas entre si, aliados as assinaturas geoquímicas e isotópicas Sr-Nd diagnósticas de subducção, são condizentes com ambiente tectônico de *arc – back-arc* e, portanto, reforçam a tese de subducção para explicar a geração das rochas da Suíte Rio Branco (ver artigo 2, submetido).

A história metamórfica do Cinturão Nova Brasilândia é ainda considerada complexa e necessita de estudos adicionais aprofundados para caracterizar, em cada domínio, a trajetória pressão-temperatura (P-T). As condições variadas de P-T foram, inicialmente, estabelecidas com base nas paragêneses de rochas metapelíticas. Rizzotto (1999) identificou condições metamórficas de alta temperatura entre 670°-800°C e baixa pressão em torno de 3.1 Kb. Na parte sul do cinturão, Tohver *et al.* (2004, 2005a) definiram condições de pico em T máxima de 750°C e P máxima de 7,9 kbars para paragêneses granulíticas. Faixas em baixo-grau ocorrem localmente ao longo de zonas de cisalhamento e, principalmente, na parte norte do Cinturão Nova Brasilândia. Estas variadas condições de P-T sugerem justaposição de domínios metamórficos de alta temperatura e baixa pressão (HT/LP) e alta temperatura e alta pressão (HT/HP), locais onde o metamorfismo atingiu condições de fácies anfíbolito superior a granulito, com migmatização do componente metassedimentar, seguido de re-equilíbrios retrometamórficos em baixo grau, reflexos dos processos de subducção, colisão e exumação do orógeno. Processos que necessitam ser avaliados em estudos futuros.

Dados geoquímicos (rocha total) da Suíte Rio Branco revelam que o componente metamáfico apresenta afinidade geoquímica subalcalina toleítica de baixo a médio Ti com sobreposição de assinaturas MORB-like (semelhante com basalto de cadeia meso-oceânica), IAT (toleito de arco de ilhas) e BABB (basalto de bacia *back-arc*) nos diagramas (ver artigo 2). Esses configuram padrões bem definidos de distribuição de elementos traços nos diagramas ETRs normalizados ao Condrito que demonstram leve enriquecimento em LREE em relação a HREE. Nos diagramas multi-elementos (*spidergrams*) normalizados ao Manto Primitivo apresentam enriquecimento LILE em relação a HFSE, enriquecimento em Pb, anomalias negativas de Nb e Ta, anomalias positivas de K e Sr e enriquecimento gradativo de Th em relação ao Nb e Ta, consideradas características diagnósticas de subducção. Além disso, razões Ti/V (entre 10 e 50), La/Yb (entre 1.74 e 12.33), Th/Yb (entre 0.10 e 3.56) e baixas razões Ce/Pb (3.3 e 20.5), Nb/U (3.2 e 16.25) e Th/La (0.01 e 0.30) sugerem e reforçam o cenário de subducção (Kessel et al., 2005; Xu et al., 2017). Nos diagramas discriminantes tectônicos de Wood (1980), Cabanis e Lecolle (1989) e de Pearce (2008) os *trends* petrogenéticos exibidos pelas rochas metamáficas da Suíte Rio Branco são característicos de ambiente de arco, mais específico de arco de ilhas, com algumas amostras sugerindo ambiente de bacia *back-arc*, entretanto, destaca-se que nos diagramas discriminantes tectônicos as amostras da Suíte Rio Branco plotam principalmente em campos específicos e de possível associação à ambiente orogenético compressivo (margem ativa).

Dados isotópicos Sr-Nd (rocha total) foram utilizados na interpretação das fontes do magmatismo máfico e dos processos ocorridos no manto (contaminação ou metassomatismo), levando-se em consideração as limitações dos resultados analíticos inerentes ao método utilizado. Os ϵ_{Nd} das rochas metamáficas da Suíte Rio Branco (recalculados para $t=1120$ Ma) apresentaram valores levemente positivos e negativos entre -2.89 e +1.66, porém próximos do CHUR, e sugerem contaminação crustal ou metassomatismo da cunha mantélica, possivelmente associados a subducção. Composições isotópicas de Sr-Nd das rochas metamáficas da Suíte Rio Branco demonstram que as rochas do Grupo 1 apresentam razões médias de $^{87}\text{Sr}/^{86}\text{Sr}$ entre 0.703 e 0.705 e razões média de $^{143}\text{Nd}/^{144}\text{Nd}$ de 0.512 e do Grupo 2 razões médias a altas de $^{87}\text{Sr}/^{86}\text{Sr}$ entre 0.708 e 0.713 e razões médias de $^{143}\text{Nd}/^{144}\text{Nd}$ de 0.512. Nesses grupos, as variações composicionais de Sr e Nd podem ser associadas a fontes mantélicas mistas (manto depletado ou manto enriquecido) e as altas razões $^{87}\text{Sr}/^{86}\text{Sr}$ indicam contaminação crustal influenciada por fluídos da placa subductante, durante subducção e geração magmática. As rochas metamáficas do Grupo 3 (4 amostras) apresentam baixas razões $^{87}\text{Sr}/^{86}\text{Sr}$, em torno de 0.702, e baixas razões $^{143}\text{Nd}/^{144}\text{Nd}$, em torno de 0.512, e conteúdo muito alto de Sr (1680-1285 ppm) considerado anômalo. Entretanto, estudos adicionais se fazem necessários para avançar no entendimento da origem e evolução das rochas do

Grupo 3, envolvendo fontes e condições específicas de pressão (P) e temperatura (T) durante a subducção e exumação do orógeno.

As características geológicas, geoquímicas e isotópicas das rochas da parte sul do Cinturão Nova Brasilândia, descritas nesta tese de doutorado, foram consideradas efetivas no diagnóstico de ambiente de subducção intraoceânica, com possível formação de arco magmático (arco de ilhas) e bacia relacionada a arco (*back-arc*), que serviram de base para definir uma fase convergente acrecionária entre 1137 e 1106 Ma na evolução do Cinturão Nova Brasilândia. Destacamos, ainda, que as idades U-Pb (zircão) muito próximas entre os episódios de sedimentação, metamorfismo de alto grau e magmatismo máfico-félsico da Suíte Rio Branco serviram, também, de critérios para caracterizar o ambiente orogênico convergente, desenvolvido durante a fase inicial da orogenia Nova Brasilândia.

5.3 Fase orogênica colisional (1096-1010 Ma)

A fase acrecionária da orogenia Nova Brasilândia evoluiu, posteriormente, para fase de colisão continente-continente, entre aproximadamente 1096 e 1010 Ma, quando provavelmente as rochas metamáficas da Suíte Rio Branco foram acrecionadas na borda sudoeste do Cráton Amazônico, durante o suturamento entre um novo bloco (constituído pelo Bloco Paraguá, acrescido de terrenos alóctones e faixas móveis) e o proto-Cráton Amazônico (parte ocidental da Província Rio Negro-Juruena), consolidando assim a formação do Cráton Amazônico em aproximadamente 1.0 Ga (Tabela 1, Fig. 7). A deformação e o metamorfismo impresso nas rochas metamáficas da Suíte Rio Branco que ocorreu posteriormente entre 1096 e 1010 Ma, pode ser o reflexo da fase colisional continente-continente. Esta fase representa as atividades orogênicas finais que culminaram com aglutinação de massas cratônicas (Laurentia e Amazônia e demais blocos, fragmentos de blocos e terrenos alóctones) para formar o Supercontinente Rodínia (Rizzotto, 1999; Rizzotto *et al.*, 1999, 2014; Tohver *et al.*, 2002, 2004, 2005b).

A fase colisional da orogenia Nova Brasilândia está consolidada na literatura geológica da região em diversas pesquisas (Rizzotto, 1999; Tohver *et al.*, 2002, 2004, 2005b). Essa foi levada em consideração na tentativa de explicar as idades U-Pb em zircão (LA-ICP-MS) de *overprint* metamórfico encontradas nas rochas paraderivadas e produtos anatéticos (Formação Rio Branco) e em ortoderivadas metamáficas (Suíte Rio Branco) da parte sul do cinturão, as quais coincidem com dados geocronológicos publicados anteriormente. As idades U-Pb (zircão) obtidas foram ainda analisadas em conjunto com as idades U-Pb de trabalhos anteriores (Rizzotto, 1999; Tohver *et al.*, 2004, 2005a; Santos *et al.*, 2008; Rizzotto *et al.*, 2014), com a finalidade de reforçar a interpretação de que as rochas do Domínio Rio Branco foram afetadas por um segundo episódio mais jovem de deformação e metamorfismo entre 1096 ± 5 Ma e $1011,3 \pm 9,6$ Ma, sobreposto ao pulso metamórfico

de alto grau mais antigo entre 1137 ± 9 Ma e $1127,6 \pm 2,3$ Ma (ver artigo 1). Portanto, optamos em sugerir que o metamorfismo mais jovem registrado no cinturão pode estar associado à fase colisional da orogenia Nova Brasilândia (Tabela 1, Fig. 7), onde o magmatismo félsico da Suíte Rio Pardo em cerca de 1005 ± 41 Ma registra o início do estágio pós-tectônico desta segunda fase evolutiva do cinturão. Nesta fase, houve a justaposição tectônica de blocos representados pelos domínios Migrantinópolis, Rio Branco e São Felipe (Figs. 3, 7).

Esse novo cenário tectônico alternativo envolvendo subducção e geração de arco magmático e bacia *back-arc*, seguido de colisão, espessamento crustal, exumação e resfriamento do orógeno caracteriza a orogenia Nova Brasilândia no sudoeste do Cráton Amazônico como do tipo acrecionária-colisional, desenvolvida entre aproximadamente 1137 e 1010 Ma (Fig. 7).

Finalizando, destacamos ainda que os dados obtidos nesta pesquisa fornecem importantes informações petrogenéticas e geocronológicas que permitem um grande avanço na definição do ambiente tectônico de geração das rochas da Suíte Rio Branco, com implicações significativas no entendimento da evolução geotectônica do Cinturão Nova Brasilândia no sudoeste do Cráton Amazônico, bem como no estabelecimento de correlações geológicas com a Província Grenville. Os produtos publicados desta pesquisa (artigos e volume da tese) servem de fonte de informações geocientíficas para o aperfeiçoamento dos cenários globais de montagem do supercontinente Rodínia.

Referências bibliográficas da Tese

- Allègre, C.J., Othman, D.B. 1980 Nd-Sr isotopic relationship in granitoid rocks and continental crust development: A chemical approach to orogenesis. *Nature* 286:335-342.
- Amaral, G. 1974. *Geologia Pré-Cambriana da Região Amazônica*. 1974. 212p. Tese (Livre Docência) - Instituto de Geociências, Universidade de São Paulo, São Paulo, 1974.
- Anders, E. e Ebihara, M. 1982. Solar-system abundances of the elements, *Geochimica et Cosmochimica Acta*, 46, p. 2363-2380, [https://doi.org/10.1016/0016-7037\(82\)90208-3](https://doi.org/10.1016/0016-7037(82)90208-3).
- Bahia, R.B.C., Silva, C.R. da. (Orgs.). 1998. Rio Pardo Folha SC.20-Z-C-VI, Estado de Rondônia. Brasília: CPRM, 1998. Escala 1:100.000. Programa levantamentos geológicos básicos do Brasil. Convênio DNPM/CPRM.
- Bergami, G.N., Prado, E.M.G, Souza, A.A de, Oliveira, C.E.S., Guerra, G.I.T., Silva, G.F. da, Corrêa, L.W.C., Silva, L.C. da; Quadros, M.L. do E.S., Graça, M.C., Adôrno, R.R., Rodrigues, T.R., Ribeiro, T. de J., Oliveira Neto, W.L. de, Silva, D.R.V. da. 2018. Mapa geológico integrado da ARIM Nova Brasilândia. Porto Velho: CPRM, 2018. Escala 1:150.000. (Projeto Evolução Crustal e Metalogenia da Faixa Nova Brasilândia).
- Bettencourt, J.S., Leite Júnior, W.B., Payolla, B.L., Scandolaro, J.E., Muzzolon, R., Vian, J.A.A.J. 1997. The rapakivi granites of the Rondônia Tin province, northern Brazil. In: *INTERNATIONAL SYMPOSIUM ON GRANITES AND ASSOCIATED MINERALIZATIONS*, 2. Salvador. Excursions Guide. Salvador: CBPM/SGM, 1997. p. 3-31.
- Bettencourt, J.S., Tosdal, R.M., Leite Júnior, W.B., Payolla, B.L. 1999. Mesoproterozoic rapakivi granites of the Rondônia Tin province, southwestern border of the Amazonian Craton, Brazil-I: reconnaissance U-Pb geochronology and regional implications. *Precambrian Research*, v. 95, p. 41-67, 1999.
- Bettencourt, J.S., Leite Jr., W.B., Ruiz, A.S., Matos, R., Payolla, B. L., Tosdal, R.M. 2010. The Rondonian-San Ignacio Province in the SW Amazonian Craton: An overview. *J. South. Am. Ear. Sci.* 29: 28-46.
- Boger, S.D., Raetz, M., Giles, D., Etchart, E., Fanning, C.M. 2005. U-Pb age data from the Sunsás region of eastern Bolivia, evidence for the allochthonous origin of the Paraguá Block. *Precam. Res.* 139: 121-146.
- Boynton, W.V. 1984. *Geochemistry of Rare Earth Elements: Meteorite Studies*. In: Henderson, P., Ed., *Rare Earth Element Geochemistry*, Elsevier, New York, 63-114. <http://dx.doi.org/10.1016/B978-0-444-42148-7.50008-3>
- Bühn, B., Pimentel, M. M., Matteini, M., Dantas, E. L. 2009. High spatial resolution analysis of Pb and U isotopes for geochronology by laser ablation multi-collector inductively coupled plasma spectroetry (L-C-ICPMS). *An. Acad. Bras. Cienc.*, 81, 99-114.
- Cabanis, B., e Lecolle, M. 1989. Le diagramme La/10–Y/15–Nb/8: Unoutil pour la discrimination des series volcaniques et la mise en evidence des processus de mélange et/ou de contamination crustale. *Comptes Rendus de l'Académie des Sciences-Series II*, 309, 2023–2029.

- Casquet, C., Pankhurs, R.J., Fanning, M., Baldo, E., Galindo, C., Rapela, C.W., González-Casado, J.M., Dahlquist, J.A. 2006. U-Pb SHRIMP zircon dating of Grenvillian metamorphism in Western Sierras Pampeanas (Argentina): correlation with the Arequipa-Antofalla Craton and constraints on the extent of the Precordillera Terrane. *Gond Res* 9(4): 524-529.
- Casquet, C., Pankhurst, R.J., Rapela, C.W., Galindo, C., Fanning, C.M, Chiaradia, M., Baldo, E., González-Casado, J.M., Dahlquist, J.A. 2008. The Mesoproterozoic Maz terrane in the Western Sierras Pampeanas, Argentina, equivalent to the Arequipa–Antofalla block of southern Peru? Implications for West Gondwana margin evolution. *Gondwana Research*. 13. 163-175. 10.1016/j.gr.2007.04.005.
- Cawood, P. A. Pisarevsky, S. A. 2017. Laurentia-Baltica-Azonian relations during Rodinia assembly. *Precambrian Research*. doi: <http://dx.doi.org/10.1016/j.precamres.2017.01.031>.
- Chen, W. T., Sun, W., Wang, W. Zhao, J., Zhou, M. 2014. “Grenvillian” intra-plate mafic magmatism in the southwestern Yangtze Block, SW China. *Precambrian Research*, 242. 138–153.
- Costa, J.B.S., Hasuy, Y.H. 1997. Evolução Geológica da Amazônia. In: Costa, M.L.C. da, Angélica, R.S. (Coords.). *Contribuições à Geologia da Amazônia*: FINEP/SBG-NO, Belém-PA. p. 15-90.
- Cordani, U.G., Teixeira, W., 2007. Proterozoic accretionary belts in the Amazonian Craton. In: Hatcher Jr., R.D., Carlson, M.P., McBride, J.H., Martinez Catalán, J.R. (Org.), *The 4D Framework of Continental Crust*. GSA Memoir. Boulder, Colorado: Geological Society of America Book Editors 200, 297–320.
- Cordani, U.G., Tassinari, C.C.G., Teixeira, W., Basei, M.A.S., Kawashita, K. 1979 Evolução tectônica da Amazônia com base nos dados geocronológicos. In: *Congresso Geológico Chileno*, 2, Arica. Actas. [s.n.]. p. 137-148
- Cordani, U.G., Sato, K., Teixeira, W., Tassinari, C.G., Basei, M.A. 2000. Crustal Evolution of the South American Platform. In: Cordani UG, Milani EJ, Thomaz Filho A and Campos DA (Eds.), *Tectonic Evolution of South America, 31st. International Geological Congress*, Rio de Janeiro, Brazil, p. 19-40.
- Costa, J.B.S. e Hasui, Y. 1991. O quadro geral da evolução tectônica da Amazônia. In: *Simpósio Nacional de Estudos Tectônicos*, 3, 1991, Rio Claro. Anais. Rio Claro: SBG-Núcleo de São Paulo, 1991. p. 142-145.
- Cox, K. G., Bell, J. D., Pankhurst, R. J. 1979. *The Interpretation of Igneous Rocks*. London: George Allen & Unwin.
- CPRM - Serviço Geológico do Brasil, 2014. Projeto Aerogeofísico Sudoeste de Rondônia–Relatório Final do Levantamento e Processamento de dados magnéticos e gamaespectrométricos. Rio de Janeiro: Lasa Engenharia e Prospecções; Prospectores Aerolevantamentos e Sistemas. 27v.
- D'Agrella-Filho, M.S., Trindade, R.I.F., Elming, S.-Å., Teixeira, W., Yokoyama, E., Tohver, E., Geraldés, M.C., Pacca, I.I.G., Silva, J.A., Barros, M.A.S., Ruiz, A.S., 2012. The 1420 Ma Indiavaí Mafic Intrusion (SW Amazonian Craton): Paleomagnetic results and implications for the Columbia Supercontinent. *Gondwana Res*. 22, 956–973.

- DePaolo, D.J. 1981 Nd isotopic studies: Some new perspective on Earth structure and evolution. *Eos* 6(14):137-140.
- Dey, A., Hussain, M. F., Barman, M. N. 2018. Geochemical characteristics of mafic and ultramafic rocks from the Naga Hills Ophiolite, India: implications for petrogenesis. *Geoscience Frontiers*, 9, 517-529.
- Dilek, Y., Furnes, H. 2011. Ophiolite genesis and global tectonics: geochemical and tectonic fingerprinting of ancient oceanic lithosphere. *GSA Bulletin*, 123(3/4), 387–411. doi: 10.1130/B30446.10.
- Elming, S.A., D'Agrella-Filho, M.S., Page, L.M., Tohver, E., Trindade, R.I.F., Pacca, I.I.G., Geraldes, M.C., Teixeira, W., 2009. A paleomagnetic and $^{40}\text{Ar}/^{39}\text{Ar}$ study of Late Precambrian sills in the SW part of the Amazonian Craton. *Geophysical Journal International* (1), 106–122. doi:10.1111/j.1365-246X.2009.04149.
- Faure, G., Powell, J.L. 1972. *Strontium Isotope Geology*. Springer-Verlag, New York, 188 p.
- Faure, G. 1986. *Principles of Isotope Geology*, 2nd, New York. 589 pp.
- Geraldes, M.C., Van Schmus, W.R., Condie, K.C., Bell, S., Teixeira, W., Babinski, M. 2001. Proterozoic Geologic Evolution of the SW Part of the Amazonian craton in Mato Grosso State, Brazil. *Precambrian Research* 111, 91-108.
- Geraldes, M.C. 2010. Introdução à Geocronologia. 1ªed. São Paulo: Sociedade Brasileira de Geociências, 146p.
- Hasui, Y., Haralyi, N.L.E., Schobbenhaus, C. 1984. Elementos geofísicos e geológicos da Região Amazônica: subsídios para o modelo geotectônico. In: *Symposium Amazonico*, 2, 1884, Manaus. Anais. Manaus: DNPM, p. 129-147.
- Isotta, C.A.L., Carneiro, J.M., Kato, H.T., Barros, R.J.L. 1978. Projeto província estanífera de Rondônia. Relatório final. Porto Velho: CPRM, 1978. 16 v., il. (Convênio DNPM/CPRM).
- Irvine, T. N., Baragar, W. R. A. 1971. A guide to the chemical classification of the common volcanic rocks. *Canadian Journal of Earth Sciences*, 8(5), 523-548.
- Jackson, S., Pearson, N. J., Griffin, W. L., Belousova, E. A. 2004. The application of laser ablation-inductively coupled plasma-mass spectrometry to in situ U–Pb zircon geochronology. *Chem. Geol.*, 211, 47-69.
- Kessel, R., Schmidt, M.W., Ulmer, P., Pettke, T., 2005. Trace element signature of subduction-zone fluids, melts and supercritical liquids at 120–180 km depth. *Nature* 437, 724-727.
- Kloosterman, J.B. 1968. Uma província do tipo nigeriano no sul da Amazônia. *Mineração e Metalurgia*, v. 47, n.278, p. 59-64.
- Kroner, A., Cordani, U. 2003. African, southern Indian and South American cratons were not part of the Rodinia supercontinent: evidence from field relationships and geochronology. *Tectonophysics*, 375, 325–352

- Kroonenberg, S.B. 1982. A Grenvillian granulite belt in the Colombian Andes and its relation to the Guiana Shield. *Geologie en Mijnbouw*, v. 61, p. 325-333, 1982.
- Lacerda filho, J.V., Abreu, W., Valente, C.R., Oliveira, C.C., Albuquerque, M.C. de. 2004. Geologia e recursos minerais do Estado de Mato Grosso: texto explicativo dos mapas geológico e de recursos minerais do Estado de Mato Grosso. Escala 1:1.000.000. Cuiabá: CPRM. 235 p. Programa Geologia do Brasil.
- Li, Z. X., Bogdanova, S. V., Collins, A. S., Davidson, A., De Waele, B., Ernst, R. E., Fitzsimons, I. C. W., Fuck, R. A., Gladkochub, D. P., Jacobs, J., Karlstrom, K. E., Lu, S., Natapov, L. M., Pease, V., Pisarevsky, S. A., Thrane, K., Vernikovsky, V. 2008. Assembly, configuration, and break-up history of Rodinia: a synthesis. *Precam. Res.* 160, 179-210.
- Litherland, M., Annells, R. N., Appleton, J. D., Berrange, J. P., Bloomfield, K., Burton, C. C. J., Darbyshire, D. P. F., Fletcher, C. J. N., Hawkins, M. P., Klinck, B. A., Llands, A., Mitchell, W. I., O'Connor, E. A., Pitfield, P. E. J., Power, G., Weeb. B. C. 1986. *The Geology and Mineral Resources of the Bolivian Precambrian Shield*. London: Brit. Geol. Surv. 153p. (Overseas Memoir 9).
- Litherland, M., Bloomfield, K. 1981. The Proterozoic History of Eastern Bolivia. *Precambrian Res.*, 15, 157-179.
- Lobato, F.P.N.S., Appel, L.E., Godoy, M.C.F.T., Ritter, J.E. 1966. Pesquisa de cassiterita no território federal de Rondônia. Relatório final. Rio de Janeiro: DNPM/DFPM, 1966. 209 p. (Boletim, 125).
- Loewy, S., Connelly, J.N., Dalziel, I.W. 2004. An orphaned basement block: the Arequipa-Antofalla Basement of the central Andean margin of South America. *Geol Soc Am Bull* 116: 171-187.
- Loewy, S., Connelly, J.N., Dalziel, I.W., Gower, C.F. 2003. Eastern Laurentia in Rodinia: Constraints from wholerock Pb and U-Pb geochronology, In: Sircombe, K.N. and McElhinny, M.W. (Eds.), *Orogenic belts, regional and global tectonics: A memorial volume to Chris McAulay Powell: Tectonophysics* 375: 169-197.
- Ludwig, K. R. 2003. User's manual for Isoplot 3.00. Berkeley Geochronology Center, 4, pp. 74.
- Ludwig, K.R. 2008. User's manual for Isoplot 3.70 - A geochronological toolkit for Microsoft® Excel. Berkeley Geochronological Center Special Publication 4, pp. 76.
- McDonough W. F., Sun S. 1995. "The composition of the Earth". *Chemical Geology* 120, p. 223-253.
- McLelland, J.M., Selleck, B.W., Bickford, M.E. 2010. Review of the Proterozoic evolution of the Grenville Province, its Adirondack outlier, and the Mesoproterozoic inliers of the Appalachians. In: Tollo, R.P., Bartholomew, M.J., Hibbard, J.P., and Karabinos, P.M., eds., *From Rodinia to Pangea: The Lithotectonic Record of the Appalachian Region: Geological Society of America Memoir* 206, p. 1-29, doi: 10.1130/2010.1206(02).
- Oliveira, I.L. 2015. Isótopos de Nd e Sr em minerais de diferentes séries petrogenéticas nos complexos alcalino-carbonatíticos de Salitre e Catalão I, 240 f., il. Dissertação (Mestrado em Geologia) - Universidade de Brasília, Brasília, 2015.

- Payolla, B.L., Bettencourt, J.S., Kozuch, M., Leite Júnior, W.B., Fetter, A., Van Schmus, W.R. 2002. Geological evolution of the basement rocks in the east-central part of the Rondônia Tin province, SW Amazonian Craton, Brazil: U-Pb and Sm-Nd isotopic constraints. *Precambrian Research*, v. 119, p. 141-169.
- Pearce, J. A. 1982. Trace element characteristics of lavas from destructive plate boundaries. In Thorps, R. S. (Ed.), *Andesites* (pp. 525–548). New York: John Wiley and Sons.
- Pearce, J. A. 2008. Geochemical fingerprinting of oceanic basalts with applications to ophiolite classification and the search for Archean oceanic crust. *Lithos*, 100, 14–48.
- Pearce, J.A., Lippard, S. J., Roberts, S. 1984. Characteristics and tectonic significance of supra-subduction zone ophiolites. Geological Society, London, Special Publications, 16, p. 77-94 (doi.org/10.1144/GSL.SP.1984.016.01.06).
- Pinto Filho, F. P., Freitas, A. F. de, Melo, C. F., Romanini, S. J. 1977. *Projeto Sudeste de Rondônia: Relatório Final* (Vol. 4). Porto Velho: CPRM.
- Priem, H. N. A., Bon, E. H., Verdumen, E. A. Th., Bettencourt, J. S. 1989. Rb-Sr chronology of Precambrian crustal evolution in Rondonia (Western margin Brazilian Craton). *Journal of South American Earth Sciences*, 2, 163-170.
- Quadros, M. L. do E. S., Rizzotto, G. J. (Orgs.). 2007. *Geologia e recursos minerais do Estado de Rondônia: texto explicativo do mapa geológico e de recursos minerais do Estado de Rondônia* (pp. 116). Escala 1:1.000.000. Porto Velho: CPRM.
- Quadros, M. L. do E.S., Palmeira, L. C., Castro, C. C. 2011. Geologia e Recursos Minerais da Folha Rio Machadinho: SC.20-X-C, escala 1:250.000 (pp. 203). Porto Velho: CPRM.
- Quadros, M.L.E.S., Palmeira, L.C.M., Souza, A.A., Costa, M.A.C. 2014. Sistema Transpressivo Sinistral Ji-Paraná –Cujubim, sudoeste do Cráton Amazônico, Rondônia. *Cong. Bras. Geol.*, 47, Anais, Salvador, 1831p.
- Rivers, T. 2008. Assembly and preservation of lower, mid, and upper orogenic crust in the Grenville Province - Implications for the evolution of large hot long-duration orogens, *Precambrian Research*, 167, p. 237-259 (doi.org/10.1016/j.precamres.2008.08.005).
- Rizzotto, G. J. 1999. *Petrologia e Geotectônica do Grupo Nova Brasilândia: Rondônia* (Dissertação de mestrado). Federal University of Rio Grande do Sul, Porto Alegre, Brazil.
- Rizzotto, G. J. 2001. Reavaliação do Ciclo Orogênico Sunsás/Aguapeí no Sudoeste do Amazonian Craton. *Abstracts Workshop on Geology of the SW Amazonian Craton: state of the art, IGC Project 426* (pp. 66-67).
- Rizzotto, G.J., Bettencourt, J.S., Teixeira, W., Pacca, I.I.G., D'Agrella-Filho, M.S., Vasconcelos, P., Basei, M.A.S., Onoe, A.T., Passarelli, C.R. 2002. Geologia e geocronologia da Suíte Metamórfica Colorado e suas encaixantes, SE de Rondônia: implicações para a evolução mesoproterozóica do SW do Cráton Amazônico. *Geologia USP - Serie Científica*. 2. 41-55.
- Rizzotto, G.J., Oliveira, J.G.F. de, Quadros, M.L. do E.S., Castro, J.M.R. de, Cordeiro, A.V., Adamy, A., Dantas, M.E., Melo Junior, H.R. de. 2005a. Projeto Rio Madeira: estudo de

- viabilidade para implantação de usinas hidrelétricas no rio Madeira. Relatório parcial AHE Jirau. Porto Velho: CPRM. 1 CD-ROM.
- Rizzotto, G.J., Oliveira, J.G.F. de, Quadros, M.L. do E.S., Castro, J.M.R. de, Cordeiro, A.V., Adamy, A., Dantas, M.E., Melo Junior, H.R. de. 2005b. Projeto Rio Madeira: estudo de viabilidade para implantação de usinas hidrelétricas no rio Madeira. Relatório parcial AHE Santo Antonio. Porto Velho: CPRM. 1 CD-ROM.
- Rizzotto, G. J., Hartmann, L. A. 2012. Geological and geochemical evolution of the Trincheira Complex, a Mesoproterozoic ophiolite in the southwestern Amazon craton, Brazil. *Lithos*, 148, 277-295.
- Rizzotto, G. J., Lima, E. F., Chemale Jr., F. 1999. Geologia e geoquímica das rochas metabásicas da sequência metavulcano-sedimentar Nova Brasilândia – sudoeste de RO. *Revista Brasileira de Geociências*, 29(2), 119-128.
- Rizzotto, G. J., Lima, E. F., Chemale Jr., F. 2001. Geologia do Grupo Nova Brasilândia, sudeste de Rondônia, acreção continental e implicações geotectônicas. In Reis, N. J., Monteiro, M. A. S. (Coord.). *Contribuições à Geologia da Amazônia*, 2, 342–442.
- Rizzotto, G.J., Quadros, M.L. do E.S., Bahia, R.B.C., Cordeiro, A.V. 2004. Folha SC.20-Porto Velho. In: Schobbenhaus, C., Gonçalves, J.H., Santos, J.O.S., Abram, M.B., Leão Neto, R., Matos, M.M., Vidotti, R.M., Ramos, M.A.B., Jesus, J.D.A. de (Ed.). Carta geológica do Brasil ao milionésimo. Sistema de informações geográficas (SIG). Programa Geologia do Brasil. Brasília: CPRM, 2004a. 1 CD-ROM.
- Rizzotto, G. J., Santos, J. O. S., Hartmann, L. A., Tohver, E., Pimentel, M. M., Mcnaughton, N. J. 2013. The Mesoproterozoic Guaporé suture in the SW Amazonian craton: geotectonic implications based on field geology, zircon geochronology and Nd-Sr isotopic geochemistry. *J South Am Ear Sci* 48, 271-295.
- Rizzotto, G. J., Hartmann, L. A., Santos, J. O. S., Mcnaughton, N. J. 2014. Tectonic evolution of the southern margin of the Amazonian craton in the late Mesoproterozoic based on field relationships and zircon U-Pb geochronology. *Anais da Academia Brasileira de Ciências*, 86 (1), 57-84.
- Rogers, J.J., Santosh, M. 2003. Supercontinents in Earth history. *Gond. Res.*, 6: 357-368.
- Romanini, S.J. 2000. Geologia e prospecção geoquímica/aluvionar da área Corumbiara/Chupinguaia-Rondônia. Porto Alegre: CPRM, 2000a. (Informe de Recursos Minerais. Série Metais do Grupo da Platina e Associados, 06).
- Ruiz, A.S. 2005. Evolução geológica do sudoeste do Cráton Amazônico, região limítrofe Brasil-Bolívia, Mato Grosso. PhD Thesis, Universidade Estadual Paulista, Rio Claro, São Paulo, Brasil. (Unpublished).
- Ruiz, A.S., Simões, L.S., Araújo, L.M., Godoy, A.M., Matos, J.B., Souza, M.Z. 2007. Cinturão Orogênico Aguapeí (1025-900 Ma): Um exemplo de Faixa Móvel Intracontinental no SW do Cráton Amazônico. In: *XI Simpósio Nacional de Estudos Tectônicos*, Natal. Anais, p. 116-118.
- Sadowski, G.R., Bettencourt, J.S. 1996. Mesoproterozoic tectonic correlations between eastern Laurentia and western border of the Amazon Craton. *Precam. Res.* 76: 213-227.

- Saccani, E., Allahyari, K., Beccaluva, L., Bianchini, G. 2013. Geochemistry and petrology of the Kermanshah ophiolites (Iran): Implication for the interaction between passive rifting, oceanic accretion, and OIB-type components in the Southern Neo-Tethys Ocean. *Gondwana Research* 24. p. 392–411 (dx.doi.org/10.1016/j.gr.2012.10.009).
- Saccani, E., Allahyari, K., Rahimzadeh, B. 2014. Petrology and geochemistry of mafic magmatic rocks from the Sarve-Abad ophiolites (Kurdistan region, Iran): Evidence for interaction between MORB-type asthenosphere and OIB-type components in the southern Neo-Tethys Ocean. *Tectonophysics*, 621.
- Santos, J.O.S., 2004. Geotectônica dos escudos das Guianas e Brasil-Central. In: Bizzi, L.A., Schobbenhaus, C., Vidotti, R.M., Gonçalves, J.H., (Coord.). *Geologia, Tectônica e Recursos Minerais do Brasil*. CPRM, Brasília, 2004.
- Santos, J.O., Hartmann, L.A., Gaudette, H.E., Groves, D.I., McNaughton, N.J., Fletcher, I.R. 2000. A new understanding of the provinces of the Amazon Craton based on integration of field mapping and U-Pb and Sm-Nd geochronology. *Gond Res* 3: 453-488.
- Santos, J.O.S., Rizzotto, G.J., Hartmann, L.A., McNaughton, N.J., Fletcher, I.R. 2001. Ages sedimentary basins related to the Sunsás and Juruena orogenies, southwest Amazon craton established by zircon U-Pb geochronology. In: *Workshop on Geology of the SW Amazonian Craton: State-of-the-art*, São Paulo. Extended Abstracts. São Paulo: Institute of Geosciences. University of São Paulo, p. 114-118.
- Santos, J.O., Rizzotto, G.J., Easton, M.R., Potter, P.E., Hartmann, L.A., McNaughton, N.J. 2002. The Sunsás Orogen in Western Amazon Craton, South America and correlation with the Grenville Orogen of Laurentia, based on U-Pb isotopic study of detrital and igneous zircons. In: *Geological Society of America, 2002 Denver Annual Meeting (October 27-30, 2002)*, *Precam. Geol.*, p. 122-128.
- Santos, J.O.S., Rizzotto, G.J., Chemale, F., Hartmann, L.A., Quadros, M.L. do E.S., McNaughton, N.J. 2003. Três orogêneses colisionais do Sudoeste do Cráton Amazonas: evidências com base em geocronologia U-Pb. In: *Simpósio Brasileiro de Geologia do Centro-Oeste*, 8, 2003, Cuiabá. Boletim de Resumos. Cuiabá: SBG-Núcleo Centro-Oeste. 211p. p.85-88.
- Santos, J.O., Rizzotto, G.J., Potter, P., McNaughton, N., Matos, R., Hartmann, L.A., Chemale, J.R., Quadros, M.L. 2008. Age and autochthonous evolution of the Sunsás Orogen in West Amazon Craton based on mapping and U Pb geochronology. *Precam Res* 165: 120-152. *An Acad Bras Cienc* (2014) 86 (1).
- Sato, K., Tassinari, C.C.G. 1997. Principais eventos de acreção continental no Cráton Amazônico baseados em idade-modelo Sm-Nd, calculada em evolução de estágio único e estágio duplo. In: *Contribuições à Geologia da Amazônia*. FINEP/SBG/Núcleo Norte. Belém, 91-142.
- Scandolara, J.E. 2006. Geologia e evolução do terreno Jamari, embasamento da faixa Sunsás/Aguapeí, centro-leste de Rondônia, sudoeste do Cráton Amazônico. 2006. 383p. Tese (Doutorado em Geologia Regional) - Instituto de Geociências, Universidade de Brasília, Brasília, 2006.

- Scandolara, J.E., Rizzotto, G.J. (Orgs.). 1998. Programa Levantamentos Geológicos Básicos do Brasil. Paulo Saldanha Folha SC.20-Z-C-V. Estado de Rondônia. Escala 1:100.000. Brasília: CPRM, 1998. 105p. il.
- Scandolara, J.E., Rizzotto, G.J., Bahia, R.B.C., Quadros, M.L. do E.S., Silva, C.R. da, Amorim, J.L. de. 1999. Mapa geológico do Estado de Rondônia. Escala 1:1.000.000. Porto Velho: CPRM, 1999.
- Shervais, J. W. 1982. Ti–V plots and the petrogenesis of ophiolitic lavas. *Earth and Planetary Science Letters*, 59, 101–118.
- Sparrenberger, I., Bettencourt, J.S., Tosdal, R.M., Wooden, J.L. 2002. Datações U-Pb convencionais versus SHRIMP do maciço estanífero Santa Bárbara, suíte Granitos Últimos de Rondônia, Brasil. *Geologia USP, Série Científica*, v. 2, p. 79-94.
- Stacey, J. S, and Kramers, Jan. 1975. Approximation of Terrestrial Lead Isotope Evolution by a 2-Stage Model. *Earth and Planetary Science Letters*, 26(2), 207-221. [https://doi.org/10.1016/0012-821X\(75\)90088-6](https://doi.org/10.1016/0012-821X(75)90088-6).
- Tassinari, C.C.G. A porção ocidental do Cráton Amazônico: evidências isotópicas de acreção continental no Proterozóico médio. In: SYMPOSIUM AMAZONICO, 2., 1984, Manaus. Atas... Manaus: DNPM, 1984. p. 439-446.
- Tassinari, C.C.G., Cordani, U.G., Nutman, A.P., Van Schmus, W.R., Bettencourt, J.S., Taylor, P.N., 1996. Geochronological systematics on basement rocks from the Rio Negro-Juruena Province (Amazonian Craton) and tectonic implications. *Int. Geol. Rev.* 38, 161–175.
- Tassinari, C.C.G., Macambira, M.J.B. 1999. Geo-chronological provinces of the Amazonian Craton. *Episodes*, v.22, n.3, p.174-182.
- Tassinari, C.C.G., Macambira, M.J.B., 2004. A evolução tectônica do Craton Amazônico. In: Mantesso-Neto, V., Bartorelli, A., Carneiro, C.R., Brito-Neves, B.B. (Eds.), *Geologia do Continente Sul-Americano*, vol. XXVIII, Beca, São Paulo, Brazil, pp. 471–485.
- Teixeira, W., Bettencourt, J.S., Girardi, V.A.V., Onoe, A.T., Sato, K., 2006. Mesoproterozoic mantle heterogeneity in SW Amazonian Craton: $^{40}\text{Ar}/^{39}\text{Ar}$ and Nd–Sr evidence from mafic–felsic rocks. In: Hansji, E., Mertanen, S., Rämö, T., Vuollo, J. (Orgs.), *Dyke Swarms – Time Markers of Crustal Evolution. Proceedings of the V International Dyke Conference, 2005*, vol. 1, Taylor and Francis Group, London, pp. 113–129.
- Teixeira, W., Geraldes, M.C., Matos, R., Ruiz, A.S., SAES, G., Vargas-Mattos, G. 2010. A review of the tectonic evolution of the Sunsás belt, SW Amazonian Craton. *Journ of South Am Earth Sci* 29(1): 47-60.
- Teixeira, W., Hamilton, M.A., Lima, G.A., Ruiz, A.S., Matos, R., Ernst, R.E., 2015. Precise ID-TIMS U-Pb baddeleyite ages (1110–1112 Ma) for the Rincón del Tigre-Huanchaca large igneous province (LIP) of the Amazonian Craton: implications for the Rodinia supercontinent. *Precamb. Res.* 265, 273–285.
- Teixeira, W., Hamilton, M. A., Girardi, V. A. V., Faleiros, F. M., Emst, R. E. 2018. U-Pb baddeleyite ages of key dyke swarms in the Amazonian Craton (Carajás/Rio Maria and Rio

- Apa areas): tectonic implications for events at 1880, 1110 Ma, 535 Ma and 200 Ma. *Precambrian Research*. doi:10.1016/j.precamres.2018.02.008
- Teixeira, W., Tassinari, C.C.G., Cordani, U.G., Kawashita, K. 1989. A review of the geochronology of the Amazonian Craton: tectonic implications. *Precambrian Research*, 42, p. 213-227.
- Tohver, E., Van Der Pluijm, B. A., Mezger, K., Essene, E., Scandolaro, J. E., Rizzotto, G. J. 2004. Significance of the Nova Brasilândia metasedimentary belt in western Brazil: redefining the Mesoproterozoic boundary of the Amazon Craton. *Tectonics*, 23(6). doi:10.1029/2003TC001563.
- Tohver, E., Van Der Pluijm, B. A., Scandolaro, J. E., Essene, E. 2005a. Late mesoproterozoic deformation of SW Amazonia (Rondonia, Brazil): geochronological and structural evidence for collision with Southern Laurentia. *J. Geol.*, 113, 309-323. doi: 10.1086/428807.
- Tohver, E., Van Der Pluijm, B. A., Mezger, K., Scandolaro, J. E., Essene, E. J. 2005b. Two stage tectonic history of the SW Amazon craton in the late Mesoproterozoic: identifying a cryptic suture zone. *Precam. Res.*, 137, 35-59.
- Tohver, E., Van Der Pluijm, B. A., Van Der Voo, R., Rizzotto, G. J., Scandolaro, J. E. 2002. Paleogeography of the Amazon Craton at 1.2 Ga: early greenvillian collision with the llano segment of Laurentia. *Earth and Planetary Science Letters*, 199, 185-200.
- Tohver, E., Teixeira, W., Van Der Pluijm, B., Geraldés, M., Bettencourt, J. S., Rizzotto, G. J. 2006. Restored transect across the exhumed Grenville orogen of Laurentia and Amazonia, with implications for crustal architecture. *Geology*, 34, 669-672.
- Vargas-Mattos, G.L. 2006. Geocronologia U/Pb en granitos post y sin-tectónicos de la Orogenia Sunsás en el Cratón Amazonico de Bolivia. Msc. Dissertation, Universidade do Estado do Rio de Janeiro, Rio de Janeiro, Brazil, p. 107.
- Wood, D. A. 1980. The application of a Th–Hf–Ta diagram to problems of tectonomagmatic classification and to establishing the nature of crustal contaminations of basaltic lavas of British tertiary volcanic province. *Earth and Planetary Science Letters*, 56, 11–30.
- Xia, L., Li, X. 2019. Basalt geochemistry as a diagnostic indicator of tectonic setting. *Gondwana Research*, 65, 43–67. <https://doi.org/10.1016/j.gr.2018.08.006>
- Xu, W., Xu, X., Zeng, G. 2017. Crustal contamination versus an enriched mantle source for intracontinental mafic rocks: Insights from early Paleozoic mafic rocks of the South China Block. *Lithos*. 286. 10.1016/j.lithos.2017.06.023.